

Identification of Opt3 as a putative ER glutathione disulfide exporter

Dissertation

zur Erlangung des Grades
des Doktors der Naturwissenschaften
der Naturwissenschaftlich-Technischen Fakultät
der Universität des Saarlandes

von

Julian Oestreicher

Saarbrücken

2021

Tag des Kolloquiums: 21.01.2022
Dekan: Prof. Dr. Jörn Erik Walter
Berichterstatter: Prof. Dr. Bruce Morgan
Prof. Dr. Katrin Philippar

Vorsitz: Prof. Dr. Uli Müller
Akad. Mitarbeiter: Dr. Jens Neunzig

Danksagung

Zuallererst möchte ich Prof. Dr. Bruce Morgan danken, der es mir ermöglichte diese Dissertation in seiner Gruppe anzufertigen. Bruce, es war eine wunderbare Zeit in deinem Labor, in der ich viel lernen durfte. Danke für die fachliche Unterstützung und dafür, dass du dir stets die Zeit genommen hast über meine Projekte, aber auch persönliche Belange zu diskutieren.

Des Weiteren möchte ich Prof. Dr. Katrin Philippar danken, für Ihre Ideen bezüglich meines Projekts, sei es bei IRTG-Seminaren oder in unseren gruppenübergreifenden Meetings. Außerdem, auch vielen Dank für die Übernahme des Zweitgutachtens.

Selbstverständlich möchte ich auch meinen alten Weggefährten danken. Vielen Dank Prince Amponsah, Gurleen Khandpur, Marie Mai und Jannik Zimmermann. Wir hatten unzählige Diskussionen bezüglich unserer Projekte und haben immer versucht uns gegenseitig zu unterstützen, ganz getreu dem Motto „geteiltes Leid ist halbes Leid“. Außerdem, danke Jannik und Gurleen, dass ihr meine Travel-Buddies wart, auch wenn wir wegen dir Jannik öfter einmal Pech mit dem Zug hatten. Nichtsdestotrotz gilt Jannik ein besonderer Dank für das Korrekturlesen meiner Arbeit.

Natürlich möchte ich auch Antje Eiden-Plach, Birgit Heider-Lips, Gabi Schon und Dr. Frank Hannemann danken. Nur dank eurem Einsatz war es möglich unseren Umzug nach Saarbrücken so schnell zu meistern. Wir sind als Team in den letzten zwei Jahren eng zusammengewachsen und dafür danke ich euch. Danke auch für die sehr unterhaltsamen Gespräche und die Unterstützung, welche ich von euch erfahren habe.

Bedanken möchte ich mich auch bei Prof. Dr. Maya Schuldiner, Dr. Jens Neunzig und Carsten Mattes für die spannenden Kollaborationen.

Außerdem möchte ich meinen ehemaligen Studentinnen Laura Buchholz und Haile Ropp danken, deren Zuarbeit mir sehr geholfen hat.

Vor allem möchte ich meinen Eltern danken. Danke, dass ich mich immer auf euch verlassen kann! Ohne eure Unterstützung hätte ich bislang wohl nicht so unbeschwert durchs Leben gehen können. Ich weiß das mehr als zu schätzen.

Abschließend möchte ich mich bei dir bedanken Myra. Du standest in den letzten vier Jahren immer an meiner Seite. Ohne dich wäre das alles sicherlich viel schwieriger gewesen. Auch wenn für mich jetzt ein neuer Lebensabschnitt beginnt, bleibst du meine Konstante.

Content

Danksagung	I
Content	II
Curriculum Vitae	III
List of Publications	IV
List of Figures	V
List of Tables	VI
Summary	VII
Zusammenfassung	VIII
1 Introduction	1
1.1 History of glutathione	1
1.2 Chemical properties of glutathione	1
1.3 Measurement of intracellular glutathione	4
1.3.1 Determination of whole cell [GSH] and [GSSG]	4
1.3.2 Genetically encoded redox biosensors	5
1.4 General functions of glutathione	8
1.4.1 GSH can reduce hydrogen peroxide.....	8
1.4.2 GSH is essential for iron-sulfur cluster biogenesis	8
1.4.3 GSH can post-translationally modify proteins.....	9
1.5 Glutathione synthesis and degradation	11
1.6 Cytosolic glutathione homeostasis	13
1.7 The vacuolar ABC-C-transporter Ycf1	16
1.8 Glutathione in the ER	18
1.8.1 Oxidative protein folding	18
1.8.2 Role of glutathione in the ER	20
1.8.3 ER glutathione transport	23
1.9 Glutathione in the Golgi apparatus	26

1.10	The oligopeptide transporter (OPT) family in <i>S. cerevisiae</i>	27
1.11	Aim of this thesis	29
2	Results	30
2.1	Opt3 genetically interacts with genes encoding Gsh1 and Gsh2	30
2.1.1	Synthetic gene array to identify genomic interaction partners of <i>OPT3</i>	30
2.1.2	<i>OPT3</i> deletion negatively affects cell growth in the absence of glutathione	32
2.2	Opt3 affects a specific cellular pool of glutathione disulfide	34
2.2.1	Opt3 expression influences cellular GSSG content.....	35
2.3	Opt3 affects a Ycf1-independent cellular GSSG pool	36
2.3.1	The effect of Opt3 on cellular GSSG levels is Ycf1 independent.....	37
2.3.2	Opt3 does not modulate vacuolar GSSG, which is imported from the cytosol	38
2.4	Opt3 affects GSSG in the endoplasmic reticulum	39
2.4.1	Opt3 co-localizes with Sec63.....	40
2.4.2	Re-localized Gsh2 restores $\Delta gsh2\Delta opt3$ growth in the absence of GSH.....	41
2.4.3	Opt3 strongly affects cellular GSSG content when Gsh2 is targeted to the ER	44
2.4.4	The effect of Opt3 on GSSG levels with ER-targeted Gsh2 is Ycf1 independent ..	47
2.5	Opt3 does not affect GSSG formed after cytosolic GSH accumulation	50
2.5.1	Opt1 dependent GSH uptake promotes cellular GSSG formation	50
2.5.2	GSSG formed during cellular GSH influx is not stored in the vacuole	52
2.5.3	The cytosol stays robustly reduced when GSH is taken up.....	54
2.5.4	Cells accumulate GSH after cellular GSSG application	55
2.5.5	GSSG is not exported to the vacuole via Ycf1 after uptake from the media	57
2.5.6	The cytosolic glutathione pool stays reduced after treatment with GSSG	59
2.5.7	Exogenous GSSG is immediately reduced after uptake into the cytosol	60
2.5.8	Cellular glutathione influx does not affect cytosolic pH.....	62

2.6	Opt3 activity is not regulated via cysteine oxidation	64
2.6.1	Opt3 cysteine mutants can maintain viability of the $\Delta gsh2\Delta opt3$ strain	65
2.6.2	Opt3 cysteine mutants affect whole cell GSSG concentrations	66
2.6.3	Opt3 cysteine modifications do not inhibit GSSG transport activity	69
2.7	Physiological relevance of Opt3	71
2.7.1	Opt3 function is independent of the thioredoxin system	71
2.7.2	<i>OPT3</i> mutant strains are resistant to ER-stress	74
2.7.3	Opt3 abundancy is important for a rapid unfolded protein response	76
2.7.4	<i>OPT3</i> expression levels do not affect E_{GSH} in the ER lumen	79
3	Discussion	82
3.1	<i>OPT3</i> expression influences cellular GSSG levels	82
3.2	Opt3 is a transmembrane protein of the ER	86
3.3	Opt3 does not influence the Ycf1-dependent GSSG pool	87
3.4	Glutathione synthesis can be re-localized to the endoplasmic reticulum	89
3.5	Two plausible pathways for GSSG depletion from the ER	92
3.6	The physiological role of Opt3	95
4	Material and Methods	99
4.1	Molecular Biology Methods	99
4.1.1	Plasmid isolation from <i>E. Coli</i>	99
4.1.2	Determination of DNA concentration.....	99
4.1.3	Preparation of chromosomal DNA of <i>S. cerevisiae</i>	99
4.1.4	Polymerase chain reaction for DNA amplification	100
4.1.5	PCR- and Agarose Gel clean up.....	101
4.1.6	Restriction digestion of DNA	101
4.1.7	Ligation of DNA fragments.....	101
4.1.8	Agarose gel electrophoresis	101
4.1.9	Chemical transformation of <i>E. Coli</i> cells.....	102
4.2	Genetic methods	102

4.2.1	p416- <i>TEF</i> - <i>OPT1</i> cloning	102
4.2.2	Cloning of <i>GSH2</i> variants	102
4.2.3	One-step transformation of <i>S. cerevisiae</i> / homologous recombination.....	105
4.2.4	Construction of yeast deletion and tagged strains.....	107
4.3	Cell Biology methods	109
4.3.1	Synthetic Genetic Array (SGA)	109
4.3.2	Growth curves	110
4.3.3	Determination of total GSH and GSSG content in cell lysates	110
4.3.4	Measurement with <i>OPT1</i> overexpression	111
4.3.5	Phluorin measurements.....	111
4.3.6	Determination of E_{GSH}	112
4.3.7	roGFP2 measurements in the ER.....	112
4.3.8	Growth test with shifted glutathione synthesis.....	112
4.3.9	Growth assay of <i>OPT3</i> Cysteine-Mutants	113
4.3.10	Drop dilution assay	113
4.3.11	Halo assay.....	113
4.3.12	ER Stress Resistance assay.....	114
4.3.13	RNA, DNA isolation and quantitative real-time PCR analysis.....	114
4.3.14	Microscopy	114
4.4	Growth Media	115
4.4.1	LB-Media.....	115
4.4.2	LB-Plates.....	115
4.4.3	YPD-media	115
4.4.4	YPD-plates	115
4.4.5	Yeast Nitrogen Base-solution (YNB).....	115
4.4.6	Ten times drop out mix	115
4.4.7	Hartwell`s complete (HC) media	116
4.4.8	HC-plates	117

References	IX
List of Abbreviations	X
Appendix	XI

Curriculum Vitae

Name	Julian Oestreicher
Date of birth	19.08.1992
Place of birth	Kaiserslautern, Deutschland

Education

09/2003 - 06/2012	Nordpfalzgymnasium Kirchheimbolanden 67292 Kirchheimbolanden Diploma: Abitur
10/2012 - 01/2016	University of Kaiserslautern, 67663 Kaiserslautern Bachelor's degree course: Biowissenschaften Diploma: Bachelor of Science (B.Sc.)
10/2015 – 10/2017	University of Kaiserslautern, 67663 Kaiserslautern Master's degree course: Molecular Cell and Neurobiology Diploma: Master of Science (M.Sc.)
10/2017 – 10/2018	University of Kaiserslautern, 67663 Kaiserslautern Start Ph.D. studies, in the group: Cellular Biochemistry
Since 10/2018	Saarland University 66123 Saarbrücken Center of Human and Molecular biology Continuation of Ph.D. studies at the Institute of Biochemistry

List of Publications

- [1] **Oestreicher, J.**, Morgan B. Glutathione: subcellular distribution and membrane transport. *Biochem Cell Biol.* 2019 Jun;97(3):270-289. Epub 2018 Nov 14. PMID: 30427707. <https://doi.org/10.1139/bcb-2018-0189>.
- [2] Zimmermann, J., **Oestreicher, J.**, Hess, S., Herrmann, J.M., Deponte, M., Morgan, B., 2020. One cysteine is enough: A monothiol Grx can functionally replace all cytosolic Trx and dithiol Grx. *Redox Biol* 36, 101598. <https://doi.org/10.1016/j.redox.2020.101598>
- [3] Zimmermann, J¹., **Oestreicher, J¹.**, Geissel, F., Deponte, M., Morgan, B., 2021. An intracellular assay for activity screening and characterization of glutathione-dependent oxidoreductases. *Free Radical Biology and Medicine* 172, 340–349. <https://doi.org/10.1016/j.freeradbiomed.2021.06.016>
- [4] Niemeyer, J., Scheuring, D., **Oestreicher, J.**, Morgan, B., Schroda, M., 2021. Real-time Monitoring of Subcellular H₂O₂ Distribution in *Chlamydomonas reinhardtii*. *The Plant Cell* <https://doi.org/10.1093/plcell/koab176>
- [5] Zimmermann, J., Laporte, H., Amponsah, P. S., Michalk, Sukmann, T., **Oestreicher, J.**, Tursch, A., Owusu, T.N.E., Roma, L.P., Riemer, J., Morgan, B. Tsa1 is the dominant peroxide scavenger and a major source of H₂O₂-dependent GSSG production in yeast – *not published*

¹Authors contributed equally.

List of Figures

Figure 1 Molecular structure of GSH and GSSG	2
Figure 2 Calculation of the glutathione redox potential	3
Figure 3 DTNB-recycling assay to determine [GSH] and [GSSG] in whole cell lysates	5
Figure 4 Model of the determination of E_{GSH} with genetically encoded Grx1-roGFP2 sensor	7
Figure 5 Non-enzymatical mechanisms of protein-S-glutathionylation	10
Figure 6 Cellular glutathione cycle	12
Figure 7 GSSG export from the cytosol	15
Figure 8 Protein structure of <i>S. cerevisiae</i> protein disulfide isomerase 1 (Pdi1) and ER oxidoreductase 1 (Ero1)	19
Figure 9 Multiple roles of glutathione in the ER	22
Figure 10 Model of ER glutathione uptake in yeast	24
Figure 11 Model of glutathione export from the ER	25
Figure 12 Illustration of the synthetic genetic array	31
Figure 13 <i>OPT3</i> has a synthetic negative growth phenotype with <i>GSH1</i> and <i>GSH2</i>	33
Figure 14 Analysis of GSH and GSSG in whole cell extracts of WT, $\Delta opt3$ and $p_{TEF}OPT3$ cells	36
Figure 15 Opt3 modulates a Ycf1 independent GSSG pool	37
Figure 16 Increased vacuolar GSSG is unaffected by Opt3	39
Figure 17 Opt3 is localized in the ER membrane	41
Figure 18 Glutathione synthesis was shifted from the cytosol to the ER	43
Figure 19 Illustration of Gsh2 constructs	44
Figure 20 Whole cell GSH content of strains expressing <i>GSH2</i> targeted to different subcellular localizations	45
Figure 21 ER localized GSH synthesis increases the effect of Opt3 on whole cell GSSG levels	46
Figure 22 Combined deletion of <i>OPT3</i> and <i>YCF1</i> does not affect GSH produced in the ER	48
Figure 23 Opt3 modulates GSSG produced upon ER-localized GSH synthesis independently of Ycf1	49
Figure 24 <i>OPT1</i> overexpression leads to a massive accumulation of cellular GSH	51
Figure 25 Whole cell GSSG content after GSH pulse is Ycf1 independent	53

Figure 26 Cytosolic glutathione remains reduced during the accumulation of GSH	55
Figure 27 <i>OPT1</i> overexpression causes a massive accumulation of cellular GSH	56
Figure 28 GSSG is not imported to the vacuole when GSSG is imported by Opt1.....	58
Figure 29 The cytosolic glutathione pool remains reduced during GSSG influx.....	60
Figure 30 Glr1 reduces immediately Opt1 imported GSSG in the cytosol	61
Figure 31 Cellular GSH influx slightly decreases cytosolic pH.....	63
Figure 32 Opt3 amino-acid sequence	64
Figure 33 Opt3 cysteine mutants rescue lethality of the $\Delta gsh2\Delta opt3$ double knock-out...	66
Figure 34 Total cellular GSH is unaffected by Opt3 cysteine mutants	67
Figure 35 Opt3 is not activated via protein cysteine modifications.....	68
Figure 36 Opt3 cysteine mutants do not affect whole cell GSH content in a $\Delta glr1\Delta opt3$ background	69
Figure 37 Opt3 is not inhibited via protein cysteine modifications	70
Figure 38 $\Delta trx1\Delta trx2\Delta opt3$ and $\Delta trx1\Delta trx2p_{TEF}OPT3$ are viable	72
Figure 39 Genetical manipulation of <i>OPT3</i> expression levels does not alter $\Delta trx1\Delta trx2$ sensitivity to H ₂ O ₂	73
Figure 40 <i>OPT3</i> expression mutants grow like WT cells during tunicamycin induced ER-stress.....	75
Figure 41 Altering <i>OPT3</i> expression levels does not influence cell viability during ER-stress.....	76
Figure 42 Low and high Opt3 copy numbers decrease the UPR	77
Figure 43 Impaired <i>HAC1</i> splicing in <i>OPT3</i> deletion and overexpression strains leads to lower expression of <i>KAR2</i> and <i>PDI1</i> during ER-stress	78
Figure 44 The ER targeted roGFP2-GRX1 redox-sensor is strongly oxidized	80
Figure 45 Opt3 exports GSSG from a cellular compartment into the cytosol.....	84
Figure 46 Opt3 is Ycf1 independent.....	88
Figure 47 Model of GSH synthesis in the ER.....	91
Figure 48 Model of GSSG export from the ER.....	94

List of Tables

Table 1 Standard PCR-components	100
Table 2 Standard PCR cycler program	100
Table 3 Primers used in this thesis	103
Table 4 Plasmids used in this thesis	105
Table 5 Strains used in this thesis	108
Table 6 10 x drop out mix composition	116
Table 7 Drop out amino acids	116

Summary

Glutathione is a small thiol-containing tripeptide, which is found in all eukaryotes, and has numerous essential functions. In mammals and yeast, glutathione is synthesized exclusively in the cytosol, yet is found in nearly all subcellular compartments. This implies the existence of glutathione transporters in most intracellular membranes, although the identity of these proteins is largely unknown. In this study, I characterized the protein product of the *Saccharomyces cerevisiae* open reading frame, *YGL114W*, hereinafter referred to as Opt3, which is a homolog of the plasma membrane glutathione transporter, Opt1. I observed a strong synthetic negative genetic interaction between *OPT3* and either *GSH1* or *GSH2*, which encode the proteins responsible for glutathione biosynthesis. Furthermore, overexpression of *OPT3* led to a strong decrease in cellular glutathione disulfide (GSSG) levels, which was independent of Ycf1-mediated vacuolar GSSG storage. I found that a genetic fusion construct between *OPT3* and the ultra-bright green fluorescent protein, ymNeonGreen, showed an exclusive endoplasmic reticulum (ER) localization. I observed that the effect of *OPT3* deletion and overexpression on cellular GSSG levels was strongly increased when glutathione biosynthesis was re-localized to the ER. Taken together, I propose that Opt3 is an ER-localized GSSG transporter, which functions to export GSSG from the ER to the cytosol, where it can be efficiently reduced.

Zusammenfassung

Glutathion ist ein kleines Thiol-haltiges Tripeptid, das in allen Eukaryonten vorkommt und diverse wichtige Funktionen hat. In Säugern und Hefen wird Glutathion ausschließlich im Zytosol synthetisiert, ist aber in fast allen Zellkompartimenten zu finden. Dies impliziert eine Existenz von Glutathiontransportern in intrazellulären Membranen, obwohl deren Identität weitgehend unbekannt ist. In dieser Studie habe ich das Proteinprodukt des offenen Leserahmens von *Saccharomyces cerevisiae*, *YGL114W*, im Folgenden als Opt3 bezeichnet, charakterisiert, welches ein Homolog des Plasmamembran-Glutathiontransporters Opt1 ist. Ich stellte eine synthetisch negative genetische Interaktion zwischen *OPT3* und *GSH1* oder *GSH2* fest, die für die Proteine der Glutathion-Biosynthese kodieren. Darüber hinaus führte die Überexpression von *OPT3* zu einem starken Rückgang des zellulären Glutathion-Disulfid (GSSG)-Gehalts, der unabhängig von der Ycf1-vermittelten vakuolären GSSG-Speicherung war. Ich zeigte, dass ein genetisches Fusionskonstrukt zwischen *OPT3* und dem ultrahellen grün fluoreszierenden Protein, ymNeonGreen, eine Lokalisierung im endoplasmatischen Retikulum (ER) aufweist. Außerdem war die Wirkung von *OPT3*-Deletion und -Überexpression auf den zellulären GSSG-Spiegel stark erhöht, wenn die Glutathion-Biosynthese in das ER verlagert wurde. Insgesamt denke ich, dass Opt3 ein im ER lokalisierter GSSG-Transporter ist, welcher GSSG aus dem ER in das Zytosol exportiert, wo es reduziert werden kann.

1 Introduction

1.1 History of glutathione

In 1888 J. de Rey-Paihade isolated a substance from yeast and different animal tissues and named it *philothion* what means “love and sulfur” in Greek. Only 33 years later in 1921 the later Nobel prize winner Sir Frederick G. Hopkins, isolated *philothion*, which he postulated to consist of glutamate and cysteine (Hopkins, 1921). He further described that the molecule was able to undergo reversible oxidation and reduction. Hopkins named it glutathione (Hopkins, 1921; Hopkins and Dixon, 1922). However, in 1927 Hunter and Eagles, using the same method as Hopkins for glutathione preparation, suggested that glutathione was rather a tripeptide than a dipeptide (Hanschmann et al., 2013; Hunter and Eagles, 1927; Simoni et al., 2002). After another two years, Hopkins confirmed Hunters and Eagles observation and proposed that glutathione is a tripeptide formed by glutamate, cysteine, and glycine (Hopkins, 1929). In the same year, Pirie and Pinhey reported that the structure of glutathione is γ -L-glutamyl-L-cysteinylglycine, by the titration of glutathione in water and formaldehyde (Pirie and Pinhey, 1929). Only six years later the prediction of Pirie and Pinhey was proven by Harington and Mead in 1935 who synthesized γ -glutamyl-cysteine out of N-carbobenzoxycystine and glycine ethyl ester (Harington and Mead, 1935).

In the past 133 years, the molecule glutathione was extensively studied. When searching for “glutathione” on the database PubMed, more than 8000 publications show up. Hopkins isolated glutathione from yeast cells, muscle tissue and mammalian liver. We now know that glutathione (γ -L-glutamyl-L-cysteinylglycine) is the most abundant small thiol present in nearly all eukaryotes with cellular concentrations of approximately 1-30 mM (Deponete, 2017; Iversen et al., 2010; Meister and Anderson, 1983; Schafer and Buettner, 2001).

1.2 Chemical properties of glutathione

Two reduced glutathione molecules (GSH) can be covalently linked between their cysteine residues (Figure 1). The resulting molecule is often referred to as oxidized glutathione (GSSG) (Deponete, 2013; Dickinson and Forman, 2002; Forman et al., 2009). However, more precise is the

designation glutathione disulfide (GSSG) as there are different oxidized glutathione species present in the cell (Meister and Anderson, 1983; Sies, 1999).

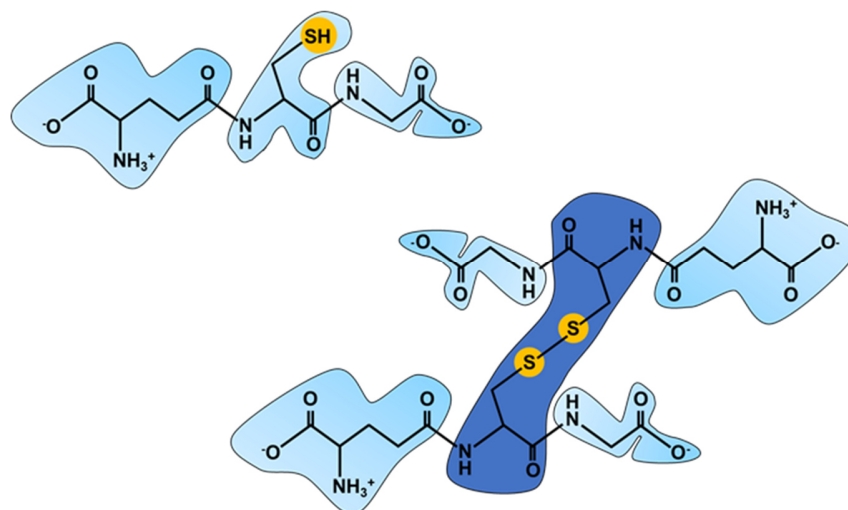


Figure 1 Molecular structure of GSH and GSSG. Individual amino acids are highlighted in blue. Modified figure from Oestreicher et al., 2018.

For the better understanding of glutathione redox homeostasis and how cellular glutathione can be studied, it is important to understand the basics of cysteine chemistry. Thereby, the thiol group (-SH) of the cysteine side chain is the reactive motif. As a nucleophile, cysteines can react with electrophiles and oxidants (McAlpine, 2019). The nucleophilicity of thiols is mostly dependent on the sulfur atom, which has two free electron pairs (LoPachin and Gavin, 2016). However, thiols are rather weak nucleophiles. The hydrogen and the sulfur atom of the thiol group are non-polar covalently bound because of minor changes in their electronegativity. Hence, thiols can be relatively easy deprotonated and are thus weak acids (McAlpine, 2019). The conjugate base of a thiol is often referred to as thiolate ($-S^-$) (Ulrich and Jakob, 2019). Thiolates are much stronger nucleophiles, because of their negative charge. Consequently, deprotonation of the thiol is important to make the cysteine reactive. The protonation state of a thiol residue depends on the pH of the surrounding environment and the pKa, which can be different for individual thiols (Reddie and Carroll, 2008; Wall et al., 2012). For instance, the pKa of cysteines within a protein can be altered by chemical properties of neighboring groups (Awoonor-Williams and Rowley, 2016). The typical pKa of a cysteine residue is ~ 9 . This implicates, that under the physiological pH of approximately 7, most cysteine residues are protonated (Krezel and Bal, 1999; Zeida et al., 2014).

However, the pKa of the cysteine residue alone does not determine glutathione reactivity (Matsui et al., 2020).

Glutathione can spontaneously react with other molecules in a redox reaction if thermodynamically favorable. Thereby, glutathione can either be reduced or oxidized (Deponte, 2017). A parameter, which describes the tendency of a substance to get reduced or oxidized in a redox reaction is the reduction oxidation (redox) potential (E). Thus, the redox potential provides information if a reaction of glutathione with another molecule is thermodynamically favored or not (Deponte, 2013; Gutscher et al., 2008).

$$\text{Equation 1} \quad E = E^{\circ'} - \frac{RT}{zF} * \ln \frac{[\text{red}]}{[\text{ox}]}$$

$$\text{Equation 2} \quad E_{\text{GSH}} = E^{\circ'}_{\text{GSH}} - \frac{RT}{2F} * \ln \frac{[\text{GSH}]^2}{[\text{GSSG}]}$$

Figure 2 Calculation of the glutathione redox potential. In Equation 1 the Nernst equation for determination of redox potentials is presented where E is the redox potential dependent on the standard redox potential, R is the universal gas constant ($8.314 \text{ J} \cdot \text{K}^{-1} \cdot \text{mol}^{-1}$), F is the Faraday constant (96485 C/mol), T is the absolute temperature in kelvin and z the number of electrons donated in the half reaction. Equation 2 demonstrates how E_{GSH} can be determined using the Nernst equation. Due to the half reaction, $[\text{GSH}]$ enters the Nernst equation in a squared term.

The redox potential of glutathione (E_{GSH}) can be calculated from the Nernst equation as illustrated in Figure 2 and is dependent on i. the total glutathione concentration (here referred to as $[\text{GSx}]$) and ii. the molar ratio between GSH and GSSG (GSH:GSSG). Since the half-cell reaction of glutathione is $\text{GSSG} + 2\text{e}^- + 2\text{H}^+ \leftrightarrow 2 \text{GSH}$, the GSH concentration enters the Nernst-equation in a squared term (Figure 2). Thus, to calculate either E_{GSH} , GSH:GSSG ratio or $[\text{GSx}]$ information on either two of these parameters are required or alternatively $[\text{GSH}] + [\text{GSSG}]$ (Lismont et al., 2017; Morgan et al., 2011; Schafer and Buettner, 2001).

However, it is not clear to which extend thermodynamic reactions are relevant within the cell. For instance, although a reaction might be less thermodynamically favorable, enzymes can catalyze the reaction. Thus, in a cellular system kinetics might be more important than thermodynamics (Berndt et al., 2014; Deponte, 2013; Flohé, 2013). Although E_{GSH} might not necessarily be the

driving force of most reactions, it can provide information on glutathione dependent reactions mediated by enzymes.

1.3 Measurement of intracellular glutathione

Several methods are available to study glutathione homeostasis (Gutscher et al., 2008; Iversen et al., 2010; Morgan et al., 2011; Rahman et al., 2006). Early studies of glutathione mostly relied on glutathione concentrations determined in whole cell extracts. However, now we have a wide variety of genetically encoded biosensors to determine compartment specific glutathione redox potentials.

1.3.1 Determination of whole cell [GSH] and [GSSG]

One commonly used method to measure glutathione concentrations in whole cell lysates is based on the enzymatic recycling assay developed in 2006 by I. Rahman (Rahman et al., 2006).

The assay relies on the reaction of GSH with 5,5'-dithio-bis(2-nitrobenzoic acid) (DTNB), in which GS-TNB and TNB are formed. The TNB formation can be monitored by absorption measurement at 412 nm and is proportional to [GSH] in the cell extract. The GS-TNB disulfide along with GSSG in the sample is reduced to GSH + TNB and 2 GSH, respectively by glutathione reductase in the presence of nicotinamide adenine dinucleotide phosphate (NADPH). Therefore, GSH enters another round of reaction with DTNB (Figure 3). Hence, the change in absorbance over time is proportional to the total glutathione [GSx] concentration in the sample. Glutathione disulfide can be determined by incubating the sample with 2-vinyl-pyridine before measurement. 2-vinyl-pyridine covalently reacts with GSH but not with GSSG thus eliminating GSH from the reaction with DTNB. While both [GSx] and [GSSG] concentrations are experimentally determined, the [GSH] is calculated ($GSx = GSH + 2 \times GSSG \rightarrow GSH = GSx - 2 \times GSSG$).

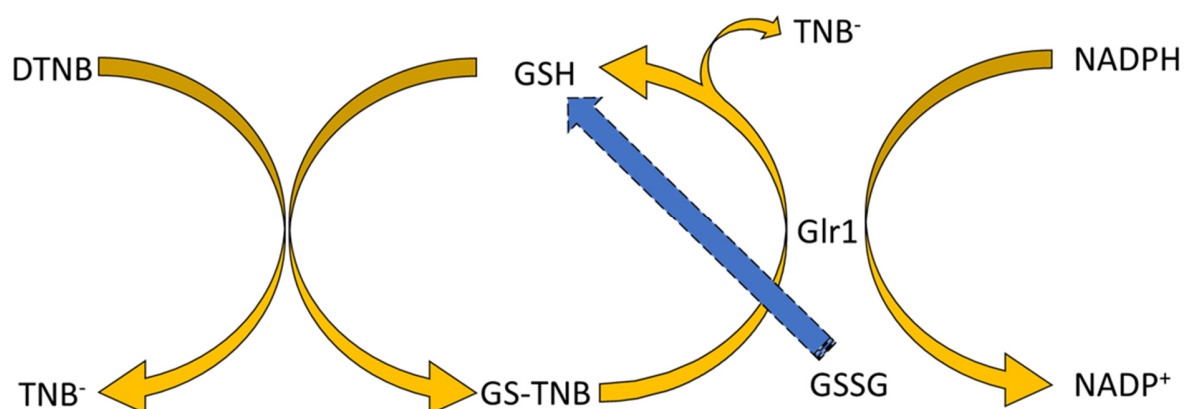


Figure 3 DTNB-recycling assay to determine [GSH] and [GSSG] in whole cell lysates. For [GSH] determination total glutathione is measured and subtracted from experimentally determined [GSSG]. [GSx] determination: GSH in the sample reacts with 5,5'-dithio-bis(2-nitrobenzoic acid) (DTNB) to TNB⁻ and GS-TNB. TNB⁻ can be determined by measuring absorption at 412 nm. GS-TNB is reduced by glutathione reductase (Glr1) to GSH and another molecule TNB⁻. Also, GSSG in the sample is reduced to GSH by Glr1. Formed GSH enters the DTNB cycle. Thus, TNB⁻ formation is proportional to glutathione concentrations in the media. Determination of [GSSG]: Before recycling assay is started, samples are incubated with 2-vinyl-pyridine, what covalently binds to reduced GSH. Hence, when DTNB assay is started, GSSG is reduced to GSH what rapidly reacts with DTNB, while 2-vinyl-pyridin bound endogenous GSH cannot enter the reaction. [GSH] is calculated as followed: $[GSx]-2*[GSSG]$ since two GSH molecules form one molecule of GSSG. Modified figure from Rahman et al., 2006.

With the absolute [GSH] and [GSSG] concentrations from whole cell extracts, the GSH:GSSG ratio and further the cellular E_{GSH} can be calculated. Although, the analysis of glutathione concentration in whole cell extracts is remarkably useful in terms of reproducibility and high glutathione specificity, the technique has limitations (Schwarzländer et al., 2016). Beside a low temporal resolution, subcellular glutathione pools get mixed during cell lysis. Therefore, it was previously not possible to study glutathione homeostasis in specific cellular compartments. Thus, novel genetically encoded biosensors were developed, which can be fused to compartment specific targeting sequences and expressed *in vivo*.

1.3.2 Genetically encoded redox biosensors

In 2004, Hanson and colleagues developed a redox sensitive GFP (roGFP) biosensor, based on the enhanced green fluorescent protein (eGFP) to measure redox potentials *in vivo* (Hanson et al., 2004). The chromophore of roGFP exists in an anionic or neutral state, depending on its protonation state. roGFP contains two cysteines close to the chromophore which can form a disulfide bond. Disulfide bond formation induces slight structural changes in the GFP β -barrel, which facilitates chromophore protonation. Depending on its redox state, roGFP has two excitation maxima. The anionic chromophore, predominantly in reduced roGFP, is excited at 490 nm, while

the neutral chromophore, predominantly in oxidized roGFP, is excited at 405 nm. Both states emit light at 512 nm (Morgan, 2014; Morgan et al., 2011; Zimmermann et al., 2020). This behaviour allows for a ratio metric readout making the probe independent of expression.

Different roGFP variants were developed containing multiple point mutations, which change the midpoint potential of certain sensors (Cannon and Remington, 2006). One commonly used roGFP variant is roGFP2. roGFP2 has a midpoint potential of -280 mV, which perfectly suits to measure redox potentials in reducing subcellular compartments like the cytosol or the mitochondrial matrix (Dooley et al., 2004; Gutscher et al., 2008; Hanson et al., 2004).

Remarkably, it was demonstrated that fluorescent protein-based biosensors expressed in the cytosol equilibrate with the 2GSH:GSSG redox couple. However, the equilibration was not directly and relied on the presence of highly abundant glutaredoxin 1 (Grx1) (Østergaard et al., 2004). Upon these findings, a fusion construct between Grx1 and roGFP2 (Grx1-roGFP2) was developed, which monitors exclusively E_{GSH} (Gutscher et al., 2008). The fusion of Grx1 to roGFP2 makes the probe independent from endogenous Grx1 and enhances the kinetics of the reaction. Thus, Grx1-roGFP2 allows for measurements of the glutathione redox potential in living cells with compartment-specific resolution (Figure 4) (Calabrese et al., 2017; Gutscher et al., 2008; Morgan et al., 2011).

Interestingly, measurements with cytosolic localized Grx1-roGFP2 revealed a glutathione redox potential of approximately -320 mV, which suggest a GSH:GSSG ratio of $\sim 50\,000:1$ with estimated cytosolic glutathione concentrations of 10 mM (Morgan, 2014). This observation is in massive discrepancy with GSH:GSSG ratios of 100:1 determined in whole cell extracts and hence suggests a compartmentalization of cellular GSSG (Morgan et al., 2013; Muller, 1996).

We now have highly sensitive E_{GSH} sensors e.g., in the cytosol, mitochondrial matrix or in peroxisomes. Furthermore, roGFP variants like roGFP1-iE or roGFP1-iL with midpoint potentials of approximately -230 mV, which are more suitable for oxidative compartments like the ER, are available. Please note that roGFP2 with a midpoint potential of approximately -280 mV is almost fully oxidized in the endoplasmic reticulum (Aller et al., 2013; Birk et al., 2013b; Hwang et al., 1992). However, there is still a controversy going on in how specifically ER targeted sensors equilibrate to the ER glutathione redox couple and thus need further characterization (Oestreicher and Morgan, 2018).

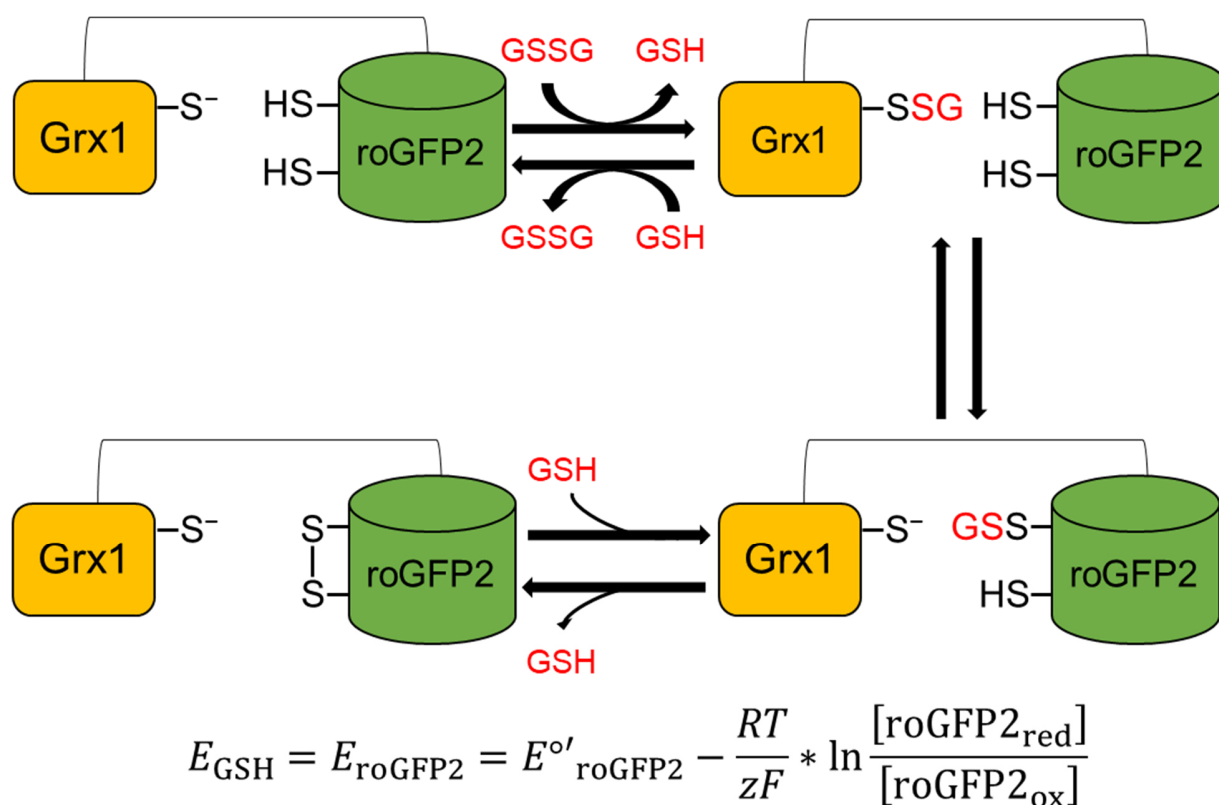


Figure 4 Model of the determination of E_{GSH} with genetically encoded Grx1-roGFP2 sensor. The fusion of Grx1 to roGFP2 leads to the thermodynamic equilibration of roGFP2 with the glutathione redox pair. Thereby, experimentally measured E_{roGFP2} equals E_{GSH} as illustrated in the lower panel with the modified Nernst equation. E_{roGFP2} is determined via fluorescent emission measurement as described in "Material and Methods". Modified figure from Morgan et al., 2011.

Recently, the combination of the yellow fluorescent protein (YFP)-based E_{GSH} sensor rxYFP, with a single cysteine Grx1 (sCGrx1p) sensor monitoring the GSH:GSSG ratio, was used to indirectly determine ER [GSx]. While the biosensor rxYFP underlies a similar mechanism than roGFP2 based probes, sCGrx1p is in equilibrium with the GSH:GSSG redox couple through autocatalyzed glutathionylation. The percentage of glutathionylated sCGrx1 can be quantified through size shift experiments in combination with non-reducing SDS-page (Iversen et al., 2010; Montero et al., 2013; Østergaard et al., 2004; Ponsero et al., 2017).

The ongoing development of novel cellular glutathione sensors sharpens our understanding of cellular glutathione redox homeostasis. Thereby it is important to study glutathione homeostasis in a subcellular context and to understand how different glutathione pools are connected.

1.4 General functions of glutathione

As a nucleophile and reductant, GSH is involved in a variety of different cellular processes including the detoxification of reactive oxygen species (ROS), the formation of iron sulfur clusters and the posttranslational modification of proteins (Grant et al., 1997; May et al., 1998; Wu et al., 2004).

1.4.1 GSH can reduce hydrogen peroxide

Although uncontrolled production of ROS such as hydrogen peroxide (H_2O_2) can be harmful for the cell, the formation of ROS is unavoidable (Murphy, 2009). For example, H_2O_2 can be formed during respiration, oxidative protein folding or beta oxidation of fatty acids (Murphy, 2009; Nakamura et al., 2019; Paranagama et al., 2010; Quijano et al., 2016). ROS potentially can react with thiolates in (certain) proteins leading to the formation of sulfenic, sulfinic or sulfonic acids on cysteine residues. The latter is irreversibly and can therefore inactivate the protein. Thus, ROS formation and reduction need to be controlled (Amponsah et al., 2021; He et al., 2017; Huang et al., 2019; Ray et al., 2012). GSH can reduce H_2O_2 directly, however the second order rate constant of $30 \text{ M}^{-1}\text{s}^{-1}$ is slow (Van Laer et al., 2013; Winterbourn and Metodiewa, 1999). Thus, GSH is rather indirectly involved in H_2O_2 scavenging as electron donor of enzymes like glutathione peroxidases (Gpx), glutaredoxins (Grx) and peroxiredoxins (Prx) (Aoyama and Nakaki, 2012; Collinson et al., 2002; Greetham and Grant, 2009; Pedrajas et al., 2010). However, it is nowadays suggested that at least in the yeast cytosol the thioredoxin system is sufficient enough for H_2O_2 scavenging, via the efficient reduction of highly abundant peroxiredoxins (Hanschmann et al., 2013; Paulo et al., 2014). Thereby, it remains largely elusive to what extent glutathione-dependent peroxiredoxin reduction contributes (Calabrese et al., 2019; Deponete, 2013; Peskin et al., 2016). Please note, that these observations cannot be interpreted as ROS detoxification in the cytosol is completely GSH independent e.g., application of exogenous H_2O_2 leads to the formation of GSSG in the cytosol and deletion of the thioredoxin system together with the glutaredoxin system is lethal (Liedgens et al., 2020; Zimmermann et al., 2021, 2020). However, since the thioredoxin system can scavenge efficiently ROS in the cytosol when GSH is depleted, the vital role for the cell of GSH must be something different.

1.4.2 GSH is essential for iron-sulfur cluster biogenesis

GSH plays a crucial role in the formation of iron-sulfur clusters (FeS). Within the cell FeS clusters are incorporated into a variety of proteins where they act as an essential co-factor for several

reactions e.g., electron transfer and activation or regulation of gene expression (Cardenas-Rodriguez et al., 2018; Johnson et al., 2005). In the yeast mitochondrial matrix, FeS clusters are formed in the iron-sulfur cluster (ISC) pathway, which consists out of at least 17 proteins (Daniel et al., 2020). One important component of the ISC is the monothiol Grx5, localized in the mitochondrial matrix, which can transfer FeS clusters to proteins. Thereby, GSH acts as the co-ligand, which allows binding of FeS to Grx5 (Deponete, 2013). Furthermore, it was demonstrated, that the Atm1 mediated export of a so far unknown FeS cluster containing compound to the cytosol is GSH dependent (Mühlenhoff et al., 2020).

Interestingly, depletion of GSH causes the same cellular iron-starvation like response as observed in cells with depleted Atm1 and leads to an upregulation of the iron-responsive transcription factors Aft1 and Aft2 (Kumar et al., 2011). Aft1 and Aft2 enhance the expression of e.g., the ferro-O₂-oxidoreductase encoding gene *FET2* and the high affinity iron permease encoding gene *FTR1* (Courel et al., 2005). Aft1 and Aft2 are activated upon interaction with the FeS cluster containing enzymes Grx2 and Grx3. Thereby it was demonstrated, that GSH is similar to Grx5 important for Grx2 and Grx3 interaction with FeS clusters (Kumar et al., 2011; Sipos et al., 2002).

Conclusively, the essential role of GSH in the cell might be rather linked to iron homeostasis and FeS cluster formation than the reduction of ROS (Kumar et al., 2011).

1.4.3 GSH can post-translationally modify proteins

The mixed disulfide formation between GSH and a protein thiol, is an important mechanism to either modulate enzyme activity, protect protein thiols from irreversible hyperoxidation, or modulate cellular signaling. The underlying mechanism of GSH-protein mixed disulfide formation is called protein-S-glutathionylation (Grant et al., 1997; Iversen et al., 2010; Mailloux, 2020). One example for protein S-glutathionylation is the plasma membrane localized Ca²⁺ transporter Cch1, which is activated upon glutathionylation on the four cysteines C587A, C606A, C636A and C642A by glutathione S-transferase Gtt1 during ER-stress (Chandel and Bachhawat, 2017).

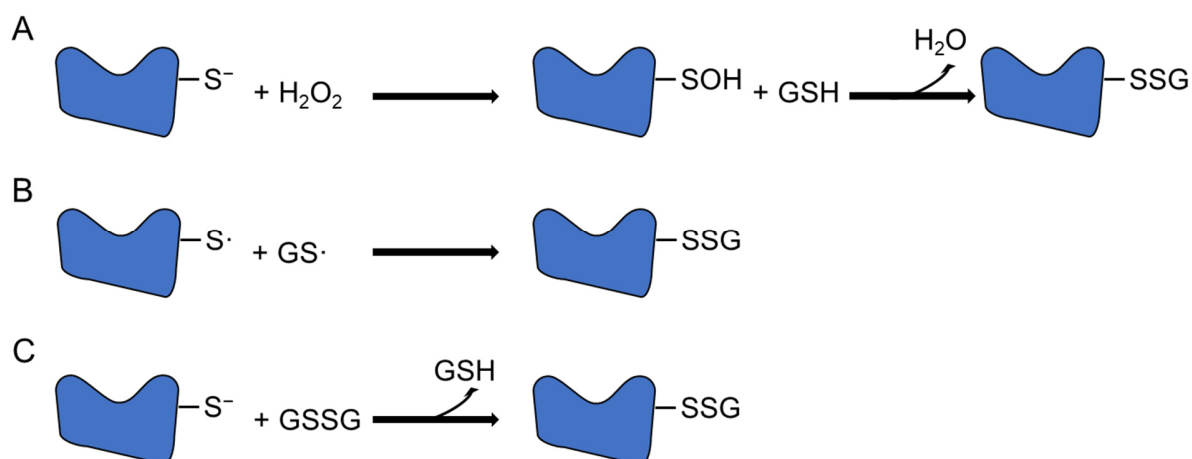


Figure 5 Non-enzymatical mechanisms of protein-S-glutathionylation. Different mechanisms are proposed of how protein thiols can be glutathionylated. In the the two-electron mechanism (A) the protein cysteine residue forms a sulfenic acid upon reaction with reactive oxygen species like H₂O₂. In a second step, the sulfenic acid reacts with GSH what forms a mixed disulfide bond between the thiol and glutathione. During the one electron mechanism (B) protein thiol and GSH form a radical after the reaction with reactive thiyl radicals. Protein-S-glutathionylation occurs via radical recombination. Another, although quite unlikely mechanism to glutathionylate protein thiols is the disulfide exchange between GSSG and the cysteine residue (C). This mechanism presupposes a relatively low GSH:GSSG ratio. Whether this occurs in most of the reduced cellular compartments remains elusive.

Beside enzymatically mediated protein-S-glutathionylation by glutaredoxins or glutathione transferases, several mechanisms were supposed how protein thiols can become non enzymatically S-glutathionylated (Mailloux, 2020). In the two-electron oxidation model (Figure 5 A), thiolates form a sulfenic acid when oxidized by e.g., hydrogen peroxides, alkyl hydroperoxides or peroxyxynitrite, followed by the rapid reaction with GSH. This leads to the formation of a mixed disulfide bond between the protein cysteine and glutathione (PSSG) (Gupta and Carroll, 2014). In the proposed one electron oxidation mechanism (Figure 5 B) protein thiols and GSH form reactive thiyl radicals after the reaction with hydroxyl, nitrogen dioxide or superoxide radical, which can be formed for example in the mitochondrial matrix during respiration. Protein S-glutathionylation may occur through radical recombination (Yun et al., 2010).

In theory it is also possible that protein thiols get non enzymatically glutathionylated in a direct reaction with glutathione disulfide as demonstrated in Figure 5 C (Musaogullari and Chai, 2020). However, such a mechanism would need an extremely low GSH:GSSG ratio and is thus, taking into concern that the yeast cytosolic GSH:GSSG ratio is 50 000:1, highly unlikely in most cellular compartments (Morgan et al., 2013). In the cytosol the glutaredoxins Grx1 and Grx2 can either reduce intramolecular protein disulfides, or de-glutathionylate proteins using GSH as an electron donor (Mailloux, 2020).

1.5 Glutathione synthesis and degradation

In *S. cerevisiae* glutathione synthesis takes exclusively place in the cytosol. Reduced GSH is synthesized in two steps. The first step of GSH synthesis is mediated by the enzyme γ -glutamylcysteine synthetase 1 (Gsh1) (Figure 6). In an ATP-dependent reaction, Gsh1 links glutamate to cysteine thereby introducing an atypical peptide bond between the amino group of cysteine and the side-chain carboxyl group of the glutamate. As a product of this reaction, the glutathione precursor γ -L-glutamyl-L-cysteine, often referred to as γ -EC or γ -GC is produced (hereinafter referred to as γ -GC) (Birk et al., 2013a; Hanschmann et al., 2013; Suzuki et al., 2011). In the second ATP consuming synthesis reaction, glutathione synthase (Gsh2) links a glycine molecule to γ -GC producing one molecule of reduced γ -L-glutamyl-L-cysteinylglycine (GSH) (Grant, 2001). As an important source of electrons, GSH is oxidized to glutathione disulfide in many different reactions for example during the reduction of protein disulfides by glutathione-dependent oxidoreductases such as glutaredoxins. Cytosolic glutathione disulfide is rapidly reduced by glutathione reductase (Glr1) in a NADPH-dependent process.

The synthesis of γ -GC by Gsh1 is negatively feedback regulated by GSH and thus is the rate limiting step in glutathione synthesis. Both, *GSH1* and *GSH2* have a *YAP1* binding site in their promoter region (Trotter and Grant, 2002; Wheeler et al., 2003; Wu and Moye-Rowley, 1994). Yeast Activator (AP1-like) protein Yap1 is a redox dependent transcription factor, which accumulates upon oxidative stress in the nucleus and promotes the expression of several redox active proteins (Fernandes et al., 1997; Kuge and Jones, 1994; Rodrigues-Pousada et al., 2019). Interestingly, yeast deleted for *GSH1* is not viable without glutathione supplemented in the media, whereas cells lacking Gsh2 survive. In cells deleted for *GSH2* the γ -GC concentration is increased (Quintana-Cabrera et al., 2012). Although γ -GC can substitute GSH, its ability to form mixed thiols with proteins is lower compared to GSH (Grant et al., 1997; Kumar et al., 2011). Counterintuitively, similar to GSH depletion a strong increase in intracellular GSH is also lethal (Kumar et al., 2011; Ponsoero et al., 2017; Srikanth et al., 2005).

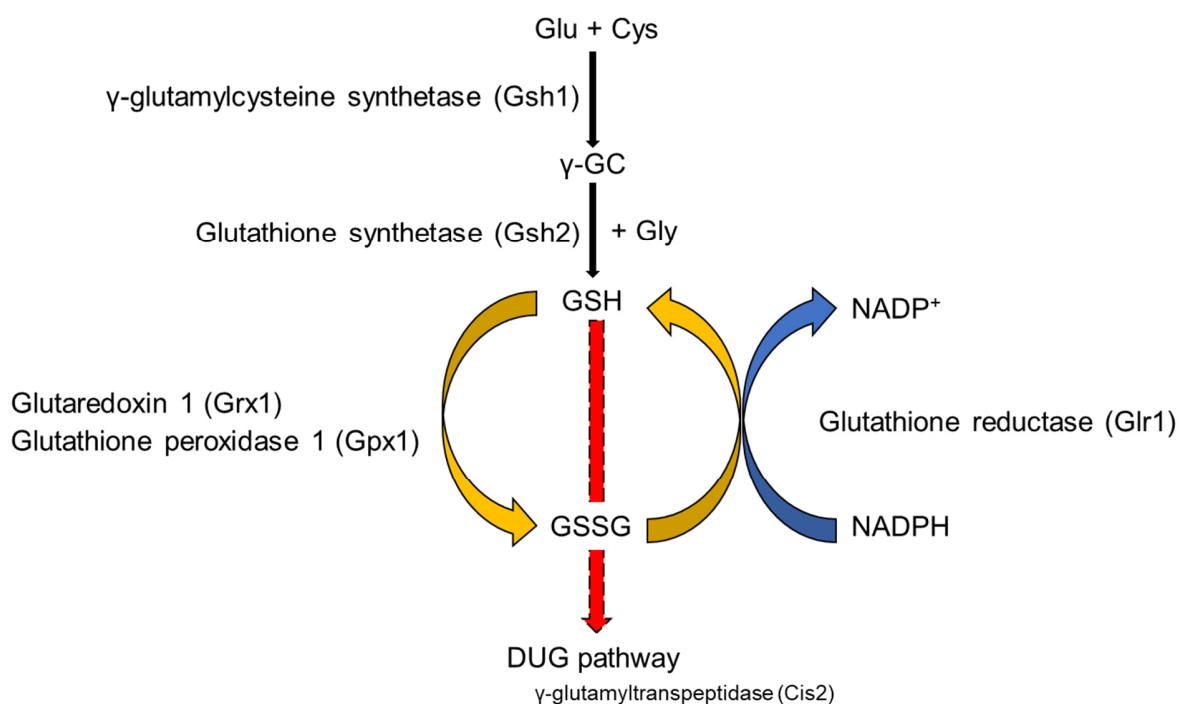


Figure 6 Cellular glutathione cycle. GSH is synthesized in the cytosol via the enzymes γ-glutamylcysteine synthetase (Gsh1) and glutathione synthetase (Gsh2). Reduced GSH is involved in a variety of different cellular functions for example electron donor for the enzymes glutaredoxin 1 (Grx1) or glutathione peroxidase 1 (Gpx1). It is also thought to be oxidized by peroxiredoxins like e.g., peroxiredoxin 1 (Prx1) and may directly reduce reactive oxygen species (ROS). Formed GSSG is predominantly reduced via NADPH consuming glutathione reductase 1 (Glr1). Glutathione degradation can either be mediated via the cytosolic DUG-pathway, or the vacuolar γ-glutamyltranspeptidase (Cis2). Modified figure from Grant (Grant, 2001).

Glutathione has a comparably long half-life in yeast cells of approximately 90 min (Baudouin-Cornu et al., 2012). Two independent mechanisms of glutathione degradation were described. For a long time, it was assumed that glutathione degradation in yeast occurs exclusively in the vacuolar lumen. Until recently, the γ-glutamyltranspeptidase (Cis2) was the only known GSH degrading enzyme (Mehdi et al., 2001). However, the DUG pathway was identified as another novel cytosolic glutathione degradation pathway (Ganguli et al., 2007). In this mechanism the enzymes Dug2 and Dug3 form a heteromeric complex, which is crucial for the aminotransferase activity of Dug3. Furthermore Dug1 is able to function as Cys-Gly dipeptidase (Kaur et al., 2012, 2009).

Glutathione synthesis and degradation are both thought to play an important role for cellular glutathione redox homeostasis (Bachhawat et al., 2009; Bachhawat and Yadav, 2018).

1.6 Cytosolic glutathione homeostasis

The cytosolic glutathione pool in *S. cerevisiae* is extremely reduced ($E_{\text{GSH}} = -320$ mV) under physiological conditions (Morgan et al., 2013). This is consistent to cytosolic E_{GSH} reported in other organisms like nematode worms, fish, plants, mice and human cell lines (Gutscher et al., 2008; Meyer et al., 2007; Morgan, 2014).

Our traditional understanding of glutathione concentration in the cytosol of ~ 10 mM is mainly based on measurements of [GSx] in whole cell lysates. Thereby, it was assumed for a long time, that [GSx] measured in whole cell lysates must mostly represent the cytosolic glutathione pool, as it was postulated that the cytosol takes in the largest volume of the cell. However, recently the group of Michel Toledano re-estimated the cytosolic [GSx] to 30 mM by the combination of a rYFP E_{GSH} probe and the sCGrx1p sensor, which equilibrates with the GSH:GSSG ratio as mentioned above (Ponsero et al., 2017). Ponsero et al. pointed out, that their measurements are in line with glutathione values examined in whole cell lysates if a correction is made, which considers the large volume of the vacuole (Ponsero et al., 2017).

Recently postulated [GSx] of 30 mM together with a reported E_{GSH} value of -320 mV indicates a cytosolic GSH:GSSG ratio of $\sim 17\,000:1$, which is equivalent to a cytosolic [GSSG] of ~ 1.8 μM . When the GSH:GSSG ratio is determined with the more traditionally reported cytosolic [GSx] of 10 mM, the GSH:GSSG ratio is $\sim 50\,000:1$ with cytosolic [GSSG] of approximately 200 nM. Conclusively this elucidates that GSSG in the cytosol is only present in a nanomolar to low micromolar range (Oestreicher and Morgan, 2018).

The extremely reduced glutathione pool in the cytosol of *S. cerevisiae* is mainly maintained by the NADPH consuming enzyme Glr1 (Grant et al., 1996). Glr1 is a flavoenzyme belonging to the nucleotide-disulfide oxidoreductase family and has high affinity to both NADPH ($K_m \sim 15$ μM) and GSSG ($K_m \sim 76$ μM) (Massey and Williams, 1965; Yu and Zhou, 2007a). Glr1 forms a heterodimer of approximately 110 kDa in which both subunits hold a flavin-adenine-dinucleotide (FAD) binding domain, which is formed by a typical Rossmann fold (Yu and Zhou, 2007a). A Rossmann fold usually consists out of a repeating chain of a α -sheet, flanked by two β -sheets (Hanukoglu, 2015). Also, the NADPH binding site is formed by a Rossmann fold and is present in each of the Glr1 subunits (Outten and Culotta, 2004). However, the substrate binding site, in which two GSSG molecules can be attached is created through dimerization of the two individual subunits, what implicates that just dimerized Glr1 is functional. Since the NADPH and GSSG binding sites are spatially separated from each other, Glr1 is first reduced by NADPH, before the electrons are

passed to GSSG (Deponte, 2013; Schulz et al., 1978). Although Glr1 is important for the reduction of GSSG in the cytosol, $\Delta glr1$ cells are viable and just slightly more sensitive to oxidants like diamide (Muller, 1996).

Interestingly, although the fruit fly *Drosophila melanogaster* (*D. melanogaster*) has no gene, which encodes for *GLR1*, the cytosolic glutathione pool is equally reduced as in yeast cells, with reported E_{GSH} values of approximately -320 mV (Albrecht et al., 2011). Intriguingly, unlike in mammals, yeast or plants, the cytosolic thioredoxin system alone is responsible for the reduction of GSSG in *D. melanogaster* (Cheng et al., 2007; Kanzok et al., 2001).

In yeast, the thioredoxin system consists of the two homologs thioredoxin 1 (Trx1) and thioredoxin 2 (Trx2), which possibly developed through whole genome duplication (Garrido and Grant, 2002; Oliveira et al., 2010). Both Trx1 and Trx2 have a typical CXXC motif in their active sites, which is required for efficient reduction of substrate proteins. Oxidized Trx1 and Trx2 are reduced by thioredoxin reductase1 (Trr1), which ultimately relates its reduced state by the oxidation of reduced NADPH (Atkinson and Babbitt, 2009). Thioredoxins together with glutaredoxins belong to the TRX superfamily sharing the characteristic TRX fold and partial redundancy in their function (Toledano et al., 2013). Thus, structural differences between and within these two groups remain elusive and move into focus of recent research (Liedgens et al., 2020; Staudacher et al., 2018; Zimmermann et al., 2021, 2020)

Remarkably, like in *D. melanogaster*, the thioredoxin system in yeast is thought to reduce GSSG. For example, $\Delta gsh1\Delta glr1$ cells which are deficient in GSH synthesis and the reduction of GSSG, can accumulate GSH when grown in GSSG containing media, whereby the additional deletion of a single thioredoxin decreases the accumulation of GSH (Greetham and Grant, 2009). Additionally, causes the overexpression of *TRX1*, *TRX2* or *TRR1* in a $\Delta glr1$ background decreased GSSG concentrations, whereas a $\Delta trx2\Delta glr1$ strain has increased whole-cell GSSG (Morgan et al., 2013; Tan et al., 2010). Moreover, *in vitro* studies with purified Trx1 from *S. cerevisiae* revealed that indeed Trx1 can reduce GSSG with a second order rate constant of $100 \text{ M}^{-1} \text{ s}^{-1}$ (Bao et al., 2009). This is comparable to second order rate constants determined in *D. melanogaster* ($170 \text{ M}^{-1} \text{ s}^{-1}$) (Kanzok et al., 2001, 2000). Nevertheless, it remains elusive to what extent GSSG reduction by Trx1 is physiological relevant in yeast. For example, the reduction of GSSG by Glr1 has a second order rate constant of $1.8 \times 10^4 \text{ M}^{-1} \text{ s}^{-1}$ and is thus 180 times faster than Trx1 (Bulger and Brandt, 1971).

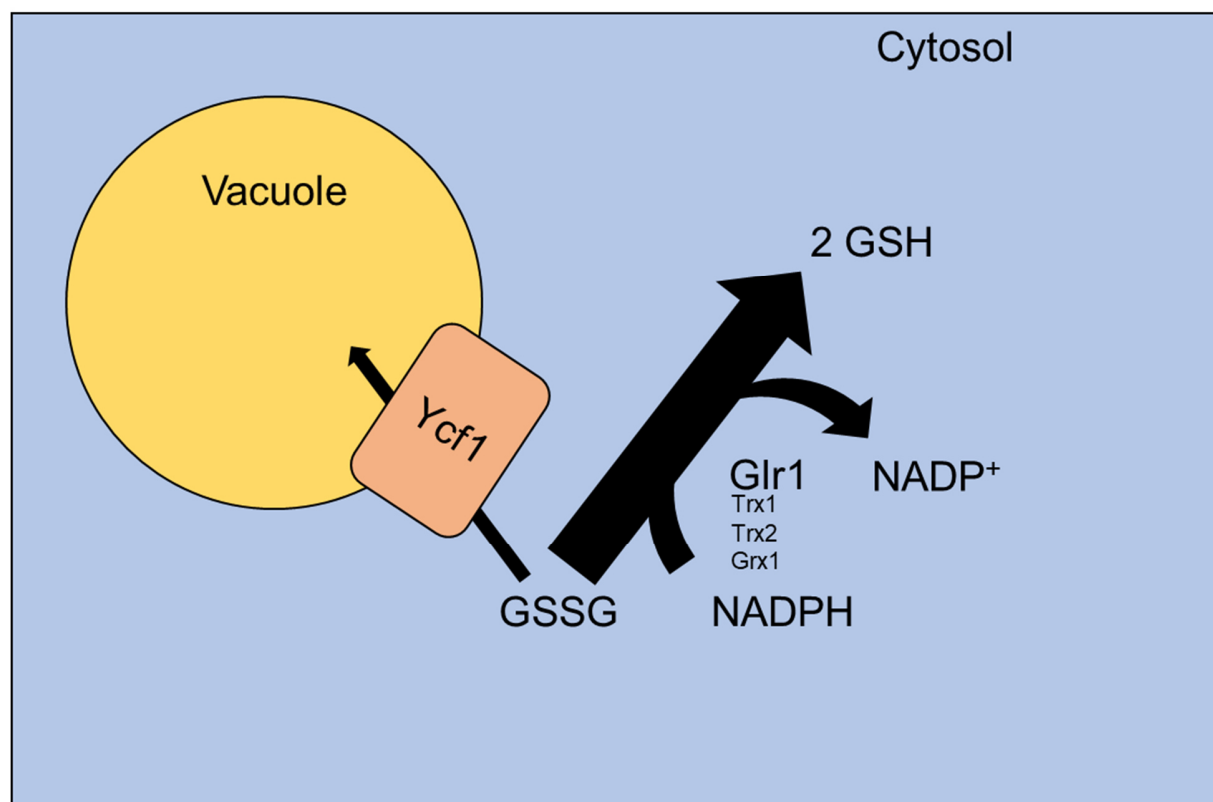


Figure 7 GSSG export from the cytosol. The formation of glutathione disulfide in the cytosol leads to both, the storage of GSSG into the vacuole via Ycf1 and the cytosolic reduction by glutathione reductase 1 (Glr1) or enzymes like Trx1, Trx2 and Grx1. Both mechanisms exist in parallel and thus compete with each other. When Glr1 is missing, large amounts of GSSG are transferred and stored in the vacuole. Thus, a robustly reduced cytosol is maintained. Modified figure from Morgan et. al., 2013.

In 2013, Morgan and colleagues identified a mechanism, in which GSSG is exported from the cytosol via the vacuolar ABC-C-transporter yeast cadmium factor 1 (Ycf1). Thereby, they impressively demonstrated that although Glr1 was missing in the cytosol, the cytosolic glutathione pool stayed robustly reduced even when GSSG was formed during the application of exogenous H_2O_2 . However, GSSG found in cell lysates of $\Delta glr1$ cells was massively increased compared to wild-type cells. When *YCF1* was overexpressed in the $\Delta glr1$ background, total [GSSG] further increased. This suggests, that GSSG formed in the cytosol is rapidly exported and stored in the vacuole. Vice versa, blocks Ycf1 depletion the import of GSSG to the vacuole and thus, GSSG remains in the cytosol. Hence, one might expect that in a $\Delta glr1 \Delta ycf1$ strain, in which Glr1 dependent reduction of GSSG is missing, GSSG accumulates in the cytosol. Surprisingly, when *YCF1* was deleted in a $\Delta glr1$ strain, there was almost no GSSG detectable in whole cell lysates (Morgan et al., 2013). This must mean that in the absence of Glr1, cytosolic GSSG reducing backup systems exist e.g., the before-mentioned thioredoxin system. Beside the thioredoxin

system, it was suggested that glutaredoxin 2 (Grx2) is involved in a yet unidentified pathway to reduce GSSG in absence of Glr1 (Morgan et al., 2013). Such a mechanism seems to be plausible, since also glutaredoxin 1 (Grx1) in the well-established biosensor Grx1-roGFP2 is sensitively oxidized by low amounts of GSSG in a nanomolar range, and can transfer the disulfides to roGFP2 (Gutscher et al., 2008).

However, the observations made by Morgan and colleagues imply that the cytosolic glutathione pool is robustly reduced even during oxidative stress, by an interplay between mainly Glr1 mediated reduction and export of GSSG via Ycf1 (Figure 7). Thus, there is almost no GSSG present in the cytosol. This implies that GSSG measured in whole cell lysates cannot have a cytosolic origin. Further, causes *YCF1* overexpression the enhanced export of GSSG from the cytosol, which increases GSSG concentrations in whole cell lysates. On the contrary, *YCF1* deletion decreases GSSG content in cell lysates. *Thus, changes in whole cell GSSG upon the expression manipulation of a putative glutathione transporter can give an indirect indication of GSSG transport between the cytosol and a specific compartment.*

1.7 The vacuolar ABC-C-transporter Ycf1

Unlike mammals, yeast has a vacuole. Due to a low pH, complex targeting of vacuolar proteins to the lumen and strong proteolytic activity in the vacuole, we lack efficient glutathione biosensors to study vacuolar glutathione redox homeostasis (Chiang, 1995; Hecht et al., 2014; Horst et al., 1999; Li and Kane, 2009). Thus, information gained about vacuolar glutathione relies mostly on either isolated vacuoles, or measurements of total [GSH] and [GSSG] in whole cell lysates (Li et al., 1996). For example, when *YCF1* is deleted, GSSG determined in whole cell lysates is decreased (Morgan et al., 2013).

Ycf1 is a member of the ABC-C-transporter family, which transports substrates by the consumption of ATP (Gueldry et al., 2003; Paumi et al., 2009; Rees et al., 2009). While Ycf1 has a strong affinity to GSSG with a K_m of 290 μM , it was also demonstrated that reduced GSH can be a substrate of Ycf1 (Lazard et al., 2011). However, the K_m value for GSH is about 15 mM what demonstrates the preferred transport of GSSG over GSH (Rebbeor et al., 1998). Although the efficient export of GSSG from the cytosol seems to be important to maintain a high cytosolic GSH:GSSG ratio, it is little known what happens with GSSG after it is stored in the vacuole. Moreover, after treatment with hydrogen peroxide, GSSG stayed stable in the vacuole for at least 60 min (Morgan et al., 2013). Whereas up to date no GSSG exporter in the vacuolar membrane

is identified, one possibility might be the GSSG degradation by γ -glutamyltranspeptidase in the vacuolar lumen as described before in chapter 1.5 (Jaspers and Penninckx, 1984; Mehdi et al., 2001).

Beside the storage of cytosolic derived glutathione disulfide, other glutathione conjugates/derivatives get transported to the vacuole (Penninckx, 2002). Interestingly, Ycf1 was first described as a vacuolar importer of Cd^{2+} -glutathione conjugates ($K_m \sim 39 \mu\text{M}$) (Li et al., 1997, 1996). The importance of Ycf1 as a glutathione transporter was further demonstrated by the finding of other glutathione conjugated substrates e.g., arsenite (Ghosh et al., 1999), Pb^{2+} (Sousa et al., 2015) and Hg^{2+} (Guedry et al., 2003).

Since Ycf1 was extensively studied, a lot of different regulatory mechanisms and potential regulatory target sites are known. *YCF1* has a *YAP1* binding site in its promoter region and thus is stronger expressed under oxidative stress conditions (Wemmie et al., 1994). Additionally numerous different post translational target sites are known for e.g., Ser^{908} and Thr^{911} which activate Ycf1 upon phosphorylation (Eraso et al., 2004). Phosphorylation of Ser^{251} negatively regulates Ycf1 activity (Paumi et al., 2008; Pickin et al., 2010). While the finding of the specific phosphorylation sites was mostly by transport studies with mutated Ycf1, Khandelwal and colleagues presented more recently, in a up to date non-peer reviewed study, two cryo-EM structures of Ycf1 at 3.4Å and 4Å. Thereby, they identified a so far not shown regulatory domain (R-domain) with the before described phosphorylation sites Ser^{908} , Thr^{911} and Ser^{914} . It is furthermore suggested that the R-domain electrostatically and hydrophobically interacts with the nucleotide-binding-domain1 (NBD1) upon phosphorylation. Consequently Ycf1 needs R-domain phosphorylation for maximal ATPase activity (Khandelwal et al., 2021). Beside phosphorylation, the redox modification of Cys^{436} by protein S-glutathionylation negatively regulates Ycf1 (Wei et al., 2014).

Except Ycf1, other transporters are present, which modulate vacuolar glutathione. The ABC-C-transporter Bpt1 can import Cd^{2+} -GS conjugates or GSH although it has a low K_m of 3 mM for latter (Klein et al., 2002; Petrovic et al., 2000). While it was shown, that another ABC-C-transporter Vmr1 can transport glutathione conjugates, it is also speculated that the dual localized proteins Gex1 and Gex2 transport glutathione as proton coupled antiporters (Dhaoui et al., 2011; Wawrzycka et al., 2010).

1.8 Glutathione in the ER

In yeast, glutathione is compartmentalized within different cellular organelles. While cellular sub-compartments like the mitochondrial matrix or peroxisomes have glutathione redox potentials comparable to the cytosol, the glutathione pool in the ER lumen is thought to be much more oxidized (Deponate, 2017; Morgan et al., 2013; Ponsero et al., 2017).

The following section provides an overview about, i. the main oxidizing machinery in the ER, ii. the potential roles glutathione has in the ER and iii. glutathione transport between the ER and the cytosol.

1.8.1 Oxidative protein folding

The endoplasmic reticulum is part of the secretory pathway (Preuss et al., 1991). All proteins, which are either secreted or embedded into the plasma membrane, the vacuolar or Golgi membrane are translocated to the ER before targeted to their final destination (Delic et al., 2013). Protein translocation into the ER can occur either co-translationally or post-translationally.

During co-translational integration, an N-terminal precursor signal peptide of the nascent protein chain is recognized by the signal recognition particle (SRP), which slows down translation and tethers the ribosome to the signal recognition particle receptors (SRPR) in the ER membrane. When the ribosome binds to the ER surface it translates the nascent protein chain through the Sec61 channel directly into the ER lumen (Potter et al., 2001; Potter and Nicchitta, 2002).

Proteins which are post-translational integrated into the ER are fully translated in the cytosol. The heat shock proteins Hsp40 and Hsp70 bind to the hydrophobic motifs of the unfolded polypeptide. Post-translational integrated precursor proteins, as well as co-translational integrated peptides, are translocated into the ER via the Sec61 translocon (Ngosuwan et al., 2003; Zimmermann et al., 2011).

In the ER lumen, protein precursors get processed e.g., by the degradation of the signal peptide, glycosylated, and oxidatively folded, before their transport to the Golgi apparatus via vesicles (Austriaco, O. P., 2012). Efficient protein folding (especially in membrane bound proteins) requires the formation of intramolecular disulfides. Therefore, the reduced cysteine residues of the unfolded protein must be oxidized (Hidaka and Shimamoto, 2013; Qin et al., 2015; Wiedemann et al., 2020). In *S. cerevisiae* oxidative protein folding is mediated by a well-studied redox relay system in which

reductive equivalents are transferred from peptides to molecular oxygen via protein disulfide isomerase 1 (Pdi1) and ER oxidoreductase 1 (Ero1) (Chakravarthi et al., 2006; Hogg, 2013; Parakh and Atkin, 2015).

Ero1 contains two cysteine pairs, which are required for Pdi1 oxidation (Figure 8). Thereby, the inner site active cysteines (C³⁵² and C³⁵⁵) of Ero1 form a disulfide upon oxidation by its FAD-cofactor, which transfers electrons to molecular oxygen (Gross et al., 2006; Kim et al., 2018; Tu et al., 2000). The reduction of molecular oxygen ultimately leads to the formation of hydrogen peroxide in the ER (Roscoe and Sevier, 2020). Oxidized cysteines in the active center of Ero1 transfer the disulfide to the outer active cysteines C¹⁰⁰ and C¹⁰⁵, which further oxidize Pdi1 (Wang et al., 2009).

Pdi1 consists of four TRX-like domains. While two domains are redox active (a, a'), the two other domains possess no redox activity (b, b'). The four TRX-like domains in Pdi1 are orientated in an abb'a' manner. The Pdi1 motives b' and a' are connected via a linker loop (x-linker) and it has a carboxyl terminal c tail (Figure 8). The redox active a and a' domains have a typical CXXC TRX active site (cys-gly-his-cys) while b and b' forms a hydrophobic binding pocket for substrate binding. Intriguingly, the binding of Ero1 to Pdi1 in yeast is weaker compared to their homologous in humans and oxidation of the yeast Pdi1 a domain is faster than a' (Masui et al., 2011; Vitu et al., 2010; Zhang et al., 2014).

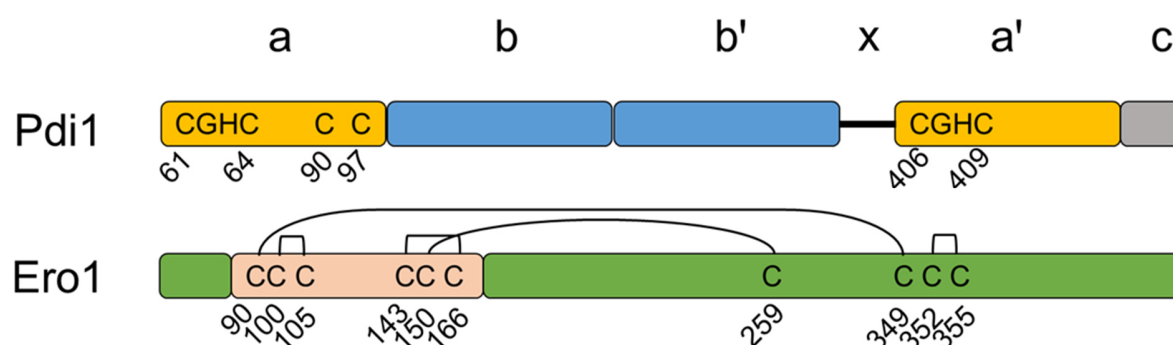


Figure 8 Protein structure of *S. cerevisiae* protein disulfide isomerase 1 (Pdi1) and ER oxidoreductase 1 (Ero1). Pdi1 consists out of the 4 TRX like domains abb'a', a linker domain x between b' and a' and a carboxylic tail c. The domains a and a' are catalytical active and have both the typical CXXC active site TRX motive (C⁶¹-C⁶⁴ and C⁴⁰⁶-C⁴⁰⁹). Domain a has a second cysteine pair which is thought to be important for Ero1 regulation (C⁶¹-C⁶⁴). The domains b and b' form a hydrophobic substrate binding pocket. Ero1 has two active inner site cysteines (C³⁵² and C³⁵⁵) and two active outer site cysteines (C¹⁰⁰ and C¹⁰⁵), which transfer oxidative equivalents to Pdi1 by the reduction of molecular oxygen via a FAD cofactor. Beside the active site cysteines three regulatory cysteine pairs are present, which inhibit Ero1 function upon disulfide bond formation (C⁹⁰-C³⁴⁹, C¹⁴³-C¹⁶⁶, C¹⁵⁰-C²⁹⁵). Modified figure from Nui et al., 2016.

To prevent the endoplasmic reticulum from over-oxidation, the Ero1-Pdi1 redox relay is feedback regulated. Yeast Ero1 has three cysteine pairs (C⁹⁰-C³⁴⁹, C¹⁴³-C¹⁶⁶, C¹⁵⁰-C²⁹⁵) beside its active site cysteines, which regulate its activity. Especially the cysteines C¹⁵⁰ and C²⁹⁵ are crucial to modulate Ero1 activity (Sevier et al., 2007). The formation of disulfides between the regulatory cysteines connect the outer active loop of Ero1 to the inner helical core, which impairs the oxidation of Pdi1 (Baker et al., 2008; Vitu et al., 2010). Consequently, the oxidation of Ero1 regulatory cysteines switches Ero1 into a low active state. Vice versa, reduction of regulatory cysteines lead to activation of Ero1 (Zhang et al., 2014). Ero1 regulatory cysteine reduction is mediated by reduced Pdi1. Please note that yeast Pdi1 has another non-catalytically active cysteine pair (C⁹⁰-C⁹⁷) in its active site, which forms a disulfide under steady state conditions. Reduction of this third cysteine pair is required for Ero1 reduction through the reduced Pdi1 active site cysteines (Byrne et al., 2009; Niu et al., 2016; Pirneskoski et al., 2004). Interestingly, *in vitro* experiments suggested that the reduction of the relatively stable C⁹⁰-C⁹⁷ disulfide only occurs in the presence of the reductant dithiothreitol (DTT) or when the glutathione redox potential is quite low. Consequentially, Ero1 is mostly in its low active state (Niu et al., 2016; Sevier et al., 2007; Wilkinson et al., 2005).

1.8.2 Role of glutathione in the ER

First insights in ER glutathione were given 1992 by the group of Harvey Lodish. For analysis they expressed a N-acetyl-Asn-Tyr-Thr-Cys-NH₂ peptide in yeast, which freely diffuses through membranes and gets trapped in the ER upon glycosylation. The peptide equilibrates with the glutathione redox-couple via a thiol disulfide exchange mechanism and hence a ER GSH:GSSG ratio of 3:1 was determined (Hwang et al., 1992). Further the measurement with ER targeted E_{GSH} sensors suggested a glutathione redox potential of approximately -208 mV to -230 mV (Appenzeller-Herzog, 2011; Avezov et al., 2013; Bass et al., 2004; Delaunay-Moisan et al., 2017; Delic et al., 2010; van Lith et al., 2011).

In the study from 1992, Hwang et al. considered, that GSSG might be the major oxidant required for disulfide bond formation in the ER (Figure 9) (Hwang et al., 1992). However, the findings of Hwang and colleagues, were made six years before Ero1 was identified. We now know, that the Ero1-Pdi1 redox relay is required for oxidative protein folding in the ER (Frandsen and Kaiser, 1998; Pollard et al., 1998). For example: *in vitro* studies revealed that Ero1 was able to force the oxidation of RNase1 when Pdi1 was present, regardless if GSSG was in the buffer or not (Tu et al., 2000). Nevertheless, these findings do not exclude that GSSG act as a backup system, which can provide oxidative equivalents to Pdi1 if necessary, as recently demonstrated for human PDI, which can reduce GSSG *in vitro* (Neves et al., 2017).

However, if the particular role of glutathione in the ER is to function as backup system for oxidative protein folding, where would GSSG be formed in the first place? Although Hwang et al. suggested that GSSG might be imported into the ER lumen from the cytosol, we now know that almost no cytosolic GSSG is present. Moreover it was proposed, that GSH and not GSSG diffuses into the ER from the cytosol, which will be explained in the following chapter in detail (Ponsero et al., 2017). Nevertheless, this indicates that glutathione in the ER must be primarily a reductant and not an oxidant.

An obvious idea how GSSG is formed in the ER is the direct oxidation of GSH via Ero1. Indeed, already early studies on Ero1 mentioned a link between GSSG formation and Ero1 activity. In 1999, Cuzzo and Kaiser demonstrated that GSSG re-generation after DTT treatment in an *ero1-1* mutant strain was slower compared to wild-type cells. Vice versa caused the overexpression of *ERO1* higher GSSG formation (Cuzzo and Kaiser, 1999). However, later *in vitro* studies suggested that GSH was a poor substrate of Ero1 (Tu and Weissman, 2002).

Thus, oxidation of ER GSH seems rather to be indirect and not directly mediated by Ero1. One explanation to this might be that H₂O₂ produced by active Ero1 gets reduced by GSH (Chakravarthi et al., 2006). Another model suggested that GSH has a role in reducing non-native disulfide bonds of nascent protein chains (Chakravarthi and Bulleid, 2004). Intriguingly, depletion of cellular GSH increases the formation of non-native intramolecular disulfides (Chakravarthi and Bulleid, 2004).

However, although proteins were able to slowly fold in a glutathione containing buffer, the addition of Pdi1 increased the folding rate noticeably (Weissman and Kimt, 1993). Thus, it remains unclear to what extent GSH reduces non-native disulfide bonds directly under physiological conditions. It is now believed, that GSH has rather an indirect effect on non-native cysteine disulfides through the reduction of ER oxidoreductases e.g., Pdi1 (Chakravarthi et al., 2006; Ponsero et al., 2017). This theory is supported by recently made *in vitro* experiments, which demonstrated that the reduction of Pdi1 and thus indirect activation of Ero1 is dependent on the GSH:GSSG ratio in the buffer solution as mentioned above (Niu et al., 2016).

While it was thought that GSH alone delivers the main reductive power necessary to maintain Pdi1 isomerase activity in the ER, and thus ensures correct protein folding, this model was challenged by a study published in 2014 (Bertoli et al., 2004; Cuzzo and Kaiser, 1999; Ponsero et al., 2017; Trotter and Grant, 2002; Tsunoda et al., 2014). Thereby, Tsunoda et al., targeted the GSH-degrading enzyme ChaC1 to the ER lumen of cultured mammalian cells. Interestingly neither oxidative protein folding, nor the reduction required degradation of alpha-1-antitrypsin was impaired when GSH was depleted from the ER (Tsunoda et al., 2014). Please note, one product

of ChaC1 mediated GSH degradation is cysteinyl-glycine, which might be sufficient to provide reduced PDI (Crawford et al., 2015; Tsunoda et al., 2014). However, Tsunoda and colleagues concluded from their experiments, that GSH cannot be the exclusive electron donor in the ER (Tsunoda et al., 2014).

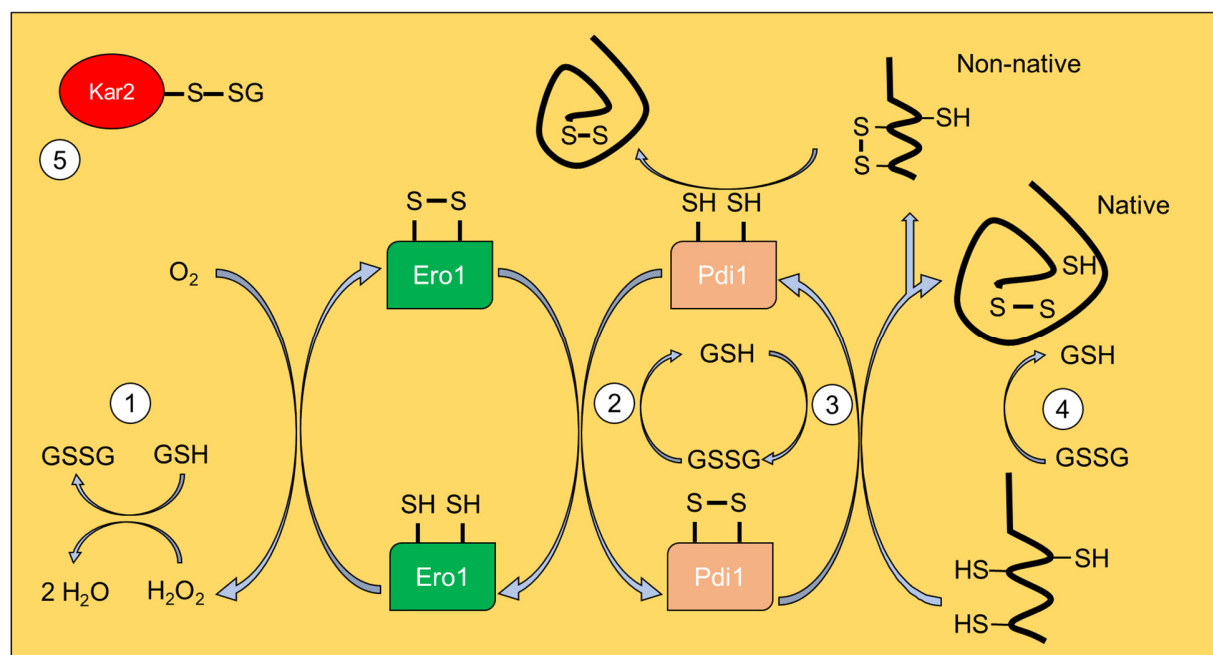


Figure 9 Multiple roles of glutathione in the ER. Glutathione is thought to fulfill multiple roles in the ER. One role is the detoxification of ROS, derived during oxidation of Ero1 (1). It was also suggested that GSSG can oxidize Pdi1 (2). Furthermore, GSH is reported to provide reductive equivalents to Pdi1 to maintain isomerase activity (3). Additionally, it was speculated whether GSSG can oxidize cysteines from nascent protein chains to enable disulfide bond formation and thus protein folding (4). Lastly it was shown that glutathione can modify cysteine residues of different proteins e.g., Kar2 to modulate their molecular function (5).

It was demonstrated in human cells that under nitrosative stress conditions PDI gets S-glutathionylated inhibiting thereby its isomerase and chaperone activity (Townsend et al., 2009; Xiong et al., 2012). Beside PDI many other ER localized proteins are target of protein-S-glutathionylation. For example, the yeast ER localized HSP70 chaperone Kar2 is glutathionylated upon increasing H₂O₂ formation during high Ero1 activity and changes in the ER GSH:GSSG ratio (Wang et al., 2014). Thereby the holdase function of Kar2 is increased, which causes a stronger binding to exposed hydrophobic domains of an unfolded protein and blocks the Sec61 translocon (Wang et al., 2014; Wang and Sevier, 2016). Thus, it was suggested that Kar2 glutathionylation upon H₂O₂ formation by Ero1 and changes in ER GSH:GSSG ratio, functions as a mechanism to

sense the oxidative load of the ER and hence, i. block the import of new nascent protein chains and ii. provide accumulation of unfolded proteins in the lumen (Wang et al., 2014; Wang and Sevier, 2016).

Although it is not clear, whether GSH is the unique ER electron donor to provide reductive equivalents to the ER, changes in the GSH:GSSG ratio clearly affect oxidative protein folding. Thus, the glutathione pool in the ER has to be precisely controlled. One proposed mechanism to maintain the ER glutathione pool, is the controlled import of GSH from the cytosol into the ER.

1.8.3 ER glutathione transport

GSH is negatively charged under physiological pH and can thus not diffuse freely across cellular membranes. Hence transporter must exist, which mediate the transport of glutathione between the cytosol and other cellular compartments (Oestreicher and Morgan, 2018; Zimmermann et al., 2021).

Glutathione import into the ER was already addressed in the early study of Hwang and colleagues 1992. Therefore, they purified microsomes from rat liver and measured the import of radioactive labeled GSH and GSSG *in vitro* (Hwang et al., 1992). While Hwang et al. suggested that only GSSG but not GSH is taken up into microsomes, this was questioned by Bánhegyi et al., who demonstrated that only GSH was transported into purified microsomes from mammalian liver and the sarcoplasmic reticulum of muscle cells (Bánhegyi et al., 1999; Hwang et al., 1992).

Recently, two groups determined ER glutathione concentrations by using a combination of ER targeted E_{GSH} sensor together with a reporter for GSH:GSSG ratio. Both reported an ER GSH:GSSG ratio of approximately 7:1, which correlates with the findings of Hwang in 1992. Also, the total glutathione concentrations of approximately 30 mM and 15 mM are in line with each other. However, their model starts to divide from each other with measured cytosolic glutathione concentrations. While Montero et al. measured ~7 mM cytosolic glutathione, and thus suggested that glutathione must be actively transported into the ER against the chemical concentration gradient, Ponsero et al. measured equally high glutathione concentrations in the cytosol and ER, and thus mentioned that an active transport of glutathione into the ER is not necessary (Montero et al., 2013; Ponsero et al., 2017).

Ponsero and colleagues demonstrated that glutathione diffuses from the cytosol into the endoplasmic reticulum. Therefore, they overexpressed the plasma membrane localized GSH transporter *OPT1* in yeast cells. *OPT1* overexpression causes an import of GSH from the growth media into the cytosol, which leads to the enormous accumulation of total [GSx] in whole cell

lysates (~30 – 40 mM) (Kumar et al., 2011; Ponsero et al., 2017; Zimmermann et al., 2021). Thereby, they assumed that high cytosolic [GSH] upon *OPT1* overexpression, increases the GSH diffusion gradient between the cytosol and the ER. Indeed, the ER total glutathione concentration increased when *OPT1* was overexpressed, but in parallel the glutathione redox-potential in the ER became more oxidized (Ponsero et al., 2017). Thus, imported GSH was oxidized to GSSG. Further they demonstrated that the diffusion of GSH into the ER is facilitated by the channel forming translocon Sec61. Additionally, glutathione diffusion through Sec61 is negatively controlled (Figure 10).

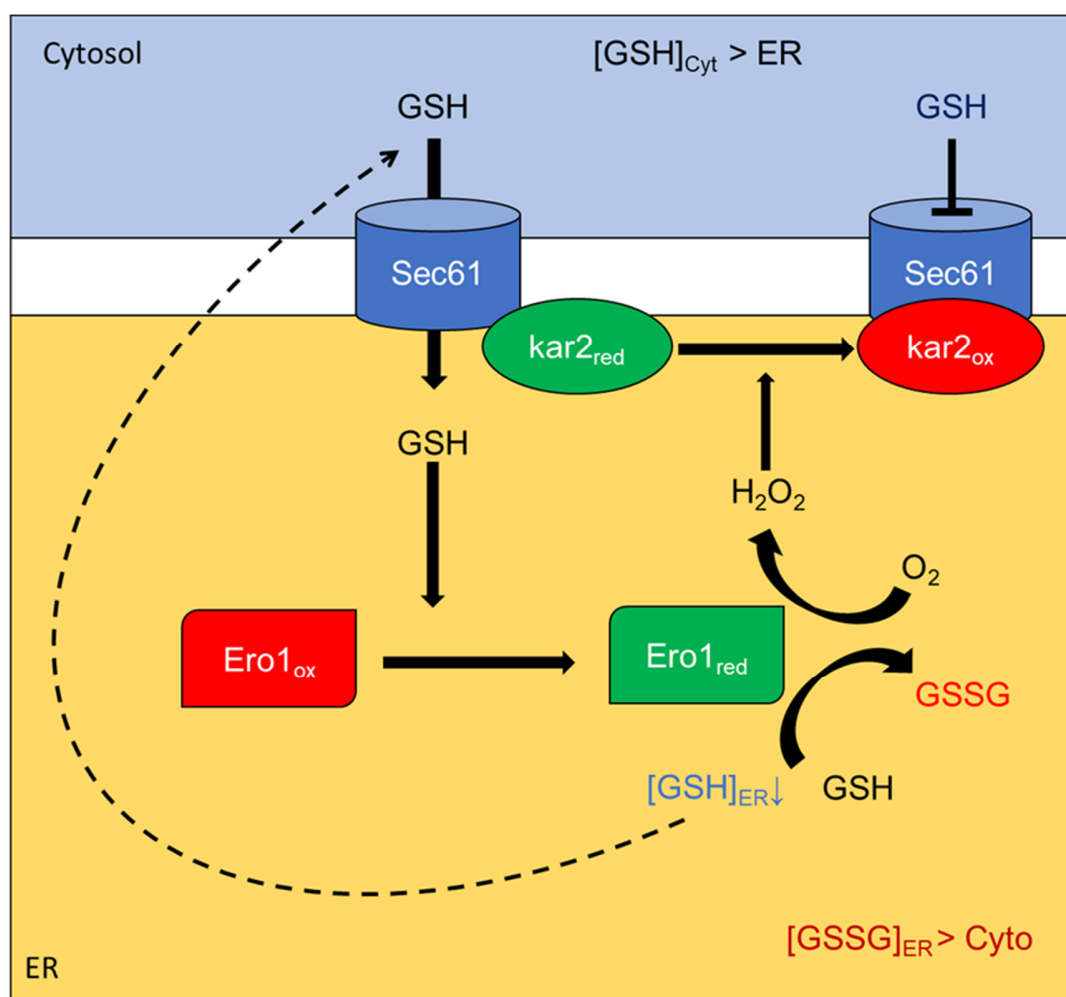


Figure 10 Model of ER glutathione uptake in yeast. GSH can enter the ER via facilitated diffusion from the cytosol through Sec61. Thereby GSH promotes indirectly the reduction of Ero1 regulatory disulfides, which leads to its activation. When Ero1 is highly active hydrogen peroxide is formed by the reduction of molecular oxygen. Additionally GSSG is formed by oxidation of GSH. H₂O₂ formation leads to the oxidation of Sec61 associated chaperon Kar2, which plugs the Sec61 channel. This mechanism prevents further influx of GSH. Thereby the activity of Ero1 can be downregulated to prevent the ER from oxidative poise. Modified figure from Ponsero et al., 2017.

The influx of reduced glutathione into the ER leads indirectly to the reduction and subsequent activation of Ero1. Active Ero1 produces hydrogen peroxide, which forms a sulfenic acid at a cysteine residue of Kar2, which is associated to the Sec complex (Ponsero et al., 2017). As mentioned above, sulfenic-acid formation leads to glutathionylation of Kar2 (Wang and Sevier, 2016). However, oxidized Kar2 clogs the Sec61 channel, and thereby inhibits further GSH influx what allows the re-oxidation of Ero1 regulatory cysteines to prevent non-native disulfide bond formation through hyperactive Ero1 (Ponsero et al., 2017).

Vice versa, promotes the accumulation of unfolded proteins, often referred to as ER-stress, the expression of *ERO1* and the formation of newly synthesized GSH, what indirectly increases ER [GSx]. Both, more Ero1 and its indirect activation through GSH influx might increase the ER folding capacity during ER stress (Ponsero et al., 2017; Wu et al., 2014).

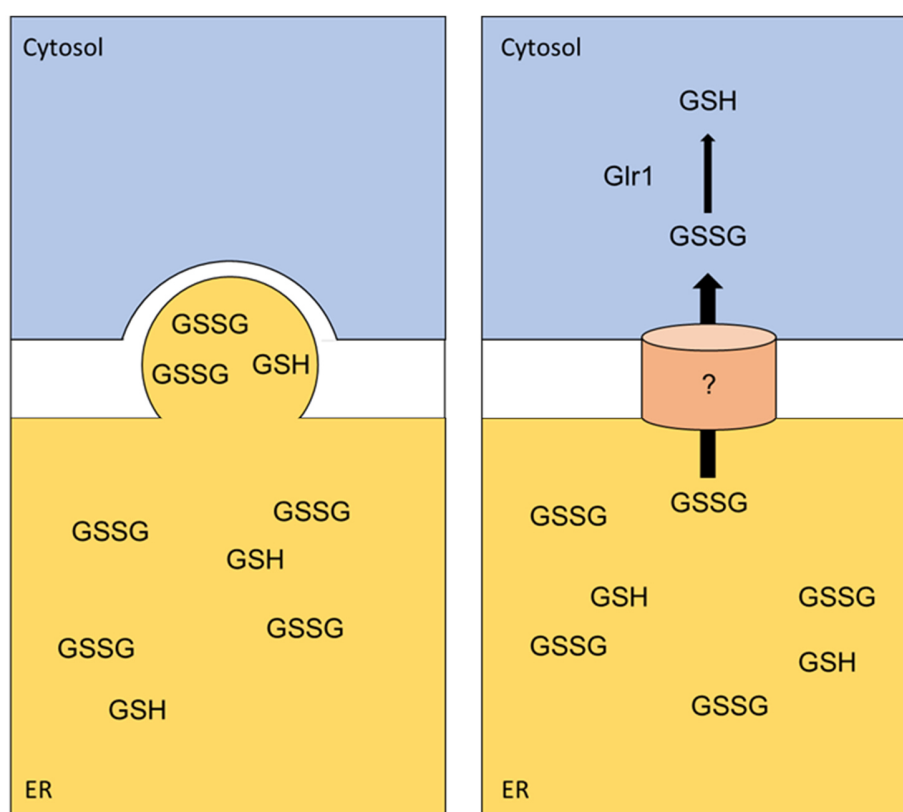


Figure 11 Model of glutathione export from the ER. GSSG is formed in the ER. Different models exist of how GSSG is depleted from the lumen. Left panel: GSSG is packed into vesicles and transferred to the Golgi apparatus and/or the vacuole. Right panel: A so far unidentified GSSG exporter in the ER membrane exports GSSG from the lumen to the cytosol where glutathione reductase 1 (Glr1) reduce it back to GSH.

Under ER-stress conditions the unfolded protein response (UPR) pathway is activated, stimulating the expression of several genes to increase the ER protein folding capacity e.g., by expression of *ERO1*, *KAR2* or *PDI1* (Chawla et al., 2011; Travers et al., 2000). In yeast UPR is mediated via the stress sensing membrane protein Ire1. ER-stress causes Ire1 autophosphorylation and oligomerization, which activates its endo-RNase activity at the cytosolic site (Lee et al., 2008; Shamu and Walter, 1996). Activated Ire1 splices the intron of inactive *HAC1* mRNA and thus allows the translation of the Hac1 transcription factor (Cox and Walter, 1996; Kawahara et al., 1998; Travers et al., 2000).

GSH mediated activation of Ero1, most likely indirectly by the direct reduction of Pdi1, leads to the formation of GSSG, which is reflected by low ER E_{GSH} and GSH:GSSG ratios. To maintain a stable glutathione redox homeostasis in the ER, GSSG must be either reduced to GSH or get removed from the lumen. Unlike the mitochondrial matrix, the ER lumen does not possess glutathione reductases or comparable reductive systems (Toledano et al., 2007). For GSSG export, two different non-exclusive mechanisms were supposed: i. Either GSSG is transported through the secretory pathway via vesicles towards the vacuole or ii. a transporter mediated direct export of GSSG from the lumen to the cytosol (Figure 11) (Appenzeller-Herzog, 2011; Oestreicher and Morgan, 2018).

1.9 Glutathione in the Golgi apparatus

Newly synthesized proteins in the ER which are secreted, are transported via vesicles to the Golgi apparatus, where they get further processed (Papanikou and Glick, 2009). Although the Golgi apparatus was extensively studied in terms of compartmental organization and protein processing, very little is known about its glutathione homeostasis (Suda and Nakano, 2012).

Interestingly, yeast has the two enzymatically active glutaredoxins Grx6 and Grx7 present in the Golgi apparatus. This further indicates the existence of a Golgi glutathione pool. Although ER/Golgi dual localized Grx6 is thought to play a role in the binding of iron-sulfur clusters it has a oxido-reductase activity (Mesecke et al., 2008b). Grx7 localizes exclusively to the Golgi and has a sensitive oxido-reductase activity, which was recently demonstrated *in vitro* and *in vivo* (Liedgens et al., 2020; Mesecke et al., 2008a; Zimmermann et al., 2020). In 2010, Braun et al. suggested that Golgi function is linked to cytosolic glutathione redox homeostasis. They showed that cells lacking Gef1, a transporter normally involved in proton coupled chloride transport across the Golgi membrane, had a decreased ability to maintain cytosolic reduced E_{GSH} , after H_2O_2

treatment. Interestingly this phenotype was mainly dependent on the proton antiporter function of Gef1. Thus, it was speculated that the proton gradient across the Golgi-membrane is important for cytosolic glutathione homeostasis (Braun et al., 2010).

Another hint for the importance of glutathione in the context of Golgi apparatus was recently given by Li et al., in 2019: The human papillomavirus (HPV) is a small DNA virus. HPV needs to integrate its viral DNA (vDNA) into the nucleus via retrograde vesicle trafficking from the plasma membrane to the trans-Golgi network (Braaten and Laufer, 2008; Day et al., 2013). Interestingly, depletion of cellular glutathione leads to decreased integration of vDNA towards the Golgi. This suggests that glutathione might play an important role for retrograde trafficking from endosomes to the trans-Golgi network during virus infection in mammals (Li et al., 2019).

Measurements of the glutathione redox potential in the Golgi apparatus is extremely difficult due to its high morphological dynamics (Presley et al., 1998). However, cellular microdomains within a specific cell compartment move into focus of redox biology (Ahmad et al., 2020). For that reason, Hatori et al. anchored a Grx1-roGFP2 sensor N-terminally to different cellular membranes in human HeLa cells. When Grx1-roGFP2 was fused to the cytosolic part of giantin, a Golgi membrane resident protein, the GSH:GSSG ratio close to the Golgi was lower compared to overall cytosolic GSH:GSSG. To determine E_{GSH} on the luminal site Grx1-roGFP2 was N-terminally fused to galactosyltransferase 1 (GALT1). Intriguingly, the sensor was almost fully oxidized when targeted to the Golgi lumen, which suggests a very oxidized glutathione pool (Hatori et al., 2020; Koreishi et al., 2013). However, if the reported oxidized glutathione pool in the Golgi of HeLa cells correlates with the Golgi in yeast remains to be shown.

So far it is not known how glutathione enters the Golgi network. Thereby different models are conceivable. To the best of my knowledge, there is no glutathione transporter identified in the Golgi to mediate GSH or GSSG import and/or export. Alternatively, glutathione might be shuttled via vesicles retrograde from the vacuole or anterograde from the ER to the Golgi.

1.10 The oligopeptide transporter (OPT) family in *S. cerevisiae*

Glutathione belongs to the large group of oligopeptides. Oligopeptides are normally defined as small peptides with a molecular mass smaller than 1 kDa, which in average, refers to less than 10 amino acids (Becerra-Rodríguez et al., 2020). The transport of oligopeptides across membranes requires energy. But, unlike Ycf1, members of the oligopeptide transporter family are not

ATP-dependent. Oligopeptide transporters are rather secondary active transporters and thus mostly energized via a proton-coupled symport mechanism (Osawa et al., 2006). Interestingly, members of the oligopeptide transporter family are not just found in yeast but also in other eukaryotes such as the plant *Arabidopsis Thaliana* (*A. Thaliana*) with its glutathione transporters *AtOPT4* and *AtOPT6* (Cagnac et al., 2004; Koh et al., 2002; Pike et al., 2009).

The best studied member of the oligopeptide transporter family in *S. cerevisiae* is Opt1/Hgt1 localized in the plasma membrane. Opt1 has a high affinity to GSH ($K_m = 54 \mu\text{M}$) and GSSG ($K_m = 92 \mu\text{M}$) and imports them into the cytosol (Bourbouloux et al., 2000; Osawa et al., 2006). While deletion of *OPT1* is not lethal under physiological conditions, it becomes essential in cells lacking Gsh1 for glutathione synthesis. Interestingly cells deleted for *GSH1* had 30% less cellular GSH compared to wild-type, although they grew in growth media supplemented with 100 μM GSH. However, when *OPT1* was overexpressed in the same deletion background, cells accumulated massive amounts of cellular GSH up to 7 times higher compared to wild-type, leading to cell death (Kumar et al., 2011). Combining these findings suggests, that Opt1 activity is predominantly regulated via its expression level. Under endogenous conditions, expression levels of *OPT1* are relatively low. This raises the question of why and how wild-type yeast cells accumulate up to 10 mM cellular GSH? The reason for this remains elusive.

The second member of the oligopeptide transporter family, Opt2, is localized in the peroxisomal membrane. Although it was so far not experimentally demonstrated that Opt2 actively transports glutathione, it has a relatively high sequence homology to Opt1. However, Opt2 function seems to be linked to cellular glutathione, since its deletion not only oxidizes the peroxisomal glutathione pool but also lowers the cytosolic capacity to maintain a reduced glutathione pool after H_2O_2 treatment (Elbaz-Alon et al., 2014).

In 2002, Pearson et al., analyzed six so far uncharacterized open reading frames (ORF) in yeast by sequence homology analysis. Thereby, the ORF *YGL114W* was described as a putative member of the oligo peptide transporter family (Pearson and Schweizer, 2002). Interestingly, the developed algorithm of Wiles and colleagues did not group *YGL114W* as a member of the OPT family due to missing homologous in other organisms and sequence homology less than 40% compared to Opt1 and Opt2 (Wiles et al., 2006). So far, very little is known about *YGL114W*. Cells, which were deleted for *YGL114W* are viable (Aouida et al., 2009; Pearson and Schweizer, 2002). However, performed genome wide screens searching for genetic interaction partners of *GSH1*, suggested a synthetic lethality between *YGL114W* and *GSH1* (Costanzo et al., 2016, 2010). Recently, Ho et al. bundled the information of 21 independent published quantitative analyses of

the yeast proteome. Thereby, they estimated the copy number of the protein encoded by *YGL114W* (Ygl114w) of approximately ~1160 copies per cell. This is comparable low e.g., the same study reported that cells have three times more molecules of Opt1 (Ho et al., 2018). Also, the localization of Ygl114w remains unclear since different high-throughput screens revealed different localizations for Ygl114w. The protein was localized in the ER when N-terminally tagged with GFP under the expression of the constitutive *NOP1* promoter. However, when expressed under a strong *TEF1* promoter in a split-Venus screen, Ygl114w was detected in the vacuole (Breker et al., 2014, 2013). In the split-Venus screen, the C-terminal part of the fluorescent protein Venus was N-terminally fused to genes of the *S. cerevisiae* genome library, whereas the N-terminal part of Venus was expressed in the cytosol (Breker et al., 2014, 2013). Please note, only when N- and C-terminal parts of Venus are in close proximity a fluorescent signal is detectable (Ohashi and Mizuno, 2014). Thus, independent of its endogenous localization, the N-terminus of Ygl114w must be exposed to the cytosol. However, GFP-tagged Ygl114w under expression of its endogenous promoter was not detectable, since fluorescence intensity was below the threshold of the preformed screen (Breker et al., 2014, 2013).

1.11 Aim of this thesis

Recently, the uncharacterized open reading frame *YGL114W* was described as a putative member of the oligopeptide transporter family (OPT family). The OPT family in *S. cerevisiae* consists out of the two transmembrane transporters Opt1 in the plasma membrane and Opt2 in peroxisomes. While it was shown, that Opt1 transports GSH and GSSG, it was suggested that Opt2 function is also linked to regulation of the cytosolic glutathione homeostasis. So far, our knowledge about *YGL114W* is based on genomic wide screens and high throughput analysis. Thus, the aim of this thesis is to characterize the open reading frame *YGL114W* (hereafter referred to as *OPT3*). Therefore, fundamental questions must be addressed. To get an idea of functions and importance of Opt3, genomic screens will be employed, to identify potential genetic interaction partners. Following the initial broad characterization, subcellular localization of Opt3 will be investigated using novel ultra-bright fluorescent protein tags. Based on these studies, assays will be applied to understand the compartment specific function of Opt3. Given that Opt3 is another member of the oligo peptide transporter family, determination of total glutathione concentrations paired with subcellular E_{GSH} measurements will be used to gain indirect information about a potential glutathione transport activity. Furthermore, the relationship between Opt3 function and important cellular reduction pathways e.g., the thioredoxin system will be analyzed.

2 Results

Glutathione is a highly abundant small thiol present in all eukaryotic cells. It plays a major role in a variety of cellular processes and thus its total depletion is lethal (Grant et al., 1997; Montero et al., 2013). In nearly all eukaryotes, glutathione can either be imported from the extracellular space or synthesized exclusively in the cytosol by the enzymes Gsh1 and Gsh2 except of plants, which have dual localized Gsh1 in the cytosol and in plastids (Galant et al., 2011; Grant, 2001; Hanschmann et al., 2013). Glutathione is found in different cell organelles (Deponete, 2017). Therefore, reduced glutathione (GSH) and the glutathione disulfide (GSSG) are transported between the cytosol and other compartments. However, under physiological pH 7 GSH and GSSG are negatively charged and can thus not cross cellular membranes (Deponete, 2017; Montero et al., 2013; Zimmermann et al., 2021). Therefore cellular glutathione shuttling is mediated by different transporters (Oestreicher and Morgan, 2018). In yeast, one group of glutathione transporters is the oligopeptide transporter (OPT) family with the two members Opt1 and Opt2 (Bourbouloux et al., 2000; Elbaz-Alon et al., 2014). However, there might be a third so far uncharacterized isoform encoded on the open reading frame (ORF) *YGL114W*. The protein encoded by *YGL114W* was described as a putative member of the oligopeptide transporter family by analyzing sequence homology (Pearson and Schweizer, 2002). However, it remains completely uncharacterized and a potential role in glutathione trafficking has thus far not been addressed. Hereinafter, the ORF *YGL114W* will be named *OPT3* throughout this thesis. Therefore, the primary aim in this work was to identify physiological functions of Opt3.

2.1 Opt3 genetically interacts with genes encoding Gsh1 and Gsh2

2.1.1 Synthetic gene array to identify genomic interaction partners of *OPT3*

Almost nothing is known about Opt3. Thereof, to gain first insights a synthetic genetic array (SGA) was performed to screen for genetic interaction partners of *OPT3*. This high throughput analysis is a very powerful tool and delivers a brought overview in which cellular processes the gene of interest might be involved and thus builds a solid base for further studies. In the Material and Methods section explained in detail, a *S. cerevisiae* SGA-starter strain deleted for *OPT3* ($\Delta opt3::nat-NT2$), was mated with the BY4741 yeast deletion library ($\Delta xzy::kanMX4$) and the mRNA Perturbation (DAmP) library ($::kanMX4$) of essential genes, in which mRNA levels of corresponding essential genes are 4- to 10-fold decreased. After mating, the strains were plated

onto sporulation inducing minimal media before being transferred to selective growth plates containing the antibiotic selection markers G418 and nourseothricin (clonNAT) to select for haploid double mutants ($\Delta opt3\Delta x$). In parallel a control strain, harboring *OPT3* with a clonNAT resistance cassette, was mated with the BY4741 yeast deletion library and DAmP library of non-essential genes and selected for haploid single mutants. Afterwards colony size of the resulting double deletion strains was compared to the size of single deletion colonies (Figure 12).

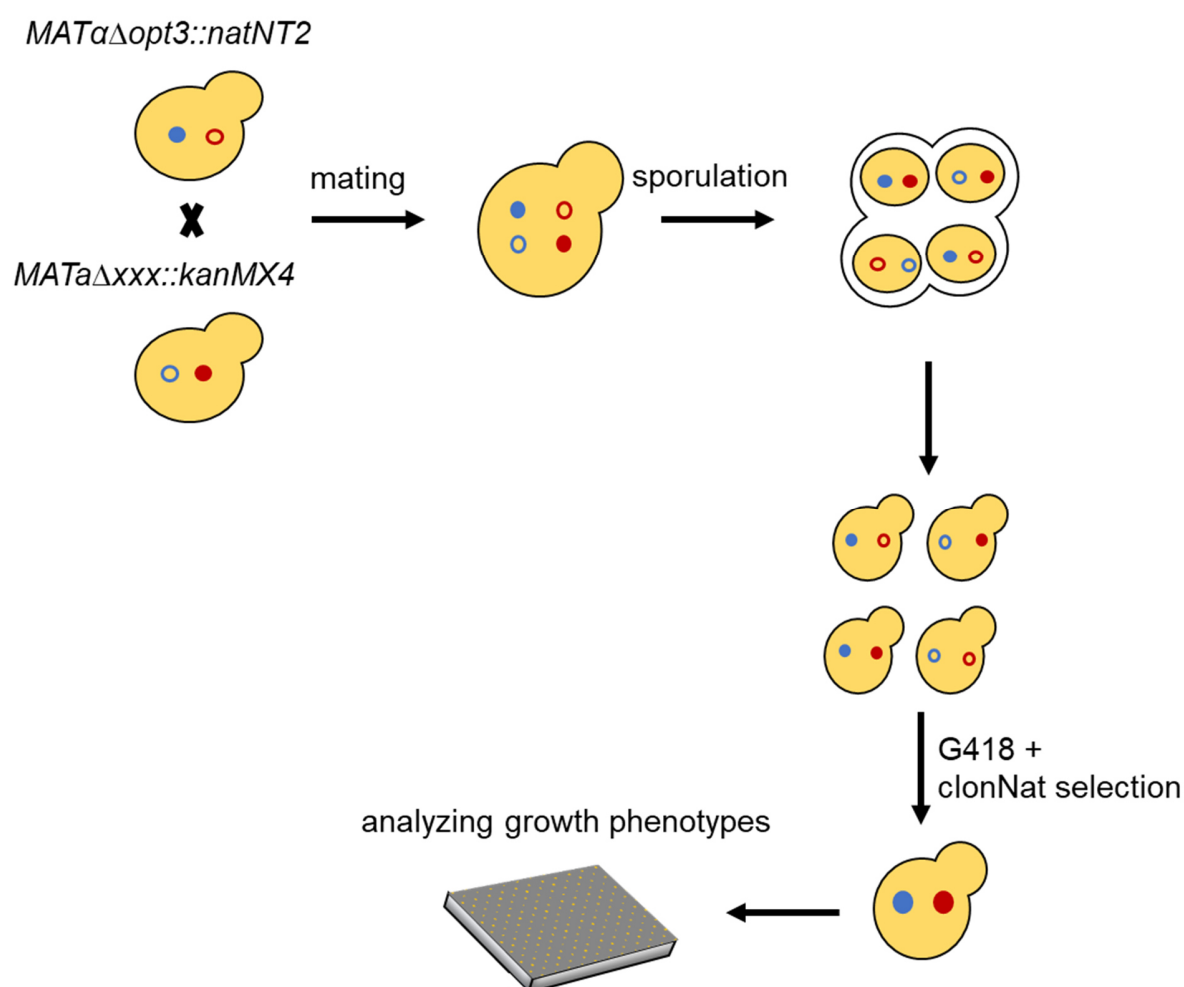


Figure 12 Illustration of the synthetic genetic array. Simplification of an *OPT3* deletion strain, which is mated with the yeast deletion library of non-essential genes and the yeast DAmP library of essential genes to identify genetic interaction partners of *OPT3*. The red arrows indicate colonies which do not grow after the selection for double mutants.

SGA analysis identified 40 different genes, which had synthetic negative interactions in combination with *OPT3* (a summary of total hits is listed in Supplements Table 1). While some hits

were so far uncharacterized open reading frames (*YAL037W*, *YDR526C*, *YIL055C*, *YLR317W*, *YPR170C*) others were genes, which are involved in transcriptional or translational processes (for example: *CRR4*, *FUN12*, *PAF1*, *SRO9* and *CEM9*). However, the screen also identified genes, which were involved in redox-processes like *GND1*, the 6-phosphogluconate dehydrogenase, which is part of the pentose phosphate pathway catalyzing the reduction of nicotinamide adenine dinucleotide phosphate (NADP⁺) to NADPH (He et al., 2007). Another interesting hit was γ -glutamylcysteine synthetase, *GSH1*. Gsh1 catalyzes the first step in the glutathione biosynthesis pathway (Birk et al., 2013a; Suzuki et al., 2011). As previously shown by Kumar et al. the depletion of cellular glutathione is lethal in yeast and thus cells deleted for *GSH1* must have extracellular GSH available to grow (Kumar et al., 2011). In the SGA screen haploid selection was carried out on GSH containing growth plates. Afterwards, the cells were transferred to media without glutathione for double mutant selection. However, $\Delta gsh1$ cells can divide up to 7 times without extracellular GSH in the media (Kumar et al., 2011). Thus, the $\Delta gsh1$ strain in the SGA screen had possibly still enough GSH present from former growth on GSH containing plates and grew when shifted to growth plates without supplemented glutathione. Remarkably, the $\Delta gsh1\Delta opt3$ double mutant showed no growth, which suggested a link between cellular GSH and Opt3 function.

2.1.2 *OPT3* deletion negatively affects cell growth in the absence of glutathione

Glutathione biosynthesis is mediated by two enzymes: γ -glutamylcysteine synthetase (Gsh1) and glutathione synthetase (Gsh2) (Forman et al., 2009; Suzuki et al., 2011). In the performed SGA analysis *GSH1*, which encodes the protein mediating the first step in glutathione biosynthesis led to impaired growth when deleted together with *OPT3*. This observation indicated a relationship between Opt3 and cellular glutathione synthesis. To verify the observation found in the SGA a new $\Delta gsh1\Delta opt3$ mutant was generated via homologous recombination and growth was analyzed by automated measurements of the OD₆₀₀ over 35h. In addition to the $\Delta gsh1\Delta opt3$ double mutant, a wild-type strain (BY4742 WT) plus the single mutant strains $\Delta gsh1$ and $\Delta opt3$ were used as controls. Furthermore, a mutant was created, which was deleted for *GSH1* and expressed *OPT3* from a strong, constitutive *TEF* promoter resulting in an overexpression of the gene ($\Delta gsh1p_{TEF}OPT3$). Since glutathione depletion is toxic in a $\Delta gsh1$ background, the cells (WT, $\Delta gsh1$, $\Delta opt3$, $\Delta gsh1\Delta opt3$ and $\Delta gsh1p_{TEF}OPT3$) were cultured overnight in synthetic *Hartwell Complete* (HC) media supplemented with 2 μ M GSH before they were shifted to either HC media containing 2 μ M glutathione or media without glutathione (Figure 13).

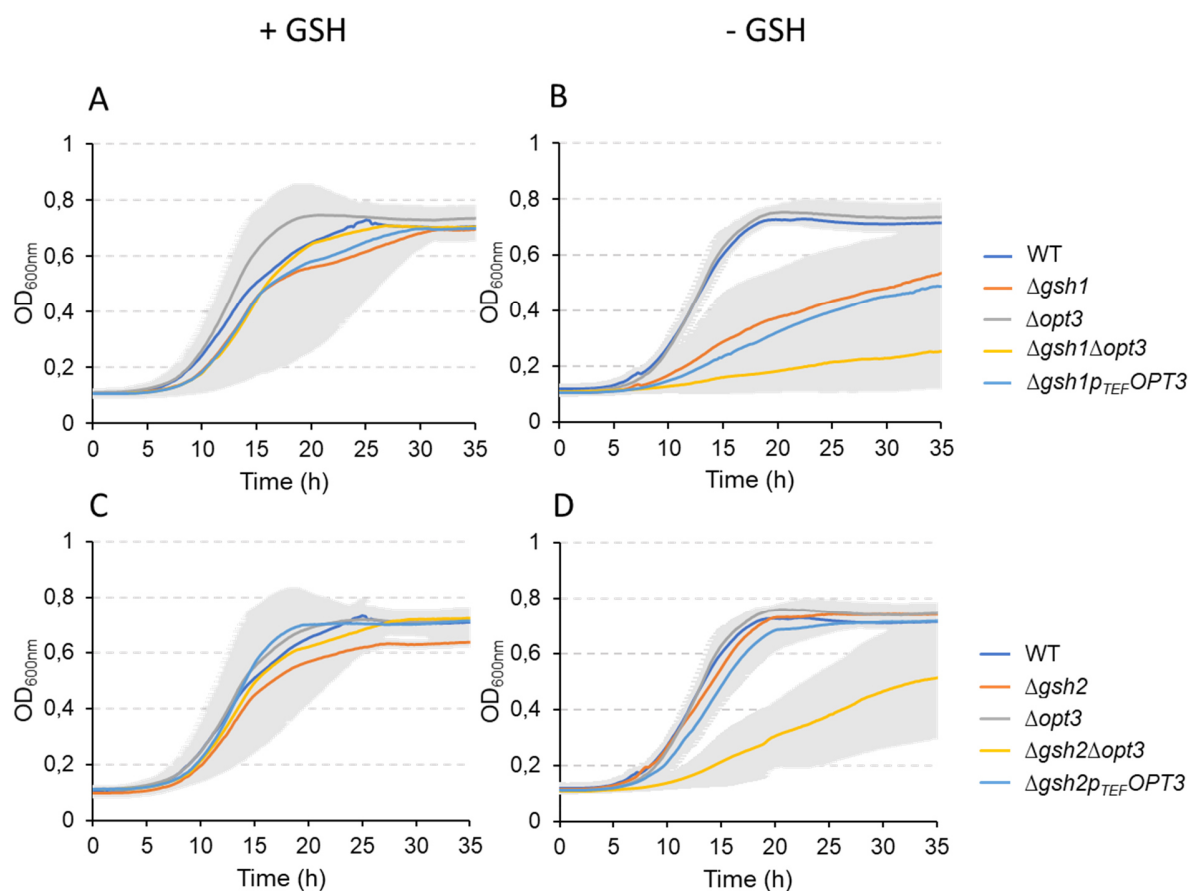


Figure 13 *OPT3* has a synthetic negative growth phenotype with *GSH1* and *GSH2*. A and B: For the analysis of yeast growth, the yeast strains BY4742 (WT), $\Delta gsh1$, $\Delta opt3$, $\Delta gsh1\Delta opt3$ and $\Delta gsh1p_{TEF}OPT3$ were cultured overnight in HC media supplemented with 2 μ M glutathione before 0.1 OD units of cells were transferred to fresh HC media with (A) or without (B) 2 μ M glutathione. OD₆₀₀ was automatically recorded every 10 min for the indicated time. In C and D, growth of the strains, BY4742 (WT), $\Delta gsh2$, $\Delta opt3$, $\Delta gsh2\Delta opt3$ and $\Delta gsh2p_{TEF}OPT3$ was analyzed as for A and B. While cells in C grew in media supplemented with 2 μ M GSH, cells in D grew without supplemented glutathione. All figures error bars illustrate the standard deviation of at least three independent repeats. Single repeats were done with the help of Laura Buchholz during her Bachelor Thesis, which was supervised by me.

In media supplemented with GSH, the growth of all tested strains did not significantly differ from WT (p -values > 0.05) (Figure 13 A). Contrarily, when cells were transferred to media without glutathione, strong growth phenotypes were observable (Figure 13 B). Whilst the $\Delta opt3$ strain grew comparable to the WT, the $\Delta gsh1$ mutant strain grew significantly slower after 15h (p -values < 0,05). Additionally, the overexpression of *OPT3* in a *GSH1* deletion ($\Delta gsh1p_{TEF}OPT3$) background did not lead to better growth compared to $\Delta gsh1$. Consistent with observations in the SGA screen, $\Delta gsh1\Delta opt3$ cells grew, although not significantly worse than $\Delta gsh1$ cells. When both genes were knocked out in the $\Delta gsh1\Delta opt3$ strain, cell growth was almost completely impaired. Since the $\Delta gsh1\Delta opt3$ double deletion strain grew on growth plates with supplemented GSH it

was presumed that *OPT3* deletion leads to an increased sensitivity when cellular glutathione was depleted.

To test this hypothesis, it was tested whether a *GSH2* knockout strain would grow, if deleted in combination with *OPT3*. Thus, a $\Delta gsh2\Delta opt3$ double mutant was generated and growth was monitored for 35h by recording the OD₆₀₀. As a control, the OD₆₀₀ of the strains WT, $\Delta opt3$, $\Delta gsh2$ and $\Delta gsh2p_{TEF}OPT3$ was monitored in parallel. All strains grew overnight in HC media supplemented with glutathione before 0.1 OD unit of each strain was inoculated in either HC media with or without glutathione (Figure 13).

All strains ($\Delta opt3$, $\Delta gsh2$, $\Delta gsh2p_{TEF}OPT3$ and $\Delta gsh2\Delta opt3$) grew similar to the WT in medium supplemented with glutathione (p-values > 0.05) (Figure 13 C). When cells grew in media without glutathione the deletion strains $\Delta opt3$, $\Delta gsh2$ and $\Delta gsh2p_{TEF}OPT3$ grew like the WT, whereas the $\Delta gsh2\Delta opt3$ strain grew significantly slower after 11h of measurement (p-values < 0.05) (Figure 13 D).

In summary, the deletion of both *GSH1* and *GSH2* in combination with a $\Delta opt3$ background negatively affected cellular growth. However, this negative growth phenotype was only observable without extracellular GSH available. Thus, analyzing the relationship of the loss of *OPT3* in combination with a lack in glutathione biosynthesis (*GSH1*, *GSH2*) indicated a strong correlation between cellular GSH and Opt3 rather than a direct interaction of Opt3 with Gsh1 or Gsh2. This first observation raised the question how exactly cellular glutathione and Opt3 function were linked. Hence, next total cellular glutathione was analyzed in cells with different *OPT3* expression levels.

2.2 Opt3 affects a specific cellular pool of glutathione disulfide

The slower growth in $\Delta gsh1\Delta opt3$ and $\Delta gsh2\Delta opt3$ mutant strains indicated negative genetic interaction between *OPT3* and *GSH1* or *GSH2* and further a potential link between Opt3 function and cellular glutathione homeostasis. The gene homology of *OPT3* to the oligopeptide transporter family members together with the identified relationship between Opt3 and cellular glutathione might indicate that Opt3 is a cellular glutathione transporter. Thus, it was next investigated whether Opt3 has a direct effect on cellular GSH or GSSG in whole cell lysates.

2.2.1 Opt3 expression influences cellular GSSG content

In order to further test if Opt3 is a cellular glutathione transporter, it was next analyzed whether Opt3 affects cellular glutathione.

Therefore, an experimental setup was used, which was previously applied by Morgan et al. to identify the yeast cadmium factor 1 (Ycf1) as vacuolar GSSG importer (Morgan et al., 2013). They demonstrated that the cytosolic glutathione pool is extremely robust reduced. Hence, GSSG in the cytosol is only present in a nanomolar or low micromolar range. The reduced cytosolic glutathione homeostasis is mainly maintained by a kinetic competition between Glr1 mediated GSSG reduction and GSSG import to the vacuole via Ycf1. Strains with either deleted or overexpressed *YCF1*, had a decreased or increased GSSG content in whole cell lysates, respectively. Conclusively, *YCF1* overexpression increased vacuolar GSSG uptake while its deletion disrupted GSSG transport and promoted the Glr1 mediated reduction. This revealed that GSSG measured in whole cell lysates represents a non-cytosolic GSSG pool. Thus, measurements of whole cell GSSG in combination with genetic manipulation of a cellular glutathione transporter can be used as an indirect indication about glutathione transport between the cytosol and a cellular compartment.

To gain further insights if Opt3 mediates the transport of glutathione between the cytosol and a subcellular compartment, total GSH and GSSG concentrations were determined in whole cell lysates of *OPT3* deletion ($\Delta opt3$) and overexpression ($p_{TEF}OPT3$) mutants and compared to wild-type glutathione concentrations (Figure 14).

As illustrated in Figure 14 A, the concentration of GSH in the WT strain was similar to $p_{TEF}OPT3$ cells and the $\Delta opt3$ strain (p-values > 0.05). Interestingly in contrast to the cellular GSH concentrations, GSSG content of both, *OPT3* deletion and overexpression changed compared to WT (Figure 14 B). In the $\Delta opt3$ strain cellular GSSG levels were slightly increased compared to WT. When *OPT3* was overexpressed in $p_{TEF}OPT3$ cells, whole cell GSSG levels were three times lower as measured in WT (p = 0.009) and $\Delta opt3$ (p = 0.005).

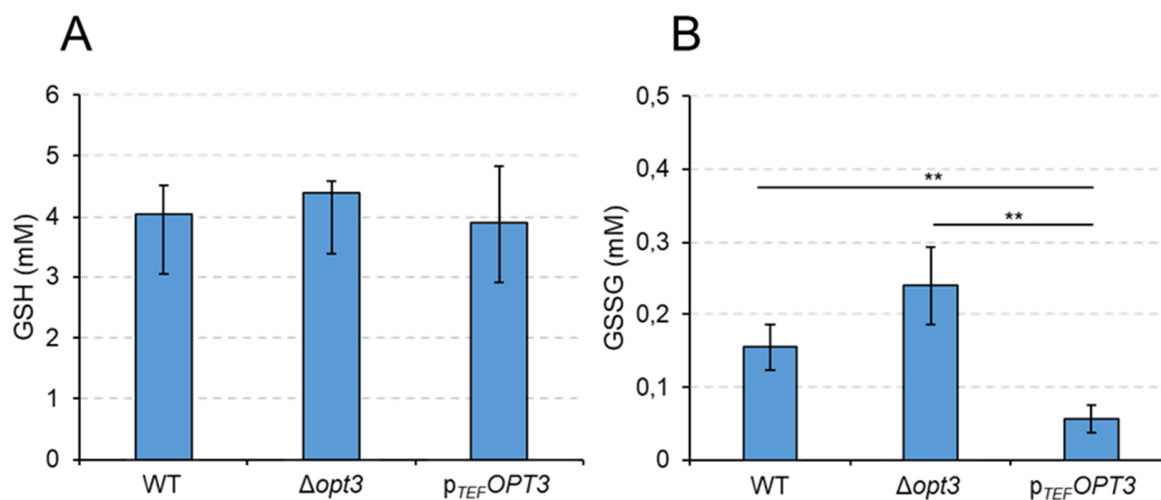


Figure 14 Analysis of GSH and GSSG in whole cell extracts of WT, $\Delta opt3$ and $p_{TEF} OPT3$ cells. Cellular GSH (A) and GSSG (B) content of WT, $\Delta opt3$ and $p_{TEF} OPT3$ was analyzed. While *OPT3* deletion and overexpression did not affect cellular GSH content, cells with overexpressed *OPT3* had a massive decrease in cellular GSSG. All figures error bars illustrate the standard deviation of at least three independent repeats. Error bars denote standard derivations. The stars represent the p-value calculated in a student's t-test for statistical analysis ($p < 0,05$: *; $p < 0,01$: **; $p < 0,001$: ***).

The changes in whole cell GSSG concentrations upon *OPT3* deletion and overexpression further supports a relationship between Opt3 and glutathione and can give a hint that Opt3 may be a transporter of cellular glutathione. Moreover, the GSSG concentrations measured in the lysate of $\Delta opt3$ and $p_{TEF} OPT3$ cells, showed an opposing pattern to those reported for Ycf1. For instance, when Morgan et al. measured GSSG in the whole cell lysate of a $\Delta ycf1$ strain the concentration was decreased compared to WT, whereas deletion of *OPT3* in the here performed experiment caused an increase in GSSG (Morgan et al., 2013). Thus, Opt3 mediated GSSG transport might be in the opposite direction to Ycf1.

2.3 Opt3 affects a Ycf1-independent cellular GSSG pool

While Ycf1 transports GSSG from the cytosol into the vacuole to maintain a reduced cytosolic glutathione pool, it was next investigated if Opt3 mediates the transport of vacuolar GSSG back into the cytosol where enzymes like glutathione reductase would recycle the oxidized glutathione to GSH (Morgan et al., 2013).

2.3.1 The effect of Opt3 on cellular GSSG levels is Ycf1 independent

To test the hypothesis if Opt3 affects the vacuolar glutathione pool I assumed, that if Opt3 exports GSSG from the vacuole into the cytosol, the effect of *OPT3* deletion and overexpression on whole cell GSSG levels must be absent, when vacuolar import of GSSG is blocked.

To impair vacuolar uptake of GSSG, *YCF1* was deleted in a BY4742 WT background. Additionally, $\Delta ycf1\Delta opt3$ and $\Delta ycf1p_{TEF}OPT3$ strains were generated and both cellular GSH and GSSG concentrations were determined (Figure 15).

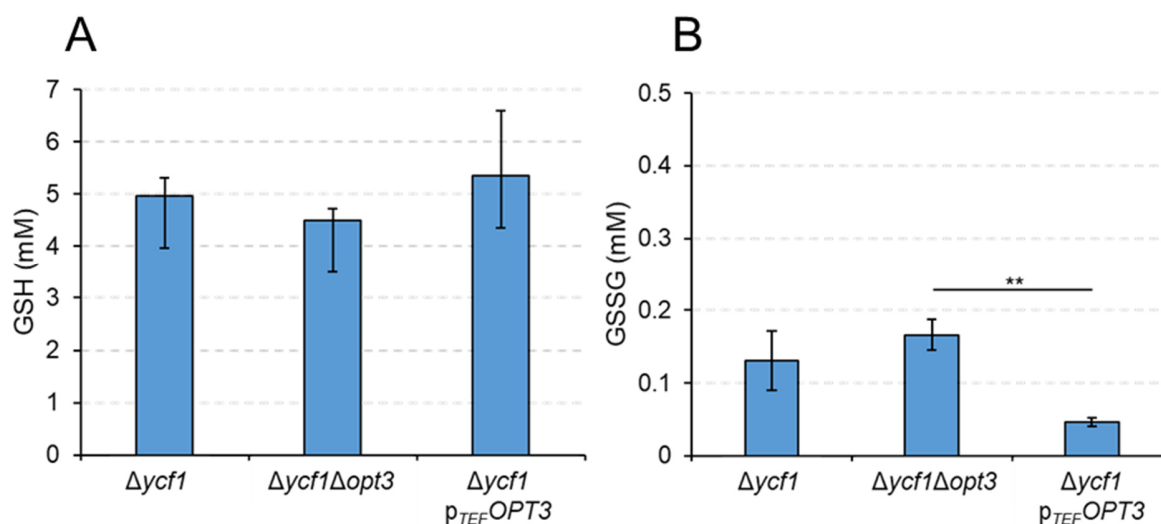


Figure 15 Opt3 modulates a Ycf1 independent GSSG pool. Both, GSH (A) and GSSG (B) content was analyzed in whole cell extracts of $\Delta ycf1$, $\Delta ycf1\Delta opt3$ and $\Delta ycf1p_{TEF}OPT3$ cells. Glutathione concentrations were determined using the DTNB-recycling assay. While all tested strains had similar GSH concentrations, the GSSG content was decreased in the $\Delta ycf1p_{TEF}OPT3$ strain compared to $\Delta ycf1$ single deletion or the $\Delta ycf1\Delta opt3$ double deletion strain. All figures error bars illustrate the standard deviation of at least three independent repeats. Error bars denote standard derivations. The stars represent the p-value calculated in a student's t-test for statistical analysis ($p < 0,05$: *; $p < 0,01$: **; $p < 0,001$: ***).

When the GSH concentration of the $\Delta ycf1$ single deletion, was compared to the double mutants $\Delta ycf1\Delta opt3$ and $\Delta ycf1p_{TEF}OPT3$ both the deletion of *OPT3* ($\Delta ycf1\Delta opt3$) and the *OPT3* overexpression ($\Delta ycf1p_{TEF}OPT3$) had comparable cellular GSH levels of approximately 5 mM with p-values of 0.194 and 0.686, respectively (Figure 15 A). However, when GSSG concentrations were measured, the double deletion mutant $\Delta ycf1\Delta opt3$ had slightly more - although not significant - GSSG compared to the single deletion strain $\Delta ycf1$. Accordingly, the $\Delta ycf1p_{TEF}OPT3$ mutation

strain had decreased cellular GSSG compared to $\Delta ycf1$ ($p = 0.108$) and $\Delta ycf1\Delta opt3$ ($p = 0.009$) (Figure 15 B).

Blocking the vacuolar uptake of cytosolic GSSG, through the deletion of *YCF1* did not affect the impact of Opt3 on cellular GSSG concentrations. Thus, this observation might indicate, that Opt3 modulates a different, Ycf1-independent, GSSG pool in the cell apart from the vacuolar pool. However, although Ycf1 is the major vacuolar GSSG importer, the experiment did not allow to rule out, that oxidized glutathione enters the vacuole via an Ycf1 independent mechanism. Hence, another test was performed to investigate whether Opt3 is involved in vacuolar GSSG export or not.

2.3.2 Opt3 does not modulate vacuolar GSSG, which is imported from the cytosol

The extremely reduced glutathione pool in the cytosol of *S. cerevisiae* is maintained by reduction of GSSG, mainly mediated by the cytosolic Glr1 as well as by pathways involving cytosolic glutaredoxins and thioredoxins, and the export of GSSG to the vacuole via Ycf1 (Garrido and Grant, 2002; Morgan et al., 2013; Oliveira et al., 2010). The deletion of *GLR1* leads to an increased uptake of GSSG into the vacuole (Morgan et al., 2013). On the understanding that Opt3 might be localized in the vacuolar membrane, increased levels of vacuolar glutathione should promote a stronger impact of *OPT3* deletion and overexpression on whole cell GSSG.

To increase the vacuolar GSSG content, a single *GLR1* deletion strain was generated ($\Delta glr1$). Furthermore, *GLR1* was knocked out in $\Delta opt3$ and $p_{TEF}OPT3$ backgrounds to generate the yeast strains $\Delta glr1\Delta opt3$ and $\Delta glr1p_{TEF}OPT3$. Afterwards whole cell concentration of GSH and GSSG was determined (Figure 16).

The *GLR1* deletion strain with overexpressed *OPT3* ($\Delta glr1p_{TEF}OPT3$) ($p = 0.414$) and the $\Delta glr1\Delta opt3$ deletion strain ($p = 0.160$) had analogous cellular GSH levels compared to WT cells (Figure 16 A). This result was consistent with former experiments and underlined that Opt3 affects cellular GSSG and not GSH. When GSSG content was measured in a $\Delta glr1$ strain, levels of around 1 mM were detected. The $\Delta glr1\Delta opt3$ double deletion strain had similar GSSG concentrations as the $\Delta glr1$ strain ($p = 0.345$). When Opt3 levels were increased in combination with deletion of *GLR1* ($\Delta glr1p_{TEF}OPT3$) the cellular GSSG content was comparable high as in the strains $\Delta glr1$ ($p = 0.462$) and $\Delta glr1\Delta opt3$ ($p = 0.757$) (Figure 16 B).

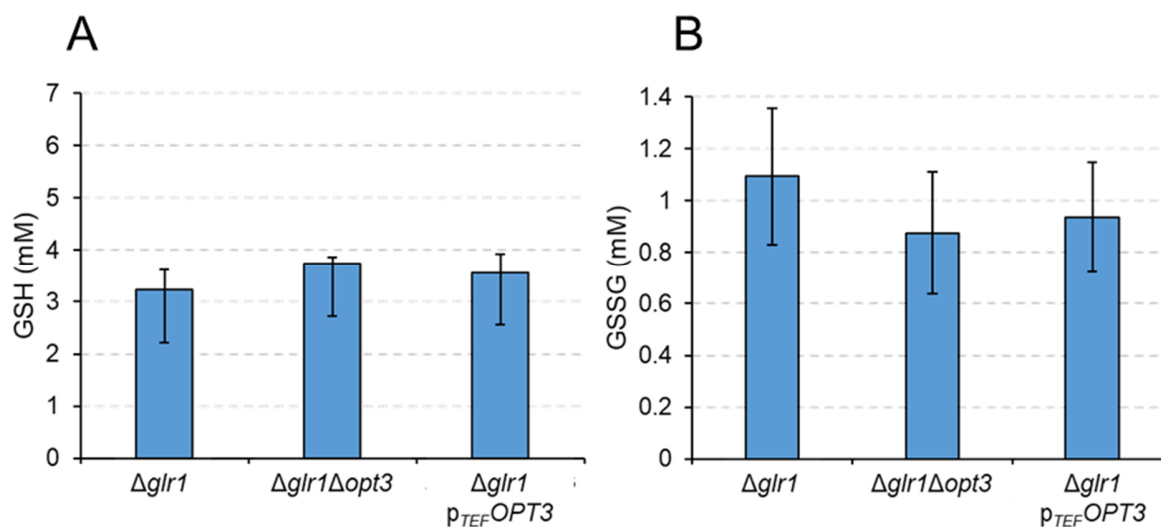


Figure 16 Increased vacuolar GSSG is unaffected by Opt3. In cell lysates of the strains $\Delta glr1$, $\Delta glr1\Delta opt3$ and $\Delta glr1 p_{TEF}OPT3$, GSH (A) and GSSG (B) content was analyzed. The deletion of *GLR1* promotes a massive import of cytosolic GSSG into the vacuole. All tested strains had similar GSH and GSSG concentrations. Thus, Opt3 does not modulate the large vacuolar GSSG concentration. Error bars illustrate the standard deviation of at least three independent repeats.

Since it is known that in cells without cytosolic Glr1 most GSSG is sequestered in the vacuole the result was in line with the former experiment suggesting, that Opt3 was not responsible for the export of GSSG from the vacuole to the cytosol.

2.4 Opt3 affects GSSG in the endoplasmic reticulum

When the results of former experiments were summarized, two facts were obvious. First, it was shown that Opt3 affects a subcellular GSSG pool and secondly the experiments suggested that Opt3 does not transport GSSG from the vacuolar lumen to the cytosol. Hence, there must exist a second cellular pool of GSSG, whose level is affected by *OPT3* expression. It is known that glutathione is present in cell organelles like mitochondria or peroxisomes (Calabrese et al., 2019; Elbaz-Alon et al., 2014). However, by analyzing the Opt3 amino acid sequence there was no obvious mitochondrial or peroxisomal targeting sequence present. Further, in contrast to the vacuole, which is a known reservoir of GSSG, cell organelles like mitochondria or peroxisomes are highly reduced (Ayer et al., 2013; Go and Jones, 2008; Toledano et al., 2013). With GSH:GSSG ratios of around 50 000:1, mitochondria and peroxisomal glutathione ratios are comparable to those of the cytosol (Calabrese et al., 2019; Iversen et al., 2010; Montero et al.,

2013; Morgan et al., 2013). Thus, the estimated GSSG concentrations in these compartments are in a nanomolar range and would not explain the huge effect of Opt3 on cellular GSSG concentration when *OPT3* was overexpressed. Beside the vacuole another cell organelle seemed to be a plausible localization of Opt3: the endoplasmic reticulum (ER). The ER is part of the secretory pathway. Proteins localized in the Golgi apparatus, vacuole or the plasma membrane are first co- or post-translationally integrated into the ER before they are translocated to their destination. In both, co- and post-translational integration processes, the polypeptide chain is integrated into the ER in an unfolded confirmation (Zimmermann et al., 2011). During oxidative protein folding in the ER, cysteines of incoming nascent protein chains get oxidized and form disulfide bonds (Braakman and Hebert, 2013). This mechanism allows a correct and stable folding from the unfolded polypeptide chain to a functional protein (Delaunay-Moisan et al., 2017). Protein folding in the ER lumen creates a highly oxidative environment (Appenzeller-Herzog, 2011; Birk et al., 2013a; Delaunay-Moisan et al., 2017). This is also reflected by the glutathione pool in the endoplasmic reticulum. Ratios between GSH and GSSG of 3:1 are reported (Appenzeller-Herzog, 2011). Thus, it was next investigated if Opt3 was localized in endoplasmic membrane.

2.4.1 Opt3 co-localizes with Sec63

For better understanding the role of Opt3 regarding glutathione homeostasis, it was necessary to identify the subcellular localization of Opt3. Since the endoplasmic reticulum seemed to be a plausible candidate, it was considered if Opt3 was localized in the ER membrane. Therefore, *OPT3* was C-terminally tagged with ymNeonGreen (*OPT3-NeonGreen*). ymNeonGreen is one of the brightest GFP-based fluorescent proteins and hence seemed to be a perfect tag for a low-copy protein like Opt3 (Botman et al., 2019). Nevertheless, *OPT3-NeonGreen* expression was very low when expressed under the control of the endogenous promoter and thus the promoter was genomically replaced by a stronger *ADH* promoter (*ADH-OPT3-NeonGreen*). For co-localization studies, *SEC63* encoding an ER resident protein was tagged with a C-terminal *mCherry* (*ADH-OPT3-ymNeonGreenSEC63-mCherry*) and both, the GFP and mCherry channels were imaged using a fluorescent microscope (Figure 17).

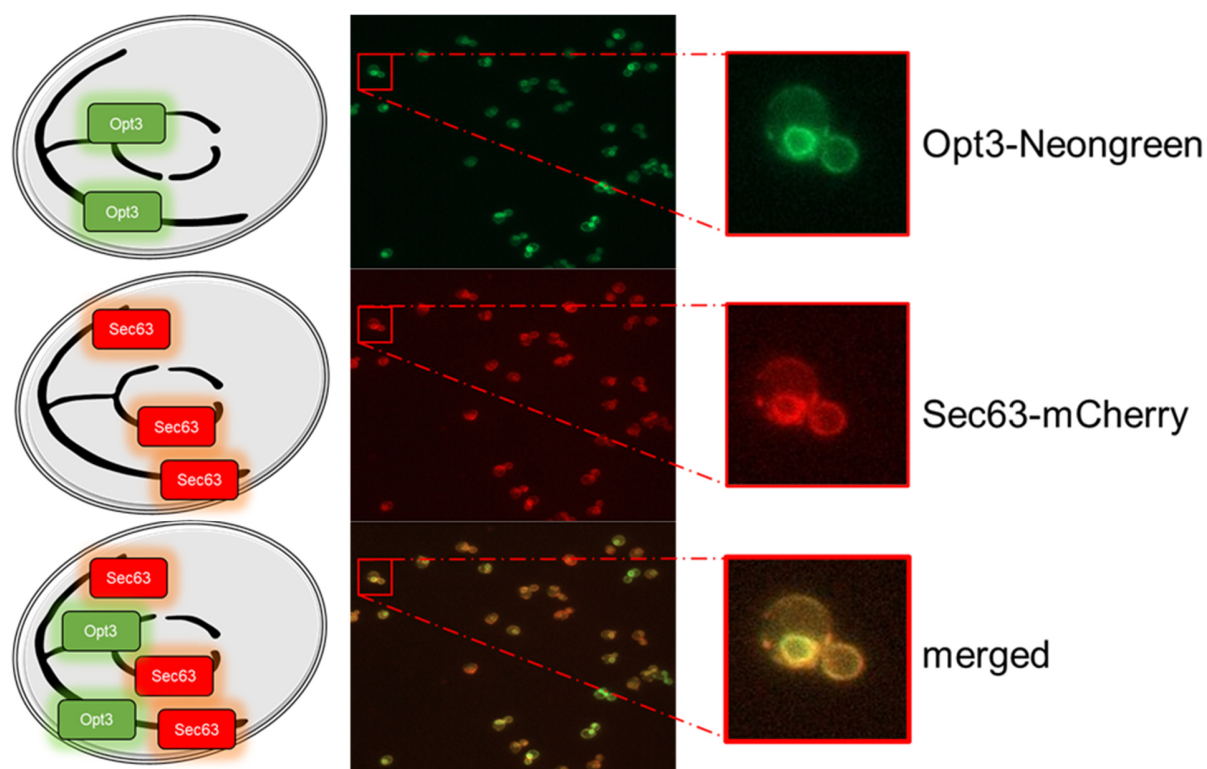


Figure 17 Opt3 is localized in the ER membrane. *OPT3* was genomically tagged at the C-terminus with the fluorescent protein ymNeonGreen (green). Due to low *OPT3* expression, the endogenous promoter was replaced through the continuously active *ADH* promoter (*ADH**OPT3*-ymNeonGreen). In parallel, a mCherry (red) fluorescent protein tag was genomically introduced at the C-terminus of *SEC63*, which encodes for an ER membrane resident protein. Both, green (upper panel) and red channels (middle panel) of the *pADH**OPT3*-ymNeonGreen*SEC63*-mCherry strain were recorded using a fluorescent microscope. Both channels were merged (lower panel) using the software *ImageJ*. At least three different cell samples were recorded.

When the green and red signal were merged, they showed strong co-localization what suggested that Opt3 was localized in the ER membrane. This clear localization of Opt3 in the ER membrane together with the before observed phenotype of that Opt3 modulates cellular GSSG, suggested the further working hypothesis that Opt3 is an ER GSSG exporter. Thus, experiments were performed, which clarified if the new hypothesis was correct or not.

2.4.2 Re-localized Gsh2 restores $\Delta gsh2\Delta opt3$ growth in the absence of GSH

First experiments, performed to characterize Opt3, revealed that Opt3 affects a vacuolar-independent GSSG pool. Since co-localization studies showed that Opt3 is an ER transmembrane protein, it was now tested whether Opt3 affects the GSSG pool of the endoplasmic reticulum. In 2017 the mechanism of GSH uptake into the ER lumen was described (Ponsero et al., 2017). It was demonstrated, that GSH can diffuse via the Sec61 translocon from the cytosol into the ER. In

the highly oxidative environment of the ER lumen, GSSG is formed. However, the diffusion of GSH into the ER is negatively regulated (Ponsero et al., 2017). Thus, GSH and GSSG content of the endoplasmic reticulum and consequently the cellular GSSG pool affected by Opt3, is limited. Overcoming the regulated import of glutathione into the ER might increase ER-glutathione content and thus increase the effect of Opt3 deletion or overexpression on GSSG in whole cell lysates. To overcome the regulated import of GSH into the ER, it was tested if the glutathione synthesis pathway could be shifted completely or partially from the cytosol into the ER.

In *S. cerevisiae* cells glutathione synthesis takes exclusively place in the cytosol. Thereby the enzyme (Gsh1) links glutamate and cysteine and forms the GSH precursor molecule γ -GC. In the second step of glutathione synthesis Gsh2 adds glycine to γ -GC and produces one molecule of GSH. Hence, either Gsh1, Gsh2 or both were shifted from the cytosol into the ER. In theory, ER-localized Gsh1 leads to the production of γ -GC in the ER lumen, while GSH synthesis takes place in the cytosol through cytosolic Gsh2. However, targeting of Gsh2 to the ER together with endogenous expressed *GSH1*, causes the synthesis of γ -GC in the cytosol and the production of GSH in the ER. Finally, targeting of both Gsh1 and Gsh2 to the ER leads to the complete synthesis of GSH in the ER lumen.

To ensure that Gsh1 and Gsh2 were targeted to the ER, the glutathione synthesis genes *GSH1* and *GSH2* were linked to a 5'- signal sequence and a 3'- ER retention tag expressed from plasmids (p415-*ADH-SS-GSH1-HDEL*, p416-*ADH-SS-GSH2-HDEL*). To realize the exclusive re-localization of the cellular glutathione synthesis machinery it was necessary to deplete either Gsh1, Gsh2 or both from the cytosol. Thus, the endogenous genes *GSH1*, *GSH2* or both were knocked out to produce the yeast mutants $\Delta gsh1$, $\Delta gsh2$, and $\Delta gsh1\Delta gsh2$. Additionally, *OPT3* was either deleted or overexpressed in strains with deficient glutathione synthesis ($\Delta gsh1\Delta opt3$, $\Delta gsh2\Delta opt3$, $\Delta gsh1\Delta gsh2\Delta opt3$ and $\Delta gsh1p_{TEF}OPT3$, $\Delta gsh2 p_{TEF}OPT3$, $\Delta gsh1\Delta gsh2 p_{TEF}OPT3$). Since further experiments in this dissertation were made in yeast strains with ER re-localized Gsh2 and endogenous *GSH1*, the focus will lie on the strains $\Delta gsh2$, $\Delta gsh2\Delta opt3$ and $\Delta gsh2p_{TEF}OPT3$. To test whether cells produce sufficient glutathione when glutathione synthesis pathway was shifted to the ER, it was tested if the cells $\Delta gsh2$, $\Delta gsh2\Delta opt3$ and $\Delta gsh2p_{TEF}OPT3$ transformed with either p415-*ADH-SS-GSH1-HDEL*, p416-*ADH-SS-GSH2-HDEL* or both, survive on growth plates without glutathione supplementation. As growth control all mutant strains and WT cells were transformed with empty p415-*ADH* and p416-*ADH*. All strains were streaked out on HC-ura-leu growth plates with either no glutathione or as positive control on HC-ura-leu plates in which 2 μ M glutathione was supplemented (Figure 18).

When the cells ($\Delta gsh2$, $\Delta gsh2\Delta opt3$ and $\Delta gsh2p_{TEF}OPT3$) with ER-localized Gsh1 and Gsh2 (p415-ADH-SS-GSH1-HDEL, p416-ADH-SS-GSH2-HDEL) were streaked out on media with supplemented glutathione all strains grew like WT p415-ADH + p416-ADH (Figure 18). In parallel, same strains grew similar on growth plates without glutathione. However, $\Delta gsh2\Delta opt3$ cells were not viable without glutathione supplementation. The synthetic negative growth phenotype between *GSH2* and *OPT3* was already known from first experiments. Intriguingly, targeting Gsh2 to the ER could rescue this lethal phenotype whereas re-localization of Gsh1 did not. The overexpression of *OPT3* combined with *GSH2* deletion in the strain $\Delta gsh2p_{TEF}OPT3$ grew as WT cells when transformed with empty plasmids. Also, the re-localization of Gsh1, Gsh2 or both did not influence the growth when *OPT3* was overexpressed.

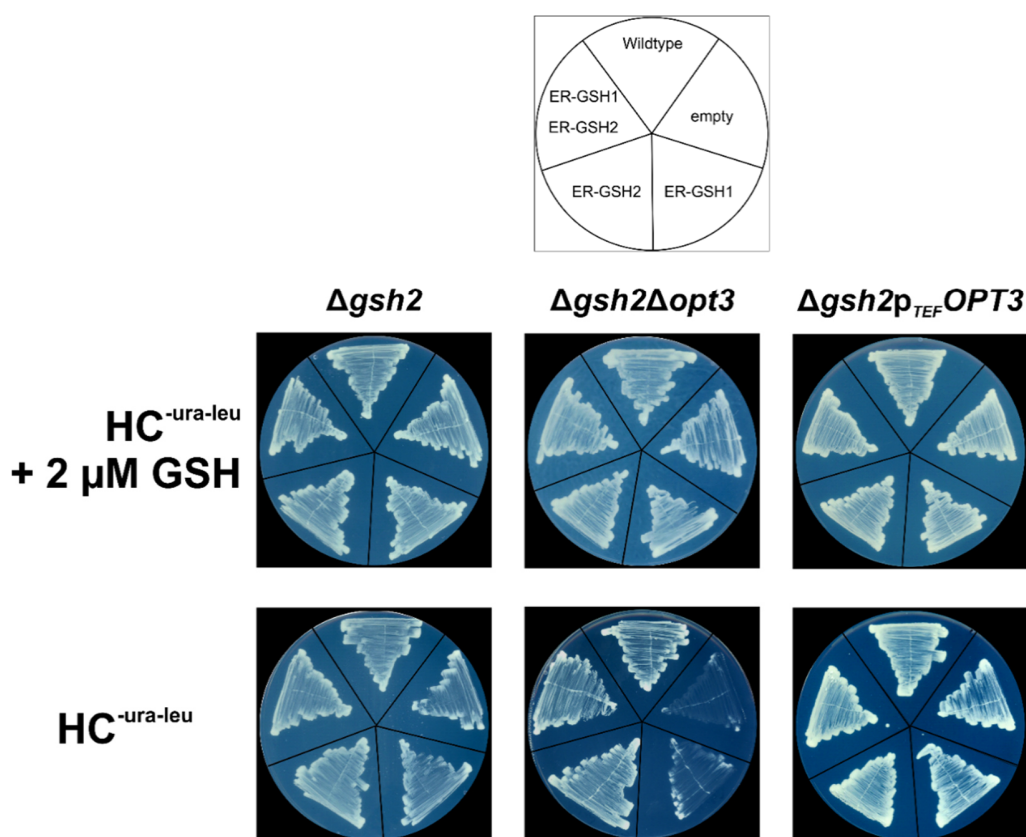


Figure 18 Glutathione synthesis was shifted from the cytosol to the ER. To test whether the cells $\Delta gsh2$, $\Delta gsh2\Delta opt3$ and $\Delta gsh2p_{TEF}OPT3$ can grow on growth plates without GSH they were transformed with plasmids containing *GSH1* and *GSH2* variants, which shifted Gsh1 and Gsh2 from the cytosol to the ER (p415-ADH-SS-GSH1-HDEL, p416-ADH-SS-GSH2-HDEL). This shift was realized by the introduction of an N-terminal ER signal peptide (SS) and a C-terminal ER retention signal (HDEL). Both plasmids were either separately or together expressed in the tested cells. To avoid amino acid marker dependent growth phenotypes, corresponding empty plasmids were transformed. Thus, all tested strains had an uracil and leucine marker gene. As growth control WT + p415-ADH + p416-ADH was used. All cells were plated on HC-ura-leu media with (2 μ M) and without glutathione. Cells were re-streaked twice before imaged. At least three independent tests were performed.

Finally, shifting the glutathione synthesis from the cytosol to the ER was sufficient to rescue the lethal phenotype of a $\Delta gsh2\Delta opt3$ double mutant. This observation suggested that glutathione synthesis can take place in the ER.

2.4.3 Opt3 strongly affects cellular GSSG content when Gsh2 is targeted to the ER

To test if Opt3 modulates the glutathione pool of the ER lumen, a tool was created to overcome regulated import of GSH in the ER and thereby elevate both, GSH and GSSG concentrations. Now, the GSH and GSSG content in whole cell lysates was analyzed to investigate, whether Opt3 had a stronger effect on cellular glutathione levels when the glutathione synthesis was taking place in the ER.

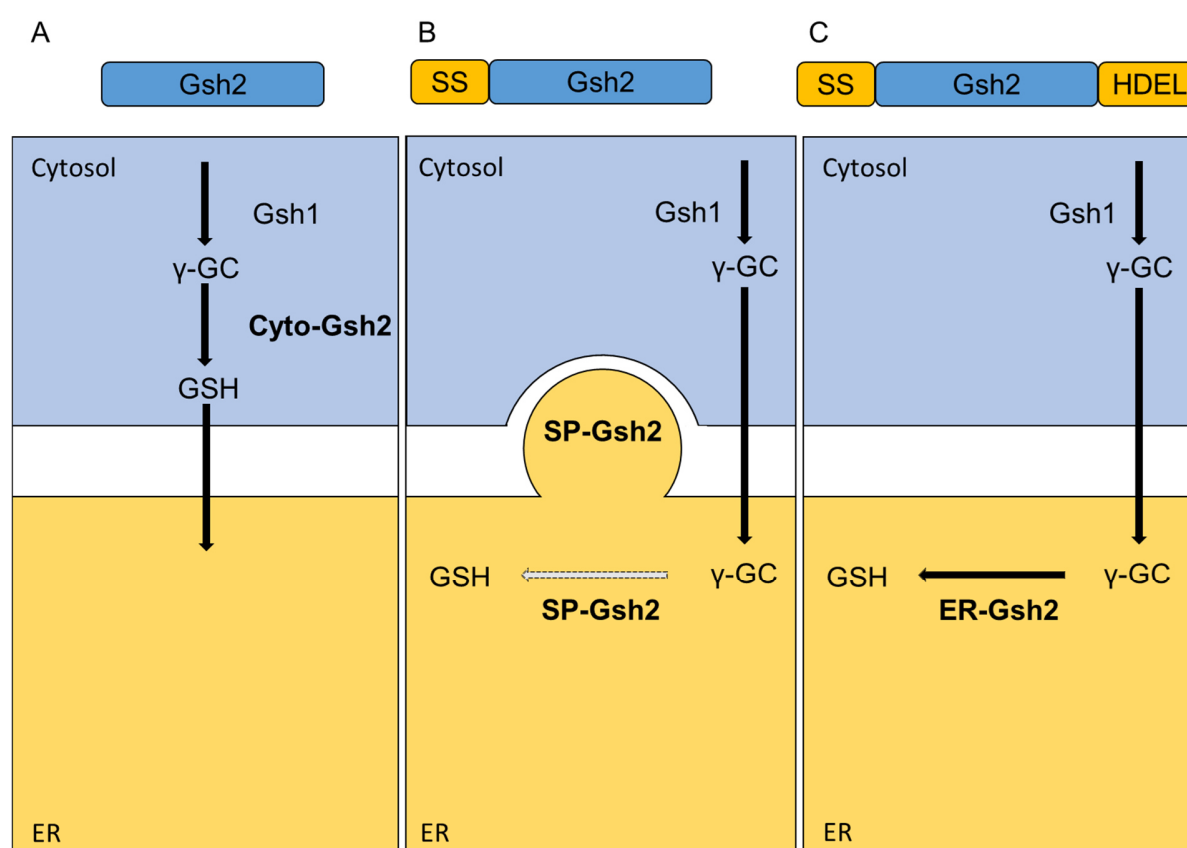


Figure 19 Illustration of Gsh2 constructs. To ensure exclusive re-localization of Gsh2 from the cytosol to the ER lumen (ER-Gsh2) a N-terminal signal peptide and a C-terminal ER retention signal was added to Gsh2 (C). To verify that ER-Gsh2 was totally integrated into the ER and was not anterograde transported through the secretory pathway or stayed back in the cytosol, two control constructs were created. Cyto-Gsh2 had neither a signal peptide nor a retention signal and thus is localized in the cytosol (A). A third Gsh2 variant (SP-Gsh2), has a N-terminal signal peptide, which allows ER-targeting, but has no retention signal and so might be exported from the ER through anterograde vesicle trafficking (B).

Beside the ER localized Gsh2 (p416ADH SS-GSH2-HDEL) two other Gsh2 constructs were cloned in a p416-ADH vector, which served as controls. One construct (p416-ADH-GSH2) contained the WT version of GSH2 which led to a cytosolic localized Gsh2 (Figure 19 A, Cyto-Gsh2). The second construct (p416-ADH-SS-GSH2) caused the integration of Gsh2 into the ER, but since the modified Gsh2 had no ER-retention signal, Gsh2 was not necessarily bound in the ER and thus could be shuttled further down the secretory pathway to the Golgi-apparatus and the vacuole (Figure 19 B, SP-Gsh2).

The constructs p416-ADH-GSH2, p416-ADH-SS-GSH2, and p416-ADH-SS-GSH2-HDEL were separately expressed in $\Delta gsh2$, $\Delta gsh2\Delta opt3$ and $\Delta gsh2p_{TEF}OPT3$ cells. Before analyzing the GSSG concentration in the strains, GSH content in whole cell lysates of all tested strains was analyzed (Figure 20).

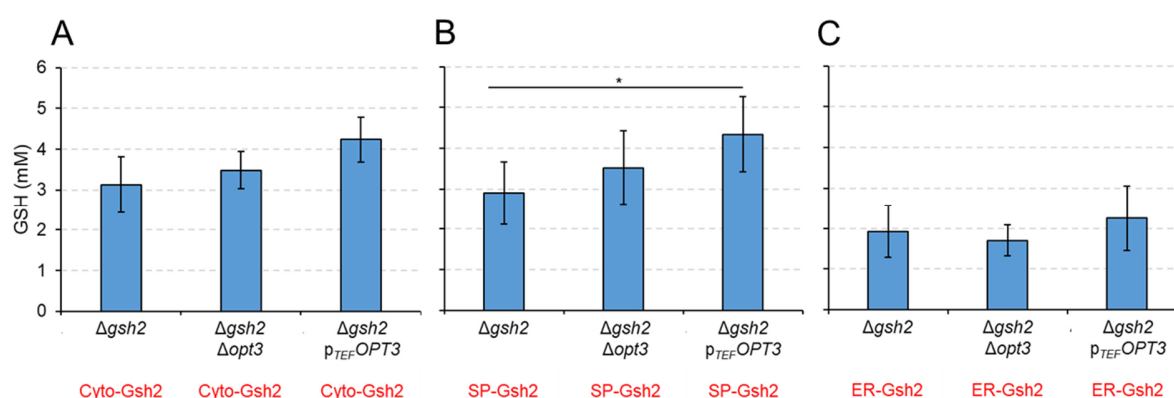


Figure 20 Whole cell GSH content of strains expressing GSH2 targeted to different subcellular localizations. The individual cells $\Delta gsh2$, $\Delta gsh2\Delta opt3$ and $\Delta gsh2p_{TEF}OPT3$ were separately transformed with plasmids carrying different GSH2 constructs. In A, the strains $\Delta gsh2$ + p416-ADH-GSH2, $\Delta gsh2\Delta opt3$ + p416-ADH-GSH2 and $\Delta gsh2p_{TEF}OPT3$ + p416-ADH-GSH2 had cytosolic localized Gsh2. B: GSH content of cells with Gsh2 localized in the secretory pathway ($\Delta gsh2$ + p416-ADH-SS-GSH2, $\Delta gsh2\Delta opt3$ + p416-ADH-SS-GSH2 and $\Delta gsh2p_{TEF}OPT3$ + p416-ADH-SS-GSH2). And C: whole cell GSH content in strains expressing ER localized GSH2 ($\Delta gsh2$ + p416-ADH-SS-GSH2-HDEL, $\Delta gsh2\Delta opt3$ + p416-ADH-SS-GSH2-HDEL and $\Delta gsh2p_{TEF}OPT3$ + p416-ADH-SS-GSH2-HDEL). At least three independent tests were performed. Error bars denote standard derivations. The stars represent the p-value calculated in a student's t-test for statistical analysis (p < 0,05: *; p < 0,01: **; p < 0,001: ***).

When WT Gsh2 was brought back in the $\Delta gsh2$ deletion strains, the GSH concentration in whole cell lysates was approximately around 3 mM (Figure 20 A). Thereby the GSH content of $\Delta gsh2\Delta opt3$ (p = 0.471) and $\Delta gsh2p_{TEF}OPT3$ (p = 0.102) cells with cytosolic Gsh2 was like the $\Delta gsh2$ + p416-ADH-GSH2 strain. When cells expressed p416-ADH-SS-GSH2, which allowed Gsh2 to enter the ER but did not anchor it to the ER lumen, GSH concentrations were also around

3 mM and comparable to GSH concentrations produced in the cytosol (Figure 20 B). Interestingly, when Opt3 levels were elevated ($\Delta gsh2p_{TEF}OPT3$), cells produced ~ 1 mM more GSH compared to cells without the *OPT3* overexpression ($p = 0.04$). When the glutathione synthesis was exclusively shifted to the ER all strains had lower GSH concentrations (~ 2 mM) compared to cells expressing the other Gsh2-constructs (Figure 20 C).

However, it is known, that the glutathione pool in the ER is heavily oxidized compared to the cytosol (Appenzeller-Herzog, 2011; Birk et al., 2013a). Thus, the GSSG content of cells expressing one of the three constructs p416-*ADH-GSH2*, p416-*ADH-SS-GSH2*, and p416-*ADH-SS-GSH2-HDEL* was analyzed and tested if Opt3 had a stronger effect on cellular GSSG when the glutathione synthesis is in the ER.

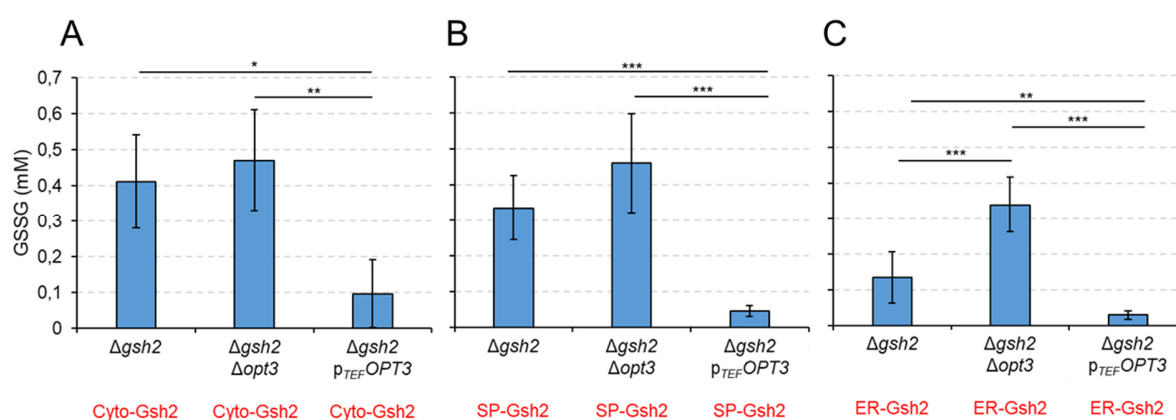


Figure 21 ER localized GSH synthesis increases the effect of Opt3 on whole cell GSSG levels. GSSG concentration measured in whole cell lysates of the cells $\Delta gsh2$, $\Delta gsh2\Delta opt3$ and $\Delta gsh2p_{TEF}OPT3$. Cells were transformed with the plasmids p416-*ADH-GSH2* (Cyto-Gsh2), p416-*ADH-SS-GSH2* (SP-Gsh2) and p416-*ADH-SS-GSH2-HDEL* (ER-Gsh2). *OPT3* deletion does not affect cellular GSSG when strains expressing p416-*ADH-GSH2* and p416-*ADH-SS-GSH2* with cytosolic (A) and secretory pathway (B) localized Gsh2, respectively. Only in cells with exclusively ER localized Gsh2 (ER-Gsh2) had strongly increased whole cell GSSG when *OPT3* was deleted (C). At least three independent tests were performed. Error bars denote standard deviations. The stars represent the p-value calculated in a student's t-test for statistical analysis ($p < 0,05$: *; $p < 0,01$: **; $p < 0,001$: ***).

When Gsh2 (p416-*ADH-GSH2*) was in the cytosol, whole cell lysates of $\Delta gsh2\Delta opt3$ cells had comparable GSSG concentrations like the $\Delta gsh2$ strain ($p = 0.627$). However, $\Delta gsh2p_{TEF}OPT3$ overexpression cells, had approximately four-fold decreased total cellular GSSG in comparison to $\Delta gsh2$ ($p = 0.026$) and $\Delta gsh2\Delta opt3$ strains ($p = 0.005$) (Figure 21 A). Analogous observations were made in whole cell lysates of cells with Gsh2 localized in the secretory pathway (p416-*ADH-SS-GSH2*). While the deletion of *OPT3* led just to a small increase in GSSG, the overexpression

strain $\Delta gsh2p_{TEF}OPT3$ had around three times less cellular GSSG than $\Delta gsh2$ ($p = 1.68 * 10^{-5}$) (Figure 21 B). Remarkably, when Gsh2 was exclusively targeted to the endoplasmic reticulum (p416-ADH-SS-GSH2-HDEL), $\Delta gsh2\Delta opt3$ cells had approximately four times more GSSG than the $\Delta gsh2$ single deletion ($p = 2 * 10^{-4}$). Additionally, the $\Delta gsh2p_{TEF}OPT3$ mutant had nearly a total depletion of GSSG (Figure 21 C).

In summary, a system was created, in which glutathione synthesis was shifted to the endoplasmic reticulum. While Gsh1 synthesized the GSH precursor γ -GC in the cytosol, Gsh2 produced GSH in the ER lumen. Therefore, I suggested that upon the production of GSH in the endoplasmic reticulum both GSH and GSSG concentrations increased in the ER. It was considered that an increase of ER GSSG concentration would increase the cellular GSSG pool affected by Opt3 and thus genetic manipulation of *OPT3* should have a stronger impact on whole cell GSSG. Hence, the system was used as an indirect indicator whether Opt3 was transporting GSSG to the cytosol. Within this system, Opt3 depletion promoted a strong increase of GSSG in whole cell lysates. This observation indicated that the formed GSSG was not transported out of the ER into the cytosol where it would be possibly reduced to GSH. Instead, the *OPT3* deletion caused an accumulation of GSSG in the ER.

However, the experimental setup could not rule out, that formed GSSG in the ER was exported to the cytosol via an unknown, Opt3-independent mechanism and imported into the vacuole by Ycf1. Thus, it was next tested if the Opt3-dependent GSSG phenotype in the system with shifted Gsh2 was independent of Ycf1 function and thus specific to the endoplasmic reticulum.

2.4.4 The effect of Opt3 on GSSG levels with ER-targeted Gsh2 is Ycf1 independent

As a further proof, that Opt3 was exclusively localized in the ER and not in the vacuole, the previous system in which the glutathione synthesis was re-localized into the ER by expressing p416-ADH-SS-GSH2-HDEL was used. In comparison to the former performed experiment, the plasmid was transformed into $\Delta gsh2\Delta ycf1$ to prevent cytosolic glutathione production and to stop the import of cytosolic GSSG into the vacuole. Additionally, to test if the effect of Opt3 on whole cell GSSG was Ycf1 independent and thus ER specific, the plasmid p416-ADH-SS-GSH2-HDEL was transformed into $\Delta gsh2\Delta ycf1\Delta opt3$ and $\Delta gsh2\Delta ycf1p_{TEF}OPT3$ cells. As a control the three strains $\Delta gsh2\Delta ycf1$, $\Delta gsh2\Delta ycf1\Delta opt3$ and $\Delta gsh2\Delta ycf1p_{TEF}OPT3$ were transformed with plasmids that carried the cytosolic localized Gsh2 (p416-ADH-GSH2) construct and the Gsh2 construct for integration of Gsh2 into the secretory pathway (p416-ADH-SS-GSH2). In all tested strains both, whole cell GSH and GSSG was analyzed (Figure 22 and Figure 23).

When Gsh2 was synthesized in the cytosol (Cyto-Gsh2) neither the deletion ($p = 0.163$), nor the overexpression ($p = 0.650$) of *OPT3* in combination with *YCF1* and *GSH2* deletion had an impact on cellular GSH levels (Figure 22 A). The same observation was true, when Gsh2 entered the endoplasmic reticulum and was transported through the secretory pathway (SP-Gsh2). In all tested strains transformed with the p416-*ADH-SS-GSH2* construct, approximately 4 mM GSH was detected in whole cell lysates (Figure 22 B).

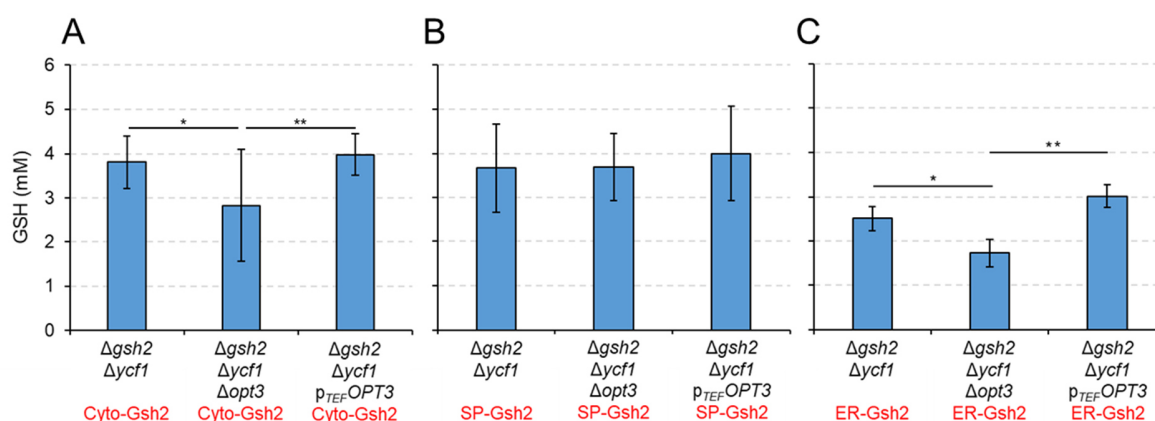


Figure 22 Combined deletion of *OPT3* and *YCF1* does not affect GSH produced in the ER. GSH concentration was measured in whole cell lysates of the cells $\Delta gsh2 \Delta ycf1$, $\Delta gsh2 \Delta ycf1 \Delta opt3$ and $\Delta gsh2 \Delta ycf1 p_{TEF}OPT3$. Cells were transformed with the plasmids p416-*ADH-GSH2* (Cyto-Gsh2), p416-*ADH-SS-GSH2* (SP-Gsh2) and p416-*ADH-SS-GSH2-HDEL* (ER-Gsh2). *OPT3* deletion together with deleted *YCF1* did not affect cellular GSSG when strains expressed p416-*ADH-GSH2* and p416-*ADH-SS-GSH2* with cytosolic (left panel) and secretory pathway (right panel) localized Gsh2, respectively. However, the strains $\Delta gsh2 \Delta ycf1$, $\Delta gsh2 \Delta ycf1 \Delta opt3$ and $\Delta gsh2 \Delta ycf1 p_{TEF}OPT3$ with ER localized Gsh2 (ER-Gsh2) had decreased total GSH compared to the same cells with cytosolic or secretory pathway Gsh2. At least three independent tests were performed. Error bars denote standard deviations. The stars represent the p-value calculated in a student's t-test for statistical analysis ($p < 0,05$: *; $p < 0,01$: **; $p < 0,001$: ***).

When Gsh2 was re-localized from the cytosol to the ER in $\Delta gsh2 \Delta ycf1$, $\Delta gsh2 \Delta ycf1 \Delta opt3$ and $\Delta gsh2 \Delta ycf1 p_{TEF}OPT3$, cells had less GSH compared to strains with cytosolic GSH production (Figure 22 A and C). Interestingly, the GSH content in $\Delta gsh2 \Delta ycf1$ cells with ER-localized Gsh2 had 1 mM more GSH compared to $\Delta gsh2 \Delta ycf1 \Delta opt3$ cells expressing the same plasmid ($p = 0.018$) (Figure 22 C). Furthermore, the GSH concentration in whole cell lysates increased about 1 mM through the stronger expression of *OPT3* in the $\Delta gsh2 \Delta ycf1 p_{TEF}OPT3$ + p416-*ADH-SS-GSH2-HDEL* strain compared to $\Delta gsh2 \Delta ycf1 \Delta opt3$ ($p = 0.004$) (Figure 22 C). When Gsh2 was re-localized to the secretory pathway, neither *OPT3* overexpression nor deletion influenced total cellular GSH (Figure 22 B).

When the glutathione synthesis was exclusively shifted into the ER (ER-Gsh2) both, *OPT3* deletion and overexpression in combination with *YCF1* deletion ($\Delta gsh2\Delta ycf1\Delta opt3$ and $\Delta gsh2\Delta ycf1p_{TEF}OPT3$) had a strong impact on cellular GSSG levels (Figure 23 C). While the overexpression strain $\Delta gsh2\Delta ycf1p_{TEF}OPT3$ had a very low GSSG content of ~ 0.05 mM, the depletion of *OPT3* in the $\Delta gsh2\Delta ycf1\Delta opt3$ strain caused significantly higher GSSG levels of more than 0.2 mM compared to $\Delta gsh2\Delta ycf1$ ($p = 1.5 \cdot 10^{-4}$) (Figure 23 C). This phenotype was specific when Gsh2 was localized in the endoplasmic reticulum since the integration of Gsh2 into the complete secretory pathway (SP-Gsh2) showed a different picture. Although cells with $p_{TEF}OPT3$ had a strongly decreased GSSG content of ~ 0.4 mM, the deletion ($\Delta gsh2\Delta ycf1\Delta opt3$) had no impact on cellular GSSG compared to the $\Delta gsh2\Delta ycf1$ strain with endogenous *Opt3* ($p = 0.829$). Interestingly, the total GSSG concentration in cells with Gsh2 in the secretory pathway was in general higher compared to those cells which had an ER-localized Gsh2 (Figure 23 B). When Gsh2 was expressed as a control in the cytosol (Cyto-Gsh2), the GSSG measured in whole cell lysates showed the same pattern as cells with Gsh2 in the secretory pathway. While the deletion of *OPT3* did not influence cellular GSSG levels (~ 2.5 mM), overexpressed *OPT3* promoted a strong decrease in total cellular GSSG (~ 0.5 mM) (Figure 23 A).

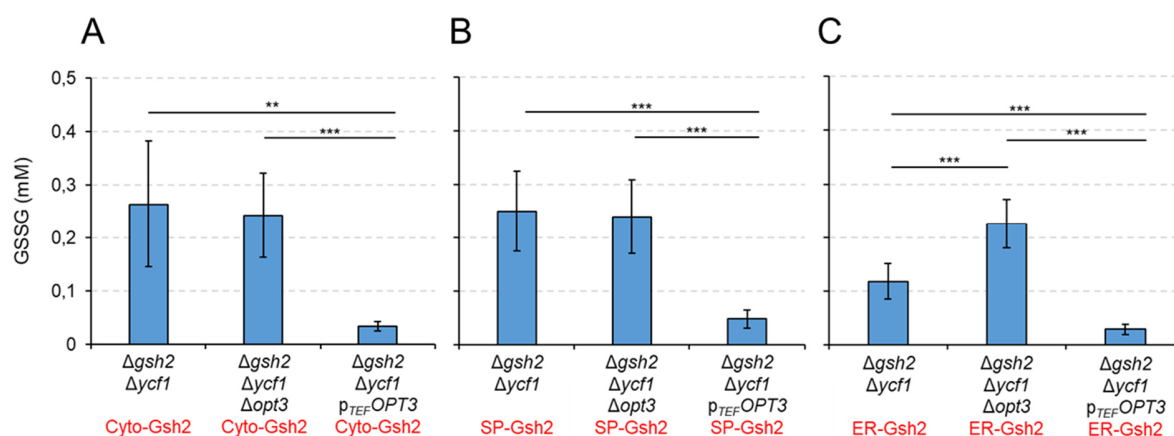


Figure 23 Opt3 modulates GSSG produced upon ER-localized GSH synthesis independently of Ycf1. GSSG content measured in whole cell lysates of the cells $\Delta gsh2\Delta ycf1$, $\Delta gsh2\Delta ycf1\Delta opt3$ and $\Delta gsh2\Delta ycf1p_{TEF}OPT3$. Cells were transformed with the plasmids p416-*ADH-GSH2* (Cyto-Gsh2), p416-*ADH-SS-GSH2* (SP-Gsh2) and p416-*ADH-SS-GSH2-HDEL* (ER-Gsh2). Deletion of *OPT3* and *YCF1* did not affect cellular GSSG when strains express either p416-*ADH-GSH2* and p416-*ADH-SS-GSH2* with cytosolic (A) and secretory pathway (B) localized Gsh2, respectively. However, cells with $\Delta gsh2\Delta ycf1\Delta opt3$ with ER-localized Gsh2 (ER-Gsh2) had increased cellular GSSG while the $\Delta gsh2\Delta ycf1p_{TEF}OPT3$ strain had almost no GSSG compared to cells with endogenous Gsh2 (C). At least three independent tests were performed. Error bars denote standard derivations. P-values were calculated in a student's t-test for statistical analysis ($p < 0,05$: *; $p < 0,01$: **; $p < 0,001$: ***).

In summary, Opt3 co-localization studies paired with analysis of GSSG levels when glutathione synthesis was shifted to the ER demonstrated that the ER glutathione pool was influenced by Opt3. However, shifting the glutathione biosynthetic pathway into the endoplasmic reticulum did not allow to analyze if Opt3 had an impact on dynamic changes in the ER glutathione pool.

2.5 Opt3 does not affect GSSG formed after cytosolic GSH accumulation

Former experiments suggested, that increasing the GSSG content in the ER, increases the effect of *OPT3* deletion and overexpression on total cellular GSSG. Thus, I decided to perform a second experiment as an ultimate proof that Opt3 exports GSSG from the ER lumen. To analyze the relationship between GSSG production and Opt3 mediated export in the ER in a time dependent manner, an inducible system was established.

2.5.1 Opt1 dependent GSH uptake promotes cellular GSSG formation

Glutathione import into the ER is regulated. GSH enters the ER via facilitated diffusion (Ponsero et al., 2017). Hence, one limiting factor of ER glutathione concentrations is the cytosolic GSH concentration. An increase in cytosolic GSH leads to a stronger diffusion gradient between the cytosol and the ER and thus to higher ER glutathione concentrations (Ponsero et al., 2017). In *S. cerevisiae* the proton-coupled oligo peptide transporter Opt1, localized in the plasma membrane, imports GSH into the cytosol (Bourbouloux et al., 2000; Kumar et al., 2011). When *OPT1* is overexpressed cells accumulate massive amounts of glutathione (Bourbouloux et al., 2000; Kumar et al., 2011; Ponsero et al., 2017; Zimmermann et al., 2021). Thus, *OPT1* overexpression was used as a tool to increase cytosolic glutathione and consequently ER glutathione.

Therefore, the overexpression plasmid p416-*TEF-OPT1* was constructed and transformed into WT cells and cells, with deleted or overexpressed *OPT3*. With the transformed strains WT + p416-*TEF-OPT1*, $\Delta opt3$ + p416-*TEF-OPT1* and p_{TEF}*OPT3* + p416-*TEF-OPT1* a pulse-chase experiment was performed. Thereby GSH and GSSG content of cell lysates was analyzed immediately before induction with 0.1 mM GSH, 30 min after the glutathione pulse and 60 min after recovery in glutathione free media (Figure 24).

Before induction with glutathione the GSH concentration in WT, $\Delta opt3$ and p_{TEF}*OPT3* containing the p416-*TEF-OPT1* plasmid was similar. All three strains had GSH concentrations of around 5 mM, what was consistent with measurements of former experiments (Figure 24 A). However,

after the incubation with extracellular reduced glutathione, the cellular GSH concentration strongly increased. While WT cells accumulated up to ~37 mM GSH, the strains $\Delta opt3$ and $p_{TEF}OPT3$ had GSH concentrations of ~27 mM and ~29 mM, respectively. In all the three tested strains GSH concentrations slightly decreased after cells were washed and recovered in fresh media without glutathione. Interestingly, the GSH levels in the WT strain were significantly higher than in $\Delta opt3$ ($p = 0.025$), whereas GSH concentrations of WT and $p_{TEF}OPT3$ were equal ($p = 0.468$) (Figure 24 A).

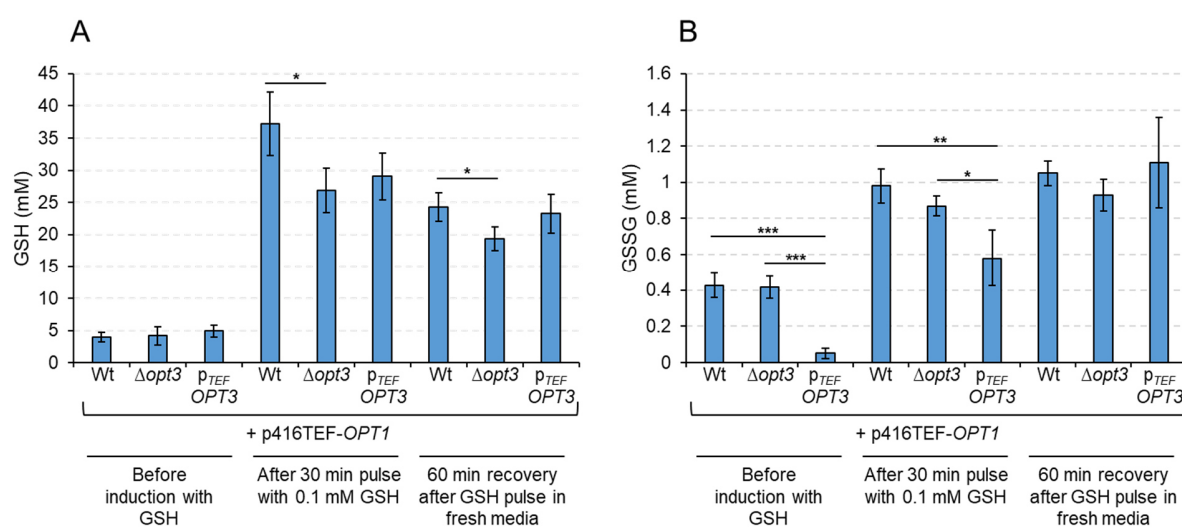


Figure 24 *OPT1* overexpression leads to a massive accumulation of cellular GSH. Whole cell lysates were analyzed for GSH and GSSG content of strains WT + p416-*TEF-OPT1*, $\Delta opt3$ + p416-*TEF-OPT1* and $p_{TEF}OPT3$ + p416-*TEF-OPT1*. All cells grew in 60 ml HC-ura selection media without supplemented glutathione till log phase, before GSH and GSSG content was determined. To the remaining culture 0.1 mM GSH was added and incubated for 30 min. After the glutathione pulse, the culture was split. In one sample glutathione content was immediately determined after the pulse. The other sample was washed twice with sterile water to remove remaining GSH and inoculated in fresh media without glutathione. After one-hour recovery GSH and GSSG concentration was determined. The GSH pulse caused massive accumulation of cellular GSH in all strains. Cellular GSSG content increased after the GSH pulse and stayed stably high for 60 min. At least three independent tests were performed. Error bars denote standard derivations. P-values were calculated in a student's t-test for statistical analysis ($p < 0,05$: *; $p < 0,01$: **; $p < 0,001$: ***).

While GSH concentrations of WT cells were nearly eight times higher after the glutathione pulse, cellular GSSG levels were just about two times higher in these cells (Figure 24 B). Before *OPT1* overexpressing cells were transferred into media with GSH, the GSSG concentration in WT cells was around 0.4 mM and equal to the GSSG content in the $\Delta opt3$ strain ($p = 0.874$). Compared to WT and *OPT3* deletion, the *OPT3* overexpression strain had approximately eight-fold lower levels of GSSG (p -values < 0.001). Interestingly, when GSH was added to the cells, the GSSG

concentrations in all three strains (WT, $\Delta opt3$ and to $p_{TEF}OPT3$) increased by approximately 0.4 mM (Figure 24 B). Thus, WT and $\Delta opt3$ strains had more absolute GSSG compared to $p_{TEF}OPT3$ but $OPT3$ overexpression had no effect on the additionally formed GSSG after glutathione treatment. After washing and incubating cells in fresh media without glutathione the GSSG concentrations in WT and $\Delta opt3$ deletion strains stayed constant, whereas the glutathione disulfide concentration in the $p_{TEF}OPT3$ overexpression further increased from approximately 0.6 mM to 1.1 mM (Figure 24 B).

In summary, overexpressing $OPT1$ led to a massive increase in cellular GSH. Taken into concern that GSH diffuses from the cytosol into the ER also the ER glutathione levels must have been increased (Ponsero et al., 2017). Because of the oxidizing environment of the endoplasmic reticulum incoming GSH might get oxidized (Appenzeller-Herzog, 2011; Ponsero et al., 2017). Interestingly, after incubation with glutathione the cellular GSSG concentration increased in wild-type, $OPT3$ deletion and overexpression strains to the same fold. This indicated that genetic manipulation of $OPT3$ had no influence on formed GSSG after the influx of GSH. However, it remained unclear whether $Opt1$ imported GSH in the media was elevating ER GSSG levels as assumed. Thus, further experiments should clarify where exactly additionally formed GSSG was localized in the cell.

2.5.2 GSSG formed during cellular GSH influx is not stored in the vacuole

First tests with overexpression of $OPT1$ lead to an enormous increase in cellular GSH and GSSG levels after cells were incubated in media supplemented with GSH. Since, neither $OPT3$ deletion nor overexpression influenced the increased cellular GSSG levels it was now tested whether the measured GSSG was formed in the cytosol and stored in the vacuole.

Therefore, strains were used, which had a deleted or overexpressed $OPT3$ gene and an additional knockout in $YCF1$ ($\Delta ycf1\Delta opt3$ and $\Delta ycf1p_{TEF}OPT3$). As a control a single $\Delta ycf1$ deletion strain was used. To enable glutathione uptake into the cells, all strains were transformed with the $OPT1$ overexpression plasmid $p416-TEF-OPT1$. Like the previous performed experiment reduced and oxidized glutathione was determined in all strains ($\Delta ycf1 + p416-TEF-OPT1$, $\Delta ycf1\Delta opt3 + p416-TEF-OPT1$ and $\Delta ycf1p_{TEF}OPT3 + p416-TEF-OPT1$) before and after incubation with 0.1 mM GSH. Additionally, GSH and GSSG content was analyzed after 1h recovery in glutathione free media.

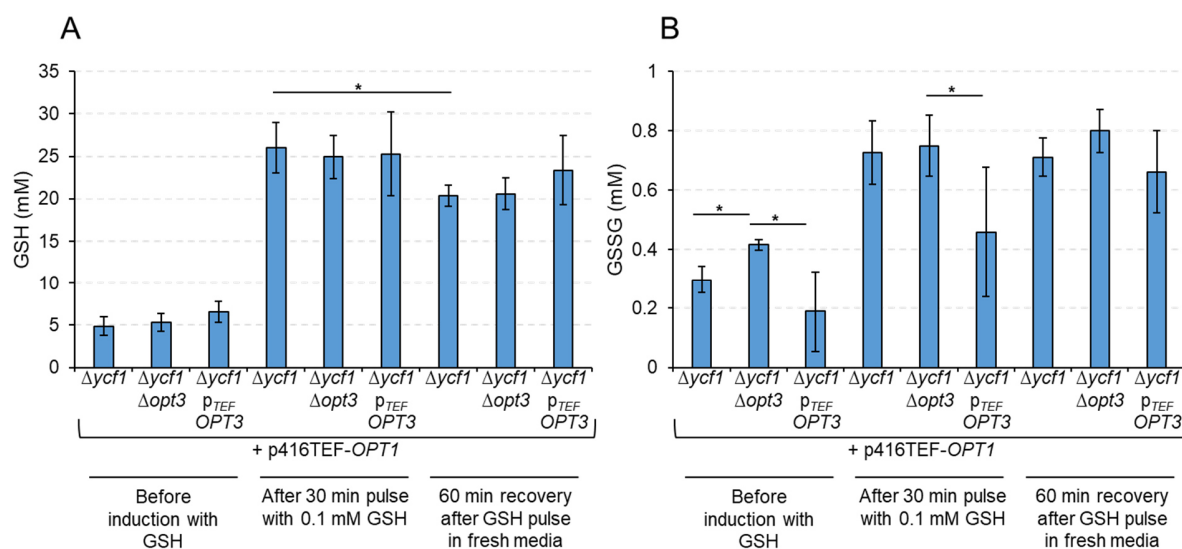


Figure 25 Whole cell GSSG content after GSH pulse is Ycf1 independent. Whole cell GSH and GSSG content of strains $\Delta ycf1 + p416-TEF-OPT1$, $\Delta ycf1\Delta opt3 + p416-TEF-OPT1$ and $\Delta ycf1 p_{TEF} OPT3 + p416-TEF-OPT1$ was analyzed. All cells grew in 60 ml HC-ura selection media without supplemented glutathione till log phase, before GSH and GSSG content was determined. To the remaining culture 0.1 mM GSH was added and incubated for 30 min. After the glutathione pulse, the culture was split. In one sample glutathione content was immediately determined after the pulse. The other sample was washed twice with water to remove remaining GSH and inoculated in fresh media without glutathione. After one-hour recovery GSH and GSSG concentrations were determined. The GSH pulse caused massive accumulation of cellular GSH in all strains. Cellular GSSG content increased after the GSH pulse and stayed stably high for 60 min. At least three independent tests were performed. Error bars denote standard derivations. P-values were calculated in a student's t-test for statistical analysis ($p < 0,05$: *; $p < 0,01$: **; $p < 0,001$: ***).

Before glutathione was added to the strains $\Delta ycf1$, $\Delta ycf1\Delta opt3$ and $\Delta ycf1 p_{TEF} OPT3$ containing $p416-TEF-OPT1$, all of them had similar GSH content of around 5 mM (Figure 25 A). After incubation in HC media supplemented with 0.1 mM GSH, all tested strains accumulated comparable amounts of total GSH (~25 mM). The GSH content in whole cell lysates remained constantly high after transferring the cells back to glutathione free media (Figure 25 A). Beside the cellular GSH content also GSSG concentrations in the tested strains increased after the GSH pulse. Thereby, the pattern of GSSG concentrations with additional knockout of *YCF1* was comparable to GSSG concentrations found when *Ycf1* was present: while the GSSG content in *OPT1* overexpressing $\Delta ycf1$ and $\Delta ycf1\Delta opt3$ was around 0.7 mM, the $\Delta ycf1 p_{TEF} OPT3 + p416-TEF-OPT1$ had approximately 0.4 mM GSSG, which was significantly less than in $\Delta ycf1\Delta opt3$ ($p = 0.048$) (Figure 25 B).

These observations suggested that accumulation of GSSG after *Opt1* mediated GSH uptake to the cytosol was *Ycf1* independent. Thus, it remained unclear where GSSG in the cell was formed.

2.5.3 The cytosol stays robustly reduced when GSH is taken up

GSSG formed in the cell after Opt1 mediated uptake of GSH is Ycf1 independent, what suggested that GSSG was not formed in the cytosol and then exported to the vacuole. However, to exclude, that GSSG was imported into the vacuole via an Ycf1-independent mechanism, it was tested if GSSG was formed in the cytosol after Opt1-mediated GSH import from the media. Thus, cytosolic GSSG formation was monitored during a pulse with 0.1 mM GSH in real time.

Therefore, the strains WT + p416-*TEF-OPT1*, $\Delta opt3$ + p416-*TEF-OPT1* and p_{TEF}*OPT3* + p416-*TEF-OPT1* were transformed with a second plasmid encoding the cytosolic glutathione sensor Grx1-roGFP2 (p415-*TEF-GRX1-roGFP2*). To additionally investigate if *YCF1* deletion has an impact on the cytosolic glutathione homeostasis during GSH uptake the strains $\Delta ycf1$, $\Delta ycf1\Delta opt3$, and $\Delta ycf1$ p_{TEF}*OPT3* were transformed with the same plasmids. Both, the untreated steady state of the cytosol as well as the sensor response during an impulse of 0.1 mM GSH were recorded (Figure 26).

Under steady state condition the Grx1-roGFP2 sensor was strongly reduced (~10% oxidized) in WT cells with overexpressed *OPT1* as shown in Figure 26 A. Also, the additional deletion or overexpression of *OPT3* did not influence the degree of Grx1-roGFP2 oxidation (OxD) (Figure 26 A), implicating that the cytosolic glutathione pool was not altered by Opt3. An additional deletion of *YCF1* in the *OPT3* deletion or overexpression backgrounds did not change the oxidation state of the Grx1-roGFP2 sensor (Figure 26 C). When 0.1 mM extracellular GSH was added, the cytosolic glutathione pool of WT stayed reduced. Neither the deletion of *OPT3* nor the overexpression affected cytosolic glutathione after the GSH pulse (Figure 26 B). In strains with additional lack of Ycf1 ($\Delta ycf1\Delta opt3$ and $\Delta ycf1$ p_{TEF}*OPT3*), the Grx1-roGFP2 sensor remained constantly reduced and did not get oxidized when GSH was entering the cytosol. Consequently, Ycf1 depletion did not affect cytosolic glutathione.

In conclusion, during the strong uptake of GSH from the media, the cytosol remains robustly reduced. This might explain why GSSG is Ycf1 independent during GSH uptake and rules out that GSSG is shunted into the vacuole via an unknown transport mechanism.

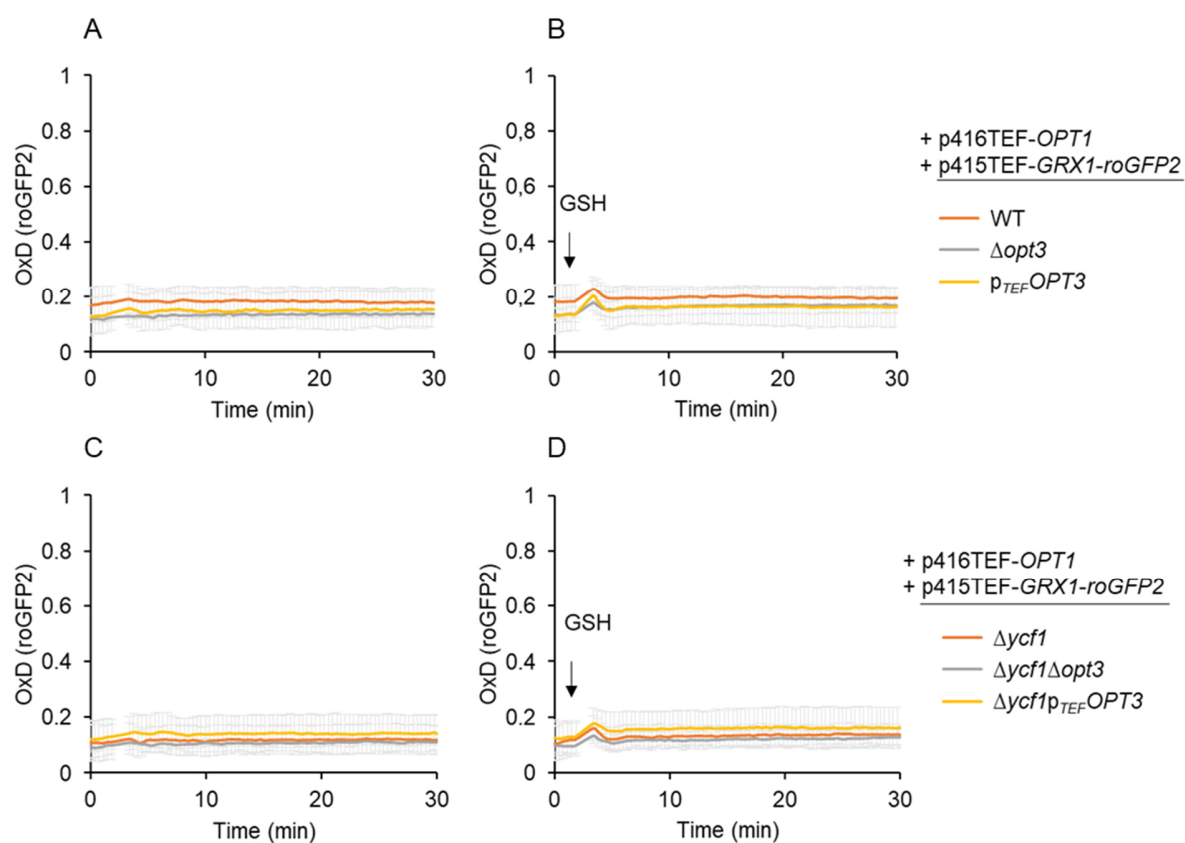


Figure 26 Cytosolic glutathione remains reduced during the accumulation of GSH. The cells BY4742 wild-type, $\Delta opt3$, $p_{TEF}OPT3$, $\Delta ycf1$, $\Delta ycf1\Delta opt3$ and $\Delta ycf1p_{TEF}OPT3$ containing a p416-TEF-OPT1 plasmid were additionally transformed with p415-TEF-GRX1-roGFP2. Cells were grown over night in corresponding growth media and resuspended the next day to an $OD_{600} = 7.5$ in fresh growth media. The cells were transferred to a 96-well plate and fluorescent roGFP2 signal was recorded in a fluorescent-plate-reader based assay. A and C: Samples without GSH treatment. B and D: measurement was paused after 5 cycles and 20 μ l of in media dissolved GSH was added to the samples (final concentration: 0.1 mM) before recording was continued. At least three independent experiments were performed. Error bars denote standard derivations. P-values were calculated with the student t-test for statistical analysis ($p < 0,05$: *, $p < 0,01$: **, $p < 0,001$: ***).

2.5.4 Cells accumulate GSH after cellular GSSG application

Previous experiments showed that an influx of GSH into the cell not just led to an increase in cellular GSH but also in GSSG. It was further shown that the cytosolic glutathione pool remained robustly reduced. This observation indicated that the measured glutathione disulfide in whole cell lysates must had a non-cytosolic origin and thus was formed in another cellular compartment. However, deletion or overexpression of *OPT3* had no effect on the newly formed GSSG.

The transport direction of secondary active transporters like oligopeptide transporter often depends on electro-chemical gradients (Becerra-Rodríguez et al., 2020; Lubkowitz, 2011). Thus,

inversion of the electrochemical gradient might alter transport direction. Hence, it was next investigated whether the induction with GSSG instead of GSH would lead to an effect of *OPT3* deletion and overexpression on the cellular GSSG content through the immense accumulation of GSSG in the cytosol.

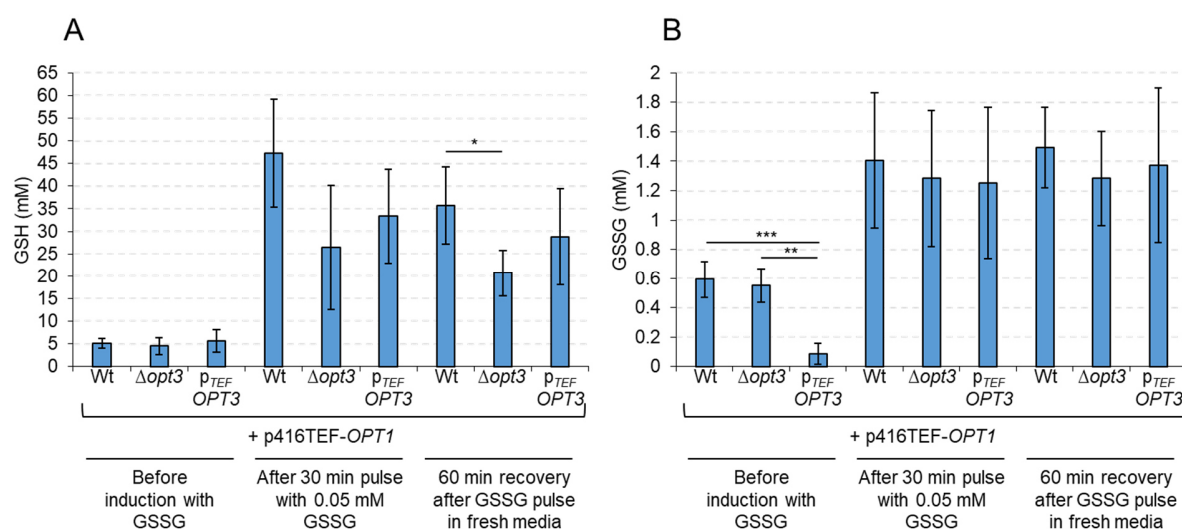


Figure 27 *OPT1* overexpression causes a massive accumulation of cellular GSH. Whole cell GSH and GSSG content of strains WT + p416-*TEF-OPT1*, $\Delta opt3$ + p416-*TEF-OPT1* and $p_{TEF}OPT3$ + p416-*TEF-OPT1* was analyzed. All cells grew in 60 ml HC-ura selection media without supplemented glutathione till log phase, before GSH and GSSG content was determined. To the remaining culture 0.05 mM GSSG was added and incubated for 30 min. After the glutathione pulse, the culture was split. In one sample glutathione content was immediately determined after the pulse. The other sample was washed twice with water to remove remaining GSSG and inoculated in fresh media without glutathione. After one-hour recovery GSH and GSSG concentrations were determined. Error bars denote standard derivations. The GSSG pulse caused massive accumulation of cellular GSH in all strains. P-values were calculated using a student's t-test for statistical analysis ($p < 0,05$: *; $p < 0,01$: **; $p < 0,001$: ***).

Therefore, wild-type cells and strains with deleted ($\Delta opt3$) or overexpressed *OPT3* ($p_{TEF}OPT3$) were transformed with a p416-*TEF* plasmid carrying *OPT1* controlled by a high expression promoter (p416*TEF-OPT1*). Like in the experiment before, whole cell glutathione in three different samples of each strain (WT + p416-*TEF-OPT1*, $\Delta opt3$ + p416-*TEF-OPT1* and $p_{TEF}OPT3$ + p416-*TEF-OPT1*) was measured. In the first sample cells grew in media without GSSG. Remaining cells were supplemented with 0.05 mM GSSG and incubated for half an hour at 30°C. Afterwards cells were divided into two samples. While one sample was measured immediately after GSSG pulse, the other sample was washed and transferred to media without glutathione and recovered for 1h at 30°C and total GSH and GSSG was determined.

When GSH concentration was analyzed in the *OPT1* overexpressing strains WT, $\Delta opt3$ and $p_{TEF}OPT3$ it was surprising that after the injection of 0.05 mM GSSG into the media the GSH levels increased much more compared to cellular GSSG (Figure 27 A). The GSH content of all the tested strains was similar after the GSSG pulse. Even after the washout of GSSG from the media all strains maintained high GSH levels, although $\Delta opt3$ had ~15 mM lower GSH levels compared to WT ($p = 0.039$). After the pulse of GSSG, all tested strains had approximately 1.2 mM total cellular GSSG (Figure 27 B). Interestingly, the cellular GSSG content was just approximately 200 μ M higher after treatment with extracellular GSSG compared to the same mutants after treatment with GSH in before performed experiments. Nevertheless, the genetic manipulation of *OPT3*, did not affect the GSSG content and thus I speculated if the additional GSSG might be exported from the cytosol into the vacuole before transported to the ER. Additionally, it was surprising that although the tested strains were treated with GSSG, they just accumulated small amounts. Instead, almost all additionally measured glutathione was present in its reduced form.

2.5.5 GSSG is not exported to the vacuole via Ycf1 after uptake from the media

Overexpression of the plasma membrane transporter *OPT1* leads to an enormous uptake of glutathione from the media into the cytosol (Bourbouloux et al., 2000; Kumar et al., 2011; Ponsero et al., 2017). Former experiments showed, that GSH as well as GSSG is taken up by Opt1 (Figure 24 and Figure 27). Interestingly it made no difference in cellular glutathione whether GSH or GSSG is transported into the cell. Under both conditions yeast cells accumulated high amounts of GSH while GSSG was comparatively low. However, cellular GSSG levels in strains incubated in media with GSSG were slightly higher compared to the same strains incubated in media with supplemented GSH. Furthermore, the manipulation of *OPT3* expression levels did not influence cellular GSSG. Thus, it was investigated if GSSG imported via Opt1 was exported from the cytosol to the vacuole by Ycf1.

To test this, GSH and GSSG content in the cells $\Delta ycf1$, $\Delta ycf1\Delta opt3$ and $\Delta ycf1p_{TEF}OPT3$ containing the plasmid p416-*TEF-OPT1* was analyzed before and after a pulse of 0.05 mM GSSG. Additional GSH and GSSG content was determined in samples ($\Delta ycf1 + p416-TEF-OPT1$, $\Delta ycf1\Delta opt3 + p416-TEF-OPT1$ and $\Delta ycf1p_{TEF}OPT3 + p416-TEF-OPT1$) which recovered for 1h after GSSG induction in glutathione free fresh media. (Figure 28).

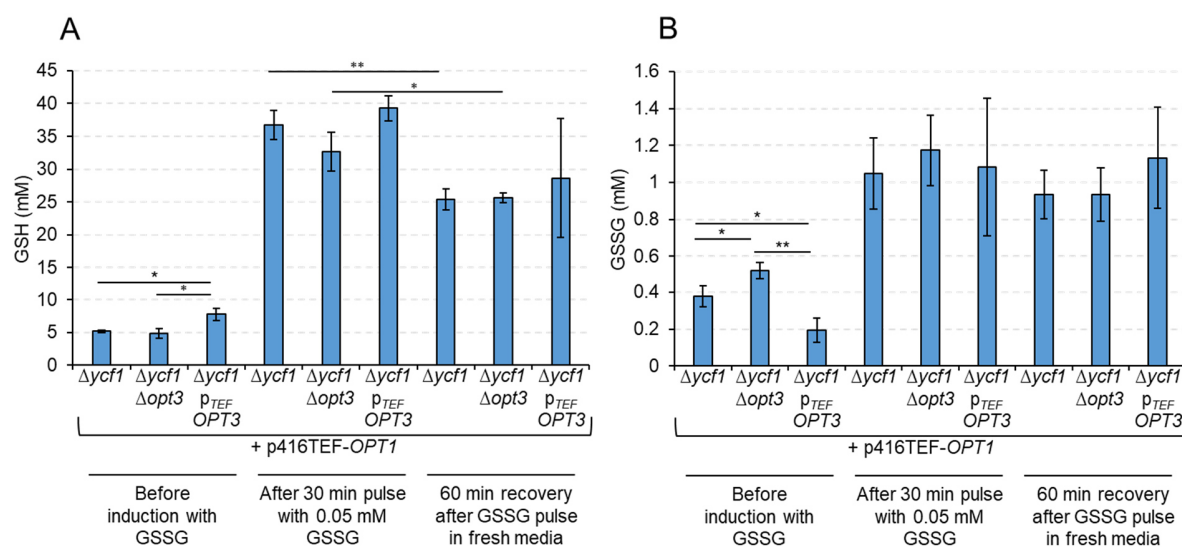


Figure 28 GSSG is not important to the vacuole when GSSG is imported by Opt1. Whole cell GSH and GSSG content of strains $\Delta ycf1 + p416\text{-TEF}\text{-OPT1}$, $\Delta ycf1\Delta opt3 + p416\text{-TEF}\text{-OPT1}$ and $\Delta ycf1 p_{TEF} OPT3 + p416\text{-TEF}\text{-OPT1}$ was analyzed. All cells grew in 60 ml HC-ura selection media without supplemented glutathione till log phase, before GSH and GSSG content was determined. To the remaining culture 0.05 mM GSSG was added and incubated for 30 min. After the glutathione pulse, the culture was split. In one sample glutathione content was immediately determined after the pulse. The other sample was washed twice with water to remove remaining GSSG and inoculated in fresh media without glutathione. After one-hour recovery GSH and GSSG concentration was determined. The GSH pulse caused massive accumulation of cellular GSH in all strains. Cellular GSSG content increased after the GSH pulse and stayed stably high for 60 min. At least three independent tests were performed. Error bars denote standard deviations. P-values were calculated using a student's t-test for statistical analysis ($p < 0,05$: *; $p < 0,01$: **; $p < 0,001$: ***).

In the tested strains $\Delta ycf1 + p416\text{-TEF}\text{-OPT1}$, $\Delta ycf1\Delta opt3 + p416\text{-TEF}\text{-OPT1}$ and $\Delta ycf1 p_{TEF} OPT3 + p416\text{-TEF}\text{-OPT1}$ the cellular GSH concentration increased approximately 25-30 mM when cells were incubated in media with supplemented GSSG. However, *YCF1* deletion alone and in combination with deleted or overexpressed *OPT3* had no effect on the elevated GSH content. Surprisingly, the GSH concentration in $\Delta ycf1$ ($p = 0.004$) and $\Delta ycf1\Delta opt3$ ($p = 0.03$) significantly decreased after glutathione washout and incubation in growth media without GSH or GSSG to 25 mM (Figure 28 A). Compared to results when cells had a functional *Ycf1* (Figure 27), the *YCF1* deletion in $\Delta ycf1$, $\Delta ycf1\Delta opt3$ and $\Delta ycf1 p_{TEF} OPT3$ strains did influence the cellular GSSG content when cells were incubated in media supplemented with GSSG and led to a decrease of approximately 200 μM GSSG in the cells (Figure 28 B). Additionally, the GSSG content in all tested cells was still higher compared to the GSSG concentration of the same strains incubated in media with supplemented GSH (Figure 25). Between the *OPT1* overexpressing cells $\Delta ycf1$, $\Delta ycf1\Delta opt3$ and $\Delta ycf1 p_{TEF} OPT3$ was no difference in whole cell GSSG content after the GSSG pulse.

In summary the uptake of extracellular GSSG via Opt1 led to both, the increase of cellular GSH and GSSG. However, Opt3 did neither affect cellular GSH nor GSSG levels. Interestingly, Ycf1 did just modulate minor GSSG amounts of cells after GSSG uptake, what suggested that indeed most GSSG was not stored in the vacuole.

2.5.6 The cytosolic glutathione pool stays reduced after treatment with GSSG

Under physiological conditions, the reduced cytosolic glutathione pool is robustly maintained by an interplay of Glr1-mediated reduction as well as other reductive systems such as glutaredoxins or thioredoxins and Ycf1-mediated vacuolar import of GSSG (Forman et al., 2009; Iversen et al., 2010; Morgan et al., 2013; Wang et al., 2014). Since in the GSSG pulse chase experiment, the genetical manipulation of *YCF1* expression had just a minor effect on the total cellular GSSG content, it was next tested how the cytosolic glutathione pool was responding to the large incoming GSSG amounts.

To retrace what happens to GSSG immediately after import to the cytosol, the cytosolic glutathione redox state was analyzed. Thus, the cytosolic glutathione sensor Grx1-roGFP2 was expressed from a plasmid in the yeast strains WT + p416-*TEF-OPT1*, $\Delta opt3$ + p416-*TEF-OPT1* +, p_{TEF}*OPT3* + p416-*TEF-OPT1*, $\Delta ycf1$ + p416-*TEF-OPT1*, $\Delta ycf1\Delta opt3$ + p416-*TEF-OPT1* and $\Delta ycf1$ p_{TEF}*OPT3* + p416-*TEF-OPT1*. In all the transformed strains roGFP2 signal was monitored in real time with and without the addition of GSSG (Figure 29).

Under steady state conditions, the degree of oxidized Grx1-roGFP2 probe in a WT cell with overexpressed *OPT1* was about 10% what reflects a strongly reduced glutathione pool (Figure 29 A). Neither the deletion nor the overexpression of *OPT3* affected the cytosolic glutathione redox state. The additional deletion of Ycf1 in the strains $\Delta ycf1$, $\Delta ycf1\Delta opt3$ and $\Delta ycf1$ p_{TEF}*OPT3* containing the *OPT1* overexpression plasmid, did also not influence cytosolic glutathione homeostasis (Figure 29 C). The addition of 0.05 mM GSSG led to the same roGFP2 response in all tested strains: probe oxidation increased immediately after GSSG injection up to ~40%. Interestingly, the probe oxidation recovered fast and after 10 min 20% of the roGFP2 molecules stayed constantly oxidized (Figure 29 B and D). However, probe oxidation did not recover completely to steady state oxidation levels.

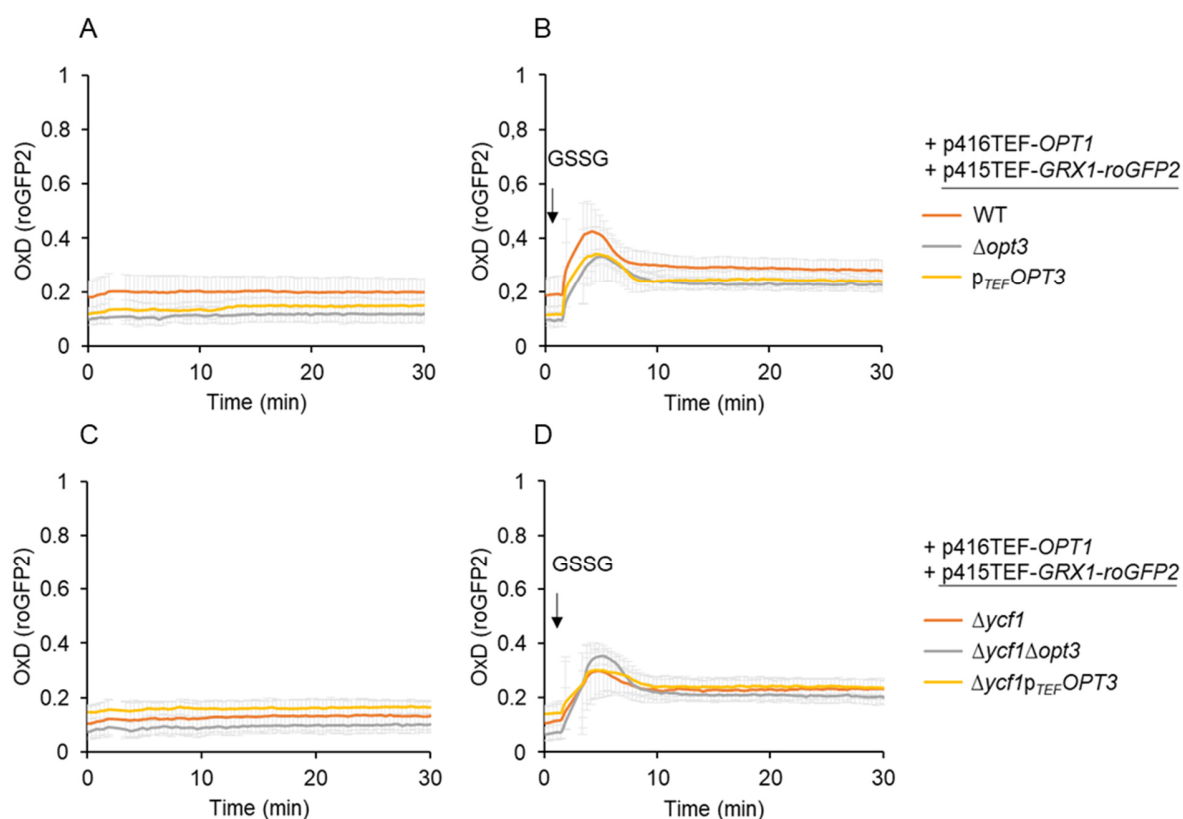


Figure 29 The cytosolic glutathione pool remains reduced during GSSG influx. The cells BY4742 WT, $\Delta opt3$, $p_{TEF}OPT3$, $\Delta ycf1$, $\Delta ycf1\Delta opt3$ and $\Delta ycf1p_{TEF}OPT3$ containing a p416-*TEF-*OPT1** plasmid were transformed with p415-*TEF-*GRX1-roGFP2**. Cells were incubated overnight in corresponding growth media and resuspended the next day to an $OD_{600} = 7.5$ in fresh growth media. The cells were transferred to a 96-well plate and fluorescent roGFP2 signal was recorded in a fluorescent-plate-reader based assay. A and C: Samples without GSSG treatment. B and D: measurement was paused after 5 cycles and 20 μ l of in media dissolved GSSG was added to the samples (final concentration: 0.05 mM) before recording was continued. At least three independent experiments were performed. Error bars denote standard deviations.

Since even in the *OPT1* overexpression containing strains $\Delta ycf1$, $\Delta ycf1\Delta opt3$ and $\Delta ycf1p_{TEF}OPT3$ the cytosol was strongly reduced after GSSG injection, it seemed possible that the reduced cytosolic glutathione pool is mainly obtained by Glr1 mediated reduction than through the export form GSSG to the vacuole.

2.5.7 Exogenous GSSG is immediately reduced after uptake into the cytosol

After the investigation that although GSSG was taken up via *Opt1* into the cell, the cytosol stayed strongly reduced it was next analyzed, if the incoming GSSG became enzymatically reduced in the cytosol. I assumed that a lack in *Glr1* paired with overexpressed *OPT1* would perturb the reduced cytosolic glutathione pool when cells are treated with GSSG.

To test this hypothesis, the plasmids p416-*TEF-OPT1* and p415-*TEF-GRX1-roGFP2* were transformed in the *GLR1* deletion strain. The roGFP2 response was recorded in the $\Delta glr1$ + p416-*TEF-OPT1* + p415-*TEF-GRX1-roGFP2* strain and steady state levels were compared to the probe response after the injection of 0.05 mM GSSG into the media.

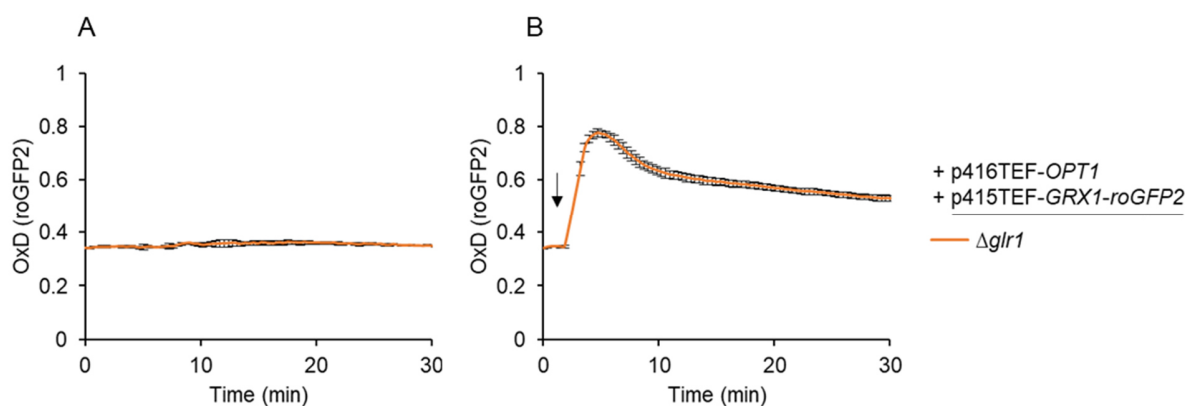


Figure 30 *Glr1* reduces immediately *Opt1* imported GSSG in the cytosol. The $\Delta glr1$ strain containing a p416-*TEF-OPT1* plasmid was transformed with p415-*TEF-GRX1-roGFP2*. Cells were incubated overnight in corresponding growth media and resuspended the next day to an $OD_{600} = 7.5$ in fresh growth media. The cells were transferred to a 96-well plate and fluorescent roGFP2 signal was recorded in a fluorescent-plate-reader based assay. A: Sample without GSSG treatment. B: Measurement was paused after 5 cycles and 20 μ l of GSSG dissolved in media was added (indicated with the black arrow) to the samples, (final concentration: 0.05 mM) before recording was continued. At least three independent experiments were performed. Error bars denote standard derivations.

The knockout of *GLR1* led to a stronger roGFP2 oxidation compared to WT cells analyzed in former experiments when cytosolic glutathione redox state was monitored (Figure 30 A). However, more exciting was the probe response after the injection of GSSG into the media. Directly after the injection 80% of the roGFP2 molecules became oxidized. Moreover, the degree of sensor oxidation dropped after 5 min to 60% and stayed constantly high (Figure 30 B). Hence, the roGFP2 response suggested a decreased cytosolic capacity to reduce GSSG. In reverse, the here made observation revealed, that GSSG imported by *Opt1* is efficiently reduced by *Glr1*.

In summary, genetical manipulation of *OPT3* did not affect GSSG formed after cellular GSH influx. Thus, I speculated, that if GSSG was formed in the ER, one reason for loss of *Opt3* function might be protein inhibition.

2.5.8 Cellular glutathione influx does not affect cytosolic pH

Members of the OPT-family are secondary active transporters, which are energized by a proton gradient (Becerra-Rodríguez et al., 2020; Kotyk, 1994; Lubkowitz, 2011; Osawa et al., 2006). Thus, Opt1 as proton coupled glutathione transporter, might influence the pH of the cytosol when highly overexpressed. Since these changes in pH eventually alter the activity of Opt3, cytosolic pH during GSH uptake was analyzed.

Therefore, the cytosolic pH was monitored during GSH induction using the well-established GFP based sensor pHluorin. Wild-type GFP has two potential excitation maxima (395 nm and 475 nm), depending on the protonation state of Tyr⁶⁶ (Remington, 2011). Since, the excitation spectra of GFP is stable in pH ranges from 5.5 to 10, Miesenböck et al. substituted several amino acids to facilitate the switch between protonated and deprotonated Tyr⁶⁶ in a pH dependent manner (Miesenböck et al., 1998). Thereby, they constructed a new sensor (pHluorin) with a sensitivity from pH 7.5 to 5.5. Hence, pHluorin has two pH dependent ratiometric excitation maxima with peaks at 395 nm (high pH) and 475 nm (low pH) (Miesenböck et al., 1998).

To test whether Opt3 function was impaired due to cytosolic pH changes during GSH influx, the yeast strains BY4742 WT, $\Delta opt3$, $p_{TEF}OPT3$ were co-transformed with a p413-MET25-PHLUORIN plasmid and p415-TEF-OPT1 ($\Delta opt3$ + p416-MET25-PHLUORIN + p415-TEF-OPT1, $p_{TEF}OPT3$ + p416-MET25-PHLUORIN + p415-TEF-OPT1 and WT + p416-MET25-PHLUORIN + p415-TEF-OPT1). In all tested strains the fluorescent excitation at wavelength 410 nm and 470 nm was recorded. After 15 cycles, 0.1 mM GSH was added to the samples and measurement was continued. While the 410 nm / 470 nm ratio of the first 15 cycles represents the steady state cytosolic pH (Figure 31 A), the difference between the 410 nm / 470 nm ratio of the last 15 cycles after GSH induction and the 410 nm / 470 nm ratio of first 15 measurement cycles before induction (Figure 31 B), represent the change in pH after glutathione induction (ΔpH).

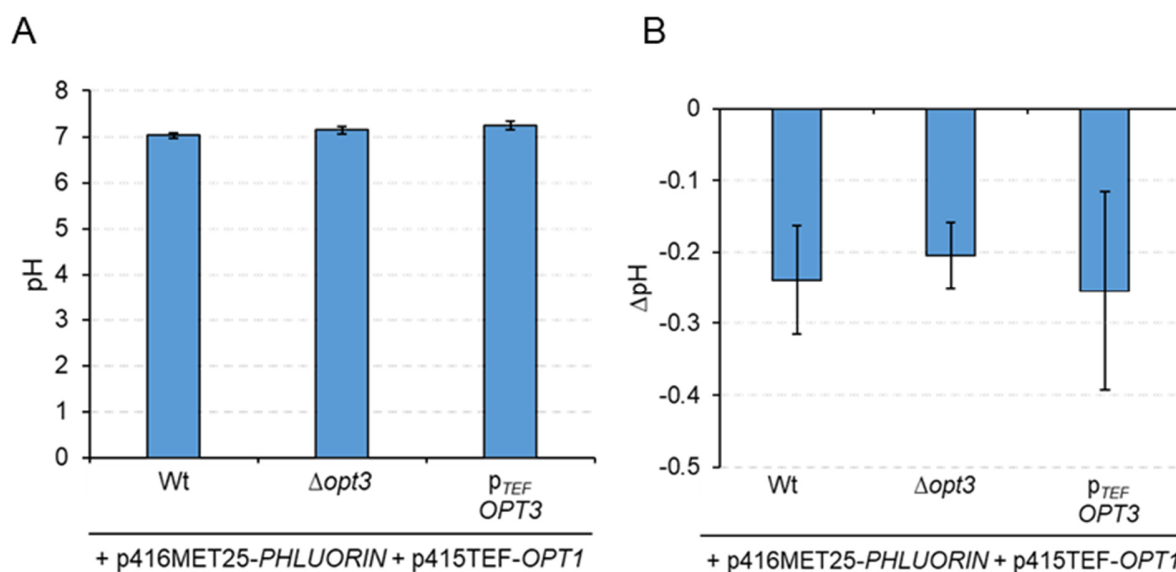


Figure 31 Cellular GSH influx slightly decreases cytosolic pH. BY4742 WT, $\Delta opt3$ and $p_{TEF} OPT3$ cells were transformed with the plasmids $p416-MET25-PHLUORIN$ and $p415-TEF-OPT1$. For pH determination cells grew overnight and next day resuspended to an $OD_{600} = 7.5$ in fresh media or buffer solutions as standards reaching from 5.5 to 7.5. Both standards and media samples were transferred to a falcon 96-well-plate and fluorescent emission intensity was recorded for excitation wavelength 410 nm and 470 nm. After 15 cycles of measurement, 0.1 mM GSH was added to the samples. While the 410 nm / 470 nm ratio of the first 15 cycles represents the cytosolic pH steady state (A), (B) the difference of steady state to the 410 nm / 470 nm ratio of the last 15 measured cycles after GSH inductions represents the GSH dependent change in pH (ΔpH). At least three independent experiments were performed. Error bars denote standard derivations.

WT cells had a cytosolic pH of ~ 7 under steady state conditions (before the induction with GSH). This neutral pH was similar in cells with $OPT3$ deletion and overexpression (Figure 31 A). Remarkably, when GSH was induced, the pH in all three tested strains decreased around 0.2, which corresponds approximately to a pH of 6.8 (Figure 31 B). Thus, there was no difference in pH change between WT and $\Delta opt3$ ($p = 0.618$) or $p_{TEF} OPT3$ ($p = 0.9$).

In summary cytosolic pHluorin measurements showed, that high Opt1 activity slightly decreases pH in the cytosol when GSH is transported into the cell. However, it remains elusive if such a small decrease in pH can alter Opt3 activity. A further hypothesis why Opt3 did not have any influence on the increased GSSG levels when Opt1 was overexpressed was, that glutathione transport via Opt3 might be regulated via post-translational modifications.

2.6 Opt3 activity is not regulated via cysteine oxidation

In some previous preformed experiments, Opt3 did not affect cellular GSSG e.g., when cellular glutathione levels were manipulated through overexpressed *OPT1* or in $\Delta glr1$ mutants. However, regulated activation and inactivation of Opt3 would possibly explain previous observations. In yeast, proteins are often regulated via post-translational modifications (Mieyal and Chock, 2012; Oliveira and Sauer, 2012; Seres et al., 1996). The thiol group (-SH) of cysteine residues is often crucial for a protein and modifications can modulate protein stability or activity (Seres et al., 1996). One important cysteine residue modification is the reversible protein-S-glutathionylation in which glutathione forms a mixed disulfide with proteins cysteine residues (PSSG) (Chandel and Bachhawat, 2017; Halloran et al., 2013; Ye et al., 2017). This mechanism can protect thiols from irreversible oxidation, modulates signals and activates or inactivates several proteins (Mailloux, 2020). Interestingly also Ycf1 function, can be regulated via post-translational cysteine modification under oxidative conditions (Paumi et al., 2008). I therefore questioned if Opt3 regulation also occurs via post translational cysteine modification.

```

1 MPQSTPSQEV QRVPWDNKPA LKQIT LRATI AGIAIGSLVL TSNFQFGLQT GW VSMMSLPS
61 ALLACAFFKN IWPLIFPNDR PFSDVENVYV QSMMAVAVGTG PLAFGFVGV PAIEKFLTND
121 ESGGLREQGQ SFTFRELLIW STALAFFGIF FAVPLRKQVI VREKLPFSPG SATATLISVL
181 NGTEILQEVS KSELLEMQR RLNECPEVLQ PNRDPEEADY LMNSSHSELG DYTATSQDGS
241 SILSTGSENY RANIIILLKT FVSSLYTMV SYFVPVIRSI PVFGKYLSNN YLWNFQPSPA
301 YIGQGIIMGL PTVSYMLIGC FLGWGVLAPL ARYKRWVPPD ADVHDWEEGV QGWILWSSLS
361 IMVADSVVAF IVVTVKSIVK FILIDDKAAL LNNIIDDTFQ SMLLEEERAI NSSRRNTYVD
421 GRQDTVRLVS RDNEIEVD SK HLVRVYTTVIS GCLVSSII CI VSIYLFGIQVIPLYAITA
481 LILALFLSIL GIRALGETDL NPVSGIGKIS QLIFAFIIPR DRPGSVLMNV VSGGIAEASA
541 QQAGDLMQDL KTGHLGASP RAQFC AQLIG ACWSIILSSF MYLCYNKVYS IPSEQFRIPT
601 AVVWIDCARL VTGKGLPKA LEC SMILGVI FAVLSLIRNT YRDYGYGWIL YIPSGVAVGV
661 GIFNSPSFTI ARFIGGWASH FWLKNHRGDL NAKTKMIVFS SGLVLGEGIF SVINMLFICL
721 NVPHY*

```

Figure 32 Opt3 amino-acid sequence. Opt3 has 725 amino-acids and a molecular mass of approximately 80 kDa. The protein has eleven cysteine residues at the positions 65, 205, 320, 452, 459, 565, 572, 584, 607, 623 and 719 (highlighted in yellow).

Opt3 has eleven cysteines at positions 65, 205, 320, 452, 459, 565, 572, 584, 607, 623 and 719 (Figure 32). While some of the cysteine residues eventually form disulfides for protein stability

e.g., in transmembrane domains, others might be potential targets for post-translational cysteine modifications. However, it was difficult to predict the Opt3 membrane domains since the results gained from different membrane prediction algorithms differed from each other (Supplement Figure 1). Consequently, to investigate if one of the cysteines is important for Opt3 function, all eleven cysteines were separately mutated to alanine and expressed from a p416-*TEF* backbone (p416-*TEF-OPT3-C65A*, p416-*TEF-OPT3-C205A*, p416-*TEF-OPT3-C320A*, p416-*TEF-OPT3-C452A*, p416-*TEF-OPT3-C459A*, p416-*TEF-OPT3-C565A*, p416-*TEF-OPT3-C572A*, p416-*TEF-OPT3-C584A*, p416-*TEF-OPT3-C607A*, p416-*TEF-OPT3-C623A*, p416-*TEF-OPT3-C719A*).

2.6.1 Opt3 cysteine mutants can maintain viability of the $\Delta gsh2\Delta opt3$ strain

Before the impact of the Opt3 cysteine mutations, in regard to their effect on cellular GSSG content was analyzed, it was tested whether the individual Opt3 mutations could rescue the lethal $\Delta gsh2\Delta opt3$ phenotype.

Therefore, the strain $\Delta gsh2\Delta opt3$ was transformed with the different Opt3 mutation constructs (p416-*TEF-OPT3-C65A*, p416-*TEF-OPT3-C205A*, p416-*TEF-OPT3-C320A*, p416-*TEF-OPT3-C452A*, p416-*TEF-OPT3-C459A*, p416-*TEF-OPT3-C565A*, p416-*TEF-OPT3-C572A*, p416-*TEF-OPT3-C584A*, p416-*TEF-OPT3-C607A*, p416-*TEF-OPT3-C623A*, p416-*TEF-OPT3-C719A*). Additionally, a Opt3 WT version was expressed from a p416-*TEF* vector as positive control. As negative control, $\Delta gsh2\Delta opt3$ cells transformed with an empty plasmid were used. All tested strains were grown on corresponding HC-ura plates supplemented with 2 μ M reduced glutathione. before they were re-streaked on HC-ura plates with and without glutathione. To ensure that the cellular glutathione was completely depleted in cells grown on HC plates without additional glutathione, a second round of re-streak was performed. Afterwards the growth phenotype of individual strains was analyzed (Figure 33).

When cells were plated on HC-ura plates supplemented with glutathione, the $\Delta gsh2\Delta opt3$ strains, transformed with Opt3 cysteine mutants, grew as well as the $\Delta gsh2\Delta opt3$ strain with Opt3 and the empty vector control (Figure 33). Interestingly, the Opt3 cysteine mutants rescued the lethal phenotype of the $\Delta gsh2\Delta opt3$ background when the cells were plated on media without supplemented GSH (Figure 33). The as negative control functioned $\Delta gsh2\Delta opt3$ p416-*TEF*-empty strain did not grow on HC-ura plates without glutathione.

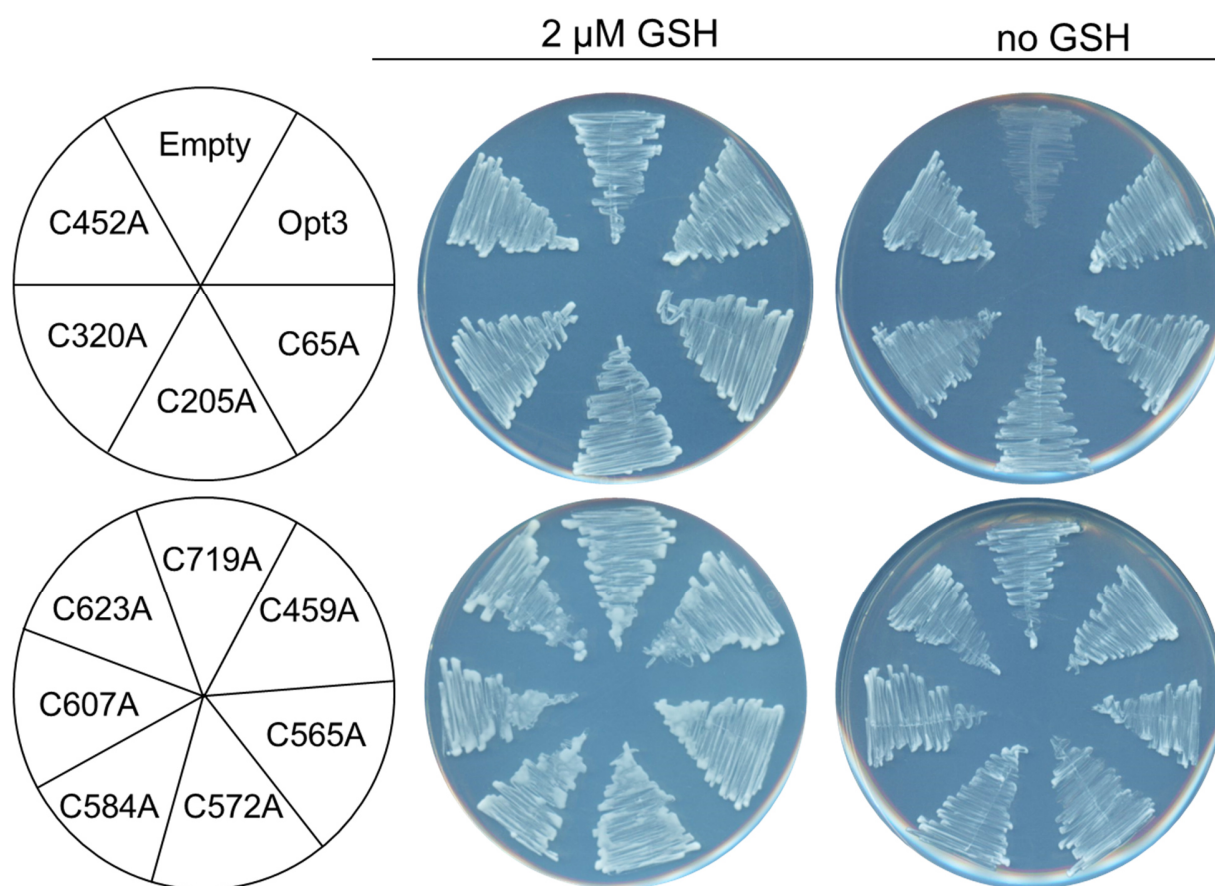


Figure 33 Opt3 cysteine mutants rescue lethality of the $\Delta gsh2\Delta opt3$ double knock-out. $\Delta gsh2\Delta opt3$ cells were transformed with plasmids containing different *OPT3* variants with individually mutated cysteine residues as indicated by the layout. As negative and positive control, the same strain was transformed with a p416-*TEF* empty plasmid and p416-*TEF*-*OPT3*, respectively. All tested strains grew on GSH containing growth plates before shifted for 24h to growth plates with or without glutathione. The cells were re-streaked twice on corresponding fresh growth plates and before imaged to ensure total cellular GSH depletion. The growth plates illustrated in this figure represents one set of at least three independent repeats.

In fact, the experiment demonstrated that the mutation of a single Opt3 cysteine does not alter Opt3 ability to rescue the lethal phenotype of the $\Delta gsh2\Delta opt3$ strain and thus suggested that Opt3 function is intact.

2.6.2 Opt3 cysteine mutants affect whole cell GSSG concentrations

The overexpression of *OPT3* leads to a decrease in whole cell GSSG content. Thus, it was next tested whether Opt3 cysteine mutants decrease the cellular GSSG content in a $\Delta opt3$ deletion strain like overexpressed endogenous *OPT3*.

Therefore, the GSH and GSSG concentration was determined in a $\Delta opt3$ strain overexpressing the different Opt3 variants (p416-TEF-OPT3-C65A, p416-TEF-OPT3-C205A, p416-TEF-OPT3-C320A, p416-TEF-OPT3-C452A, p416-TEF-OPT3-C459A, p416-TEF-OPT3-C565A, p416-TEF-OPT3-C572A, p416-TEF-OPT3-C584A, p416-TEF-OPT3-C607A, p416-TEF-OPT3-C623A, p416-TEF-OPT3-C719A). Further $\Delta opt3$ was transformed with p416-TEF empty and p416-TEF-OPT3 plasmids as negative and positive controls, respectively (Figure 34 and Figure 35).

When compared to overexpressed OPT3 none of the cysteine mutations significantly affected the cellular GSH concentration. Thereby, all cells overexpressing the different OPT3 mutations including the wild-type OPT3 overexpressing strain had GSH concentrations of approximately 8 mM and thus no significant difference to the $\Delta opt3$ empty control (Figure 34).

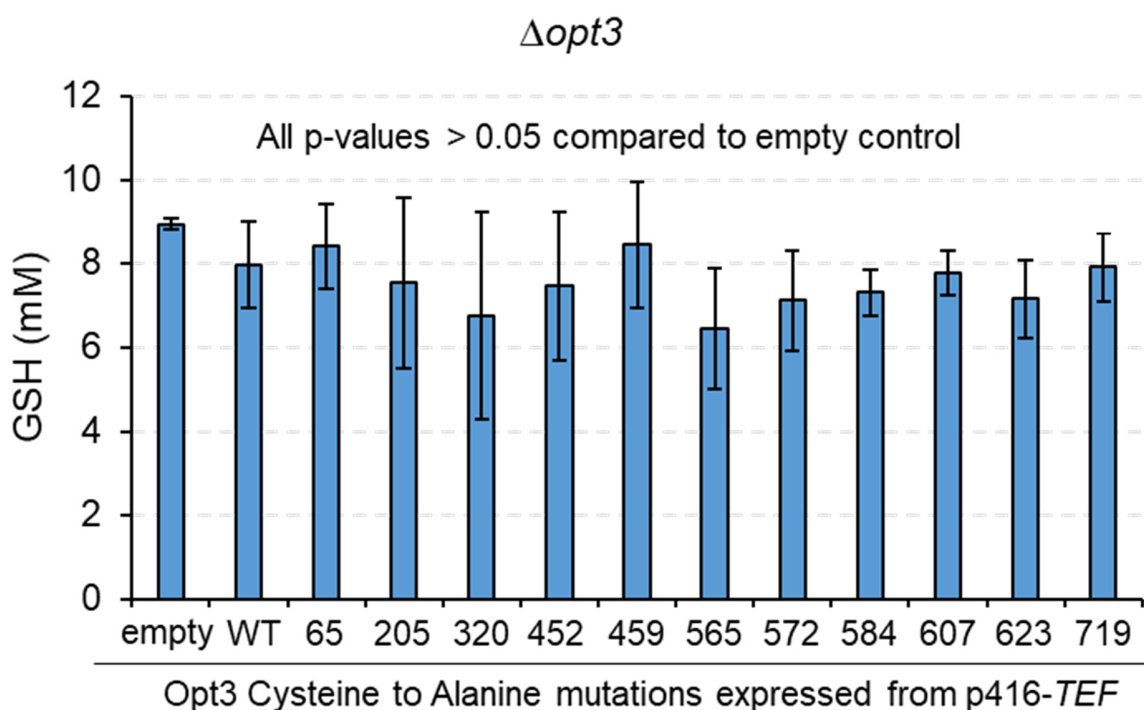


Figure 34 Total cellular GSH is unaffected by Opt3 cysteine mutants. BY4742 $\Delta opt3$ cells were transformed with plasmids containing different OPT3 mutations. Each mutation variant has a single Opt3 cysteine to alanine substitution. As positive and negative control, $\Delta opt3$ expressing OPT3 and transformed with an empty plasmid was used, respectively. Whole cell lysates of all tested strains were prepared and total GSH was determined using the DTNB-recycling assay. At least three independent experiments were performed. Error bars denote standard deviations.

The $\Delta opt3$ p416-*TEF* empty strain had approximately 0.8 mM GSSG. This result was comparable to the GSSG concentrations of a $\Delta opt3$ strain in previous experiments. Whole cell lysates of the $\Delta opt3$ strain with Opt3 as positive control, had decreased GSSG concentrations of around 0.2 mM. Interestingly, all the *OPT3* cysteine mutants expressing $\Delta opt3$ strains a decreased total GSSG content of around 0.2 mM, which was significantly lower than $\Delta opt3$ cells transformed with the empty plasmid (p-values < 0.001) (Figure 35). This observation suggested that the single mutation of the different Opt3 cysteines to alanine had no impact on Opt3 function and thus it excluded that Opt3 activity was activated via cysteine modifications during physiological growth conditions.

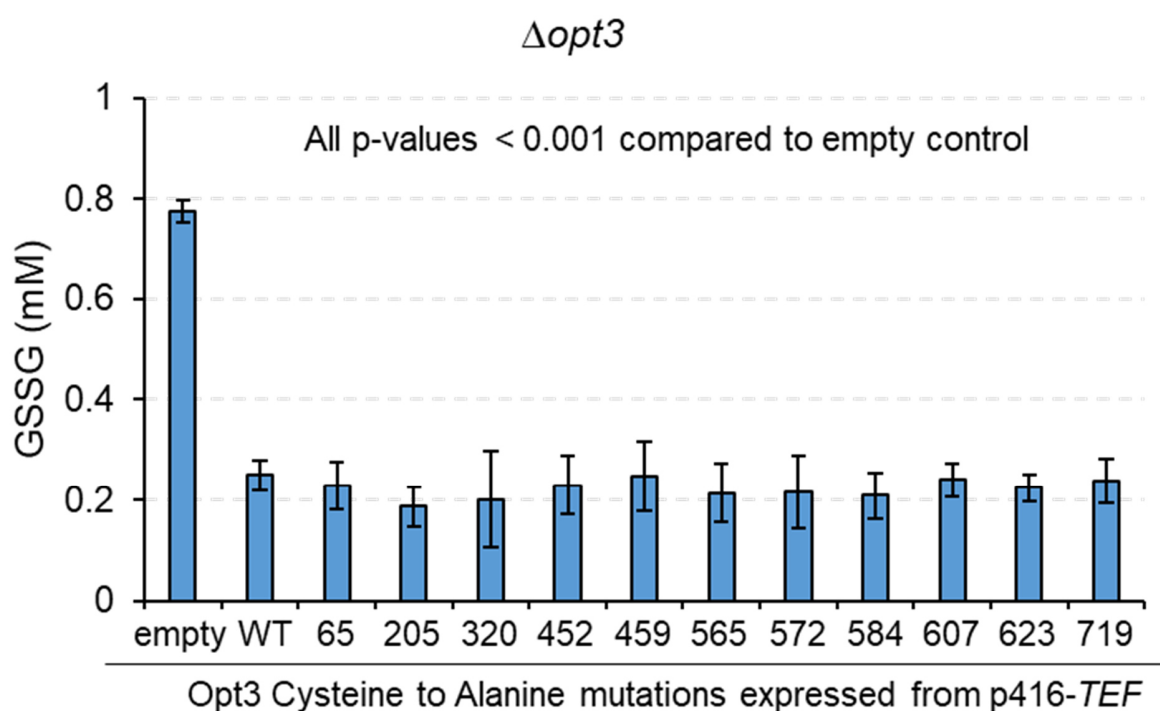


Figure 35 Opt3 is not activated via protein cysteine modifications. BY4742 $\Delta opt3$ cells were transformed with plasmids containing different *OPT3* mutations. Each mutation variant has a single Opt3 cysteine to alanine substitution. As positive and negative control, $\Delta opt3$ expressing *OPT3* and transformed with an empty plasmid was used, respectively. Whole cell lysates of all tested strains were prepared and GSSG was determined using the DTNB-recycling assay. At least three independent experiments were performed. Error bars denote standard derivations.

Previous experiments identified different conditions in which *OPT3* deletion and overexpression had no effect on cellular GSSG. Thus, it was next tested whether under such conditions transport activity was inhibited by cysteine modification.

2.6.3 Opt3 cysteine modifications do not inhibit GSSG transport activity

First tests, in which the Opt3 cysteines were individually mutated to alanine and expressed in cells, revealed that Opt3 function was not affected by the mutations showing that regulation is possibly independent of posttranslational cysteine modifications. In previous experiments situations were observed in which *OPT3* overexpression had no effect on cellular GSSG levels e.g., when *OPT3* was overexpressed in a $\Delta glr1$ background. Since, deleting *GLR1* results in a massive influx of GSSG into the vacuole I decided to rule out that a potential inhibition of Opt3 when *GLR1* was deleted, would falsify the before made observation that Opt3 function was Ycf1 independent.

A strain lacking *OPT3* and *GLR1* was transformed with plasmids containing *OPT3* as control and the different *OPT3* cysteine mutants. In all strains, both GSH and GSSG concentration was analyzed (Figure 36 and Figure 37).

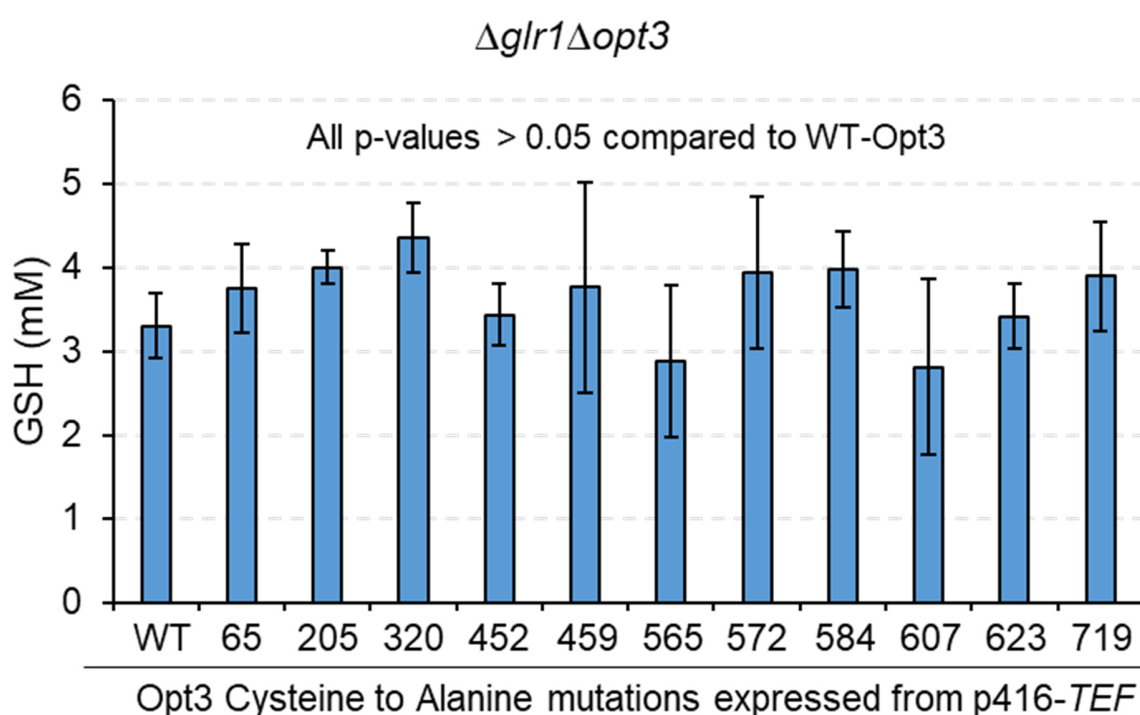


Figure 36 Opt3 cysteine mutants do not affect whole cell GSH content in a $\Delta glr1\Delta opt3$ background. $\Delta glr1\Delta opt3$ cells were transformed with plasmids containing different *OPT3* mutations. Each mutation variant had a single Opt3 cysteine to alanine substitution. As positive control, a $\Delta glr1\Delta opt3$ strain transformed with Opt3 was used. Whole cell lysates of all tested strains were prepared and GSH was determined using the DTNB-recycling assay. At least three independent experiments were performed. Error bars denote standard derivations.

The GSH concentration of $\Delta glr1\Delta opt3$ cells was similar when *OPT3* cysteine mutants or *OPT3* were overexpressed (p-values > 0.05). All strains had cellular GSH concentrations of approximately 3 mM (Figure 36). When GSSG concentration of the same strains was analyzed, cells containing the Opt3 mutants C65A, C320A, C584A, C607A and C719 had significant more GSSG than cells with the non-mutated Opt3 (p-values < 0.05). However, the GSSG content in these strains was maximum increased by ~0.18 mM. All other mutant strains had high GSSG concentrations of approximately 1 mM (Figure 37).

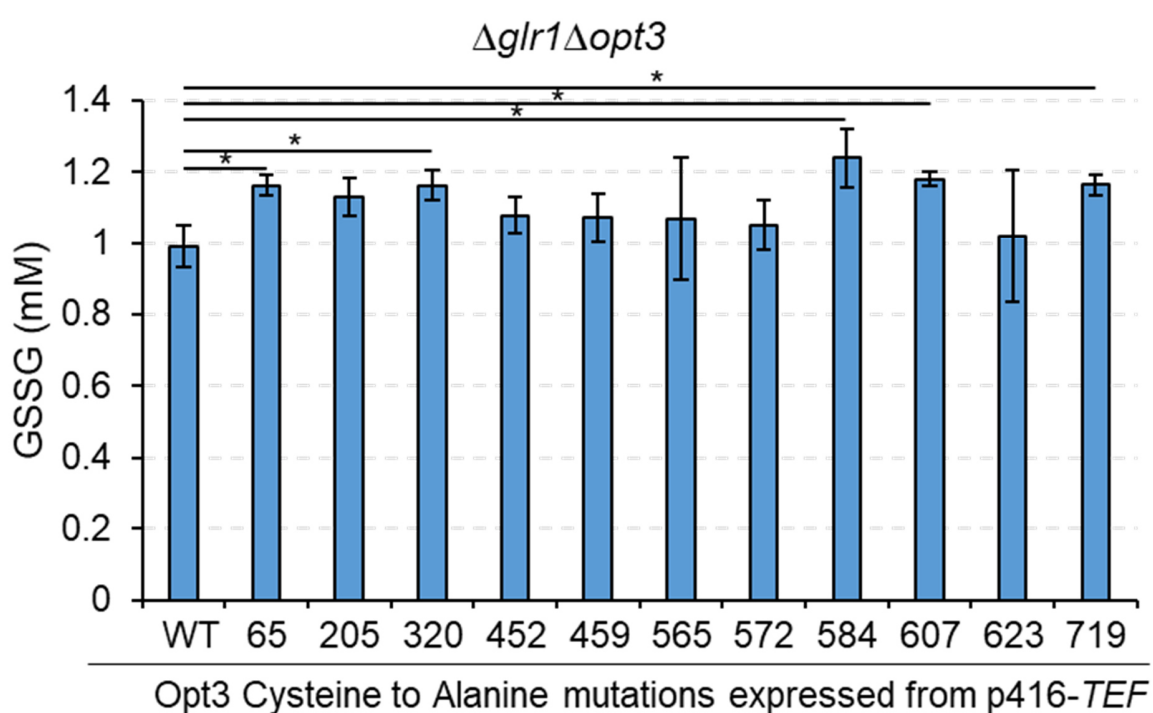


Figure 37 Opt3 is not inhibited via protein cysteine modifications. $\Delta glr1\Delta opt3$ cells were transformed with plasmids containing different *OPT3* mutations. Each mutation variant had a single Opt3 cysteine to alanine substitution. As positive control, a $\Delta glr1\Delta opt3$ strain transformed with wild-type Opt3 (p416-*TEF-OPT3*) was used. Whole cell lysates of all tested strains were prepared and GSH was determined using the DTNB-recycling assay. Error bars denote standard derivations. At least three independent experiments were performed. P-values were calculated using a student's t-test for statistical analysis (p < 0,05: *; p < 0,01: **; p < 0,001: ***).

The high GSSG content in cells expressing the different Opt3 cysteine mutation constructs verified former made observations that Opt3 was not localized in the vacuolar membrane and inhibited via post-translational cysteine modifications on Opt3 cysteine residues when *GLR1* was deleted.

In summary, the phenotype of single cysteine mutations did neither differ from Opt3 wild-type overexpression in a $\Delta opt3$ background nor when expressed in $\Delta glr1\Delta opt3$ mutant strain. These observations suggested that Opt3 was not activated or inhibited via post-translational cysteine modifications like protein-S-glutathionylation.

Up to this point the study on Opt3 revealed that the protein was localized in the membrane of the endoplasmic reticulum of *S. cerevisiae* cells and affected cellular GSSG levels when deleted or overexpressed. This effect on the cellular glutathione pool was increased with higher glutathione concentrations in the ER. However, when large amounts of GSH were imported into the cell through *OPT1* overexpression, the deletion or overexpression of *OPT3* had no effect on cellular GSSG. However, the results suggested that Opt3 as an ER transmembrane protein might mediate the export of GSSG from the ER lumen to the cytosol.

2.7 Physiological relevance of Opt3

After analyzing the molecular function of Opt3 the physiological relevance of Opt3 for the cell was analyzed. Thereby it was focused on the physiological coherences between Opt3 function and the thioredoxin system and its relevance in oxidative protein folding.

2.7.1 Opt3 function is independent of the thioredoxin system

S. cerevisiae has two partially redundant reducing systems in the cytosol: the thioredoxin (TRX) and glutaredoxin (GRX) system (Bao et al., 2009; Kumar et al., 2011; Montero et al., 2013; Morgan et al., 2013; Toledano et al., 2013; Zimmermann et al., 2020). In the cytosol the TRX system is represented by the reductases thioredoxin 1 (Trx1) and thioredoxin 2 (Trx2), which are reduced by the NADPH consuming enzyme thioredoxin reductase1 (Trr1) (Cheng et al., 2007). Interestingly, it was recently reported, that thioredoxin mutants paradoxically are not only sensitive to oxidative stress but also to reductive stress. As reason for the increased sensitivity to reductive stress, the high cellular GSH content in the $\Delta trx1\Delta trx2$ mutant was suggested (Trotter and Grant, 2002). Additionally, high cellular GSH levels were thought to cause a highly activated unfolded protein response (UPR) (Cuozzo and Kaiser, 1999; Trotter and Grant, 2002). Since according to the results presented so far in this dissertation, Opt3 is an ER GSSG exporter and thus might be crucial for ER glutathione redox homeostasis, it was investigated whether *OPT3* deletion and overexpression in a $\Delta trx1\Delta trx2$ deletion strain had a general growth effect and if Opt3 influences cell sensitivity to oxidative and reductive stress.

Therefore, the strains BY4742 WT, $\Delta opt3$, $p_{TEF}OPT3$, $\Delta trx1\Delta trx2$, $\Delta trx1\Delta trx2\Delta opt3$ and $\Delta trx1\Delta trx2p_{TEF}OPT3$ were serially diluted from 1 OD₆₀₀ to 1^{10⁻⁴} OD₆₀₀, dropped on a HC plate and incubated overnight before growth of the individual strains was compared (Figure 38).

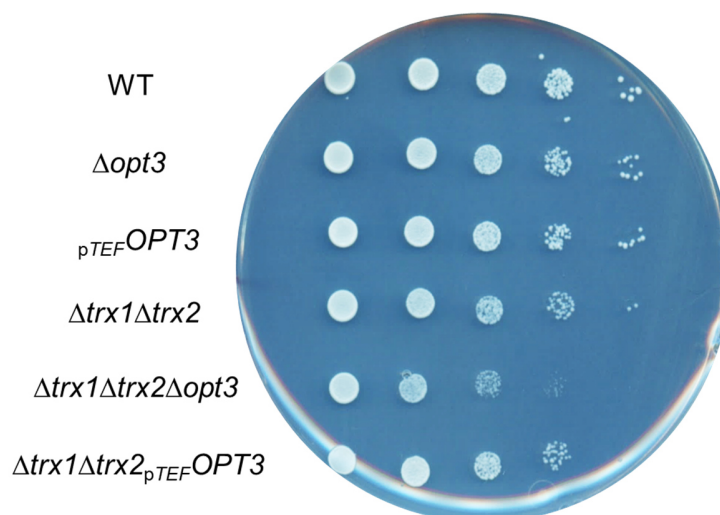


Figure 38 $\Delta trx1\Delta trx2\Delta opt3$ and $\Delta trx1\Delta trx2p_{TEF}OPT3$ are viable. BY4742 WT and the strains $\Delta opt3$, $p_{TEF}OPT3$, $\Delta trx1\Delta trx2$, $\Delta trx1\Delta trx2\Delta opt3$, $\Delta trx1\Delta trx2p_{TEF}OPT3$ grew 17h overnight before washed and resuspended to an OD₆₀₀ = 1 in sterile water. Next all tested strains got serial diluted and 3 μ l per dilution sample was dropped on a HC complete growth plate. Growth plates were incubated 24h before analyzed. At least three independent experiments were performed.

OPT3 single deletion ($\Delta opt3$) and *Opt3* overexpression ($p_{TEF}OPT3$) grew as wild-type. Also, the $\Delta trx1\Delta trx2$ double deletion strain had no difference in growth when compared to wild-type cells. Interestingly, when *OPT3* was deleted along with the two thioredoxins ($\Delta trx1\Delta trx2\Delta opt3$), cells grew slightly slower compared to a $\Delta trx1\Delta trx2$ and WT, whereas the strain $\Delta trx1\Delta trx2p_{TEF}OPT3$ had no growth phenotype (Figure 38). Since, the $\Delta trx1\Delta trx2\Delta opt3$ mutant had just a mild growth phenotype, I addressed whether reductive or oxidative stress would cause a stronger growth phenotype.

To test this a Halo-assay was performed. Therefore, the strains $\Delta opt3$, $p_{TEF}OPT3$, $\Delta trx1\Delta trx2$, $\Delta trx1\Delta trx2\Delta opt3$, $\Delta trx1\Delta trx2p_{TEF}OPT3$ and a BY4742 WT were equally plated on HC plates before a small filter pad was placed in the center of the plate. On the filter pad either 5 μ l of 3 M H₂O₂ or 3 M DTT solution was dropped as oxidant and reductant, respectively. Via diffusion of H₂O₂ or DTT through the growth plate a chemical concentration gradient was formed with high

concentrations in the center towards lower concentrations at the edge of the plate. After overnight growth at 30°C, growth was analyzed (Figure 39).

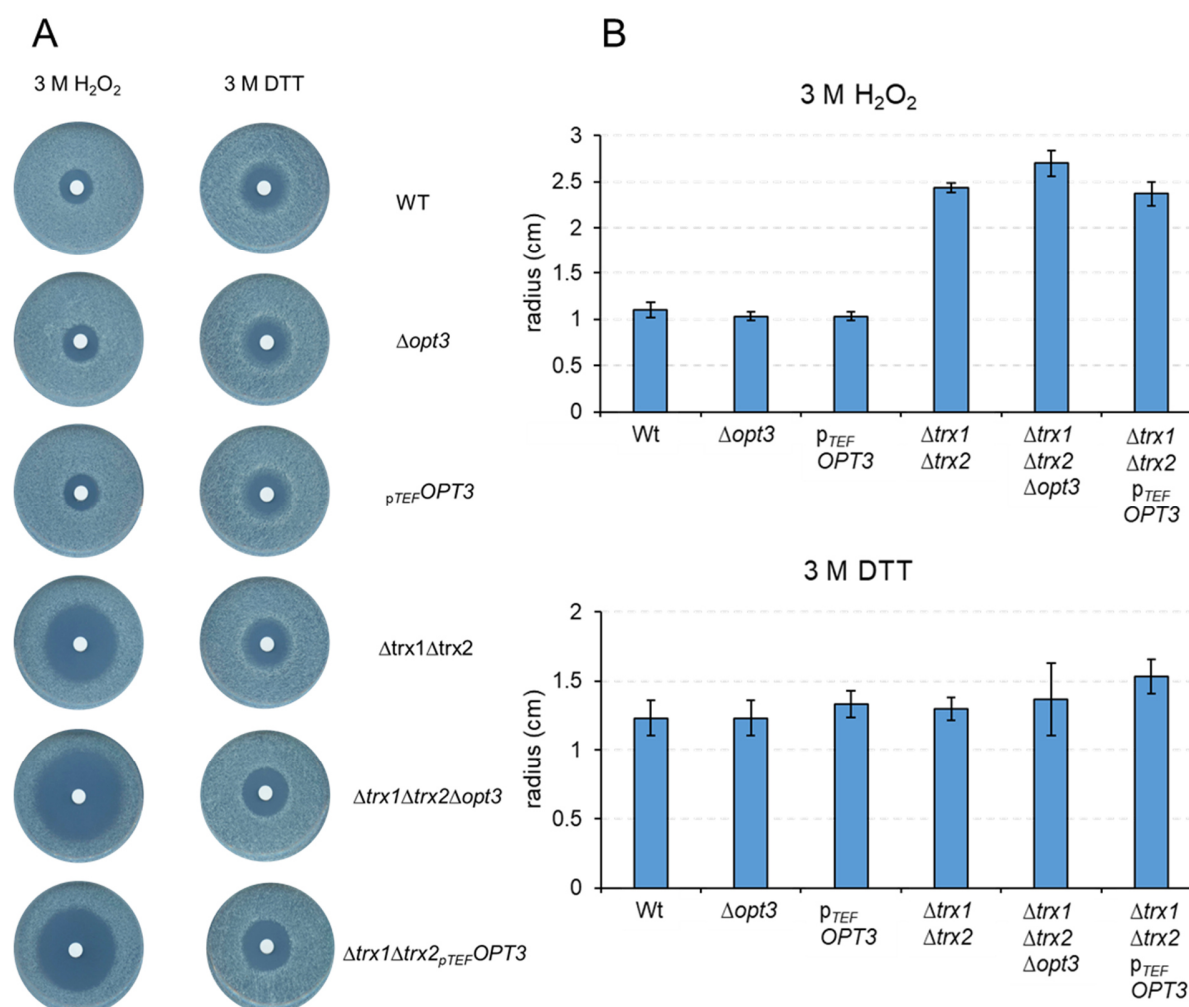


Figure 39 Genetical manipulation of *OPT3* expression levels does not alter $\Delta trx1\Delta trx2$ sensitivity to H₂O₂. To analyze sensitivity of the strains $\Delta opt3$, $p_{TEF}OPT3$, $\Delta trx1\Delta trx2$, $\Delta trx1\Delta trx2\Delta opt3$ and $\Delta trx1\Delta trx2 p_{TEF}OPT3$ to reductive and oxidative stress, Halo-tests with 3 M DTT and 3 M diamide were performed, respectively. Therefore, cells grew overnight to log-phase, washed and resuspended to an OD₆₀₀ of 0.1 and plated on a HC growth plate. 5 μ l of corresponding chemical treatment was applied on a test filter in the middle of the plate. Samples were incubated at 30°C for 17h before scanned (A) and the Halo radius was determined (B). At least three independent experiments were performed.

Interestingly, all the different mutant strains ($\Delta opt3$, $p_{TEF}OPT3$, $\Delta trx1\Delta trx2$, $\Delta trx1\Delta trx2\Delta opt3$, $\Delta trx1\Delta trx2 p_{TEF}OPT3$) had the same sensitivity to DTT as the BY4742 wild-type since there was no difference in the size of the formed Halos (p -values > 0.05) (Figure 39 B). When sensitivity of the

mutants $\Delta opt3$, $p_{TEF}OPT3$, $\Delta trx1\Delta trx2$, $\Delta trx1\Delta trx2\Delta opt3$, $\Delta trx1\Delta trx2p_{TEF}OPT3$ to H_2O_2 was tested and compared to WT cells it was obvious that the deletion of *TRX1* and *TRX2* in the $\Delta trx1\Delta trx2$ strain had a massive impact on H_2O_2 tolerance. While the wild-type formed a halo with a radius of approximately 1 cm, the halo in the $\Delta trx1\Delta trx2$ background had a size of 2.5 cm ($p = 3.6 * 10^{-5}$). Overexpressed *OPT3* in the $\Delta trx1\Delta trx2$ background had a similar halo size of approximately 2.5 cm. However, when *OPT3* was deleted in combination with the TRX system the halo was slightly, although not significantly, larger compared to $\Delta trx1\Delta trx2$ ($p = 0.064$) (Figure 39 B).

In summary deletion or overexpression of *OPT3* paired with deleted TRX system affected growth only moderately and did not affect the resistance to reductants and oxidants. However, it was surprising that $\Delta trx1\Delta trx2$ were not sensitive to DTT treatment as reported before (Trotter and Grant, 2002).

2.7.2 *OPT3* mutant strains are resistant to ER-stress

In 2017, Ponsero and colleagues observed a relationship between high cytosolic glutathione and ER stress, mentioning that under ER-stress conditions, cytosolic GSH concentration is increased and thus more GSH is diffusing into the ER. Beside the stimulation of GSH production, ER-stress activates the unfolded protein response (UPR), which promotes the expression of *ERO1*. Paradoxically both, a higher influx of GSH into the ER and the upregulated *ERO1* expression increase the ER oxidative capacity at least to a certain threshold as GSH import is negatively feedback regulated (Ponsero et al., 2017). As reason for this Ponsero et al. suggest that GSH in can indirectly lead to the reduction of the Ero1 regulatory disulfide bonds, which switches Ero1 into its high activity state (Ponsero et al., 2017). Since, there was an obvious relation between ER glutathione and the UPR, I wondered if *Opt3* has an influence on ER-stress tolerance and UPR activation.

As a first test if *OPT3* deletion or overexpression had an impact on ER-stress tolerance a drop dilution assay was performed. Thereby, the strains $\Delta opt3$, $p_{TEF}OPT3$ and WT grew overnight at 30°C, serially diluted the next day. 5 μ l per dilution was dropped on HC plates containing 1 μ g/ml tunicamycin (Figure 40). Tunicamycin is a commonly used antibiotic to introduce ER-stress and thus is often used for UPR activation. Thereby, tunicamycin is inhibiting the N-linked-glycosylation of proteins in the ER resulting in an accumulation of unfolded proteins (Guha et al., 2017).

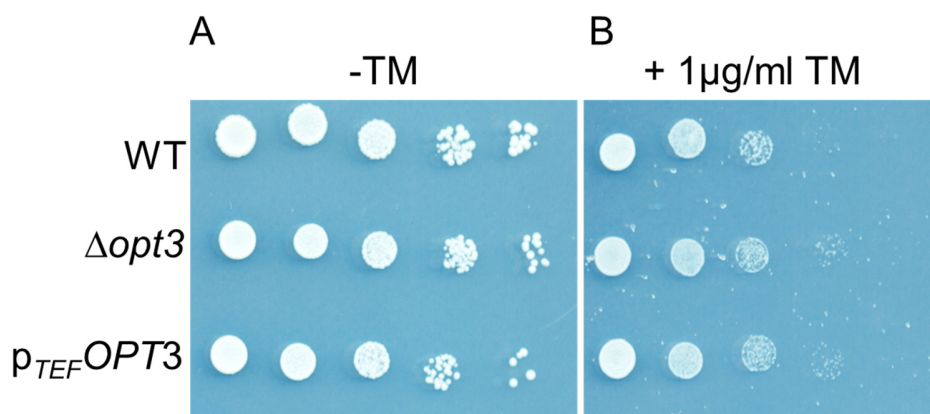


Figure 40 *OPT3* expression mutants grow like WT cells during tunicamycin induced ER-stress. Resistance of the strains BY4742 WT, $\Delta opt3$ and $p_{TEF}OPT3$ to tunicamycin induced ER-stress was analyzed. All tested strains were incubated in HC and grew overnight to an OD_{600} of approximately 3.5. Next day, 1 OD_{600} was harvested and resuspended into 1 ml sterile water after washing once. Serial dilutions of each sample were dropped onto HC plates containing either 1 $\mu\text{g/ml}$ tunicamycin (B) or no tunicamycin (A). All growth plates were incubated for 24h at 30°C before growth of the tested strains was compared. The experiment was repeated at least three times.

When the strains $\Delta opt3$ and $p_{TEF}OPT3$ were dropped on HC plates without tunicamycin, they grew similar as WT cells (Figure 40 A). However, when grown on HC plates with 1 $\mu\text{g/ml}$ tunicamycin, all tested strains grew worse compared to untreated cells (Figure 40 B).

To verify that *OPT3* deletion and overexpression did not alter ER-stress tolerance, a second experiment was performed. Thus, Carsten Mattes from the department of *Medical Biochemistry & Molecular Biology* in *Homburg, Germany* carried out a growth assay addressing the induction of UPR. In this assay, the strains $\Delta opt3$ and $p_{TEF}OPT3$ were mixed with serial diluted tunicamycin solutions with final concentrations reaching from 0 to 2 $\mu\text{g/ml}$. A wild-type and $\Delta ire1$ mutant strain, deficient in activating the UPR, served as positive and negative growth controls, respectively. After 18h incubation overnight at 30°C, the OD_{600} of each sample was determined (Figure 41 B).

The strains $\Delta opt3$, $p_{TEF}OPT3$ and wild-type grew in absence of tunicamycin to an OD_{600} of 1 while $\Delta ire1$ grew to an OD_{600} of 0.9. When the tunicamycin concentration in the growth media was 0.5 $\mu\text{g/ml}$ cell growth of all tested strains was impaired. WT, $\Delta opt3$ and $p_{TEF}OPT3$ cells grew to an OD_{600} of approximately 0.8. Notably, $\Delta ire1$ cells which were exposed to 0.5 $\mu\text{g/ml}$ or higher did not grow. At tunicamycin concentrations of 0.8 $\mu\text{g/ml}$ the growth of wild-type was 50% slower compared to growth in tunicamycin free media ($p = 1.01 \cdot 10^{-9}$). Like WT cells, $\Delta opt3$ and $p_{TEF}OPT3$ cells grew to comparable OD_{600} of 0.4 in media with 0.8 $\mu\text{g/ml}$ (p -values > 0.05). When tunicamycin in the media reached a concentration of around 1.2 $\mu\text{g/ml}$, WT, $\Delta opt3$ and $p_{TEF}OPT3$ were not viable.

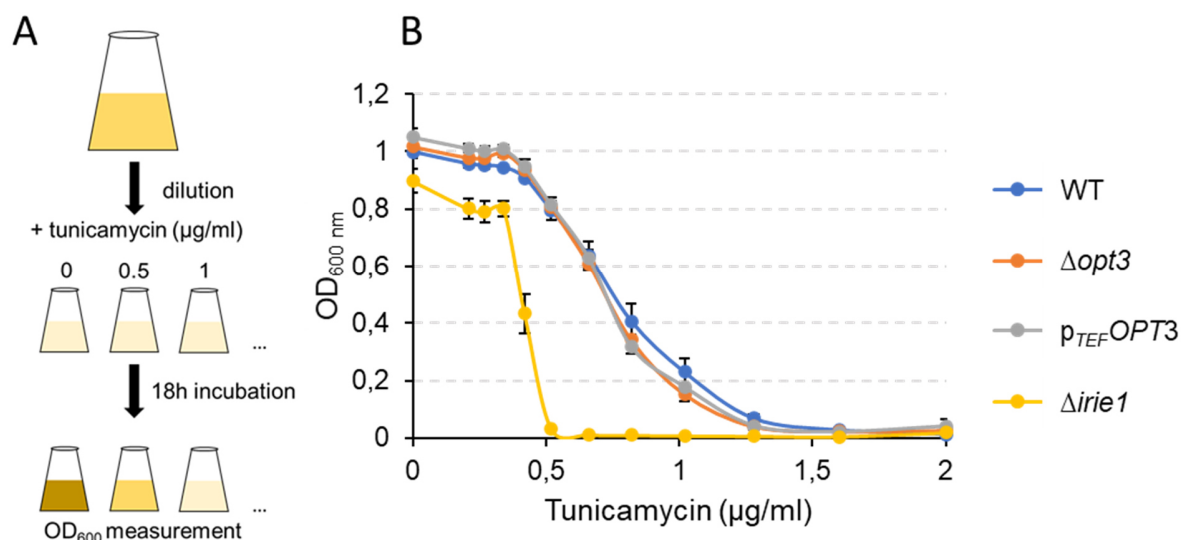


Figure 41 Altering *OPT3* expression levels does not influence cell viability during ER-stress. As illustrated in A, BY4742 WT, $\Delta opt3$, $p_{TEF}OPT3$ grew in HC media overnight before harvested and resuspended in fresh media to an $OD_{600} \sim 0.01$. To induce ER-stress, samples were treated with different concentrations of tunicamycin (from 0 to 2 µg/ml) before incubated for 18h at 30°C. After incubation the OD_{600} of each sample was analyzed (B). For statistical purpose the experiment was repeated at least three times. Error bars denote standard derivations.

In summary, these results suggested that Opt3 has no impact on ER-stress resistance. While cells depleted for the UPR transmitting protein Ire1 showed a strong sensitivity to tunicamycin, cells without or enhanced levels of Opt3 showed the same growth behavior as wild-type cells.

2.7.3 Opt3 abundance is important for a rapid unfolded protein response

Viability assays demonstrated that manipulation of *OPT3* expression levels had no impact on cellular tolerance to tunicamycin. Since the effect of a protein on cell viability under certain conditions can easily be masked by suppressors, experiments were performed, which investigated the role of Opt3 on UPR activation shortly after induction of ER-stress (Hou and Schacherer, 2017; Liebman and Sherman, 1976; van Leeuwen et al., 2020). In *S. cerevisiae* the unfolded protein response is mediated by the homodimerization and autophosphorylation of the membrane embedded protein Ire1 (Chakraborty et al., 2016; Chawla et al., 2011). Activated Ire1 splices the cytosolic localized *HAC1* mRNA, which leads to its translation and the production of Hac1p transcription factor (Kawahara et al., 1998). Hac1p promotes the transcription of several genes including: *PDI1* and *KAR2* a member of the HSP70 chaperone family, localized in the ER lumen (Ogawa and Mori, 2004).

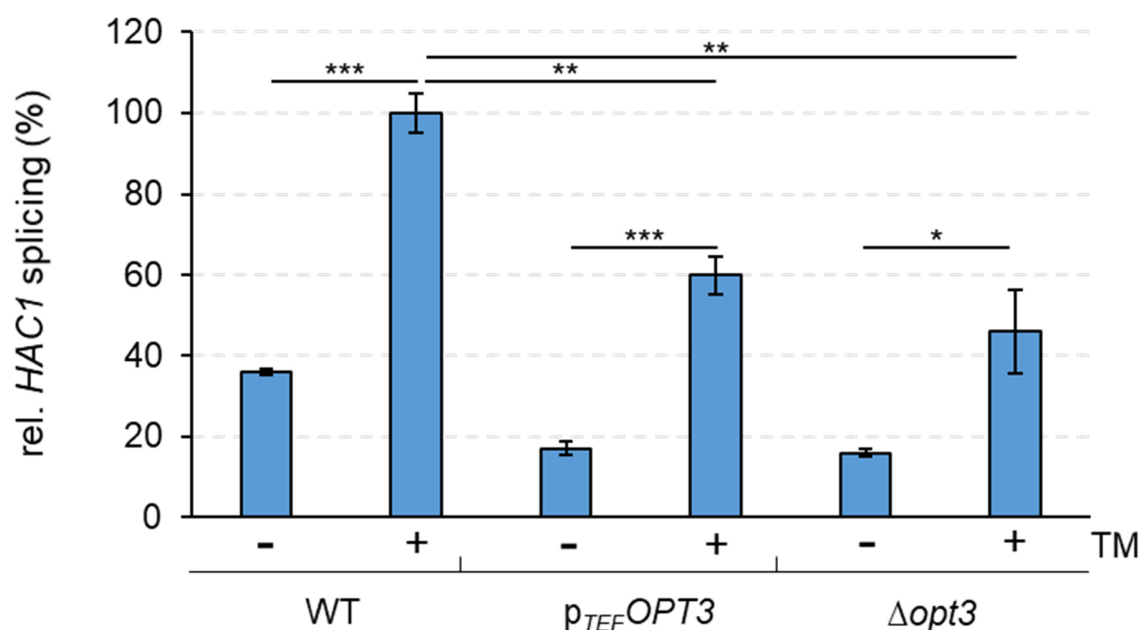


Figure 42 Low and high Opt3 copy numbers decrease the UPR. *HAC1* splicing of the strains BY4742 WT, $\Delta opt3$ and $p_{TEF}OPT3$ was analyzed. RNA was isolated from 5 OD₆₀₀ units of each tested strains treated with 1.5 μ g/ml tunicamycin or without tunicamycin (TM) treatment using the *RNeasy RNA Isolation Kit from QIAGEN*. Next, cDNA was synthesized. Afterwards, quantitative-real time PCR (qPCR) was performed with primers binding to spliced *HAC1* cDNA for quantification. Analysis of relative gene expression was carried out using the 2^{-DDCT} method as described by Livak et al. (Livak and Schmittgen, 2001). The experiment was repeated at least three times. The experiment was performed in a collaboration with the department of *Medical Biochemistry & Molecular Biology in Homburg* by Carsten Mattes. Error bars denote standard derivations. P-values were calculated using a student's t-test for statistical analysis ($p < 0,05$: *; $p < 0,01$: **; $p < 0,001$: ***).

To test if Opt3 function is related to the UPR, it was first tested whether *OPT3* deletion or overexpression had an impact on *HAC1* splicing. Therefore, the cells $\Delta opt3$, $p_{TEF}OPT3$ and wild-type were incubated for 1h in media with and without 1.5 μ g/ml tunicamycin. Afterwards the mRNA levels of spliced *HAC1* were analyzed by quantitative PCR (qPCR) (Figure 42). In Figure 42 relative *HAC1* splicing is illustrated. Thereby, measured values were normalized to tunicamycin treated wild-type. Hence, the amount of *HAC1* splicing in wild-type cells treated with tunicamycin represents 100%. Interestingly, both the deletion and overexpression of *OPT3* caused approximately 50% less *HAC1* splicing under non-stressed growth conditions compared to WT (p -values < 0.001). When $\Delta opt3$, $p_{TEF}OPT3$ and WT were treated with tunicamycin all strains had significantly increased *HAC1* splicing (p -values < 0.05). Remarkably, *HAC1* splicing in the backgrounds $\Delta opt3$ and $p_{TEF}OPT3$ was approximately 40% less after TM treatment in contrast to WT cells (p -values < 0.01). But there was no difference in *HAC1* splicing between cells with *OPT3* deletion or overexpression ($p = 0.16$). This observation suggested that Opt3 function might

modulate short time activation of UPR. Hence, it was now tested whether the influence of *OPT3* expression levels on *HAC1* splicing was also represented in the expression levels of genes, activated by the Hac1 transcription factor.

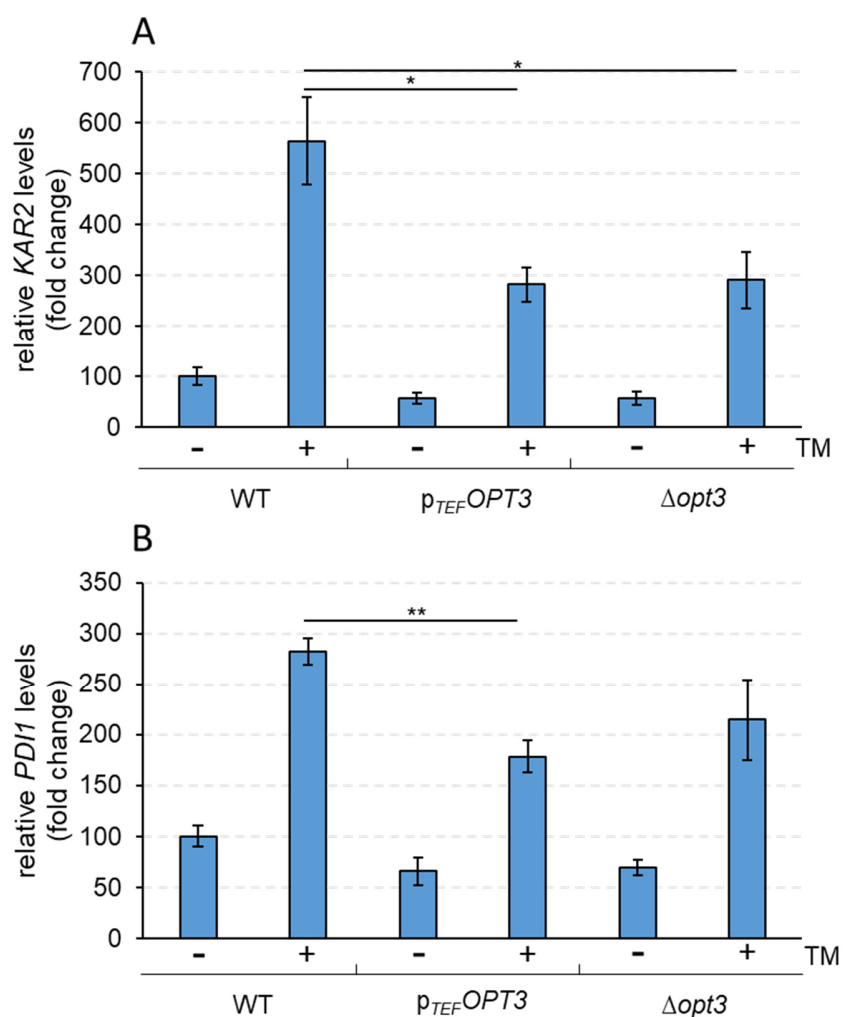


Figure 43 Impaired *HAC1* splicing in *OPT3* deletion and overexpression strains leads to lower expression of *KAR2* and *PDI1* during ER-stress. *KAR2* (A) and *PDI1* (B) expression levels of the strains BY4742 WT, $\Delta opt3$ and *p_{TEF}OPT3* were analyzed. RNA was isolated from 5 OD₆₀₀ units of each tested strain treated with 1.5 μ g/ml tunicamycin (TM) or without tunicamycin treatment using the *RNeasy RNA Isolation Kit from QIAGEN*. Next, cDNA was synthesized. Afterwards, quantitative-real time PCR (qPCR) was performed with primers binding to spliced *HAC1* cDNA for quantification. Analysis of relative gene expression was carried out using the 2^{-DDCT} method as described by Livak et. al. (Livak and Schmittgen, 2001). The experiment was performed in a collaboration with the department of *Medical Biochemistry & Molecular Biology in Homburg* by Carsten Mattes. Error bars denote standard derivations. The experiment was repeated at least three times for statistical analysis. P-values were calculated using a student's t-test for statistical analysis (p < 0,05: *; p < 0,01: **; p < 0,001: ***).

Therefore, the mRNA levels of *PDI1* and *KAR2* were analyzed by qPCR with and without induced ER-stress by 1.5 µg/ml tunicamycin. In Figure 43, the expression levels of *PDI* and *KAR2* are normalized to WT expression levels without tunicamycin treatment.

In parallel to the before observed phenotypes in *HAC1* splicing, both deletion and overexpression of *OPT3* influenced *KAR2* expression after treatment with tunicamycin. Hence, *KAR2* mRNA levels in the tunicamycin treated strains $\Delta opt3$ and $p_{TEF}OPT3$ were about 50% lower compared to mRNA levels measured in the WT background (p -values < 0.05) (Figure 43 A). A similar pattern was observed when *PDI1* expression in $\Delta opt3$ and $p_{TEF}OPT3$ was compared to WT expression levels. However, while the difference in *PDI1* expression after tunicamycin treatment was significantly lower in $p_{TEF}OPT3$ cells ($p = 0.002$) it was not in the $\Delta opt3$ strain ($p = 0.08$) when compared to WT (Figure 43 B).

In summary inducing ER-stress revealed interesting observations. Manipulating *OPT3* expression levels decreased the UPR and thus, impaired the response of cells to ER-stress. Since both deletion and overexpression of *OPT3* decreased UPR, I next speculated how *Opt3* frequency could manipulate the activation of the UPR.

2.7.4 *OPT3* expression levels do not affect E_{GSH} in the ER lumen

It was recently reported that protein-S-glutathionylation of PDI in humans might influence UPR activation (Halloran et al., 2013; Townsend et al., 2009). For protein-S-glutathionylation the GSH:GSSG ratio can be important, since lowering the glutathione ratio might facilitate the disulfide exchange between GSSG and protein thiols (Wang et al., 2014; Wang and Sevier, 2016). Because deletion and overexpression of *OPT3* potentially lead to an accumulation and depletion of ER GSSG respectively, I speculated whether a change in *OPT3* expression would alter the E_{GSH} in the ER and thus UPR activation was impaired.

To monitor the ER glutathione redox state of wild-type, $\Delta opt3$ and $p_{TEF}OPT3$, cells were transformed with the plasmid p416-*MET25-SS-roGFP2-GRX1-HDEL*, containing a roGFP2-GRX1 sensor with a N-terminal ER targeting signal sequence (SS) and a C-terminal ER retention tag (HDEL). In the same experiment it was tested whether ER glutathione in WT, $\Delta opt3$ and $p_{TEF}OPT3$ was influenced during an oxidative burst of H_2O_2 . H_2O_2 treatment indirectly leads to the formation of cellular GSSG. Thus, the roGFP2 signal was measured with and without serial diluted H_2O_2 samples (Figure 44).

In WT cells, the steady state oxidation of ER-targeted roGFP2-Grx1 was about 70%. Interestingly, the ER glutathione pool remained stable even after the addition of 1 mM H₂O₂ in WT cells (Figure 44 A). However, when the ER glutathione redox state in $\Delta opt3$ and $p_{TEF}OPT3$ was determined roGFP2 steady state oxidation was similar to the roGFP2 signal in WT (Figure 44 B, C). Also, comparable to the observation in WT cells, extracellular application of H₂O₂ did not alter the sensor oxidation state in $\Delta opt3$ and $p_{TEF}OPT3$ mutant backgrounds, implying a robust non-effected ER glutathione redox state.

Although, monitoring E_{GSH} of the redox couple 2GSH:GSSG in the strains $\Delta opt3$ and $p_{TEF}OPT3$ did not show any difference to WT, the experiment demonstrated, that the endoplasmic reticulum was strongly oxidized. However, it remains unclear why an oxidative burst like treatment with 1 mM H₂O₂ did not promote a sensor response in the ER.

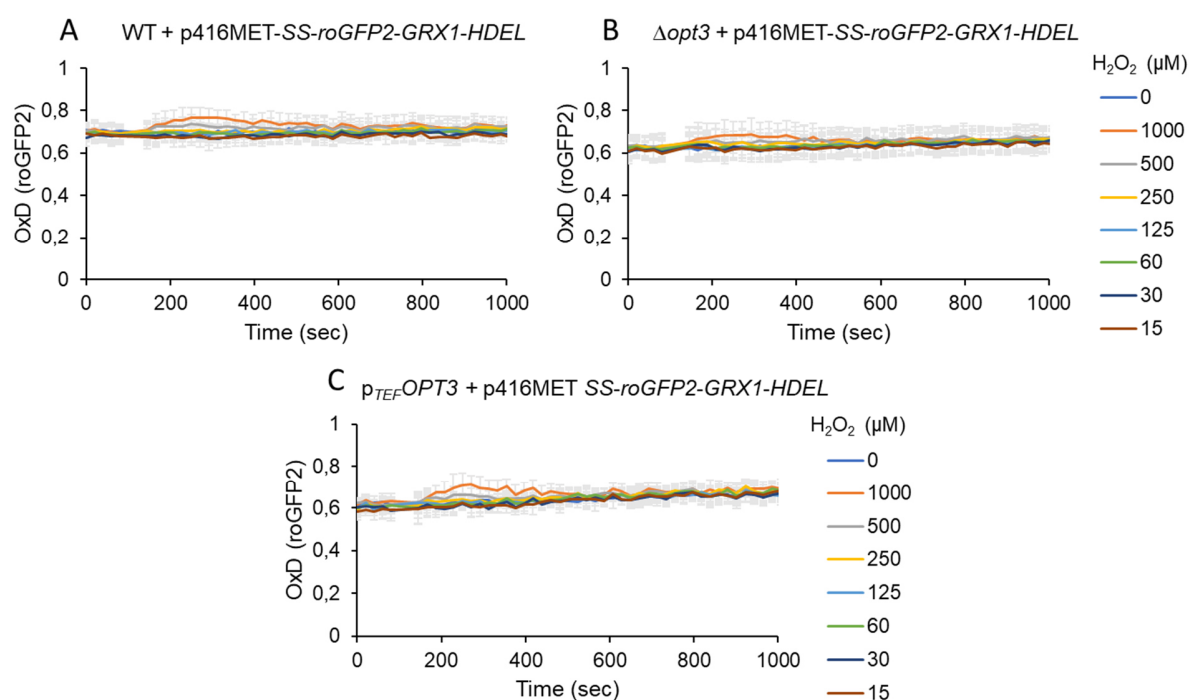


Figure 44 The ER targeted roGFP2-GRX1 redox-sensor is strongly oxidized. The strains BY4742 WT, $\Delta opt3$ and $p_{TEF}OPT3$ containing the ER-localized E_{GSH} sensor roGFP2-GRX2 (p416-MET25-SS-roGFP2-GRX2-HDEL) grew overnight before 7.5 OD₆₀₀ units (where one unit represents 1_{OD600} / 1 ml) were resuspended in MES/TRIS pH 6 buffer and transferred into a 96 well plate. Fluorescent signal of the samples was recorded for 10 cycles before paused and application of buffer or linear diluted H₂O₂ concentrations. Immediately after treatment measurement was continued. All measurements were repeated for at least three times. Error bars denote standard derivations.

In summary experiments demonstrated that Opt3 is an ER transmembrane protein, important for cellular glutathione homeostasis. Thereby, Opt3 might export formed GSSG from the ER lumen to the cytosol.

3 Discussion

Glutathione (GSH) is the most abundant small thiol in almost all eukaryotic cells (Zechmann et al., 2011). It is involved in a variety of cellular processes like the detoxification of ROS or xenobiotics (Hanschmann et al., 2013). Moreover, e.g., during the reduction of ROS two GSH molecules can be covalently linked and glutathione disulfide (GSSG) is produced (Wu et al., 2004).

In *S. cerevisiae* glutathione can either be imported into the cell or is synthesized exclusively in the cytosol (Bourbouloux et al., 2000). However, glutathione is present in all cellular compartments (Morgan et al., 2013; Oestreicher and Morgan, 2018; Scirè et al., 2019). While the glutathione redox potential in the cytosol, the mitochondrial matrix or in peroxisomes is extremely reduced, it appears that the glutathione pool in the secretory pathway is more oxidized (Hwang et al., 1992; Morgan et al., 2013). GSH and GSSG are negatively charged molecules under physiological pH and hence, cannot freely diffuse through biological membranes (Bachhawat et al., 2013). Thus, cellular glutathione transporter must exist, which mediate glutathione transport between cellular compartments. One well-studied glutathione transporter in yeast is the proton-coupled oligopeptide transporter Opt1 localized in the plasma membrane (Bourbouloux et al., 2000). Opt1 belongs to the oligopeptide transporter (OPT) family of which a second member (Opt2) exists in yeast. Opt2 is localized in the peroxisomal membrane and its deletion perturbs cytosolic glutathione homeostasis (Elbaz-Alon et al., 2014). However, a direct transport of GSH and GSSG by Opt2 was not demonstrated (Elbaz-Alon et al., 2014). Recently, the uncharacterized ORF *YGL114W* was reported to encode a third member of the OPT-family, named Opt3 in this dissertation (Pearson and Schweizer, 2002).

Since so far nothing is known about the putative oligopeptide transporter Opt3, the aim of this thesis was to characterize Opt3 and to investigate a potential role in glutathione homeostasis. Thereby, I identified Opt3 as an ER-localized GSSG exporter.

3.1 *OPT3* expression influences cellular GSSG levels

Since Opt3 was described as a putative member of the oligopeptide transporter family, it was tested if *OPT3* deletion or overexpression mutants showed changes in whole cell GSSG concentration. One must consider that GSSG measured in whole cell lysates cannot have a cytosolic origin, since the cytosolic glutathione pool is robustly reduced (Morgan et al., 2013).

Thus, GSSG is highly compartmentalized within the cell. Changes of whole cell GSSG concentration upon genomic manipulation of a glutathione transporter can provide indirect information of GSSG transport between the cytosol and a cellular compartment, as previously shown for the vacuolar GSSG transporter Ycf1 (Morgan et al., 2013). Hence, these measurements might also serve as a suitable approach for investigation of the elusive function of other putative glutathione transporters (Morgan et al., 2013). In so doing, I observed an effect of *OPT3* deletion and overexpression on whole cell GSSG concentration. Although not significant, the deletion of *OPT3* led to slightly higher GSSG concentrations. However, in the *OPT3* overexpression strain almost all GSSG was depleted (Figure 14).

Interestingly, the pattern of GSSG changes observed in *OPT3*-mutants was opposing to the previously reported *YCF1*-mutant strains (Morgan et al., 2013). Ycf1 is an ABC-C-transporter, which transports GSSG from the cytosol into the vacuole where it is stored. The overexpression of *YCF1* caused an increase of total cellular GSSG when measured in whole cell lysates, while its deletion decreased the GSSG content, since GSSG remains in the cytosol where it becomes efficiently reduced by Glr1 (Morgan et al., 2013). Thus, observations made from whole cell GSSG measurements of Opt3-mutant strains strongly suggest that cells without Opt3 accumulate GSSG (Figure 45 E), while high levels of Opt3 promote the export of GSSG to the cytosol, where it is reduced by Glr1 (Figure 45 F).

Of course, determining transport activity only based on measurements of the putative substrate concentration in cell lysates has limitations. One might speculate, that Opt3 rather directly reduces GSSG of a certain subcellular compartment. However, enzymes known to reduce GSSG e.g., glutaredoxins are soluble enzymes, which have a specific TRX-fold (Hanschmann et al., 2013). Also, the main GSSG reducing enzyme in the cytosol and mitochondrial matrix, Glr1, is a soluble enzyme which uses NADPH as an electron donor with FAD as coenzyme (Outten and Culotta, 2004). FAD binding domains are often formed by a conserved Rossmann fold, which tertiary structure typically consists out of a repeating series of a α -sheet flanked by two β -sheets ($\beta\alpha\beta$) (Outten and Culotta, 2004; Yu and Zhou, 2007b). However, Opt3 does neither possess a TRX- nor a typical Rossmann fold suggesting that it does not reduce GSSG directly.

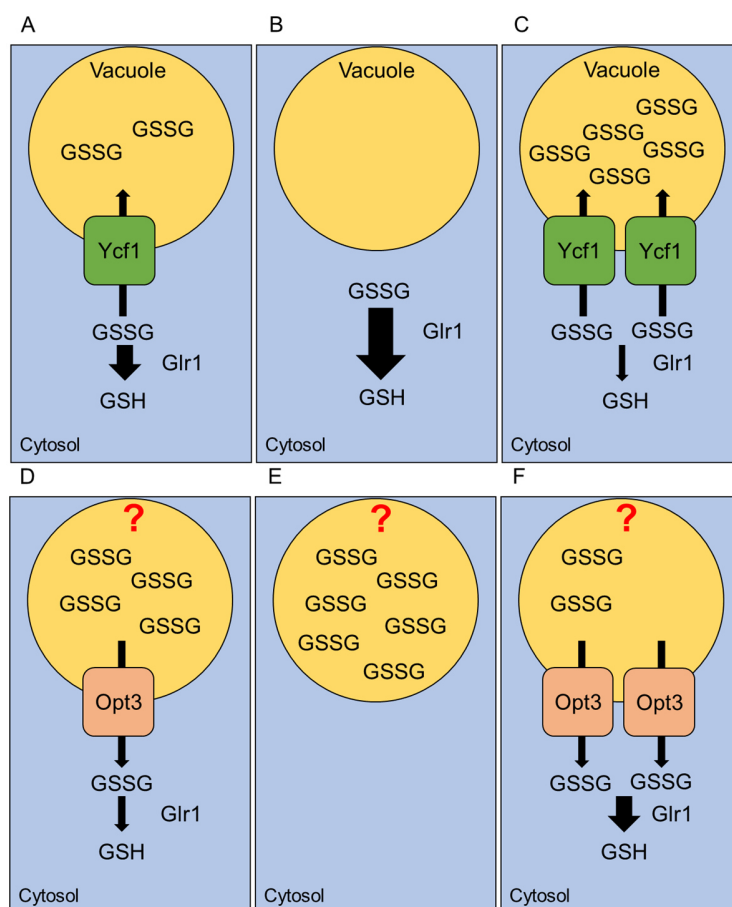


Figure 45 Opt3 exports GSSG from a cellular compartment into the cytosol. (A) Glr1 mediated GSSG reduction and GSSG transport via Ycf1 from the cytosol into the vacuole are in a kinetic competition under endogenous conditions. Total depletion of Ycf1 leads to the complete reduction of cytosolic GSSG by Glr1, which causes low GSSG concentrations in whole cell lysates (B). Vice versa, increases *YCF1* overexpression GSSG transport into the vacuole, where it is stored. Hence, GSSG content measured in whole cell lysates is increased (C). However, the pattern of GSSG concentration found in whole cell lysates of *OPT3* mutant strains was opposite to *YCF1* mutants. In a wild-type cell GSSG is exported by Opt3 from a subcellular compartment into the cytosol where it is reduced by Glr1 (D). When *OPT3* is deleted, GSSG accumulates in the compartment and is not reduced (E). Vice versa, *OPT3* overexpression leads to an increased export of GSSG, which lowers the GSSG content found in whole cell lysates (F).

It was recently speculated, that in mammals a mechanism must exist, which provides reductive equivalents to the ER, analogous to the well-studied DsbD-enzyme in bacteria (Elgaard et al., 2018). In bacteria the transmembrane protein DsbD transfers reductive equivalents from cytosolic thioredoxins to the periplasm localized DsbC, which is important to maintain its isomerase activity. DsbD consists out of three structural motifs: i. the thioredoxin-like domain DsbD α , ii. DsbD γ and iii. the transmembrane bound domain DsbD β (Goulding et al., 2002). The transfer of electrons from the cytosol to the periplasm is mediated via multiple thiol-disulfide exchange reactions between cysteine pairs of the individual subunits (Pan and Bardwell, 2006; Rietsch et al., 1997,

1996). Usually redox-active cysteine pairs in a protein are in close proximity, like the typical CXXC-motif in many TRX-fold proteins e.g., thioredoxins and glutaredoxins (Schultz et al., 1999). Although, analysis of Opt3 topology with different algorithms show that it has ~12 transmembrane domains (depending on the algorithm) and eleven cysteine residues (Supplementary Figure 1), cysteines in Opt3 are equally distributed and do not possess a TRX-like CXXC active site motif. Aside from that I could demonstrate that mutation of individual cysteines, did not alter the effect of *OPT3* overexpression on cellular GSSG and thus it is highly unlikely that Opt3 can be considered a DsbD-like protein, either transferring electrons directly to GSSG or via reduction of an unknown GSSG reducing enzyme (Figure 35).

Interestingly, cellular GSSG was strongly decreased as consequence of *OPT3* overexpression, while *OPT3* deletion cells had not a significant change in cellular GSSG concentration compared to WT. How can this be explained? Ho et al. summarized information of 21 different proteome data sets, to estimate protein copy numbers of approximately 90% of *S. cerevisiae* proteins (Ho et al., 2018). According to this study, Opt3 in yeast WT cells is not abundant with approximately 1160 molecules per cell. However, the protein copy number might be even as low as 21 molecules per cell (Kulak et al., 2014). Overexpression of the *OPT3* gene was realized by substitution of the endogenous promoter with the strong and constitutive *TEF1* promoter. *TEF1* encodes for the translation elongation factor EF1-alpha, of which ~750 000 copies are present in the cell (Ho et al., 2018). Thus, *OPT3* overexpression might have a dramatic effect on cellular GSSG compared to the deletion mutant. Apart from that, it might be that GSSG formation in the corresponding subcellular compartment is regulated. Hence, deletion of *OPT3* does not further increase total cellular GSSG. For instance, recently the mechanism of glutathione transport into the ER was identified (Ponsero et al., 2017). Through high Ero1 activity in the ER lumen, GSH is indirectly oxidized to GSSG. However, the import of GSH into the ER is regulated and thus GSH, and consequently the GSSG content in the ER lumen, is limited (Ponsero et al., 2017).

Altogether, first experiments shown in this dissertation indicate that Opt3, as a member of the OPT family, is transporting GSSG from a subcellular compartment into the cytosol where it is reduced to GSH. Accordingly, this raises the question, where Opt3 is localized. Most cellular compartments are known to be highly reduced and thus cannot be the reservoir of cellular GSSG e.g., the mitochondrial matrix or peroxisomes have GSH:GSSG ratios of 50 000:1 similar to ratios found in the cytosol (Calabrese et al., 2019; Elbaz-Alon et al., 2014). While GSSG can be stored in the vacuole, the ER has a reported GSH:GSSG ratio of approximately 3:1 and thus the ER might be a second cellular pool of GSSG (Hwang et al., 1992).

3.2 Opt3 is a transmembrane protein of the ER

Measurements of GSSG in cell lysates of *OPT3* deletion and overexpression mutants, revealed that Opt3 exports GSSG from a subcellular compartment. Hence, it was next addressed, which cellular GSSG pool was affected by Opt3. Therefore, Opt3 localization in the cell was analyzed.

To determine Opt3 localization it was C-terminally tagged with the fluorescent protein ymNeonGreen. Additionally, the expression of *OPT3-NeonGreen* was increased by substitution of the endogenous *OPT3* promoter with the *ADH1* promoter. To visualize the ER, Sec63 was tagged with mCherry, a red fluorescent protein tag. Indeed, the Opt3 signal co-localized with Sec63. Thus, co-localization studies clearly demonstrated, that Opt3 was an ER transmembrane protein.

Using the strong *ADH1* promoter was necessary because no signal was detectable expressing *OPT3-NeonGreen* under the control of the endogenous *OPT3* promoter. *ADH1* encodes the cytosolic localized alcohol dehydrogenase 1 (Adh1) of which approximately 100 000 copies are present in the cell (Ho et al., 2018). These are about ten times more molecules than reported for Opt3 (Ho et al., 2018). Please note, that protein frequency is not only dependent upon gene expression. Furthermore, translation and protein degradation can regulate protein abundance (Wu et al., 2021). Nevertheless, the expression of *OPT3-NeonGreen* under the control of an *ADH1* promoter allowed visualization. Curiously, previous experiments demonstrated that expressing N-terminally GFP-tagged *OPT3* under the strong constitutive *GPD* promoter led to dual localization of Opt3 in the ER and the vacuole (Supplementary Figure 2).

ER-membrane proteins can get transported from the ER to the vacuole for degradation. This process is called ER-phagy (Lipatova and Segev, 2015). Therefore, specific receptors in the ER membrane recruit the autophagy machinery to the ER (Liang et al., 2020; Lipatova and Segev, 2015; Molinari, 2020). Lipatova and colleagues demonstrated that during physiological conditions 20-50% of certain ER-membrane proteins are targeted to the vacuole for degradation. Interestingly up to 95% of the same proteins were transported to the vacuole during the overexpression of the ER accumulating transmembrane protein GFP-Snc1-PEM (Lipatova et al., 2013). Thus, overexpressing *GFP-OPT3* with the strong constitutive *GPD* promoter might stimulate ER-phagy, which results in the targeting of excessive amounts of GFP-Opt3 to the vacuole.

Interestingly researchers of our collaborating partners in Israel observed that also GFP-tags can change protein localization. In a high throughput analysis, they demonstrated that protein localization changes, depending on the protein termini GFP is fused to (Weill et al., 2019). This is

an interesting point, since the NeonGreen-tag was fused to the C-terminus of Opt3, while the dual localized Opt3 with the GFP-tag was N-terminally. Intriguingly, when protein localization of 5330 genes in a high throughput screen was performed with N-terminally fused GFP under the constitutive *NOP1* promoter, Opt3 localized in the ER (Breker et al., 2014, 2013). The *NOP1* promoter is stronger than an *ADH1* promoter, but weaker as the *GPD* promoter (Lee et al., 2013; Mumberg et al., 1995; Weill et al., 2019). This might indicate that rather the expression of tagged *OPT3* might determinate Opt3 localization than the position of the fluorescent tag. Since endogenous expression of Opt3 is comparable low, it is likely that endogenous Opt3 is localized in the ER and not the vacuole.

3.3 Opt3 does not influence the Ycf1-dependent GSSG pool

Although co-localization studies suggested that endogenous Opt3 is localized in the ER-membrane, further experiments were performed to rule out that overexpressed *OPT3* might affect both the ER and the vacuolar GSSG pool. Hence, it was tested whether an *OPT3* overexpression strain can export GSSG from the vacuolar lumen back to the cytosol. Therefore, it was speculated, that if Opt3 was functional in the vacuole, a lack in vacuolar uptake of GSSG by the deletion of *YCF1* would vanish the effect of *OPT3* overexpression on whole cell GSSG levels. Thus, vacuolar import of GSSG was blocked by the deletion of *YCF1* in combination with *OPT3* deletion and overexpression. When GSSG content was determined in these backgrounds, the pattern of GSSG concentrations was comparable to the pattern of *OPT3* deletion and overexpressing cells with intact Ycf1 (Figure 14). While cells with deleted *YCF1* and *OPT3* had slightly more GSSG compared to the *YCF1* single deletion strain, overexpressed *OPT3* led to a strong decrease when Ycf1 was missing (Figure 15). This strongly suggests, that Opt3 function is independent of Ycf1. Additionally, the results indicate that under physiological conditions just minor amounts of GSSG are transported from the cytosol to the vacuole, since a $\Delta ycf1$ strain had just marginally decreased GSSG than WT cells (Figure 14 and 15). These findings are consistent with observations made by Morgan and colleagues and can be explained by highly abundant Glr1, which reduces GSSG efficiently to 2GSH before it can get imported into the vacuole (Morgan et al., 2013).

As a second proof that *OPT3* overexpression did not lead to vacuolar GSSG export, another experiment was performed. *GLR1* was deleted in combination with deletion and overexpression of *OPT3*. As previous shown by Morgan et al. the depletion of cytosolic Glr1 leads to an enormous

increase of vacuolar GSSG mediated by Ycf1 (Morgan et al., 2013). Strikingly, neither *OPT3* overexpression nor deletion did affect GSSG in the *GLR1* deletion background, which clearly indicates that even if overexpression of *OPT3* leads to mis-localization and targeting to the vacuole, it does not transport GSSG from the vacuole to the lumen.

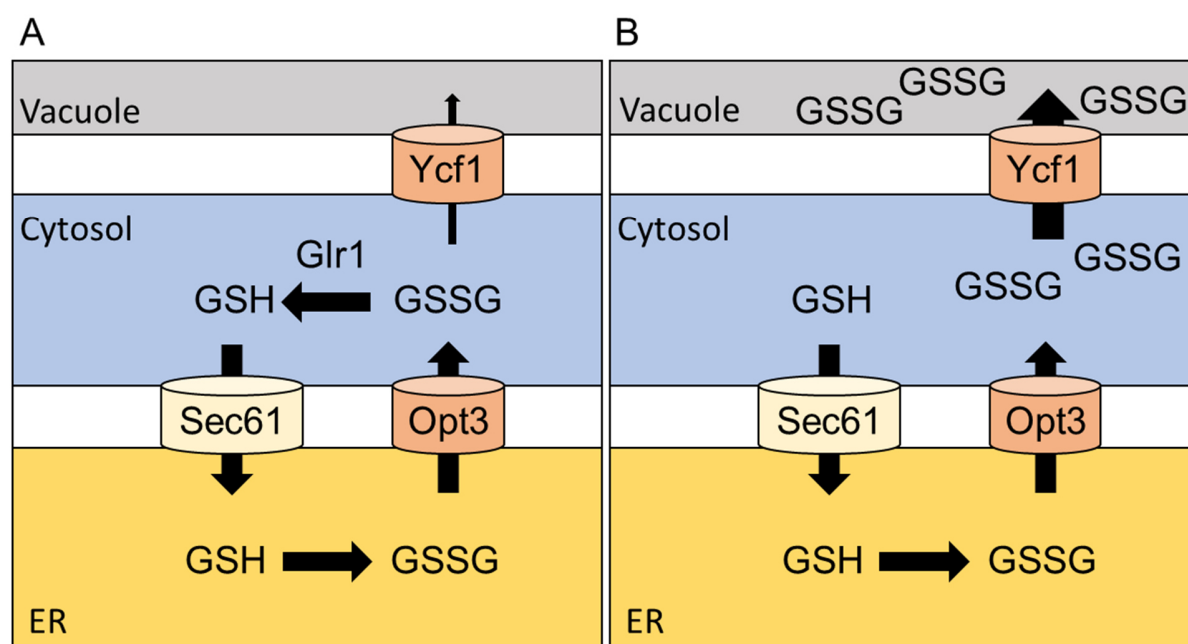


Figure 46 Opt3 is Ycf1 independent. Physiological growth conditions (A): GSSG formed in the cytosol is mostly reduced by Glr1 and small amounts are transported into the vacuole via Ycf1. Thereby GSSG formed in the ER can be transported to the cytosol and is also reduced by Glr1. When Glr1 is depleted, large amounts of GSSG formed in the cytosol are transported to the vacuole (B). However, Opt3 does not affect this increasing GSSG pool what clearly suggests that Opt3 is not in the vacuole and cannot modulate cytosolic derived GSSG.

It was previously shown that cellular transporters can be regulated via post-translational modifications (Czuba et al., 2018; Mieyal and Chock, 2012). For instance, Ycf1 is thought to be negatively regulated by protein-S-glutathionylation on a cysteine residue (Wei et al., 2014). While it was suggested that import of GSH into the ER is regulated via oxidation of Kar2 in yeast, it was recently demonstrated in humans, that also the function of the Kar2 homolog BiP can be modulated via protein-S-glutathionylation (Musaogullari and Chai, 2020; Wang and Sevier, 2016; Zhang et al., 2020). Finally, to rule out that GSSG accumulation in *GLR1* deletion cells was not due to Opt3 inactivation via post-translational cysteine modification, the GSSG content of cells

lacking *GLR1* with overexpressed *OPT3* cysteine mutants was analyzed (Figure 36). Excitingly, the mutations of Opt3 cysteines had no impact on total cellular GSSG in the *GLR1* deletion strain.

These observations clearly underline the model that under physiological conditions, GSSG measured in whole cell lysates is mostly formed in the ER, where Opt3 exports GSSG to the cytosol (Figure 46 A). Simultaneously, only small amounts of GSSG are exported via Ycf1 from the cytosol to the vacuole. When Glr1 is depleted, GSSG formed in the cytosol cannot be efficiently reduced, resulting in an enhanced uptake of GSSG into the vacuole. This vacuolar GSSG pool is independent of Opt3 as discussed previously (Figure 46 B).

3.4 Glutathione synthesis can be re-localized to the endoplasmic reticulum

After co-localization studies revealed Opt3 localization in the ER and further studies demonstrated that Opt3 does not export GSSG out of the vacuole, an experimental set up was created to proof if Opt3 exports GSSG exclusively from the ER lumen. As it is now known that GSH import into the ER is regulated, it was speculated that overcoming regulated GSH import into the ER might increase ER-glutathione content (Ponsero et al., 2017). Thus, depletion of Opt3 might have a stronger effect on GSSG found in whole cell lysates. Therefore, glutathione synthesis was partially shifted to the ER by expressing an ER targeted variant of Gsh2 from a plasmid. ER-localized Gsh2 was able to rescue the lethal phenotype of the $\Delta gsh2\Delta opt3$ deletion mutant when grown on glutathione-free medium (Figure 18).

Although it might sound unconventional to shift a cytosolic pathway into the ER, comparable experiments have been done. For instance, re-localization of the pyruvate decarboxylase (PDC) from the cytosol into the periplasm was shown in the bacteria *Zymomonas mobilis* (Balodite et al., 2019). The purpose of this study was to increase the yield of acetaldehyde, a volatile by-product of aerobic fermentation, which is normally rapidly metabolized in the cytosol. The shift of PDC to the periplasm was realized by introducing a N-terminally signal peptide, comparable to the technique used in this dissertation to re-localize Gsh2 (Balodite et al., 2019). Interestingly, there is a certain analogy between bacterial periplasm and the eukaryotic ER (Miller and Salama, 2018). In both compartments proteins are oxidatively folded (Goemans et al., 2014). Thus, the study from 2019 might not only indicate that cytosolic proteins can be transferred to another compartment but also demonstrates that some cytosolic proteins maintain functionality in this oxidative challenging environment (Balodite et al., 2019).

Not only in bacteria but also in *S. cerevisiae* metabolic pathways were re-localized from one subcellular compartment to another. The endogenous mitochondrial matrix proteins ketol-acid reductoisomerase (Ilv5) and dihydroxy-acid dehydratase 3 (Ilv3) were successfully targeted to the cytosol in order to increase cellular isobutanol production (Park and Hahn, 2019).

Above all, Quintana-Cabera and colleagues demonstrated already in 2012 that it is possible to target one enzyme of the glutathione synthesis machinery into a subcellular compartment. Thereby, they re-localized Gsh1 to the mitochondrial matrix to force an accumulation of γ -GC in the mitochondria. Interestingly this experimental set up revealed that γ -GC can reduce ROS such as H_2O_2 , irrespective of cellular glutathione concentrations (Quintana-Cabrera et al., 2012).

The successful synthesis of GSH by Gsh2 in the ER requires the import of γ -GC and glycine from the cytosol. However, since GSH can enter the ER via facilitated diffusion through the channel forming translocon Sec61, other molecules with smaller or equal sizes as GSH are thought to be able to diffuse in and out of the ER through Sec61 (Ponsero et al., 2017). Thus, γ -GC might enter the ER via facilitated diffusion through Sec61.

Intriguingly, diffusion of γ -GC into the ER might explain the lethality of a $\Delta gsh2\Delta opt3$ mutant strain without GSH in the media (Figure 13). In general $\Delta gsh2$ deletion mutants are viable and do not require GSH import from the surrounding media (Inoue et al., 1998). This implies, that the glutathione precursor γ -GC can take over the essential function of GSH in the cell. However, $\Delta gsh2$ strains contain large amounts of γ -GC (Grant et al., 1997). Furthermore, γ -GC is a redox-active molecule since it can substitute the antioxidant function of GSH. This results in the formation of γ -GC-disulfide (Grant et al., 1997; Quintana-Cabrera et al., 2012). Thus, γ -GC in the $\Delta gsh2$ background, which diffuses into the ER might be oxidized to γ -GC-disulfide. Through continuous formation of γ -GC-disulfide in the ER, the γ -GC concentration gradient between the cytosol and the ER is maintained. Additionally, according to the model that Opt3 is an ER-localized GSSG exporter, Opt3 might be able to transport γ -GC-disulfide back to the cytosol, where it is reduced (Figure 47 A).

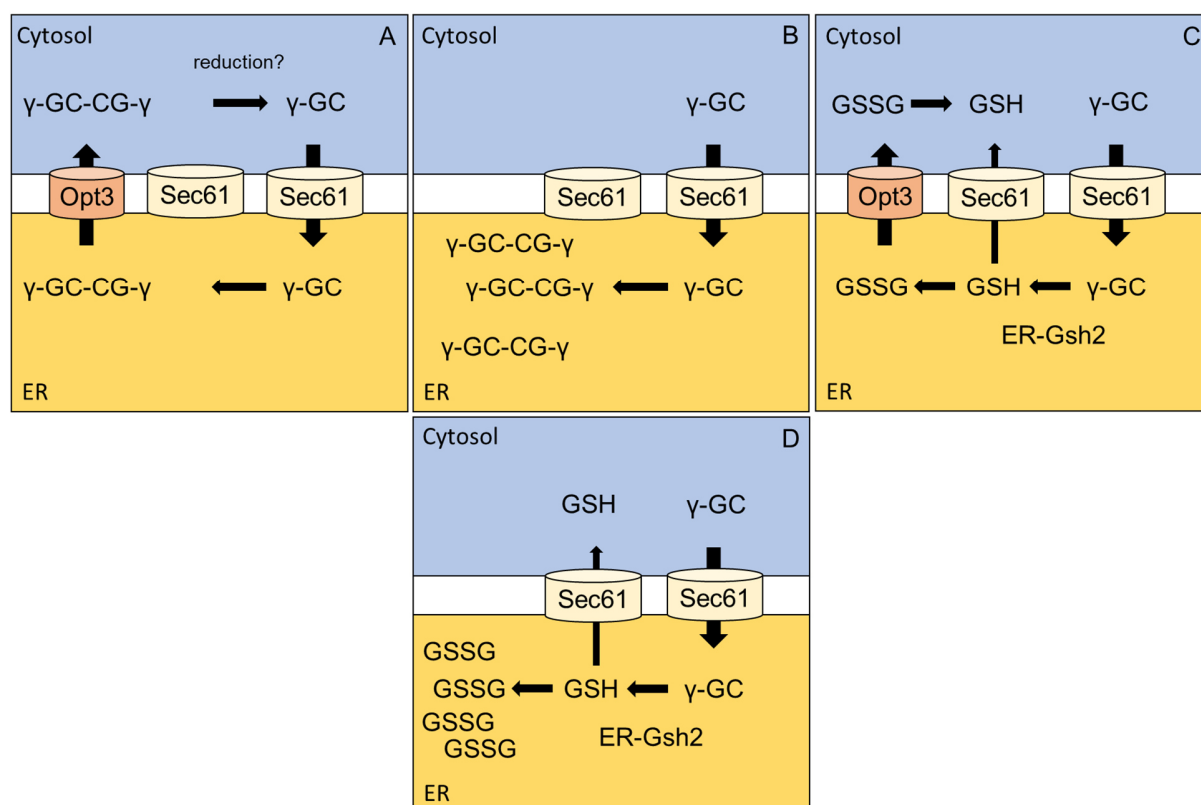


Figure 47 Model of GSH synthesis in the ER. In a $\Delta gsh2$ deletion strain γ -GC is synthesized in the cytosol and diffuses permanently into the ER through the Sec61 channel. In the ER γ -GC is oxidized. γ -GC-disulfide can be exported by Opt3 (A) maintaining high cytosolic γ -GC and thus viability. When *OPT3* is deleted in a $\Delta gsh2$ background, γ -GC-disulfide accumulates in the ER resulting in depletion of the cytosolic γ -GC content, which is lethal (B). When Gsh2 is targeted to the endoplasmic reticulum (ER-Gsh2), ER localized γ -GC is synthesized to GSH (C, D). While GSSG can be exported via Opt3 (C) cells missing Opt3 accumulate GSSG in the ER (D). However, synthesized GSH in the ER, which is not directly oxidized might diffuse into the cytosol via Sec61 and thereby rescues lethality of the $\Delta gsh2\Delta opt3$ double deletion mutant.

When Opt3 is depleted together with Gsh2, γ -GC-disulfide is trapped in the ER. Thus, γ -GC-disulfide cannot be re-reduced in the cytosol, what decreases the cytosolic γ -GC concentration. Consequently, there might be not enough γ -GC available, to maintain crucial functions in other subcellular compartments (Figure 47 B). Please consider, that it is nowadays assumed that the vital role of GSH is linked to iron-sulfur cluster homeostasis in the cytosol and the mitochondrial matrix (Kumar et al., 2011). Thereby, the here made findings support the hypothesis that the essential role of GSH is related to FeS cluster homeostasis in the cytosol or the mitochondrial matrix, as γ -GC in the ER lumen is not sufficient to maintain viability. But how does ER-localized Gsh2 rescue this lethal phenotype? When Gsh2 is present in the ER, GSH is synthesized from γ -GC and can be oxidized to GSSG. However, when GSH is synthesized in the ER a diffusion gradient arises from the ER to the cytosol. Thus, there might be an equilibrium

between ER-localized GSH oxidation and GSH diffusion into the cytosol (Figure 47 C). While formed GSSG is trapped in the ER of the $\Delta gsh2\Delta opt3$ mutant, GSH diffusion to the cytosol is sufficient to maintain cell viability (Figure 47 D).

3.5 Two plausible pathways for GSSG depletion from the ER

Since shifting Gsh2 from the cytosol into the ER seemed to be possible, it was tested whether ER-localized glutathione synthesis would increase ER GSSG levels and in turn increases the impact of *OPT3*-mutants on whole cell GSSG content. Strikingly, *OPT3* deletion caused a strong increase of GSSG found in whole cell lysates, while overexpression cells had almost no GSSG. This observation indeed suggests that the effect of *Opt3* on cellular GSSG was ER specific. For control, GSH and GSSG content of *OPT3*-mutants was measured, which expressed a cytosolic Gsh2 construct (Cyto-Gsh2) and a Gsh2 construct which could enter the ER but was not necessarily kept in there, since the ER-retention signal was missing (SP-Gsh2). While $\Delta gsh2\Delta opt3$ cells with SP-Gsh2 had slightly more GSSG than $\Delta gsh2$ cells with the same construct, *OPT3* deletion had no effect on the GSSG content when Gsh2 was present in the cytosol. Interestingly, regardless which construct was expressed, *OPT3* overexpression cells always had a strongly decreased GSSG content. In general, GSH synthesis was more efficient in the cytosol and the secretory pathway since cells containing Cyto-Gsh2 and SP-Gsh2 had almost 30% more GSH than the same cells with ER-Gsh2 (Figure 20).

Gsh2 is a cytosolic protein, thus it is not surprising, that GSH synthesis in cells with Cyto-Gsh2 is very efficient and cells expressing the construct have GSH concentrations comparable to those in WT cells, as shown in previous experiments. Although the experiment clearly demonstrated that GSH synthesis in the ER is possible, several circumstances might have decreased GSH production in the ER. For example, it remains unclear how efficiently ER-Gsh2 can be fold. By N-terminal fusion of the signal peptide to Gsh2, it is co-translationally imported into the ER and thus must fold in the ER-lumen (Aza et al., 2021; Fitzgerald and Glick, 2014; Rothe and Lehle, 1998). Since the ER has a strongly oxidative environment, native protein folding might be difficult. In the ER, proteins are not just oxidatively folded, but also processed (Thibault and Ng, 2012). This includes cleavage of the signal peptide and post-translational modifications in the form of glycosylation of specific amino acid residues (Tanner and Lehle, 1987). The latter might be a critical point for Gsh2 activity, since glycosylation can alter protein stability and activity (Karki et al., 2021). However, independent of total [GSx], only when Gsh2 was present in the ER *OPT3*

deletion caused an accumulation of GSSG. This indicates that the effect of *OPT3* deletion on total cellular GSSG must be ER-specific.

Conversely, although *OPT3* deletion only affected total [GSSG] when Gsh2 was re-localized to the ER, it remains unclear why high levels of Opt3 almost completely decreased the cellular GSSG content, independently if Gsh2 was expressed in the cytosol or the ER (Figure 20). As discussed before, under physiological conditions, GSSG found in whole cell lysates seems to mainly descend from the ER. Thus, *OPT3* overexpression might always cause low GSSG concentration, since formed GSSG is immediately exported back into the cytosol for reduction. However, if the latter is correct, how can it be that the effect of *OPT3* deletion on total [GSSG] in cells with ER-localized GSH synthesis increases, although total [GSSG] in whole cell lysates of cells with cytosolic localized GSH synthesis is higher?

This might implicate, that a second mechanism exists, which can export GSSG from the lumen. Such a mechanism cannot be the direct transport of GSSG into the cytosol as seen from Opt3 because this would decrease cellular GSSG through Glr1 activity (Morgan et al., 2013). Thus, the Opt3-independent pathway might rather be the export of GSSG from the ER by vesicular glutathione transport (VGT). Thereby, GSSG might be stored e.g., in the vacuole. Furthermore, VGT might depend on ER GSSG levels and is regulated in a GSSG concentration-dependent manner. Thus, targeting Gsh2 to the ER might not as expected increase GSH in the ER but rather decrease GSH and GSSG in the lumen. Under moderate GSSG concentrations, ER GSSG export mainly relies on the Opt3 pathway. Hence, *OPT3* deletion has a strong effect when Gsh2 is in the ER. However, with increasing ER GSSG, VGT is stimulated and GSSG is exported via vesicular transport. Conclusively, in cells with *OPT3* overexpression, GSSG can be efficiently exported to the cytosol, thus VGT activity remains low (Figure 48).

The model, that the Opt3-pathway and the VGT-pathway exist in parallel and that upon increasing GSSG concentration VGT was activated, is supported by other interesting findings in this thesis. For instance, the overexpression of *OPT1* leads to a massive influx of GSH from the media into the cytosol. High cytosolic GSH promotes its diffusion into the ER where it indirectly activates Ero1 (Ponsero et al., 2017). Ero1 activation leads to the oxidation of GSH and as a result of that increased GSSG concentration in the ER (Kumar et al., 2011; Ponsero et al., 2017). While *OPT3* overexpressing cells had very low levels of GSSG before the growth media was supplemented with GSH, GSSG was accumulating nearly as much as in WT or *OPT3* deletion cells after the GSH pulse. This indicates that before GSH was induced, the Opt3 amount in the ER was high enough to export almost all GSSG. However, after the pulse of GSH the GSSG concentration was

dramatically increased, which stimulated VGT to export GSSG from the ER. Supportive to this model, Kumar and colleagues demonstrated, that genes involved in vesicular trafficking from the ER to the Golgi are upregulated during GSH influx in *OPT1* overexpressing cells (Kumar et al., 2011).

It was further demonstrated in this thesis, that even when large amounts of GSSG were imported from the media, the cytosol stayed almost totally reduced (Figure 29). This was mainly maintained by Glr1. However, in *OPT3*-mutant strains overexpressing *OPT1*, GSSG remained constantly high after the wash-out of GSH followed by 1h incubation in GSH-free media (Figure 24). This means, that GSSG formed during the GSH pulse was stored and not transported back to the cytosol, where it could have been reduced. If GSSG was stored in the ER, *OPT3* overexpressing cells could export GSSG to the cytosol and thus GSSG concentration in these cells would decrease over time. Interestingly, GSSG stored in the vacuole seems to be stable, since Ycf1 imported GSSG formed in $\Delta glr1$ cells after a pulse of H_2O_2 remained unchanging for at least 1h (Morgan et al., 2013). Thus, GSSG formed in the ER during high GSH influx, might be stored in the vacuole.

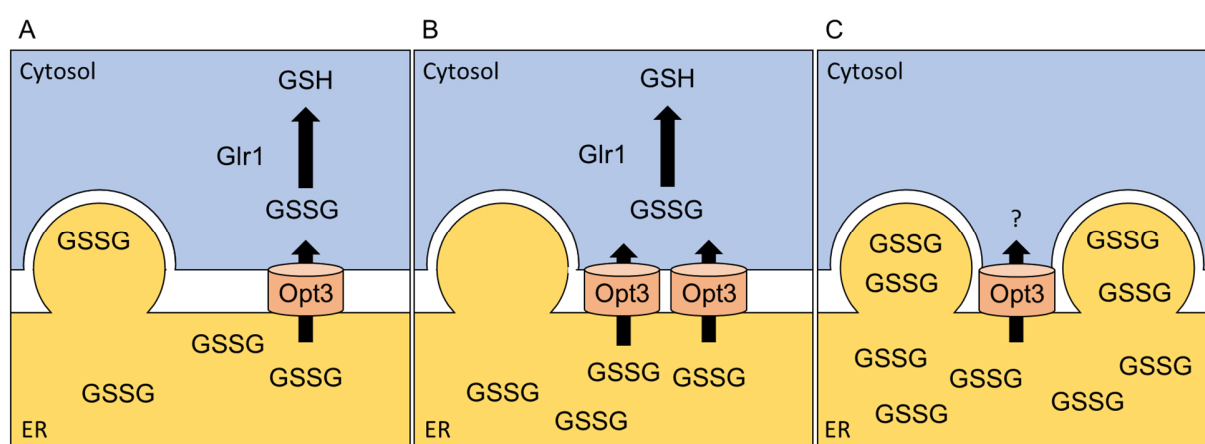


Figure 48 Model of GSSG export from the ER. Under physiological conditions (A), GSSG is formed in the ER and exported via Opt3 and vesicular GSSG export (VGT). When *OPT3* is overexpressed, mostly all GSSG is exported to the cytosol where it gets reduced (B). However, when ER GSSG is increased, VGT is stimulated and large amounts of GSSG get transported to the vacuole (C). Thereby it remains elusive, if Opt3 is inactivated or not.

Lastly, it remains unclear if Opt3 function is inhibited during active VGT. However, comparing GSSG concentrations of cells with endogenous Opt3 to an *OPT3* overexpressing strain during physiological growth conditions suggest that Opt3 transport capacity is mainly determined by its expression levels. Additionally, the amount of Opt3 in the ER membrane seems to be limited,

since the localization studies suggest that strong overexpression of *OPT3* results in mis-localization of Opt3 to the vacuole.

Interestingly, a strain lacking Gsh1 with endogenous Opt1 has approximately 30% less GSH than a WT strain (Kumar et al., 2011). However, overexpression of *OPT1* leads to a more than seven-fold increase of cellular GSH, which suggests that Opt1 function might also mainly, if not exclusively, be regulated by expression levels (Kumar et al., 2011). This in general indicates that modulating expression levels is the key regulator for OPT-family members.

3.6 The physiological role of Opt3

When GSSG is formed in the ER, it might be exported via two pathways, as discussed in previous sections. Interestingly VGT alone seems to be enough to maintain cell viability, since Opt3-mutants grew as WT cells throughout all experiments in different conditions. Furthermore, also the resistance to reductive or oxidative stress was not impaired when *OPT3* was deleted (Figure 39). Even when cells were treated with tunicamycin to induce ER-stress, Opt3-mutant strains were as resistant as WT cells (Figure 40). Surprisingly, when UPR activity in Opt3-mutant strains was analyzed, both deletion and overexpression of *OPT3* led to less *HAC1* splicing, suggesting a decreased UPR. This was consistent when cells were treated with tunicamycin where *OPT3* deletion and overexpression strains had less *HAC1* splicing activity than WT cells (Figure 42). This latter observation was surprising for many reasons: On the one hand one would expect that impaired UPR decreases tunicamycin resistance, which might lead to decreased cell viability (Torres-Quiroz et al., 2010). On the other hand, it is unexpected, that both deletion and overexpression of a protein, causes the same UPR-repressing phenotype.

During ER-stress, the oxidative folding capacity of the ER is impaired and nascent or incorrectly folded protein chains begin to accumulate (Pincus et al., 2010). One key-player, who is crucial to prevent proteins from aggregation or support the correct folding of newly post-translational integrated nascent protein chains, is the HSP70-family member Kar2 (Ngosuwan et al., 2003; Sharma and Masison, 2009). Kar2 possesses a nucleotide-binding domain (NBD) and a substrate-binding domain (SBD) (Xu et al., 2016). While, the SBD binds to hydrophobic residues of a protein, NBD activity is important for dissociation of Kar2 from the unfolded substrate (Kimata et al., 2003). Under physiological conditions, cycles of ATP- and ADP-binding to the NBD allow association and dissociation of the SBD at specific hydrophobic substrate regions (Xu et al., 2016). Interestingly, it was demonstrated that a cysteine (C63) in the Kar2 NBD can be

post-translationally modified by glutathionylation, resulting in an increased holdase activity (Wang and Sevier, 2016). This modification seems to be a sensing mechanism to increase ER-stress resistance under redox-conditions, which might be unfavourable for protein folding. Thus, glutathionylated Kar2 can prevent protein accumulation to a certain degree (Wang et al., 2014). Intriguingly, Kar2 oxidation is thought to be the main regulator of GSH import into the ER by blocking the Sec61 translocation channel (Ponsero et al., 2017). Finally, glutathionylation of Kar2 occurs either via the formation of a sulfenic acid followed by the reaction with GSH (two-electron mechanism) or directly via thiol-exchange reaction with GSSG. The latter would require an increase in ER E_{GSH} (Wang and Sevier, 2016). The sulfenic acid formation on C63 of Kar2 can be formed through thiol reaction with H_2O_2 (Wang et al., 2014). The main producer of H_2O_2 in the ER is the oxidoreductase Ero1, which transfers electrons from Pdi1 directly to molecular oxygen (Tu and Weissman, 2002; Zito, 2015). However, Ero1 activity in eukaryotes is regulated (Niu et al., 2016). This regulation is maintained by several cysteines, which can form intramolecular disulfides, causing a conformational change and inhibit Ero1 activity (Sevier et al., 2007). Please note, that recently a model was presented suggesting that unlike in human cells, oxidized regulatory cysteines in yeast Ero1 maintain low oxidase activity and can be thus rather switch from a low activity state into a high activity state (Niu et al., 2016). The switch from low activity to high activity states require the regulatory disulfide reduction by Pdi1 (Zhang et al., 2014). However, Ero1 and Pdi1 in yeast are mostly oxidized during physiological conditions, suggesting that the low activity state of Ero1 is sufficient to maintain oxidized Pdi1 (Niu et al., 2016). Nevertheless, the increase of the GSH:GSSG ratio can lead to the reduction of Pdi1 cysteines and consequently the switch of Ero1 into its high active state (Niu et al., 2016). This stimulates the formation of H_2O_2 and facilitates sulfenic acid formation on the cysteine residue of Kar2 (Wang et al., 2014).

The enhanced export of GSSG during *OPT3* overexpression, eventually increases the ER GSH:GSSG ratio, which might initiate sulfenic acid formation and therefore glutathionylation on Kar2. Glutathionylated Kar2 with its increased holdase activity, ultimately prevents proteins from accumulation during tunicamycin treatment, what would explain lower UPR in a *OPT3* overexpressing strain. This is supported by preliminary data in which Ero1 in *OPT3* overexpression strains remained in its reduced high active state after reduction with DTT, whereas Ero1 in WT or $\Delta opt3$ cells returned quickly into the oxidized low active confirmation (Supplementary Figure 3). In contrast to *OPT3* overexpression, the deletion of *OPT3* prevents direct GSSG export from the ER, what eventually decreases the GSH:GSSG ratio. Although, according to the presented model, GSSG is mainly exported by VGT in a $\Delta opt3$ strain, even a small increase in ER GSSG might decrease GSH:GSSG ratio in the lumen. Thus, increased

GSSG in $\Delta opt3$ cells could be sufficient to favour thiol exchange between Kar2 and GSSG. Again, this would lead to an increased holdase activity of Kar2 and thus less protein aggregation in the ER. Finally, the described model explains, how both deletion and overexpression of *OPT3* can cause the same phenotype for UPR induction.

The described mechanisms, which might explain how both deletion and overexpression of *OPT3* decreases UPR activation, rely on changes in ER GSSG, which can consequently cause a change in ER E_{GSH} . However, when E_{GSH} in WT, $\Delta opt3$ and *OPT3* overexpressing cells was analyzed, there was no detectable difference between the E_{GSH} of different strains observable (Figure 44). Even the treatment with H_2O_2 to agitate the cellular glutathione pool did not cause a sensor response.

Studying E_{GSH} in the ER was done by other groups before. In their studies, roGFP-based probes or other E_{GSH} sensors e.g., rxYFP were used (Meyer et al., 2007; Østergaard et al., 2004). However, these sensors were not fused to a glutaredoxin, although in the cytosol equilibration between roGFP2 and the 2GSH:GSSG redox couple requires glutaredoxin activity (Gutscher et al., 2008). Hence it remains unclear, where the glutaredoxin activity for sensors targeted into the ER might come from. Nevertheless, other groups reported equal ER E_{GSH} values when they measured with the same sensors fused to Grx1 (Birk et al., 2013a; Ponsoero et al., 2017). However, this raises further questions e.g., how redox-probes (roGFP1-iL, rxYFP), of which no clear mechanism exist, equilibrate with the 2GSH:GSSG redox-couple (if they do at all) in absence of an active glutaredoxin facilitating this equilibration. Similar response patterns of genetic fusions or unfused constructs might indicate that both types of probes do rather equilibrate with a different and not the glutathione redox-couple in the ER.

I recently fused Pdi1 to roGFP2 and expressed the construct in a strain lacking cytosolic Grx1, Grx2 and Glr1. Interestingly, I now have preliminary data, which suggest that influx of GSSG from the media cause a Pdi1 dependent roGFP2 oxidation (Supplementary Figure 4). Our new findings convincingly demonstrate, that Pdi1 can interact with roGFP2. Thus, it remains elusive to which degree measurements with roGFP- or rxYFP-based probes monitor the glutathione redox-couple in the ER or in which way highly abundant oxidoreductases can manipulate the recorded probe signal.

In summary I think that Opt3 is a GSSG exporter in the ER. I furthermore conclude that the export of GSSG is mainly regulated by Opt3 expression levels. The extremely low endogenous expression of Opt3 causes a slow export rate of GSSG from the ER, which is beneficial to maintain low ER GSH:GSSG ratios under physiological conditions. However, I assume that GSSG can

freely diffuse through the ER and thus can be packed into ER-vesicles and transported to the vacuole. Moreover, the vesicular transport rate of GSSG might be dependent on total ER GSSG concentration – as more GSSG is present, as more molecules diffuse into vesicles. Nevertheless, massive production of GSSG in the ER upon highly active Ero1 leads to a loss of Opt3 function and eventually an increase of vesicular trafficking towards the vacuole. Thus, under ER-stress conditions most GSSG in the ER is transferred to the vacuole where it is stored. How Opt3 is inactivated during high ER GSSG conditions remains elusive. However, Opt3 inactivation during high-Ero1 activity is plausible. Highly active Ero1 produces H₂O₂, which can diffuse into the cytosol. Thus, under oxidative stress conditions Opt3 inactivation supports the cytosol in maintaining a reduced glutathione pool, since ER derived GSSG is trapped in the secretory pathway.

4 Material and Methods

4.1 Molecular Biology Methods

4.1.1 Plasmid isolation from *E. Coli*

Plasmid containing *E. Coli* (*TOP10*) were inoculated in 5 ml LBamp and incubated overnight at 37°C with shaking (140 rpm). Next day, 3 ml of culture was harvested by centrifugation (1 min, 13 000 rpm). For cell lysis and plasmid purification the *NucleoSpin® Plasmid Quick Pure* Kit from *Marchery-Nagel* was used. All steps were performed exactly like documented in the user manual. In short: Cells were resuspended in 250 µl cooled buffer A1 and immediately 250 µl buffer A2 was added. After careful inversion of the samples and incubation for 5 min at room temperature, 300 µl of the neutralization buffer was added followed by another inversion step. Next the supernatant was loaded on a *NucleoSpin®* Column and centrifuged for 1 min at 11 000 rpm. After washing the column twice with AE buffer (1 min, 11 000 rpm), DNA was collected in a fresh reaction tube by elution from the membrane with 30 µl elution buffer incubated for 2 min and centrifugation for 1 min at 11 000 rpm.

4.1.2 Determination of DNA concentration

For the plasmid DNA determination, after isolation from *E. Coli*, the *QuickDrop* from *Molecular Devices* was used. After blanking the machine with 1 µl H₂O followed by cleaning of the sensor with tissue paper, 1 µl of the DNA sample was added. DNA content was determined by absorption measurements at 260 nm.

4.1.3 Preparation of chromosomal DNA of *S. cerevisiae*

Yeast cells were picked and transferred from growth plates to 30 µl 0.2% SDS. After shaking on a *VortexGenie2* (*Scientific Industries*) samples were cooked for 10 min at 95°C followed by another round of shaking. A centrifugation step (1 min, 13 200 x g) was used to separate the DNA containing aqueous fraction from the remaining cell components. 10 µl of DNA containing supernatant was transferred to a fresh reaction tube.

4.1.4 Polymerase chain reaction for DNA amplification

For DNA amplification different protocols were used. When genes were amplified from a plasmid or genomic DNA the reaction mix listed in Table 1 was used. 5 x Fusion HF buffer and Fusion polymerase were ordered from *Mobidaig*.

Table 1 Standard PCR-components. Ingredients and volumes used for gene amplification from a plasmid, or the genome are listed. When genomic DNA was used as template, 5x fusion HF buffer was substituted by 5x GC-rich buffer.

PCR-Components	Volume
5 x Fusion HF buffer	10 µl
Forward Primer	1 µl
Reverse Primer	1 µl
dTNPs	1 µl
Template	1 µl
Fusion Polymerase	0.3 µl
dH ₂ O	35.7 µl

For template amplification with high GC-content, for example amplification of the *natNT2* cassette, the PCR reaction mix was adapted. Thereby the 5x Fusion HF buffer was replaced by 1 µl of 5 x GC rich buffer from *Mobidaig*. If not other mentioned in the text, the protocol described in Table 2 was used.

Table 2 Standard PCR cycler program. Temperatures and time frames for the individual PCR steps denaturation, annealing and elongation are listed. PCR reaction was started with a 5 min denaturation step and ended with a final elongation step.

Heat	Time	Cycles
98°C	5 min	1
98°C	0.5 min	
65°C	0.5 min	35
72°C	3 min	
72°C	10 min	1

4.1.5 PCR- and Agarose Gel clean up

Both, PCR-clean up and agarose gel extraction was carried out with the *NucleoSpin^R Gel and PCR* clean up kit from *Machery-Nagel*.

4.1.6 Restriction digestion of DNA

For cloning the DNA template (30 µl of cleaned up PCR product or 1 µg plasmid DNA) was mixed with 5 µl 10 times concentrated *cutsmart* from *New England Biolabs^R (NEB)* and 2 µl of each corresponding restriction enzyme. The reaction mix was adjusted to 50 µl with dH₂O and incubated for 2h at 37°C. Restriction digest was also used to verify the correct integration of insert in the plasmid backbone after ligation reaction. Therefore 2 µl of ligated and purified plasmid was cut with 0.5 µl of corresponding enzymes in 3 µl *cutsmart* buffer and 19 µl dH₂O. The reaction mix was incubated for 30 min at 37°C. All enzymes used in this study were ordered from *NEB*.

4.1.7 Ligation of DNA fragments

Ligation was performed by using the *FAST-LINKTM DNA LIGATION* Kit (*Lucigen*). Thereby the relationship of plasmid/insert concentration was calculated with help of *NEBioCalculator^R* (<https://nebiocalculator.neb.com/#/ligation>).

Plasmid and insert were mixed with reaction buffer, ATP and ligase as described in manufacturers protocol and total reaction volume was adjusted to 15 µl with dH₂O. Ligation reaction was performed in a thermo cycler (*Peltier Thermal Cycler DTC-200*) as mentioned in the Kit manual.

4.1.8 Agarose gel electrophoresis

To separate restricted DNA fragments after restriction digest according to their size, agarose gel electrophoresis was used. Therefore 1% agarose (*Biozym*) was solubilized in TAE buffer (40 mM Tris, 1.14% acetic acid, 10 mM EDTA pH 8) by heating in a microwave. For DNA detection 2 µl *MidoriGreen (NipponGenetics)* was added to 50 ml gel solution before it polymerized for 30 min at 26°C. Before the samples were transferred on the gel, 6 x loading dye (*NEB*) was added. For size determination additionally a 1 kb DNA ladder from (*NEB*) was loaded next to the samples. DNA separation was carried out at 90 V for 45 min in 1x TAE buffer. Afterwards fragments were visualized with UV light recorded by the Molecular imager^R *ChemiDocTMXRS* from *BIORAD*.

4.1.9 Chemical transformation of *E. Coli* cells

Chemo competent *TOP10* cells were transformed with plasmid DNA by a heat shock-based approach. Therefore, 50 µl cells were incubated on ice with 1 µl corresponding plasmid for 30 min. After acclimatization cells were transferred for heat shock to a 42°C warm water bath for 1 min, followed by a cooldown on ice for 2 min. Next, cells were resuspended in 100 µl LB media and incubated for 1h at 37°C with shaking (750 rpm). Afterwards cells were plated on LB+Amp selection plates and incubated over night at 37°C.

4.2 Genetic methods

All cloned constructs in this thesis are based of the plasmid backbones described by Mumberg et al. in 1995 (Mumberg et al., 1995). The individual primers and plasmids used in this thesis are mentioned in Table 3 and 4.

4.2.1 p416-*TEF-OPT1* cloning

OPT1 was amplified from the genome. Thereby the designed primers introduced a 5' *SpeI* (*SpeI*_Opt1 F) and a 3' *Sall* restriction site (*Sall*_Opt1 R). The resulting PCR construct as well as the p416-*TEF* empty plasmid were digested with the corresponding enzymes *SpeI* and *Sall* and mixed in a ligation reaction to generate the construct p416-*TEF-OPT1*.

4.2.2 Cloning of *GSH2* variants

To shift Gsh1 and Gsh2 in the endoplasmic reticulum the enzymes had to be cloned on specific expression vectors with an integrated targeting sequence. In a first step to introduce the endoplasmic targeting sequence on the N-terminus of either Gsh1 or Gsh2 the plasmid p415-*TEF-SS-PHluorin-HDEL* was cut with *NheI* and *NotI*. PCR amplified *GSH1* (*SpeI*_GSH1-ATG F; *NotI*_GSH-Stop R) lacking the start and stop codon was cut with *SpeI* and *NotI* and ligated in p415-*TEF* empty to generate p415-*TEF-SS-GSH1-HDEL*. *GSH2* (*NheI*_GSH2-ATG F; *NotI*_GSH2-Stop R) also amplified without start and stop codons, was cut with the same enzymes and mixed in a ligation reaction with digested p415-*TEF-SS-PHluorin-HDEL* plasmid. The resulting plasmid p415-*TEF-SS-GSH2-HDEL* was further cut with *XbaI* and *HindIII* to ligate it in a p416-*TEF* empty vector. The advantage of having *GSH1* and *GSH2* on plasmids containing different amino acid markers was to select for both enzymes in parallel. Since the expression of the ER-targeted Gsh1 and Gsh2 constructs was lethal under a *TEF* promoter a weaker promoter

was introduced. Therefore, p415-*TEF-SS-GSH1*-HDEL and p416-*TEF-SS-GSH2*-HDEL were cut with XbaI and HindIII and further cloned in a p415-*ADH* empty plasmid. Finally, p415-*ADH-SS-GSH2-HDEL* was cut with SacI and HindIII to shift the construct *ADH-SS-GSH2-HDEL* on a p416 backbone and generate the plasmid p416-*ADH-SS-GSH2-HDEL*.

To produce p415-*ADH-SS-GSH2*, *GSH2* was amplified from the genome with primers introducing a 5' NheI cutting site (NheI_GSH2 F) and 3' terminal XhoI restriction site (XhoI_GSH2 R). The resulting PCR product was digested and ligated into a p415-*ADH-SS-GSH2-HDEL* plasmid digested with the same restriction enzymes. The plasmid p415-*ADH-GSH2* was constructed by cutting p415-*ADH* with NheI and XhoI. A PCR amplified *GSH2* gene with corresponding flanking restriction sites was ligated in (NheI_GSH2 F; XhoI_GSH2 R). All primer sequences used for cloning are listed in Table 3.

Table 3 Primers used in this thesis. All primers used in this thesis are listed in this table with their sequence and final usage. Cloning primers were used for gene integration into a plasmid. Gene deletion primers have homologous overhangs which bind the flanking gene regions for homologous recombination. Check primer were used to verify correct gene manipulation. N- and C- terminal tagging primers to introduce a tag of interest on the N- or C- terminal gene end. qPCR primers were used to quantify RNA levels in a qPCR reaction.

Primer	Sequence	Usage
SpeI_Opt1 F	CTGGACCACTAGTATGAGTACCATTATAGGGAG	cloning
Sall_Opt1 R	GTCCTATGAGTCGACTTACCACCATTATC	cloning
SpeI_GSH1-ATG F	CATTACGACTAGTGGACTCTTAGCTTTGGGCAC	cloning
NotI_GSH1-Stop R	CTTACAGGCGGCCGCACATTTGCTTTCTATTGAAG GC	cloning
NheI_GSH2 -ATG F	CATTACGGCTAGCGCACACTATCCACCTTCC	cloning
NotI_GSH2 -Stop R	CTTACAGGCGGCCCGTAAAGAATAATACTGTCCA AACATCCG	cloning
NheI_GSH2 F	CATTACGGCTAGCACCATGGCACACTATCCACCTT CC	cloning
XhoI_GSH2 R	CTTACAGCTCGAGCTAGTAAAGAATAATACTGTCCA AACATCCG	cloning
S1 GSH2	CAAAGGTAGCAAAGTGCCACTTCAAGCAATTATAG GAAGAAAGCACTACTCCTATAAAATATGCGTACGCT GCAGGTGCAC	gene deletion
S2 GSH2	CTTAAC TAATTGTTAATCAAGTTCTAGCATCATCTTC CTAGCATCTATGTGTATAGTACATGTACACCTAATC GAT	gene deletion

S1 OPT3	CAGTATAGAGGACTAACCGTTAAAGATTCTAAATCG GTA CTGTAAATACTTTGAAATGCGTACGCTGCAGGT CGAC	gene deletion
S2 OPT3	ATAATTTAAAATTTGTAAACTTTGTAAATTCTTTATTA GTAAATATTATATACCTAATCGATGAATTCGAGCT CG	gene deletion
S3 OPT3	GGTGGAGGTATCTTTAGCGTAATAAACATGCTCTTC ATCTGCTTAAATGTCCCTCACTATCGTACGCTGCAG GTGCGAC	C-terminal tagging
S4 OPT3	CAAAGCAGGTTTATTATCCCATGGTACACGCTGTAC TTCTTGACTTGGAGTAGATTGAGGCATCGATGAATT CTCTGTGCG	N-terminal tagging
OPT3-Neongreen F	GTATCTTTAGCGTAATAAACATGCTCTTCATCTGCT TAAATGTCCCTCACTATATGGTCTCTAAGGGTGAAG	C-terminal tagging
OPT3-Neongreen R	AAATTTGTAAACTTTGTAAATTCTTTATTAGTAAAAT ATTATATACCTAATCGATGAATTCGAGCTCG	C-terminal tagging
S2 SEC63	AAGAGCTAAAATGAAAACTATACTAATCACTTATAT CTGAATTCGAGCTCGTTTAAAC	C-terminal tagging
S3 SEC63	CGATACGGATACAGAAGCTGAAGATGATGAATCAC CAGAA	C-terminal tagging
SEC63 5'UTR CHK F	TGGTGAATGTGAAGTTTGTG	check primer
SEC63 3'UTR CHK R	AATACCAGTGGGTGGTTTG	check primer
GSH2 5'UTR CHK F	TGGAATAATTGGACAAGTGC	check primer
GSH2 3'UTR CHK R	GTGCAGCTAAATGGTGTACTTCGCTAC	check primer
GSH1 5'UTR CHK F	GTTGTGCTGGAGTAGTTGGATCTTTCC	check primer
GSH1 3'UTR CHK R	GGTCGTTGCTTTTTCAATCACCG	check primer
OPT3 5'UTR CHK F	CGTGAGATCTATCTCAAGGCATC	check primer
OPT3 3'UTR CHK R	GGAAATCTAAGACATCGAATTATGTG	check primer
YCF1 5'UTR CHK F	CTATGTGGAAGCTGGTTTACAACCTAC	check primer
YCF1 3'UTR CHK R	CATCCTACGTACGTACCAGATTGTGCG	check primer
GLR1 5'UTR CHK F	GATAGTTTAATTCATTTGCACGGCG	check primer
GLR1 3'UTR CHK R	CTTCTTTGAAGGCTTAAAGTTAGAAAGCAG	check primer
TRX1 5'UTR CHK F	CGATATGTATATTCTTTTCGTTGGAAAAGATGTC	check primer
TRX1 3'UTR CHK R	CCTCTTGTGTGAAAAATTAATTGTTTCCTCC	check primer
TRX2 5'UTR CHK F	CGGAACCAACGTATTTAGAG	check primer

TRX2 5'UTR CHK R	AATGTTCCAGTTGAAGCAAG	check primer
HAC1_{spliced} F	CTTTGTCGCCCAAGAGTATGCG	q-PCR
HAC1_{spliced} R	ACTGCGCTTCTGGATTACGC	q-PCR
PDI1 F	GATCGATTACGAGGGACCTAGA	q-PCR
PDI1 R	GCGGAGGGCAAGTAAATAGAA	q-PCR
KAR2 F	GAAGCCCCTGTAGAAGTAAG	q-PCR
KAR2 R	AGTACCACCACCCAAATCATAAA	q-PCR

4.2.3 One-step transformation of *S. cerevisiae* / homologous recombination

Cells were inoculated in 10 ml YPD for 17h at 30°C with shaking (140 rpm). The next day 1 ml of cells were collected by centrifugation (3 min, 3000 rpm) and washed once with 1 ml dH₂O. After removing the water, cells were resuspended in 100 µl One-step buffer (40% polyethylene glycol, 0.2 M lithium acetate and 0.1 M Dithiothreitol (DTT)) and 5 µl Salomon sperm single-strand DNA (*SIGMA-ALDRICH*) along with 1 µl plasmid DNA was added. After mixing with a Vortex, samples were heat shocked at 42°C for 30 min with continues shaking at 750 rpm. The heat shock was followed by incubation overnight at 30°C on corresponding HC selection plates.

Table 4 Plasmids used in this thesis. All plasmids used in this thesis are listed with their selection marker, the vector backbone, the corresponding gene insert and the source of plasmid origin.

Plasmid	Resistance Marker	Backbone	Insert	Source
p415-TEF	Amp ^R /LEU2	p415-TEF		Mumberg et al.
p416-TEF	Amp ^R /URA3	p416-TEF		Mumberg et al.
p415-ADH	Amp ^R /LEU2	p415-ADH		Mumberg et al.
p415-ADH-SS-GSH2	Amp ^R /LEU2	p415-ADH	SS-GSH2	This study
p415-ADH-GSH2	Amp ^R /LEU2	p415-ADH	ADH-GSH2	This study

p415-ADH-SS-GSH2-HDEL	Amp ^R /LEU2	p415-ADH	SS-GSH2-HDEL	This study
p415-TEF-SS-GSH2-HDEL	Amp ^R /LEU2	p415-TEF	SS-GSH2-HDEL	This study
p415-TEF-SS-PHLUORIN-HDEL	Amp ^R /LEU2	p415-TEF	SS-PHLUORIN-HDEL	This study
p416-MET25-SS-PHLUORIN-HDEL	Amp ^R /URA3	p416-TEF	SS-PHLUORIN-HDEL	Bruce Morgan
p416-TEF-OPT1	Amp ^R /URA3	p416-TEF	OPT1	This study
p415-TEF-OPT1	Amp ^R /LEU2	p415-TEF	OPT1	This study
p416-MET25-PHLUORIN	Amp ^R /URA3	p416-MET25	PHLUORIN	This study
p415-TEF-GRX1-roGFP2	Amp ^R /LEU2	p415-TEF	GRX1-roGFP2	Gutscher et al., 2008
p416-MET25-SS-roGFP2-GRX1-HDEL	Amp ^R /MET25	p416-MET25	SS-roGFP2-GRX1 HDEL	Bruce Morgan
p416-TEF-OPT3	Amp ^R /URA3	p416-TEF	OPT3	GeneScript
p416-TEF-OPT3-C65A	Amp ^R /URA3	p416-TEF	OPT3-C65A	GeneScript
p416-TEF-OPT3-C205A	Amp ^R /URA3	p416-TEF	OPT3-C205A	GeneScript
p416-TEF-OPT3-C320A	Amp ^R /URA3	p416-TEF	OPT3-C320A	GeneScript
p416-TEF-OPT3-C452A	Amp ^R /URA3	p416-TEF	OPT3-C452A	GeneScript
p416-TEF-OPT3-C459A	Amp ^R /URA3	p416-TEF	OPT3-C459A	GeneScript
p416-TEF-OPT3-C565A	Amp ^R /URA3	p416-TEF	OPT3-C565A	GeneScript
p416-TEF-OPT3-C572A	Amp ^R /URA3	p416-TEF	OPT3-C572A	GeneScript
p416-TEF-OPT3-C584A	Amp ^R /URA3	p416-TEF	OPT3-C584A	GeneScript
p416-TEF-OPT3-C607A	Amp ^R /URA3	p416-TEF	OPT3-C607A	GeneScript
p416-TEF-OPT3-C623A	Amp ^R /URA3	p416-TEF	OPT3-C623A	GeneScript
p416-TEF-OPT3-C719A	Amp ^R /URA3	p416-TEF	OPT3-C719A	GeneScript
pFA6α-natNT2	Amp ^R /natNT2	PEG202	natNT2	Janke et al.
pFA6α-hphNTI	Amp ^R /hphNTI	p425-GAL1	hphNTI	Janke et al.

pFA6α-kanMX4	Amp ^R /kanMX4	pYM3	<i>kanMX4</i>	Janke et al.
pFA6α-cherry-HIS3MX6	Amp ^R /HIS3	pFA6 α	<i>cherry-HIS3MX6</i>	Janke et al.
pYM-N18	Amp ^R /kanMX4	p413- <i>TEF</i>	<i>kanMX4</i>	Janke et al.
pYM-N7	Amp ^R /natNT2	p413- <i>ADH</i>	pADH	Janke et al.
pFA6α-ymNeonGreen-CaURA3	Amp ^R /URA3	pFA6 α	ymNEONgreen	Botman et al.

4.2.4 Construction of yeast deletion and tagged strains

If not otherwise indicated throughout the text, yeast strains come from the *S. cerevisiae* wild-type BY4742 (*his3 Δ 1leu2 Δ 0lys2 Δ 0ura3 Δ 0*) yeast strain. Deletion strains were constructed by using homologous recombination approach previous described by Janke et al., 2004 (Janke et al., 2004). Therefore, antibiotic resistance cassettes (*NatNT2*, *kanMX4* or *hphNTI*), which replaced the gene of interest were amplified via PCR from the donor plasmids pFA6 α -*natNT2*, pFA6 α -*hphNTI* and pFA6 α -*kanMX4*. For knock-out strain production, primers to amplify the antibiotic resistance cassettes had 50-60 bp long overhangs, which were homologue to genomic regions up and downstream of the replaced gene. The manipulation of endogenous promoters was also a PCR based tagging approach. Corresponding primers were designed as recommended by Janke et al. in 2014 (Janke et al., 2004). As donor-plasmids the pYM based plasmids, pYM-N18, and pYM-N7 were used. Endogenous promoters were replaced by either a *TEF1* or an *ADH1* promoter. The strain *ADH-OPT3-ymNeonGreenSEC63-mCherry* was produced stepwise. First *ymNeonGreen* was introduced by PCR based tagging using a *URA3* marker for selection. In a second step *SEC63* in the same strain was C-terminally tagged with *mCHERRY* linked to a *HIS3* marker for selection (donor plasmid: pFA6 α -cherry-HIS3MX6). Finally, the endogenous promoter was replaced by an *ADH* promoter with a *natNT2* selection marker. The donor plasmid pFA6 α -ymNeonGreen-CaURA3 was a gift from Bas Teusink (Addgene plasmid #125703) (Botman et al., 2019). All primer used are listed in Table 3.

For homologous recombination, the above-mentioned amplified resistance cassettes were transformed into the yeast cells by a lithium acetate/polyethyleneglycol-based protocol. In short, cells were grown over night. The next day, 1 ml culture was collected by centrifugation (3 min, 3000 rpm, 25°C) washed with 1 ml distilled water before and taken up in 200 μ l of one-step transformation buffer (40% polyethylene glycol, 0.2 M lithium acetate and 0.1 M Dithiothreitol (DTT)). Next, 10 μ l salmon sperm single-strand DNA (*SIGMA-ALDRICH*) and the corresponding

PCR product was supplemented. Cells were kept for 30 min at 42°C with continuous shaking (750 rpm). Positive knock out clones were selected on growth plates supplemented with corresponding antibiotics. All strains were confirmed by PCR. For further information see Table 5.

Table 5 Strains used in this thesis. All strains which were used in this thesis are listed with their corresponding genotypes and the source of origin.

Strain	Genotype	Source
BY4742	MAT α his3 Δ 1leu2 Δ 1lys2 Δ 0ura3 Δ 0	Euroscarf
Δgsh1	BY4742 Δ gsh1::kanMX4	Euroscarf
Δgsh2	BY4742 Δ gsh2::kanMX4	Euroscarf
Δgsh1Δgsh2	BY4742 Δ gsh1::kanMx4 Δ gsh2::natNT2	This study
Δopt3	BY4742 Δ opt3::natNT2	This study
p_{TEF}OPT3	BY4742 p _{TEF} OPT3::natNT2	This study
Δgsh1Δopt3	BY4742 Δ gsh1::kanMx4 Δ opt3::hphNTI	This study
Δgsh2Δopt3	BY4742 Δ gsh2::kanMx4 Δ opt3::hphNTI	This study
Δgsh1Δgsh2Δopt3	BY4742 Δ gsh1::kanMx4 Δ gsh2::natNT2 Δ opt3::hphNTI	This study
Δgsh1_{p_{TEF}OPT3}	BY4742 Δ gsh1::kanMX4 p _{TEF} OPT3::hphNTI	This study
Δgsh2_{p_{TEF}OPT3}	BY4742 Δ gsh2::kanMX4 p _{TEF} OPT3::hphNTI	This study
Δgsh1Δgsh2_{p_{TEF}OPT3}	BY4742 Δ gsh1::kanMx4 Δ gsh2::natNT2 p _{TEF} OPT3::hphNTI	This study
Δycf1	BY4742 Δ ycf1::kanMX4	Euroscarf
Δycf1Δopt3	BY4742 Δ ycf1::kanMX4 Δ opt3::natNT2	This study
Δycf1_{p_{TEF}OPT3}	BY4742 Δ ycf1::kanMX4 p _{TEF} OPT3::natNT2	This study
Δgsh2Δycf1	BY4742 Δ gsh2::kanMX4 Δ ycf1::natNT2	This study
Δgsh2Δycf1Δopt3	BY4742 Δ gsh2::kanMX4 Δ ycf1::natNT2 Δ opt3::hphNTI	This study

$\Delta gsh2\Delta ycf1_{p_{TEF}OPT3}$	BY4742 $\Delta gsh2::kanMX4 \Delta ycf1::natNT2$ $p_{TEF}OPT3::hphNTI$	This study
$\Delta glr1$	BY4742 $\Delta glr1::kanMX4$	Euroscarf
$\Delta glr1\Delta opt3$	BY4742 $\Delta glr1::kanMX4 \Delta opt3::natNT2$	This study
$\Delta glr1_{p_{TEF}OPT3}$	BY4742 $\Delta glr1::kanMX4 p_{TEF}OPT3::natNT2$	This study
$\Delta gsh2\Delta glr1$	BY4742 $\Delta gsh2::kanMX4 \Delta glr1::natNT2$	This study
$\Delta gsh2\Delta glr1\Delta opt3$	BY4742 $\Delta gsh2::kanMX4 \Delta glr1::natNT2$ $\Delta opt3::hphNTI$	This study
$\Delta gsh2\Delta glr1_{p_{TEF}OPT3}$	BY4742 $\Delta gsh2::kanMX4 \Delta glr1::natNT2$ $p_{TEF}OPT3::hphNTI$	This study
$\Delta trx1\Delta trx2$	BY4742 $\Delta trx1::kanMX4 \Delta trx2::HIS3$	Morgan et al.
$\Delta trx1\Delta trx2\Delta opt3$	BY4742 $\Delta trx1::kanMX4 \Delta trx2::HIS3 \Delta opt3::natNT2$	This study
$\Delta trx1\Delta trx2_{p_{TEF}OPT3}$	BY4742 $\Delta trx1::kanMX4 \Delta trx2::HIS3$ $p_{TEF}OPT3::natNT2$	This study
$\Delta ire1$	BY4741	Carsten Mattes
<i>OPT3-ymNeongreen</i>	BY4742 $p_{ADH}OPT3::natNT2 ymNeongreen::URA3$	This study
<i>OPT3-ymNeongreen SEC63-mCherry</i>	BY4742 $ymNeongreen::URA3 SEC63-$ $mCherry::HIS3$	This study
$p_{ADH}OPT3-ymNeongreen SEC63-mCherry$	BY4742 $ymNeongreen::URA3 SEC63-$ $mCherry::HIS3 p_{ADH}OPT3::natNT2$	This study
SGA-starter strain	$his3\Delta1 leu2\Delta0 lys2+ MET+ ura3\Delta0 can1\Delta::STE2pr-$ $sp HIS5 lyp1\Delta::STE3pr-LEU2 cyh2$	Cohen et al.

4.3 Cell Biology methods

4.3.1 Synthetic Genetic Array (SGA)

For the identification of genetically interaction partners of *OPT3* a SGA-starter strain ($his3\Delta1 leu2\Delta0 lys2+ MET+ ura3\Delta0 can1\Delta::STE2pr-sp HIS5 lyp1\Delta::STE3pr-LEU2 cyh2$) was mated with the BY4741 $xx::kanMX2$ deletion library and BY4741 DAMP library of essential genes followed by the analysis of cell growth as described by Cohen et al. in 2011 (Cohen and Schuldiner, 2011).

4.3.2 Growth curves

The yeast strains By4742 wild-type (WT), $\Delta gsh1$, $\Delta gsh2$, $\Delta opt3$, $p_{TEF}OPT3$, $\Delta gsh1\Delta opt3$, $\Delta gsh2\Delta opt3$, $\Delta gsh1_{p_{TEF}OPT3}$ and $\Delta gsh2_{p_{TEF}OPT3}$ were transformed with an empty p415-TEF empty plasmid. Precultures grew in HC medium without supplemented leucine and additional 2 μ M GSH. Next day the cultures were diluted to 0.5 OD₆₀₀ and grown for another 4h before 1 OD₆₀₀ unit (1 OD₆₀₀ unit represents 1 OD₆₀₀ in 1 ml) was harvested, washed with 1 ml distilled water, and diluted 1:100 in 100 μ l HC-leu without any GSH. Cells were incubated at 30°C with continuous shaking using a *BioTek*-Microplate Reader. The OD₆₀₀ was measured every 10 min for as a minimum 30h. Three individual repeats were performed.

4.3.3 Determination of total GSH and GSSG content in cell lysates

Determination of whole cell GSH and GSSG is based on the DTNB-recycling assay described by Rahman et al., 2006 (Rahman et al., 2006). 50 OD₆₀₀ units of cells were harvested by centrifugation (3 min, 3000 rpm, 25°C). After washing the cells once with 10 ml Milli-Q H₂O the cell pellet was taken up in 250 μ l ice-cold SSA/HCl buffer (1.3% sulfosalicylic acid, 8 mM HCL) and transferred on ice. Approximately 500 μ l of glass beads (*Scientific Industries*) were added to the cell suspension. Cells were automatically lysed at 4°C using a cell disruptor (*Scientific Industries*) and after 3 min of disruption another 100 μ l of ice-cold SSA/HCl buffer was inserted to each tube, followed by a further disruption step for 5 min. After protein precipitation by incubation of the cell suspension on ice for 15 min, samples were centrifuged at 16 000 g for 15 min at 4°C and the lysate was transferred to a fresh tube. For determination of total glutathione, 10 μ l of supernatant was diluted 1:100 in ice-cold KPE buffer (100 mM KH₂PO₄, 100 mM K₂HPO₄, 5 mM EDTA, pH 7.5). For determination of GSSG, 100 μ l supernatant was treated for 1h at 25°C with 2 μ l of 20% 2-vinylpyridine (*SIGMA-ALDRICH*) in 100% ethanol and 40 μ l 1 M MES/TRIS pH 7.0, to raise the pH and allow GSH to get alkylated. GSSG samples were agitated briefly every 10 min to prevent lysate from settling. GSH and GSSG standards were prepared by serially diluting GSH (1 mg/ml stock, diluted in KPE buffer, *SIGMA-ALDRICH*) in KPE buffer or GSSG (2 mg/ml stock, diluted in KPE buffer, *SIGMA-ALDRICH*) in SSA/HCl buffer. For the recycling assay, 120 μ l of ice-cold KPE buffer with supplemented 0.9 mg/ml NADPH (*AppliChem*) and 0.9 mg/ml DTNB (*SIGMA-ALDRICH*) was inserted to either 20 μ l of GSH or GSSG samples and the corresponding standards in a 96-well plate (*Falcon*). Each sample was analyzed in duplicate. Absorbance was measured at 412 nm by a *CLARIOstar* microplate reader (*BMG labtech*, Ortenberg, Germany) and after 5 measurement cycles, 6.0 U of glutathione reductase (diluted in KPE buffer, *SIGMA-ALDRICH*) was added to start the reaction. Total GSH and GSSG content was determined using a standard

curve derived from a linear regression analysis of a known GSH and GSSG standard curve. GSH concentration was obtained subtracting GSSG concentration from the total glutathione pool.

4.3.4 Measurement with *OPT1* overexpression

Whole cell glutathione was analyzed by a DTNB-based assay. Therefore, BY4742 wild-type, $\Delta opt3$, $p_{TEF}OPT3$, $\Delta ycf1$, $\Delta ycf1\Delta opt3$ and $\Delta ycf1p_{TEF}OPT3$ strains were transformed with $p416-TEF-OPT1$. Cells were grown in HC-ura medium overnight (30°C, 24h) and diluted the next day to grow another 17h to 3.5 OD₆₀₀. Next, 50 OD₆₀₀ units per strain were separated in *Falcon* tubes. To the remaining cells 100 μ M GSH and 50 μ M GSSG was added. Whilst the treated cells incubated for another 1h at 30°C, the before separated cells were collected by centrifugation (3000 rpm, 3 min, 25 °C) washed once with distilled water, taken up in 250 μ l ice cold SSA/HCL buffer and kept on ice. Analysis of whole cell GSH and GSSG was carried out as described in 4.3.3.

4.3.5 Phluorin measurements

The yeast strains $\Delta opt3$, $p_{TEF}OPT3$ and a BY4742 wild-type were co-transformed with the plasmids $p415-TEF-OPT1$ and $p416-MET-PHLUORIN$. For background subtraction a WT was transformed with $p415-TEF-OPT1$ plus an empty $p416-MET$ plasmid. Cells were grown in corresponding selection media for 24h diluted 1:800 in fresh selection media. After 17h cultivation, 1.5 OD₆₀₀ unit per measurement condition was collected by centrifugation for 3 min at 3000 rpm. 200 μ l of each individual strain was resuspended in fresh HC-ura-leu-met growth media and 0.1 M Mes/Tris buffer solutions with pH of 5.5, 6, 6.5, 7 and 7.5 to establish a standard curve for probe calibration.

Afterwards samples were shifted to a 96 well plate (*Falcon*) and analyzed in a Clariostar (*BMG labtech*). For pH determination the samples were excited with 410 nm and 470 nm and emission at 508 nm was detected. After 15 cycles of measurement, cells resuspended in HC-ura-leu-met were treated with 20 μ l of 100 μ M GSH (solubilized in HC-ura-leu-met) and measurement was continued for 1h. For analyzation the 470/410 nm ratio of each calibration sample was calculated. Next, the average of the ratio from the first 10 cycles was build and a standard curve was calculated using *Excel*. To determine the pH before and after the treatment with GSH not only the average of the first 10 cycles before GSH induction, but also of the last 10 cycles after induction was built. With help of the standard curve the pH was calculated. The calculated Δ pH corresponds to the subtraction of pH after GSH treatment and before treatment.

4.3.6 Determination of E_{GSH}

Yeast strains were transformed with either p415-*TEF-GRX1-roGFP2* or a p415-*TEF* empty plasmid and p416-*TEF-OPT1*. The cells were inoculated in corresponding HC-ura-leu selection media and grown for 24h at 30°C. After overnight growth, cells were diluted 1:400 in fresh media and incubated for another 17h at 30°C till they reached an OD₆₀₀ of approximately 3.5. 1.5 OD₆₀₀ units per well (1 OD₆₀₀ unit equals 1 ml culture with and OD₆₀₀ of 1) were collected by centrifugation (3 min, 3000 rpm) and resuspended in 200 µl HC-ura-leu aliquots with a density of 7.5 OD₆₀₀/ml. The aliquots were transferred into a *Falcon* 96-well plate and treated with 20 mM diamide (*SIGMA-ALDRICH*) or 100 mM DTT (*SIGMA-ALDRICH*) as oxidized and reduced controls or treated with either 100 µM GSH (*SIGMA-ALDRICH*) or 50 µM GSSG (*SIGMA-ALDRICH*). For fluorescence background subtraction, cells transformed with the p415-*TEF* empty plasmid were used. roGFP2 has two excitation maxima dependent on the oxidation state of the close to the chromophore introduced cysteines. While the roGFP2 chromophore is mostly in its anionic form when roGFP2 is oxidized and shows predominantly an excitation maximum at ~400 nm, the chromophore of reduced roGFP2 is mostly protonated and thus has an excitation maximum at ~480 nm. For both excitation wavelength the emission was recorded at 510 nm. Data was analyzed using *MARS* software (*BMG labtech*). The degree of roGFP2 oxidation was calculated with equation below.

$$OxDroGFP2 = \frac{1390 * 1480red - 1390red * 1480}{1390 * 1480red - 1390 * 1480ox + 1390ox * 1480 - 1390red * 1480}$$

4.3.7 roGFP2 measurements in the ER

The strains $\Delta opt3$, $p_{TEF}OPT3$ and wild-type were transformed with a p416-*MET25-SS-roGFP2-GRX1-HDEL* plasmid and grown over night in HC media lacking methionine and uracil. After 24h growth cells were diluted 1:400 in fresh HC-ura-met and incubated for 17h till they reached an OD₆₀₀ of approximately 3.5. The harvesting procedure was carried out like described in 4.3.6 except that samples were resuspended in 0.1 M MES/TRIS buffer (pH 6) instead of fresh media. For measurement, cells were treated with diamide or DTT as oxidized and reduced control or in 0.1 M MES/TRIS buffer (pH 6) serial diluted H₂O₂ (*SIGMA-ALDRICH*) with 8 concentrations from 1000 µM to 0 µM.

4.3.8 Growth test with shifted glutathione synthesis

The BY4742 strains $\Delta gsh2$, $\Delta gsh2\Delta opt3$ and $\Delta gsh2p_{TEF}OPT3$ were transformed with the different plasmid combinations p416-*TEF* empty + p415-*TEF* empty, p415-*TEF-SS-GSH1-HDEL* + p416-

TEF empty, p416-*TEF-SS-GSH2-HDEL* + p415-*TEF* empty or p415-*TEF-SS-GSH1-HDEL* + p416-*TEF-SS-GSH2-HDEL* and selected on 2 μ M GSH containing HC-ura-leu plates. For control a BY4742 WT strain was transformed with the empty plasmids p415-*TEF* and p416-*TEF* before selected on same growth plates. Strains were streaked on HC-ura-leu plates supplemented with 2 μ M GSH and HC-ura-leu plates without GSH and incubated over night at 30°C. After two more rounds of re-streaking, potential growth phenotypes were analyzed, and the plates were scanned.

4.3.9 Growth assay of *OPT3* Cysteine-Mutants

OPT3 and single cysteine mutants of *OPT3* were created and ordered from *GeneScript* (sequences in Appendix). The strain Δ *gsh2* Δ *opt3* was transformed with the plasmids p416-*TEF*; p416-*TEF-OPT3-C65A*; p416-*TEF-OPT3-C205A*; p416-*TEF-OPT3-C320A*; p416-*TEF-OPT3-C452A*; p416-*TEF-OPT3-C459A*; p416-*TEF-OPT3-C565A*; p416-*TEF-OPT3-C572A*; p416-*TEF-OPT3-C584A*; p416-*TEF-OPT3-C607A*; p416-*TEF-OPT3-C623A*; p416-*TEF-OPT3-C719A* and plated on HC-ura plates, supplemented with 2 μ M GSH and incubated for 24h at 30°C. Next, cells were re-streaked on both: HC-ura plates supplemented with 2 μ M and on HC-ura plates without GSH followed by an incubation time of 24 hours. Afterwards a second re-streak was performed on fresh plates. After another 24 hours incubation time the growth plates were analyzed.

4.3.10 Drop dilution assay

Cells were cultured for 17h at 30°C in HC media and diluted the next day to 0.5 OD₆₀₀. After cells grew for another 4h at 30°C in HC media, 1 OD₆₀₀ unit per sample was harvested and washed once in 1 ml MiliQ-water and finally resuspended in 1 ml fresh MiliQ-water. A dilution series of each resuspended sample was performed in MiliQ-water (from 1 OD to 1x10⁻⁵ OD). 5 μ l of each concentration was dropped on corresponding growth plates. The plates were incubated for 42h at 30°C and scanned afterwards. Drop dilution assay of each strain was repeated at least 3 times.

4.3.11 Halo assay

Cells were inoculated in HC medium overnight (17h). The next day cultures were diluted to 0.1 OD₆₀₀ in HC media and incubated for another 4h. Afterwards, 1 OD₆₀₀ unit per strain was harvested, washed in 1 ml MiliQ-water, and finally diluted to 0.1 OD₆₀₀ unit in MiliQ-water. 100 μ l of each diluted strain was plated in duplicates on HC plates. Next, a 9 mm filter paper (*CarlRoth*) was arranged in the middle of the agar plate and 5 μ l of either 3 mM DTT, 3 mM H₂O₂ or MiliQ-water as control, was dropped on the filter paper. After incubation for 42h at 30°C the

radius of each halo was measured and plates were scanned. The assay was repeated at least 3 times per strain in technical duplicates.

4.3.12 ER Stress Resistance assay

BY4742 WT, $\Delta opt3$, $p_{TEF}OPT3$ and BY4741 $\Delta ire1$ were inoculated in YPD media and incubated for 19h at 30°C. The next day pre-cultures were diluted in 3 ml fresh YPD with a starting OD₆₀₀ of approximately 0.2. After another 6h growth at 30°C samples were diluted to 0.05 OD₆₀₀ in 10 ml YPD. Aliquots of 50 μ l sample were transmitted into a 96 well plate and 180 μ l YPD was added. Finally, 20 μ l of a tunicamycin dilution series with the concentrations 0.21, 0.27, 0.34, 0.42, 0.52, 0.66, 0.82, 1.02, 1.28, 1.6 or 2 μ g/ml were added to the samples resulting in an OD of 0.01 per well. After tunicamycin treatment for 18h at 30°C, 200 μ l of cell suspension was transferred to a new 96 *Falcon* plate and OD₆₀₀ was measured.

4.3.13 RNA, DNA isolation and quantitative real-time PCR analysis

RNA was obtained from 5 OD₆₀₀ units of cells treated with and without tunicamycin (1 μ g/ml), following the instructions of the *RNeasy RNA Isolation Kit (QIAGEN)*. Afterwards, 500 ng of the RNA samples served as a qPCR template. For the synthesis of the corresponding cDNA the Oligo(dT) Primer and the *SuperscriptTM* from *Invitrogen* were used. For the quantitative real-time PCR, qPCR SYBR Green Mix (Thermo Scientific) was used in the magnetic Induction Cycler (*bio molecular systems*). The cDNA of interest was amplified with the primer pairs listed in Table 3 with a final concentration of 400 nM.

The qPCR program started with denaturation step for 15 min at 95 °C, followed by a 3-step cycle amplification (95°C 20 sec; 58°C 20 sec; 72°C 30 sec) for a total of 40 cycles. Subsequent analysis of the relative gene expression was carried out using the $2^{-\Delta\Delta CT}$ method as described by Livak and colleagues (Livak and Schmittgen, 2001).

4.3.14 Microscopy

Cells were streaked out freshly on a HC plate and grown for 17h at 30 °C. The next day, cells were imaged with a Zeiss AxioScan7 using 63x and 100x oil objectives. For GFP detection samples were excited with light at 495 nm and emission was recorded at 509 nm. mCherry was observed by excitation at 587 nm and its emission was recorded at 610 nm. Pictures were analyzed using the software *ImageJ*.

4.4 Growth Media

4.4.1 LB-Media

LB media was produced by autoclaving 20 g of *Difco*[™] *LB Broth, Lennox (BD)* dissolved in 1l dH₂O.

4.4.2 LB-Plates

LB media was produced by autoclaving 20 g of *Difco*[™] *LB Agar, Lennox (BD)* and dissolved in 1l dH₂O. Afterwards the media was filled in petri dishes.

4.4.3 YPD-media

1.1% yeast extract (*SERVA*) and 2.1 % bacto pepton (*Roth*) were dissolved in water. Afterwards, pH was adapted to 5.5 with HCl before autoclaving the solution. As carbon source 2% glucose (*Roth*) was added to the autoclaved YP (YPD).

4.4.4 YPD-plates

1.1% yeast extract (*SERVA*) and 2.1 % bacto pepton (*Roth*) were mixed in water and pH was adjusted to 5.5 before 2% Agar (*SIGMA-ALDRICH*) was added. After autoclaving 2% glucose (*Roth*) was added and solution was poured into petri dishes.

4.4.5 Yeast Nitrogen Base-solution (YNB)

To generate YNB solution 2% of yeast nitrogen base (*Difco*[™]) and 2.5% ammonium sulphate ((NH₄)₂SO₄, *Gössing*) were dissolved in distilled H₂O and autoclaved.

4.4.6 Ten times drop out mix

Drop out mix is an essential component of the defined yeast growth media used in this study. For 10 x drop out mix defined amounts of amino acids (Table 6) were dissolved in 1l distilled H₂O.

Table 6 10 x drop out mix composition. The amino acids mixed in the 10 x HC drop out mix and their corresponding concentrations.

Amino acid	g/l
Arginine	0.2
Isoleucine	0.8
Methionine	0.2
Phenylalanine	0.5
Threonine	2
Tyrosine	0.6
Valine	1.5
Glutamic acid	1
Aspartic acid	1
Serine	2.5

For experiments in which DNA was under control of a *MET25* promoter a 10 x drop out mix without methionine was used.

4.4.7 Hartwell's complete (HC) media

If not other mentioned in the text, HC media was used in most experiments. To produce HC media 100 ml YNB solution was mixed with 100 ml 10 x drop out mix and 50 ml of 40% stock glucose (*Roth*) was added. Additionally, amino acid solutions were added (Table 7) and media was adjusted to 1l with dH₂O. Afterwards the media was sterile filtered using a sterile bottle top filter (0.2 µM) (*VWR*).

Table 7 Drop out amino acids. Variable amino acids in HC media. Individual amino acids can be dropped out for plasmid selection.

Amino acid	g/l
Uracil	0.8
Adenine	3.2
Lysine	0.8
Tryptophan	2
Leucine	8
Histidine	2.4

Commonly, HC media is used for plasmid selection. Thereby one or more of the amino acid solutions listed in Table 7 can be dropped out. In this study predominately HC-ura, HC-leu and HC-ura-leu were used.

4.4.8 HC-plates

For 1l HC-plates: YNB, 10 x drop out mix, glucose and the individual amino acids were mixed as mentioned in 4.4.7. In parallel 2% agar (*SIGMA-ALDRICH*) were dissolved in 670 ml dH₂O and autoclaved. After autoclaving the solubilized agar was added to the remaining components and the solution was poured in petri dishes.

References

- Ahmad, M., Anjum, N.A., Asif, A., Ahmad, A., 2020. Real-time monitoring of glutathione in living cells using genetically encoded FRET-based ratiometric nanosensor. *Sci. Rep.* 10, 992. <https://doi.org/10.1038/s41598-020-57654-y>
- Albrecht, S.C., Barata, A.G., Großhans, J., Teleman, A.A., Dick, T.P., 2011. In Vivo Mapping of Hydrogen Peroxide and Oxidized Glutathione Reveals Chemical and Regional Specificity of Redox Homeostasis. *Cell Metab.* 14, 819–829. <https://doi.org/10.1016/j.cmet.2011.10.010>
- Aller, I., Rouhier, N., Meyer, A.J., 2013. Development of roGFP2-derived redox probes for measurement of the glutathione redox potential in the cytosol of severely glutathione-deficient *rml1* seedlings. *Front. Plant Sci.* 4, 506. <https://doi.org/10.3389/fpls.2013.00506>
- Amponsah, P.S., Yahya, G., Zimmermann, J., Mai, M., Mergel, S., Mühlhaus, T., Storchova, Z., Morgan, B., 2021. Peroxiredoxins couple metabolism and cell division in an ultradian cycle. *Nat. Chem. Biol.* 17, 477–484. <https://doi.org/10.1038/s41589-020-00728-9>
- Aouida, M., Khodami-Pour, A., Ramotar, D., 2009. Novel role for the *Saccharomyces cerevisiae* oligopeptide transporter Opt2 in drug detoxification. *Biochem. Cell Biol. Biochim. Biol. Cell.* 87, 653–661. <https://doi.org/10.1139/o09-045>
- Aoyama, K., Nakaki, T., 2012. Inhibition of GTRAP3-18 May Increase Neuroprotective Glutathione (GSH) Synthesis. *Int. J. Mol. Sci.* 13, 12017–12035. <https://doi.org/10.3390/ijms130912017>
- Appenzeller-Herzog, C., 2011. Glutathione- and non-glutathione-based oxidant control in the endoplasmic reticulum. *J. Cell Sci.* 124, 847–855. <https://doi.org/10.1242/jcs.080895>
- Atkinson, H.J., Babbitt, P.C., 2009. An Atlas of the Thioredoxin Fold Class Reveals the Complexity of Function-Enabling Adaptations. *PLOS Comput. Biol.* 5, e1000541. <https://doi.org/10.1371/journal.pcbi.1000541>
- Austriaco, O. P., N., 2012. Endoplasmic reticulum involvement in yeast cell death. *Front. Oncol.* 2, 87. <https://doi.org/10.3389/fonc.2012.00087>
- Avezov, E., Cross, B.C.S., Kaminski Schierle, G.S., Winters, M., Harding, H.P., Melo, E.P., Kaminski, C.F., Ron, D., 2013. Lifetime imaging of a fluorescent protein sensor reveals surprising stability of ER thiol redox. *J. Cell Biol.* 201, 337–349. <https://doi.org/10.1083/jcb.201211155>
- Awoonor-Williams, E., Rowley, C.N., 2016. Evaluation of Methods for the Calculation of the pKa of Cysteine Residues in Proteins. *J. Chem. Theory Comput.* 12, 4662–4673. <https://doi.org/10.1021/acs.jctc.6b00631>
- Ayer, A., Sanwald, J., Pillay, B.A., Meyer, A.J., Perrone, G.G., Dawes, I.W., 2013. Distinct Redox Regulation in Sub-Cellular Compartments in Response to Various Stress Conditions in *Saccharomyces cerevisiae*. *PLOS ONE* 8, e65240. <https://doi.org/10.1371/journal.pone.0065240>
- Aza, P., Molpeceres, G., de Salas, F., Camarero, S., 2021. Design of an improved universal signal peptide based on the α -factor mating secretion signal for enzyme production in yeast. *Cell. Mol. Life Sci.* 78, 3691–3707. <https://doi.org/10.1007/s00018-021-03793-y>
- Bachhawat, A.K., Ganguli, D., Kaur, J., Kasturia, N., Thakur, A., Kaur, H., Kumar, A., Yadav, A., 2009. Glutathione Production in Yeast, in: Satyanarayana, T., Kunze, G. (Eds.), *Yeast Biotechnology: Diversity and Applications*. Springer Netherlands, Dordrecht, pp. 259–280. https://doi.org/10.1007/978-1-4020-8292-4_13
- Bachhawat, A.K., Thakur, A., Kaur, J., Zulkifli, M., 2013. Glutathione transporters. *Biochim. Biophys. Acta BBA - Gen. Subj., Cellular functions of glutathione* 1830, 3154–3164. <https://doi.org/10.1016/j.bbagen.2012.11.018>

- Bachhawat, A.K., Yadav, S., 2018. The glutathione cycle: Glutathione metabolism beyond the γ -glutamyl cycle. *IUBMB Life* 70, 585–592. <https://doi.org/10.1002/iub.1756>
- Baker, K.M., Chakravarthi, S., Langton, K.P., Sheppard, A.M., Lu, H., Bulleid, N.J., 2008. Low reduction potential of Ero1 α regulatory disulphides ensures tight control of substrate oxidation. *EMBO J.* 27, 2988–2997. <https://doi.org/10.1038/emboj.2008.230>
- Balodite, E., Strazdina, I., Martynova, J., Galinina, N., Rutkis, R., Lasa, Z., Kalnenieks, U., 2019. Translocation of *Zymomonas mobilis* pyruvate decarboxylase to periplasmic compartment for production of acetaldehyde outside the cytosol. *MicrobiologyOpen* 8, e00809. <https://doi.org/10.1002/mbo3.809>
- Bánhegyi, G., Lusini, L., Puskás, F., Rossi, R., Fulceri, R., Braun, L., Mile, V., di Simplicio, P., Mandl, J., Benedetti, A., 1999. Preferential transport of glutathione versus glutathione disulfide in rat liver microsomal vesicles. *J. Biol. Chem.* 274, 12213–12216. <https://doi.org/10.1074/jbc.274.18.12213>
- Bao, R., Zhang, Y., Lou, X., Zhou, C.-Z., Chen, Y., 2009. Structural and kinetic analysis of *Saccharomyces cerevisiae* thioredoxin Trx1: Implications for the catalytic mechanism of GSSG reduced by the thioredoxin system. *Biochim. Biophys. Acta BBA - Proteins Proteomics* 1794, 1218–1223. <https://doi.org/10.1016/j.bbapap.2009.04.001>
- Bass, R., Ruddock, L.W., Klappa, P., Freedman, R.B., 2004. A Major Fraction of Endoplasmic Reticulum-located Glutathione Is Present as Mixed Disulfides with Protein*. *J. Biol. Chem.* 279, 5257–5262. <https://doi.org/10.1074/jbc.M304951200>
- Baudouin-Cornu, P., Lagniel, G., Kumar, C., Huang, M.-E., Labarre, J., 2012. Glutathione Degradation Is a Key Determinant of Glutathione Homeostasis*. *J. Biol. Chem.* 287, 4552–4561. <https://doi.org/10.1074/jbc.M111.315705>
- Becerra-Rodríguez, C., Marsit, S., Galeote, V., 2020. Diversity of Oligopeptide Transport in Yeast and Its Impact on Adaptation to Winemaking Conditions. *Front. Genet.* 11, 602. <https://doi.org/10.3389/fgene.2020.00602>
- Berndt, C., Lillig, C.H., Flohé, L., 2014. Redox regulation by glutathione needs enzymes. *Front. Pharmacol.* 5, 168. <https://doi.org/10.3389/fphar.2014.00168>
- Bertoli, G., Simmen, T., Anelli, T., Molteni, S.N., Fesce, R., Sitia, R., 2004. Two Conserved Cysteine Triads in Human Ero1 α Cooperate for Efficient Disulfide Bond Formation in the Endoplasmic Reticulum *. *J. Biol. Chem.* 279, 30047–30052. <https://doi.org/10.1074/jbc.M403192200>
- Birk, J., Meyer, M., Aller, I., Hansen, H.G., Odermatt, A., Dick, T.P., Meyer, A.J., Appenzeller-Herzog, C., 2013a. Endoplasmic reticulum: reduced and oxidized glutathione revisited. *J. Cell Sci.* 126, 1604–1617. <https://doi.org/10.1242/jcs.117218>
- Birk, J., Ramming, T., Odermatt, A., Appenzeller-Herzog, C., 2013b. Green fluorescent protein-based monitoring of endoplasmic reticulum redox poise. *Front. Genet.* 0. <https://doi.org/10.3389/fgene.2013.00108>
- Botman, D., de Groot, D.H., Schmidt, P., Goedhart, J., Teusink, B., 2019. In vivo characterisation of fluorescent proteins in budding yeast. *Sci. Rep.* 9, 2234. <https://doi.org/10.1038/s41598-019-38913-z>
- Bourbouloux, A., Shahi, P., Chakladar, A., Delrot, S., Bachhawat, A.K., 2000. Hgt1p, a high affinity glutathione transporter from the yeast *Saccharomyces cerevisiae*. *J. Biol. Chem.* 275, 13259–13265. <https://doi.org/10.1074/jbc.275.18.13259>
- Braakman, I., Hebert, D.N., 2013. Protein folding in the endoplasmic reticulum. *Cold Spring Harb. Perspect. Biol.* 5, a013201. <https://doi.org/10.1101/cshperspect.a013201>
- Braaten, K.P., Laufer, M.R., 2008. Human Papillomavirus (HPV), HPV-Related Disease, and the HPV Vaccine. *Rev. Obstet. Gynecol.* 1, 2–10.
- Braun, N.A., Morgan, B., Dick, T.P., Schwappach, B., 2010. The yeast CLC protein counteracts vesicular acidification during iron starvation. *J. Cell Sci.* 123, 2342–2350. <https://doi.org/10.1242/jcs.068403>

- Breker, M., Gymrek, M., Moldavski, O., Schuldiner, M., 2014. LoQAtE--Localization and Quantitation ATlas of the yeast proteome. A new tool for multiparametric dissection of single-protein behavior in response to biological perturbations in yeast. *Nucleic Acids Res.* 42, D726-730. <https://doi.org/10.1093/nar/gkt933>
- Breker, M., Gymrek, M., Schuldiner, M., 2013. A novel single-cell screening platform reveals proteome plasticity during yeast stress responses. *J. Cell Biol.* 200, 839–850. <https://doi.org/10.1083/jcb.201301120>
- Bulger, J.E., Brandt, K.G., 1971. Yeast glutathione reductase. II. Interaction of oxidized and 2-electron reduced enzyme with reduced and oxidized nicotinamide adenine dinucleotide phosphate. *J. Biol. Chem.* 246, 5578–5587.
- Byrne, L.J., Sidhu, A., Wallis, A.K., Ruddock, L.W., Freedman, R.B., Howard, M.J., Williamson, R.A., 2009. Mapping of the ligand-binding site on the b' domain of human PDI: interaction with peptide ligands and the x-linker region. *Biochem. J.* 423, 209–217. <https://doi.org/10.1042/BJ20090565>
- Cagnac, O., Bourbonloux, A., Chakrabarty, D., Zhang, M.-Y., Delrot, S., 2004. AtOPT6 Transports Glutathione Derivatives and Is Induced by Primisulfuron. *Plant Physiol.* 135, 1378–1387. <https://doi.org/10.1104/pp.104.039859>
- Calabrese, G., Morgan, B., Riemer, J., 2017. Mitochondrial Glutathione: Regulation and Functions. *Antioxid. Redox Signal.* 27, 1162–1177. <https://doi.org/10.1089/ars.2017.7121>
- Calabrese, G., Peker, E., Amponsah, P.S., Hoehne, M.N., Riemer, T., Mai, M., Bienert, G.P., Deponte, M., Morgan, B., Riemer, J., 2019. Hyperoxidation of mitochondrial peroxiredoxin limits H₂O₂-induced cell death in yeast. *EMBO J.* 38, e101552. <https://doi.org/10.15252/embj.2019101552>
- Cannon, M.B., Remington, S.J., 2006. Re-engineering redox-sensitive green fluorescent protein for improved response rate. *Protein Sci. Publ. Protein Soc.* 15, 45–57. <https://doi.org/10.1110/ps.051734306>
- Cardenas-Rodriguez, M., Chatzi, A., Tokatlidis, K., 2018. Iron–sulfur clusters: from metals through mitochondria biogenesis to disease. *J. Biol. Inorg. Chem.* 23, 509–520. <https://doi.org/10.1007/s00775-018-1548-6>
- Chakraborty, R., Baek, J.H., Bae, E.Y., Kim, W.-Y., Lee, S.Y., Kim, M.G., 2016. Comparison and contrast of plant, yeast, and mammalian ER stress and UPR. *Appl. Biol. Chem.* 59, 337–347. <https://doi.org/10.1007/s13765-016-0167-6>
- Chakravarthi, S., Bulleid, N.J., 2004. Glutathione is required to regulate the formation of native disulfide bonds within proteins entering the secretory pathway. *J. Biol. Chem.* 279, 39872–39879. <https://doi.org/10.1074/jbc.M406912200>
- Chakravarthi, S., Jessop, C.E., Bulleid, N.J., 2006. The role of glutathione in disulphide bond formation and endoplasmic-reticulum-generated oxidative stress. *EMBO Rep.* 7, 271–275. <https://doi.org/10.1038/sj.embor.7400645>
- Chandel, A., Bachhawat, A.K., 2017. Redox regulation of the yeast voltage-gated Ca²⁺ channel homolog Cch1p by glutathionylation of specific cysteine residues. *J. Cell Sci.* 130, 2317–2328. <https://doi.org/10.1242/jcs.202853>
- Chawla, A., Chakrabarti, S., Ghosh, G., Niwa, M., 2011. Attenuation of yeast UPR is essential for survival and is mediated by IRE1 kinase. *J. Cell Biol.* 193, 41–50. <https://doi.org/10.1083/jcb.201008071>
- Cheng, Z., Arscott, L.D., Ballou, D.P., Williams, C.H., 2007. The relationship of the redox potentials of thioredoxin and thioredoxin reductase from *Drosophila melanogaster* to the enzymatic mechanism: reduced thioredoxin is the reductant of glutathione in *Drosophila*. *Biochemistry* 46, 7875–7885. <https://doi.org/10.1021/bi700442r>
- Chiang, H.-L., 1995. Protein targeting and degradation in the yeast vacuole. *Can. J. Bot.* 73, 347–351. <https://doi.org/10.1139/b95-266>

- Cohen, Y., Schuldiner, M., 2011. Advanced methods for high-throughput microscopy screening of genetically modified yeast libraries. *Methods Mol. Biol.* Clifton NJ 781, 127–159. https://doi.org/10.1007/978-1-61779-276-2_8
- Collinson, E.J., Wheeler, G.L., Garrido, E.O., Avery, A.M., Avery, S.V., Grant, C.M., 2002. The yeast glutaredoxins are active as glutathione peroxidases. *J. Biol. Chem.* 277, 16712–16717. <https://doi.org/10.1074/jbc.M111686200>
- Costanzo, M., Baryshnikova, A., Bellay, J., Kim, Y., Spear, E.D., Sevier, C.S., Ding, H., Koh, J.L.Y., Toufighi, K., Mostafavi, S., Prinz, J., St Onge, R.P., VanderSluis, B., Makhnevych, T., Vizeacoumar, F.J., Alizadeh, S., Bahr, S., Brost, R.L., Chen, Y., Cokol, M., Deshpande, R., Li, Z., Lin, Z.-Y., Liang, W., Marback, M., Paw, J., San Luis, B.-J., Shuteriqi, E., Tong, A.H.Y., van Dyk, N., Wallace, I.M., Whitney, J.A., Weirauch, M.T., Zhong, G., Zhu, H., Houry, W.A., Brudno, M., Ragibzadeh, S., Papp, B., Pál, C., Roth, F.P., Giaever, G., Nislow, C., Troyanskaya, O.G., Bussey, H., Bader, G.D., Gingras, A.-C., Morris, Q.D., Kim, P.M., Kaiser, C.A., Myers, C.L., Andrews, B.J., Boone, C., 2010. The genetic landscape of a cell. *Science* 327, 425–431. <https://doi.org/10.1126/science.1180823>
- Costanzo, M., VanderSluis, B., Koch, E.N., Baryshnikova, A., Pons, C., Tan, G., Wang, W., Usaj, M., Hanchard, J., Lee, S.D., Pelechano, V., Styles, E.B., Billmann, M., van Leeuwen, J., van Dyk, N., Lin, Z.-Y., Kuzmin, E., Nelson, J., Piotrowski, J.S., Srikumar, T., Bahr, S., Chen, Y., Deshpande, R., Kurat, C.F., Li, S.C., Li, Z., Usaj, M.M., Okada, H., Pascoe, N., San Luis, B.-J., Sharifpoor, S., Shuteriqi, E., Simpkins, S.W., Snider, J., Suresh, H.G., Tan, Y., Zhu, H., Malod-Dognin, N., Janjic, V., Przulj, N., Troyanskaya, O.G., Stagljar, I., Xia, T., Ohya, Y., Gingras, A.-C., Raught, B., Boutros, M., Steinmetz, L.M., Moore, C.L., Rosebrock, A.P., Caudy, A.A., Myers, C.L., Andrews, B., Boone, C., 2016. A global genetic interaction network maps a wiring diagram of cellular function. *Science* 353, aaf1420. <https://doi.org/10.1126/science.aaf1420>
- Courel, M., Lallet, S., Camadro, J.-M., Blaiseau, P.-L., 2005. Direct Activation of Genes Involved in Intracellular Iron Use by the Yeast Iron-Responsive Transcription Factor Aft2 without Its Paralog Aft1. *Mol. Cell. Biol.* 25, 6760–6771. <https://doi.org/10.1128/MCB.25.15.6760-6771.2005>
- Cox, J.S., Walter, P., 1996. A novel mechanism for regulating activity of a transcription factor that controls the unfolded protein response. *Cell* 87, 391–404. [https://doi.org/10.1016/s0092-8674\(00\)81360-4](https://doi.org/10.1016/s0092-8674(00)81360-4)
- Crawford, R.R., Prescott, E.T., Sylvester, C.F., Higdon, A.N., Shan, J., Kilberg, M.S., Mungrue, I.N., 2015. Human CHAC1 Protein Degrades Glutathione, and mRNA Induction Is Regulated by the Transcription Factors ATF4 and ATF3 and a Bipartite ATF/CRE Regulatory Element. *J. Biol. Chem.* 290, 15878–15891. <https://doi.org/10.1074/jbc.M114.635144>
- Cuozzo, J.W., Kaiser, C.A., 1999. Competition between glutathione and protein thiols for disulphide-bond formation. *Nat. Cell Biol.* 1, 130–135. <https://doi.org/10.1038/11047>
- Czuba, L.C., Hillgren, K.M., Swaan, P.W., 2018. Post-translational Modifications of Transporters. *Pharmacol. Ther.* 192, 88–99. <https://doi.org/10.1016/j.pharmthera.2018.06.013>
- Daniel, T., Faruq, H.M., Laura Magdalena, J., Manuela, G., Christopher Horst, L., 2020. Role of GSH and Iron-Sulfur Glutaredoxins in Iron Metabolism—Review. *Molecules* 25, 3860. <https://doi.org/10.3390/molecules25173860>
- Day, P.M., Thompson, C.D., Schowalter, R.M., Lowy, D.R., Schiller, J.T., 2013. Identification of a Role for the trans-Golgi Network in Human Papillomavirus 16 Pseudovirus Infection. *J. Virol.* 87, 3862–3870. <https://doi.org/10.1128/JVI.03222-12>
- Delaunay-Moisan, A., Ponsero, A., Toledano, M.B., 2017. Reexamining the Function of Glutathione in Oxidative Protein Folding and Secretion. *Antioxid. Redox Signal.* 27, 1178–1199. <https://doi.org/10.1089/ars.2017.7148>

- Delic, M., Mattanovich, D., Gasser, B., 2010. Monitoring intracellular redox conditions in the endoplasmic reticulum of living yeasts. *FEMS Microbiol. Lett.* 306, 61–66. <https://doi.org/10.1111/j.1574-6968.2010.01935.x>
- Delic, M., Valli, M., Graf, A.B., Pfeffer, M., Mattanovich, D., Gasser, B., 2013. The secretory pathway: exploring yeast diversity. *FEMS Microbiol. Rev.* 37, 872–914. <https://doi.org/10.1111/1574-6976.12020>
- Deponte, M., 2017. The Incomplete Glutathione Puzzle: Just Guessing at Numbers and Figures? *Antioxid. Redox Signal.* 27, 1130–1161. <https://doi.org/10.1089/ars.2017.7123>
- Deponte, M., 2013. Glutathione catalysis and the reaction mechanisms of glutathione-dependent enzymes. *Biochim. Biophys. Acta BBA - Gen. Subj., Cellular functions of glutathione* 1830, 3217–3266. <https://doi.org/10.1016/j.bbagen.2012.09.018>
- Dhaoui, M., Auchère, F., Blaiseau, P.-L., Lesuisse, E., Landoulsi, A., Camadro, J.-M., Haguener-Tsapis, R., Belgareh-Touzé, N., 2011. Gex1 is a yeast glutathione exchanger that interferes with pH and redox homeostasis. *Mol. Biol. Cell* 22, 2054–2067. <https://doi.org/10.1091/mbc.e10-11-0906>
- Dickinson, D.A., Forman, H.J., 2002. Glutathione in defense and signaling: lessons from a small thiol. *Ann. N. Y. Acad. Sci.* 973, 488–504. <https://doi.org/10.1111/j.1749-6632.2002.tb04690.x>
- Dooley, C.T., Dore, T.M., Hanson, G.T., Jackson, W.C., Remington, S.J., Tsien, R.Y., 2004. Imaging Dynamic Redox Changes in Mammalian Cells with Green Fluorescent Protein Indicators*. *J. Biol. Chem.* 279, 22284–22293. <https://doi.org/10.1074/jbc.M312847200>
- Elbaz-Alon, Y., Morgan, B., Clancy, A., Amoako, T.N.E., Zalckvar, E., Dick, T.P., Schwappach, B., Schuldiner, M., 2014. The yeast oligopeptide transporter Opt2 is localized to peroxisomes and affects glutathione redox homeostasis. *FEMS Yeast Res.* 14, 1055–1067. <https://doi.org/10.1111/1567-1364.12196>
- Ellgaard, L., Sevier, C.S., Bulleid, N.J., 2018. How Are Proteins Reduced in the Endoplasmic Reticulum? *Trends Biochem. Sci.* 43, 32–43. <https://doi.org/10.1016/j.tibs.2017.10.006>
- Eraso, P., Martínez-Burgos, M., Falcón-Pérez, J.M., Portillo, F., Mazón, M.J., 2004. Ycf1-dependent cadmium detoxification by yeast requires phosphorylation of residues Ser908 and Thr911. *FEBS Lett.* 577, 322–326. <https://doi.org/10.1016/j.febslet.2004.10.030>
- Fernandes, L., Rodrigues-Pousada, C., Struhl, K., 1997. Yap, a novel family of eight bZIP proteins in *Saccharomyces cerevisiae* with distinct biological functions. *Mol. Cell. Biol.* 17, 6982–6993.
- Fitzgerald, I., Glick, B.S., 2014. Secretion of a foreign protein from budding yeasts is enhanced by cotranslational translocation and by suppression of vacuolar targeting. *Microb. Cell Factories* 13, 125. <https://doi.org/10.1186/s12934-014-0125-0>
- Flohé, L., 2013. The fairytale of the GSSG/GSH redox potential. *Biochim. Biophys. Acta BBA - Gen. Subj., Cellular functions of glutathione* 1830, 3139–3142. <https://doi.org/10.1016/j.bbagen.2012.10.020>
- Forman, H.J., Zhang, H., Rinna, A., 2009. Glutathione: Overview of its protective roles, measurement, and biosynthesis. *Mol. Aspects Med., Glutathione in Health and Disease* 30, 1–12. <https://doi.org/10.1016/j.mam.2008.08.006>
- Frand, A.R., Kaiser, C.A., 1998. The ERO1 gene of yeast is required for oxidation of protein dithiols in the endoplasmic reticulum. *Mol. Cell* 1, 161–170. [https://doi.org/10.1016/s1097-2765\(00\)80017-9](https://doi.org/10.1016/s1097-2765(00)80017-9)
- Galant, A., Preuss, M.L., Cameron, J.C., Jez, J.M., 2011. Plant Glutathione Biosynthesis: Diversity in Biochemical Regulation and Reaction Products. *Front. Plant Sci.* 2, 45. <https://doi.org/10.3389/fpls.2011.00045>
- Ganguli, D., Kumar, C., Bachhawat, A.K., 2007. The Alternative Pathway of Glutathione Degradation Is Mediated by a Novel Protein Complex Involving Three New Genes in *Saccharomyces cerevisiae*. *Genetics* 175, 1137–1151. <https://doi.org/10.1534/genetics.106.066944>

- Garrido, E.O., Grant, C.M., 2002. Role of thioredoxins in the response of *Saccharomyces cerevisiae* to oxidative stress induced by hydroperoxides. *Mol. Microbiol.* 43, 993–1003. <https://doi.org/10.1046/j.1365-2958.2002.02795.x>
- Ghosh, M., Shen, J., Rosen, B.P., 1999. Pathways of As(III) detoxification in *Saccharomyces cerevisiae*. *Proc. Natl. Acad. Sci.* 96, 5001–5006. <https://doi.org/10.1073/pnas.96.9.5001>
- Go, Y.-M., Jones, D.P., 2008. Redox compartmentalization in eukaryotic cells. *Biochim. Biophys. Acta* 1780, 1273–1290. <https://doi.org/10.1016/j.bbagen.2008.01.011>
- Goemans, C., Denoncin, K., Collet, J.-F., 2014. Folding mechanisms of periplasmic proteins. *Biochim. Biophys. Acta BBA - Mol. Cell Res., Protein trafficking and secretion in bacteria* 1843, 1517–1528. <https://doi.org/10.1016/j.bbamcr.2013.10.014>
- Goulding, C.W., Sawaya, M.R., Parseghian, A., Lim, V., Eisenberg, D., Missiakas, D., 2002. Thiol–Disulfide Exchange in an Immunoglobulin-like Fold: Structure of the N-Terminal Domain of DsbD. *Biochemistry* 41, 6920–6927. <https://doi.org/10.1021/bi016038l>
- Grant, C.M., 2001. Role of the glutathione/glutaredoxin and thioredoxin systems in yeast growth and response to stress conditions. *Mol. Microbiol.* 39, 533–541. <https://doi.org/10.1046/j.1365-2958.2001.02283.x>
- Grant, C.M., Collinson, L.P., Roe, J.H., Dawes, I.W., 1996. Yeast glutathione reductase is required for protection against oxidative stress and is a target gene for yAP-1 transcriptional regulation. *Mol. Microbiol.* 21, 171–179. <https://doi.org/10.1046/j.1365-2958.1996.6351340.x>
- Grant, C.M., Maclver, F.H., Dawes, I.W., 1997. Glutathione synthetase is dispensable for growth under both normal and oxidative stress conditions in the yeast *Saccharomyces cerevisiae* due to an accumulation of the dipeptide gamma-glutamylcysteine. *Mol. Biol. Cell* 8, 1699–1707.
- Greetham, D., Grant, C.M., 2009. Antioxidant activity of the yeast mitochondrial one-Cys peroxiredoxin is dependent on thioredoxin reductase and glutathione in vivo. *Mol. Cell. Biol.* 29, 3229–3240. <https://doi.org/10.1128/MCB.01918-08>
- Gross, E., Sevier, C.S., Heldman, N., Vitu, E., Bentzur, M., Kaiser, C.A., Thorpe, C., Fass, D., 2006. Generating disulfides enzymatically: reaction products and electron acceptors of the endoplasmic reticulum thiol oxidase Ero1p. *Proc. Natl. Acad. Sci. U. S. A.* 103, 299–304. <https://doi.org/10.1073/pnas.0506448103>
- Gueldry, O., Lazard, M., Delort, F., Dauplais, M., Grigoras, I., Blanquet, S., Plateau, P., 2003. Ycf1p-dependent Hg(II) detoxification in *Saccharomyces cerevisiae*. *Eur. J. Biochem.* 270, 2486–2496. <https://doi.org/10.1046/j.1432-1033.2003.03620.x>
- Guha, P., Kaptan, E., Gade, P., Kalvakolanu, D.V., Ahmed, H., 2017. Tunicamycin induced endoplasmic reticulum stress promotes apoptosis of prostate cancer cells by activating mTORC1. *Oncotarget* 8, 68191–68207. <https://doi.org/10.18632/oncotarget.19277>
- Gupta, V., Carroll, K.S., 2014. Sulfenic acid chemistry, detection and cellular lifetime. *Biochim. Biophys. Acta BBA - Gen. Subj., Current methods to study reactive oxygen species - pros and cons* 1840, 847–875. <https://doi.org/10.1016/j.bbagen.2013.05.040>
- Gutscher, M., Pauleau, A.-L., Marty, L., Brach, T., Wabnitz, G.H., Samstag, Y., Meyer, A.J., Dick, T.P., 2008. Real-time imaging of the intracellular glutathione redox potential. *Nat. Methods* 5, 553–559. <https://doi.org/10.1038/nmeth.1212>
- Halloran, M., Parakh, S., Atkin, J.D., 2013. The Role of S-Nitrosylation and S-Glutathionylation of Protein Disulphide Isomerase in Protein Misfolding and Neurodegeneration. *Int. J. Cell Biol.* 2013, 797914. <https://doi.org/10.1155/2013/797914>
- Hanschmann, E.-M., Godoy, J.R., Berndt, C., Hudemann, C., Lillig, C.H., 2013. Thioredoxins, Glutaredoxins, and Peroxiredoxins—Molecular Mechanisms and Health Significance: from Cofactors to Antioxidants to Redox Signaling. *Antioxid. Redox Signal.* 19, 1539–1605. <https://doi.org/10.1089/ars.2012.4599>
- Hanson, G.T., Aggeler, R., Oglesbee, D., Cannon, M., Capaldi, R.A., Tsien, R.Y., Remington, S.J., 2004. Investigating Mitochondrial Redox Potential with Redox-sensitive Green Fluorescent

- Protein Indicators*. *J. Biol. Chem.* 279, 13044–13053. <https://doi.org/10.1074/jbc.M312846200>
- Hanukoglu, I., 2015. Proteopedia: Rossmann fold: A beta-alpha-beta fold at dinucleotide binding sites. *Biochem. Mol. Biol. Educ.* 43, 206–209. <https://doi.org/10.1002/bmb.20849>
- Harington, C.R., Mead, T.H., 1935. Synthesis of glutathione. *Biochem. J.* 29, 1602–1611.
- Hatori, Y., Kubo, T., Sato, Y., Inouye, S., Akagi, R., Seyama, T., 2020. Visualization of the Redox Status of Cytosolic Glutathione Using the Organelle- and Cytoskeleton-Targeted Redox Sensors. *Antioxidants* 9, 129. <https://doi.org/10.3390/antiox9020129>
- He, L., He, T., Farrar, S., Ji, L., Liu, T., Ma, X., 2017. Antioxidants Maintain Cellular Redox Homeostasis by Elimination of Reactive Oxygen Species. *Cell. Physiol. Biochem.* 44, 532–553. <https://doi.org/10.1159/000485089>
- He, W., Wang, Y., Liu, W., Zhou, C.-Z., 2007. Crystal structure of *Saccharomyces cerevisiae* 6-phosphogluconate dehydrogenase Gnd1. *BMC Struct. Biol.* 7, 38. <https://doi.org/10.1186/1472-6807-7-38>
- Hecht, K.A., O'Donnell, A.F., Brodsky, J.L., 2014. The proteolytic landscape of the yeast vacuole. *Cell. Logist.* 4, e28023. <https://doi.org/10.4161/cl.28023>
- Hidaka, Y., Shimamoto, S., 2013. Folding of peptides and proteins: role of disulfide bonds, recent developments. *Biomol. Concepts* 4, 597–604. <https://doi.org/10.1515/bmc-2013-0022>
- Ho, B., Baryshnikova, A., Brown, G.W., 2018. Unification of Protein Abundance Datasets Yields a Quantitative *Saccharomyces cerevisiae* Proteome. *Cell Syst.* 6, 192-205.e3. <https://doi.org/10.1016/j.cels.2017.12.004>
- Hogg, P.J., 2013. Targeting allosteric disulphide bonds in cancer. *Nat. Rev. Cancer* 13, 425–431. <https://doi.org/10.1038/nrc3519>
- Hopkins, F.G., 1929. ON GLUTATHIONE: A REINVESTIGATION. *J. Biol. Chem.* 84, 269–320. [https://doi.org/10.1016/S0021-9258\(18\)77062-2](https://doi.org/10.1016/S0021-9258(18)77062-2)
- Hopkins, F.G., 1921. On an Autoxidisable Constituent of the Cell. *Biochem. J.* 15, 286–305. <https://doi.org/10.1042/bj0150286>
- Hopkins, F.G., Dixon, M., 1922. On Glutathione. II. A Thermostable Oxidation-Reduction System. *J. Cell Biol.* 54, 527–563.
- Horst, M., Knecht, E.C., Schu, P.V., 1999. Import into and Degradation of Cytosolic Proteins by Isolated Yeast Vacuoles. *Mol. Biol. Cell* 10, 2879–2889.
- Hou, J., Schacherer, J., 2017. Fitness Trade-Offs Lead to Suppressor Tolerance in Yeast. *Mol. Biol. Evol.* 34, 110–118. <https://doi.org/10.1093/molbev/msw225>
- Huang, H., Ullah, F., Zhou, D.-X., Yi, M., Zhao, Y., 2019. Mechanisms of ROS Regulation of Plant Development and Stress Responses. *Front. Plant Sci.* 0. <https://doi.org/10.3389/fpls.2019.00800>
- Hunter, G., Eagles, B.A., 1927. NON-PROTEIN SULFUR COMPOUNDS OF BLOOD: II. GLUTATHIONE. *J. Biol. Chem.* 72, 133–146. [https://doi.org/10.1016/S0021-9258\(18\)84367-8](https://doi.org/10.1016/S0021-9258(18)84367-8)
- Hwang, C., Sinskey, A.J., Lodish, H.F., 1992. Oxidized redox state of glutathione in the endoplasmic reticulum. *Science* 257, 1496–1502. <https://doi.org/10.1126/science.1523409>
- Inoue, Y., Sugiyama, K., Izawa, S., Kimura, A., 1998. Molecular identification of glutathione synthetase (GSH2) gene from *Saccharomyces cerevisiae*. *Biochim. Biophys. Acta* 1395, 315–320. [https://doi.org/10.1016/s0167-4781\(97\)00199-1](https://doi.org/10.1016/s0167-4781(97)00199-1)
- Iversen, R., Andersen, P.A., Jensen, K.S., Winther, J.R., Sigurskjold, B.W., 2010. Thiol–Disulfide Exchange between Glutaredoxin and Glutathione. *Biochemistry* 49, 810–820. <https://doi.org/10.1021/bi9015956>
- Janke, C., Magiera, M.M., Rathfelder, N., Taxis, C., Reber, S., Maekawa, H., Moreno-Borchart, A., Doenges, G., Schwob, E., Schiebel, E., Knop, M., 2004. A versatile toolbox for PCR-based tagging of yeast genes: new fluorescent proteins, more markers and promoter substitution cassettes. *Yeast* Chichester Engl. 21, 947–962. <https://doi.org/10.1002/yea.1142>

- Jaspers, C.J., Penninckx, M.J., 1984. Glutathione metabolism in yeast *Saccharomyces cerevisiae*. Evidence that gamma-glutamyltranspeptidase is a vacuolar enzyme. *Biochimie* 66, 71–74. [https://doi.org/10.1016/0300-9084\(84\)90193-7](https://doi.org/10.1016/0300-9084(84)90193-7)
- Johnson, D.C., Dean, D.R., Smith, A.D., Johnson, M.K., 2005. Structure, function, and formation of biological iron-sulfur clusters. *Annu. Rev. Biochem.* 74, 247–281. <https://doi.org/10.1146/annurev.biochem.74.082803.133518>
- Kanzok, S.M., Fechner, A., Bauer, H., Ulschmid, J.K., Müller, H.-M., Botella-Munoz, J., Schneuwly, S., Schirmer, R.H., Becker, K., 2001. Substitution of the Thioredoxin System for Glutathione Reductase in *Drosophila melanogaster*. *Science* 291, 643–646. <https://doi.org/10.1126/science.291.5504.643>
- Kanzok, S.M., Schirmer, R.H., Türbachova, I., Iozef, R., Becker, K., 2000. The Thioredoxin System of the Malaria Parasite *Plasmodium falciparum*: GLUTATHIONE REDUCTION REVISITED *. *J. Biol. Chem.* 275, 40180–40186. <https://doi.org/10.1074/jbc.M007633200>
- Karki, R., Rimal, S., Rieth, M.D., 2021. Predicted N-terminal N-linked glycosylation sites may underlie membrane protein expression patterns in *Saccharomyces cerevisiae*. *Yeast* 38, 497–506. <https://doi.org/10.1002/yea.3657>
- Kaur, H., Ganguli, D., Bachhawat, A.K., 2012. Glutathione degradation by the alternative pathway (DUG pathway) in *Saccharomyces cerevisiae* is initiated by (Dug2p-Dug3p)₂ complex, a novel glutamine amidotransferase (GATase) enzyme acting on glutathione. *J. Biol. Chem.* 287, 8920–8931. <https://doi.org/10.1074/jbc.M111.327411>
- Kaur, H., Kumar, C., Junot, C., Toledano, M.B., Bachhawat, A.K., 2009. Dug1p Is a Cys-Gly Peptidase of the γ -Glutamyl Cycle of *Saccharomyces cerevisiae* and Represents a Novel Family of Cys-Gly Peptidases. *J. Biol. Chem.* 284, 14493–14502. <https://doi.org/10.1074/jbc.M808952200>
- Kawahara, T., Yanagi, H., Yura, T., Mori, K., 1998. Unconventional splicing of HAC1/ERN4 mRNA required for the unfolded protein response. Sequence-specific and non-sequential cleavage of the splice sites. *J. Biol. Chem.* 273, 1802–1807. <https://doi.org/10.1074/jbc.273.3.1802>
- Khandelwal, N.K., Millan, C.R., Zangari, S.I., Avila, S., Williams, D., Thaker, T.M., Tomasiak, T.M., 2021. The structural basis for regulation of the glutathione transporter Ycf1 by regulatory domain phosphorylation. <https://doi.org/10.1101/2021.06.18.449046>
- Kim, S., Kim, C.M., Son, Y.-J., Choi, J.Y., Siegenthaler, R.K., Lee, Y., Jang, T.-H., Song, J., Kang, H., Kaiser, C.A., Park, H.H., 2018. Molecular basis of maintaining an oxidizing environment under anaerobiosis by soluble fumarate reductase. *Nat. Commun.* 9, 4867. <https://doi.org/10.1038/s41467-018-07285-9>
- Kimata, Y., Kimata, Y.I., Shimizu, Y., Abe, H., Farcasanu, I.C., Takeuchi, M., Rose, M.D., Kohno, K., 2003. Genetic Evidence for a Role of BiP/Kar2 That Regulates Ire1 in Response to Accumulation of Unfolded Proteins. *Mol. Biol. Cell* 14, 2559–2569. <https://doi.org/10.1091/mbc.E02-11-0708>
- Klein, M., Mamnun, Y.M., Eggmann, T., Schüller, C., Wolfger, H., Martinoia, E., Kuchler, K., 2002. The ATP-binding cassette (ABC) transporter Bpt1p mediates vacuolar sequestration of glutathione conjugates in yeast. *FEBS Lett.* 520, 63–67. [https://doi.org/10.1016/S0014-5793\(02\)02767-9](https://doi.org/10.1016/S0014-5793(02)02767-9)
- Koh, S., Wiles, A.M., Sharp, J.S., Naider, F.R., Becker, J.M., Stacey, G., 2002. An Oligopeptide Transporter Gene Family in *Arabidopsis*. *Plant Physiol.* 128, 21–29. <https://doi.org/10.1104/pp.010332>
- Koreishi, M., Gniadek, T.J., Yu, S., Masuda, J., Honjo, Y., Satoh, A., 2013. The Golgin Tether Giantin Regulates the Secretory Pathway by Controlling Stack Organization within Golgi Apparatus. *PLoS ONE* 8, e59821. <https://doi.org/10.1371/journal.pone.0059821>
- Kotytk, A., 1994. Dependence of the kinetics of secondary active transports in yeast on H(+)-ATPase acidification. *J. Membr. Biol.* 138, 29–35. <https://doi.org/10.1007/BF00211066>
- Krezel, A., Bal, W., 1999. Coordination chemistry of glutathione. *Acta Biochim. Pol.* 46, 567–580.

- Kuge, S., Jones, N., 1994. YAP1 dependent activation of TRX2 is essential for the response of *Saccharomyces cerevisiae* to oxidative stress by hydroperoxides. *EMBO J.* 13, 655–664.
- Kulak, N.A., Pichler, G., Paron, I., Nagaraj, N., Mann, M., 2014. Minimal, encapsulated proteomic-sample processing applied to copy-number estimation in eukaryotic cells. *Nat. Methods* 11, 319–324. <https://doi.org/10.1038/nmeth.2834>
- Kumar, C., Igarria, A., D'Autreaux, B., Planson, A.-G., Junot, C., Godat, E., Bachhawat, A.K., Delaunay-Moisan, A., Toledano, M.B., 2011. Glutathione revisited: a vital function in iron metabolism and ancillary role in thiol-redox control. *EMBO J.* 30, 2044–2056. <https://doi.org/10.1038/emboj.2011.105>
- Lazard, M., Ha-Duong, N.-T., Mounié, S., Perrin, R., Plateau, P., Blanquet, S., 2011. Selenodiglutathione uptake by the *Saccharomyces cerevisiae* vacuolar ATP-binding cassette transporter Ycf1p. *FEBS J.* 278, 4112–4121. <https://doi.org/10.1111/j.1742-4658.2011.08318.x>
- Lee, K.P.K., Dey, M., Neculai, D., Cao, C., Dever, T.E., Sicheri, F., 2008. Structure of the dual enzyme Ire1 reveals the basis for catalysis and regulation in nonconventional RNA splicing. *Cell* 132, 89–100. <https://doi.org/10.1016/j.cell.2007.10.057>
- Lee, K.-S., Kim, J.-S., Heo, P., Yang, T.-J., Sung, Y.-J., Cheon, Y., Koo, H.M., Yu, B.J., Seo, J.-H., Jin, Y.-S., Park, J.C., Kweon, D.-H., 2013. Characterization of *Saccharomyces cerevisiae* promoters for heterologous gene expression in *Kluyveromyces marxianus*. *Appl. Microbiol. Biotechnol.* 97, 2029–2041. <https://doi.org/10.1007/s00253-012-4306-7>
- Li, S., Bronnimann, M.P., Williams, S.J., Campos, S.K., 2019. Glutathione contributes to efficient post-Golgi trafficking of incoming HPV16 genome. *PLoS One* 14, e0225496. <https://doi.org/10.1371/journal.pone.0225496>
- Li, S.C., Kane, P.M., 2009. The yeast lysosome-like vacuole: Endpoint and crossroads. *Biochim. Biophys. Acta BBA - Mol. Cell Res., Lysosomes* 1793, 650–663. <https://doi.org/10.1016/j.bbamcr.2008.08.003>
- Li, Z.-S., Lu, Y.-P., Zhen, R.-G., Szczycka, M., Thiele, D.J., Rea, P.A., 1997. A new pathway for vacuolar cadmium sequestration in *Saccharomyces cerevisiae*: YCF1-catalyzed transport of bis(glutathionato)cadmium. *Proc. Natl. Acad. Sci.* 94, 42–47. <https://doi.org/10.1073/pnas.94.1.42>
- Li, Z.-S., Szczycka, M., Lu, Y.-P., Thiele, D.J., Rea, P.A., 1996. The Yeast Cadmium Factor Protein (YCF1) Is a Vacuolar Glutathione S-Conjugate Pump (*). *J. Biol. Chem.* 271, 6509–6517. <https://doi.org/10.1074/jbc.271.11.6509>
- Liang, J.R., Lingeman, E., Luong, T., Ahmed, S., Muhar, M., Nguyen, T., Olzmann, J.A., Corn, J.E., 2020. A Genome-wide ER-phagy Screen Highlights Key Roles of Mitochondrial Metabolism and ER-Resident UFMylation. *Cell* 180, 1160–1177.e20. <https://doi.org/10.1016/j.cell.2020.02.017>
- Liebman, S.W., Sherman, F., 1976. Inhibition of growth by amber suppressors in yeast. *Genetics* 82, 233–249. <https://doi.org/10.1093/genetics/82.2.233>
- Liedgens, L., Zimmermann, J., Wäschenbach, L., Geissel, F., Laporte, H., Gohlke, H., Morgan, B., Deponte, M., 2020. Quantitative assessment of the determinant structural differences between redox-active and inactive glutaredoxins. *Nat. Commun.* 11, 1725. <https://doi.org/10.1038/s41467-020-15441-3>
- Lipatova, Z., Segev, N., 2015. A Role for Macro-ER-Phagy in ER Quality Control. *PLOS Genet.* 11, e1005390. <https://doi.org/10.1371/journal.pgen.1005390>
- Lipatova, Z., Shah, A.H., Kim, J.J., Mulholland, J.W., Segev, N., 2013. Regulation of ER-phagy by a Ypt/Rab GTPase module. *Mol. Biol. Cell* 24, 3133–3144. <https://doi.org/10.1091/mbc.e13-05-0269>
- Lismont, C., Walton, P.A., Fransen, M., 2017. Quantitative Monitoring of Subcellular Redox Dynamics in Living Mammalian Cells Using RoGFP2-Based Probes. *Methods Mol. Biol. Clifton NJ* 1595, 151–164. https://doi.org/10.1007/978-1-4939-6937-1_14

- Livak, K.J., Schmittgen, T.D., 2001. Analysis of Relative Gene Expression Data Using Real-Time Quantitative PCR and the $2^{-\Delta\Delta CT}$ Method. *Methods* 25, 402–408. <https://doi.org/10.1006/meth.2001.1262>
- LoPachin, R.M., Gavin, T., 2016. REACTIONS OF ELECTROPHILES WITH NUCLEOPHILIC THIOLATE SITES: RELEVANCE TO PATHOPHYSIOLOGICAL MECHANISMS AND REMEDIATION. *Free Radic. Res.* 50, 195–205. <https://doi.org/10.3109/10715762.2015.1094184>
- Lubkowitz, M., 2011. The Oligopeptide Transporters: A Small Gene Family with a Diverse Group of Substrates and Functions? *Mol. Plant* 4, 407–415. <https://doi.org/10.1093/mp/ssr004>
- Mailloux, R.J., 2020. Protein S-glutathionylation reactions as a global inhibitor of cell metabolism for the desensitization of hydrogen peroxide signals. *Redox Biol.* 32, 101472. <https://doi.org/10.1016/j.redox.2020.101472>
- Massey, V., Williams, C.H., 1965. On the reaction mechanism of yeast glutathione reductase. *J. Biol. Chem.* 240, 4470–4480.
- Masui, S., Vavassori, S., Fagioli, C., Sitia, R., Inaba, K., 2011. Molecular bases of cyclic and specific disulfide interchange between human ERO1 α protein and protein-disulfide isomerase (PDI). *J. Biol. Chem.* 286, 16261–16271. <https://doi.org/10.1074/jbc.M111.231357>
- Matsui, R., Ferran, B., Oh, A., Croteau, D., Shao, D., Han, J., Pimentel, D.R., Bachschmid, M.M., 2020. Redox Regulation via Glutaredoxin-1 and Protein S-Glutathionylation. *Antioxid. Redox Signal.* <https://doi.org/10.1089/ars.2019.7963>
- May, M.J., Vernoux, T., Leaver, C., Montagu, M.V., Inzé, D., 1998. Glutathione homeostasis in plants: implications for environmental sensing and plant development. *J. Exp. Bot.* 49, 649–667. <https://doi.org/10.1093/jxb/49.321.649>
- McAlpine, C.C., 2019. Thiols: Structure, Properties and Reactions. Nova Science Publishers, Incorporated, New York, UNITED STATES.
- Mehdi, K., Thierie, J., Penninckx, M.J., 2001. γ -Glutamyl transpeptidase in the yeast *Saccharomyces cerevisiae* and its role in the vacuolar transport and metabolism of glutathione. *Biochem. J.* 359, 631–637.
- Meister, A., Anderson, M.E., 1983. Glutathione. *Annu. Rev. Biochem.* 52, 711–760. <https://doi.org/10.1146/annurev.bi.52.070183.003431>
- Mesecke, N., Mittler, S., Eckers, E., Herrmann, J.M., Deponte, M., 2008a. Two Novel Monothiol Glutaredoxins from *Saccharomyces cerevisiae* Provide Further Insight into Iron-Sulfur Cluster Binding, Oligomerization, and Enzymatic Activity of Glutaredoxins. *Biochemistry* 47, 1452–1463. <https://doi.org/10.1021/bi7017865>
- Mesecke, N., Spang, A., Deponte, M., Herrmann, J.M., 2008b. A Novel Group of Glutaredoxins in the cis-Golgi Critical for Oxidative Stress Resistance. *Mol. Biol. Cell* 19, 2673–2680. <https://doi.org/10.1091/mbc.e07-09-0896>
- Meyer, A.J., Brach, T., Marty, L., Kreye, S., Rouhier, N., Jacquot, J.-P., Hell, R., 2007. Redox-sensitive GFP in *Arabidopsis thaliana* is a quantitative biosensor for the redox potential of the cellular glutathione redox buffer. *Plant J. Cell Mol. Biol.* 52, 973–986. <https://doi.org/10.1111/j.1365-313X.2007.03280.x>
- Miesenböck, G., De Angelis, D.A., Rothman, J.E., 1998. Visualizing secretion and synaptic transmission with pH-sensitive green fluorescent proteins. *Nature* 394, 192–195. <https://doi.org/10.1038/28190>
- Mieyal, J.J., Chock, P.B., 2012. Posttranslational Modification of Cysteine in Redox Signaling and Oxidative Stress: Focus on S-Glutathionylation. *Antioxid. Redox Signal.* 16, 471–475. <https://doi.org/10.1089/ars.2011.4454>
- Miller, S.I., Salama, N.R., 2018. The gram-negative bacterial periplasm: Size matters. *PLoS Biol.* 16, e2004935. <https://doi.org/10.1371/journal.pbio.2004935>
- Molinari, M., 2020. ER-phagy: Eating the Factory. *Mol. Cell* 78, 811–813. <https://doi.org/10.1016/j.molcel.2020.05.002>

- Montero, D., Tachibana, C., Rahr Winther, J., Appenzeller-Herzog, C., 2013. Intracellular glutathione pools are heterogeneously concentrated. *Redox Biol.* 1, 508–513. <https://doi.org/10.1016/j.redox.2013.10.005>
- Morgan, B., 2014. Reassessing cellular glutathione homeostasis: novel insights revealed by genetically encoded redox probes. *Biochem. Soc. Trans.* 42, 979–984. <https://doi.org/10.1042/BST20140101>
- Morgan, B., Ezeriņa, D., Amoako, T.N.E., Riemer, J., Seedorf, M., Dick, T.P., 2013. Multiple glutathione disulfide removal pathways mediate cytosolic redox homeostasis. *Nat. Chem. Biol.* 9, 119–125. <https://doi.org/10.1038/nchembio.1142>
- Morgan, B., Sobotta, M.C., Dick, T.P., 2011. Measuring EGSH and H₂O₂ with roGFP2-based redox probes. *Free Radic. Biol. Med.* 51, 1943–1951. <https://doi.org/10.1016/j.freeradbiomed.2011.08.035>
- Mühlenhoff, U., Braymer, J.J., Christ, S., Rietzschel, N., Uzarska, M.A., Weiler, B.D., Lill, R., 2020. Glutaredoxins and iron-sulfur protein biogenesis at the interface of redox biology and iron metabolism. *Biol. Chem.* 401, 1407–1428. <https://doi.org/10.1515/hsz-2020-0237>
- Muller, E.G., 1996. A glutathione reductase mutant of yeast accumulates high levels of oxidized glutathione and requires thioredoxin for growth. *Mol. Biol. Cell* 7, 1805–1813.
- Mumberg, D., Müller, R., Funk, M., 1995. Yeast vectors for the controlled expression of heterologous proteins in different genetic backgrounds. *Gene* 156, 119–122. [https://doi.org/10.1016/0378-1119\(95\)00037-7](https://doi.org/10.1016/0378-1119(95)00037-7)
- Murphy, M.P., 2009. How mitochondria produce reactive oxygen species. *Biochem. J.* 417, 1–13. <https://doi.org/10.1042/BJ20081386>
- Musaogullari, A., Chai, Y.-C., 2020. Redox Regulation by Protein S-Glutathionylation: From Molecular Mechanisms to Implications in Health and Disease. *Int. J. Mol. Sci.* 21, 8113. <https://doi.org/10.3390/ijms21218113>
- Nakamura, T., Naguro, I., Ichijo, H., 2019. Iron homeostasis and iron-regulated ROS in cell death, senescence and human diseases. *Biochim. Biophys. Acta Gen. Subj.* 1863, 1398–1409. <https://doi.org/10.1016/j.bbagen.2019.06.010>
- Neves, R.P.P., Fernandes, P.A., Ramos, M.J., 2017. Mechanistic insights on the reduction of glutathione disulfide by protein disulfide isomerase. *Proc. Natl. Acad. Sci.* 114, E4724–E4733. <https://doi.org/10.1073/pnas.1618985114>
- Ngosuwana, J., Wang, N.M., Fung, K.L., Chirico, W.J., 2003. Roles of Cytosolic Hsp70 and Hsp40 Molecular Chaperones in Post-translational Translocation of Presecretory Proteins into the Endoplasmic Reticulum*. *J. Biol. Chem.* 278, 7034–7042. <https://doi.org/10.1074/jbc.M210544200>
- Niu, Y., Zhang, L., Yu, J., Wang, C., Wang, L., 2016. Novel Roles of the Non-catalytic Elements of Yeast Protein-disulfide Isomerase in Its Interplay with Endoplasmic Reticulum Oxidoreductin 1*. *J. Biol. Chem.* 291, 8283–8294. <https://doi.org/10.1074/jbc.M115.694257>
- Oestreicher, J., Morgan, B., 2018. Glutathione: subcellular distribution and membrane transport. *Biochem Cell Biol* 97, 270–289. <https://doi.org/10.1139/bcb-2018-0189>
- Ogawa, N., Mori, K., 2004. Autoregulation of the HAC1 gene is required for sustained activation of the yeast unfolded protein response. *Genes Cells Devoted Mol. Cell. Mech.* 9, 95–104. <https://doi.org/10.1111/j.1365-2443.2004.00704.x>
- Ohashi, K., Mizuno, K., 2014. A novel pair of split venus fragments to detect protein-protein interactions by in vitro and in vivo bimolecular fluorescence complementation assays. *Methods Mol. Biol. Clifton NJ* 1174, 247–262. https://doi.org/10.1007/978-1-4939-0944-5_17
- Oliveira, A.P., Sauer, U., 2012. The importance of post-translational modifications in regulating *Saccharomyces cerevisiae* metabolism. *FEMS Yeast Res.* 12, 104–117. <https://doi.org/10.1111/j.1567-1364.2011.00765.x>

- Oliveira, M.A., Discola, K.F., Alves, S.V., Medrano, F.J., Guimarães, B.G., Netto, L.E.S., 2010. Insights into the specificity of thioredoxin reductase-thioredoxin interactions. A structural and functional investigation of the yeast thioredoxin system. *Biochemistry* 49, 3317–3326. <https://doi.org/10.1021/bi901962p>
- Osawa, H., Stacey, G., Gassmann, W., 2006. ScOPT1 and AtOPT4 function as proton-coupled oligopeptide transporters with broad but distinct substrate specificities. *Biochem. J.* 393, 267–275. <https://doi.org/10.1042/BJ20050920>
- Østergaard, H., Tachibana, C., Winther, J.R., 2004. Monitoring disulfide bond formation in the eukaryotic cytosol. *J. Cell Biol.* 166, 337–345. <https://doi.org/10.1083/jcb.200402120>
- Outten, C.E., Culotta, V.C., 2004. Alternative Start Sites in the *Saccharomyces cerevisiae* GLR1 Gene Are Responsible for Mitochondrial and Cytosolic Isoforms of Glutathione Reductase*. *J. Biol. Chem.* 279, 7785–7791. <https://doi.org/10.1074/jbc.M312421200>
- Pan, J.L., Bardwell, J.C.A., 2006. The origami of thioredoxin-like folds. *Protein Sci. Publ. Protein Soc.* 15, 2217–2227. <https://doi.org/10.1110/ps.062268106>
- Papanikou, E., Glick, B.S., 2009. The yeast Golgi apparatus: insights and mysteries. *FEBS Lett.* 583, 3746–3751. <https://doi.org/10.1016/j.febslet.2009.10.072>
- Parakh, S., Atkin, J.D., 2015. Frontiers | Novel roles for protein disulphide isomerase in disease states: a double edged sword? | Cell and Developmental Biology [WWW Document]. URL <https://www.frontiersin.org/articles/10.3389/fcell.2015.00030/full> (accessed 8.3.21).
- Paranagama, M.P., Sakamoto, K., Amino, H., Awano, M., Miyoshi, H., Kita, K., 2010. Contribution of the FAD and quinone binding sites to the production of reactive oxygen species from *Ascaris suum* mitochondrial complex II. *Mitochondrion* 10, 158–165. <https://doi.org/10.1016/j.mito.2009.12.145>
- Park, S.-H., Hahn, J.-S., 2019. Development of an efficient cytosolic isobutanol production pathway in *Saccharomyces cerevisiae* by optimizing copy numbers and expression of the pathway genes based on the toxic effect of α -acetolactate. *Sci. Rep.* 9, 3996. <https://doi.org/10.1038/s41598-019-40631-5>
- Paulo, E., García-Santamarina, S., Calvo, I.A., Carmona, M., Boronat, S., Domènech, A., Ayté, J., Hidalgo, E., 2014. A genetic approach to study H₂O₂ scavenging in fission yeast – distinct roles of peroxiredoxin and catalase. *Mol. Microbiol.* 92, 246–257. <https://doi.org/10.1111/mmi.12548>
- Paumi, C.M., Chuk, M., Chevelev, I., Stagljar, I., Michaelis, S., 2008. Negative Regulation of the Yeast ABC Transporter Ycf1p by Phosphorylation within Its N-terminal Extension *. *J. Biol. Chem.* 283, 27079–27088. <https://doi.org/10.1074/jbc.M802569200>
- Paumi, C.M., Chuk, M., Snider, J., Stagljar, I., Michaelis, S., 2009. ABC Transporters in *Saccharomyces cerevisiae* and Their Interactors: New Technology Advances the Biology of the ABCC (MRP) Subfamily. *Microbiol. Mol. Biol. Rev.* 73, 577–593. <https://doi.org/10.1128/MMBR.00020-09>
- Pearson, B.M., Schweizer, M., 2002. Basic functional analysis of six unknown open reading frames from *Saccharomyces cerevisiae*: four from chromosome VII and two from chromosome XV. *Yeast Chichester Engl.* 19, 123–129. <https://doi.org/10.1002/yea.809>
- Pedrajas, J.R., Padilla, C.A., McDonagh, B., Bárcena, J.A., 2010. Glutaredoxin participates in the reduction of peroxides by the mitochondrial 1-CYS peroxiredoxin in *Saccharomyces cerevisiae*. *Antioxid. Redox Signal.* 13, 249–258. <https://doi.org/10.1089/ars.2009.2950>
- Penninckx, M.J., 2002. An overview on glutathione in *Saccharomyces* versus non-conventional yeasts. *FEMS Yeast Res.* 2, 295–305. [https://doi.org/10.1016/S1567-1356\(02\)00081-8](https://doi.org/10.1016/S1567-1356(02)00081-8)
- Peskin, A.V., Pace, P.E., Behring, J.B., Paton, L.N., Soethoudt, M., Bachschmid, M.M., Winterbourn, C.C., 2016. Glutathionylation of the Active Site Cysteines of Peroxiredoxin 2 and Recycling by Glutaredoxin. *J. Biol. Chem.* 291, 3053–3062. <https://doi.org/10.1074/jbc.M115.692798>
- Petrovic, S., Pascolo, L., Gallo, R., Cupelli, F., Ostrow, J.D., Goffeau, A., Tiribelli, C., Bruschi, C.V., 2000. The products of YCF1 and YLL015w (BPT1) cooperate for the ATP-dependent

- vacuolar transport of unconjugated bilirubin in *Saccharomyces cerevisiae*. *Yeast* Chichester Engl. 16, 561–571. [https://doi.org/10.1002/\(SICI\)1097-0061\(200004\)16:6<561::AID-YEA551>3.0.CO;2-L](https://doi.org/10.1002/(SICI)1097-0061(200004)16:6<561::AID-YEA551>3.0.CO;2-L)
- Pickin, K.A., Ezenwajiaku, N., Overcash, H., Sethi, M., Knecht, M.R., Paumi, C.M., 2010. Suppression of Ycf1p function by Cka1p-dependent phosphorylation is attenuated in response to salt stress. *FEMS Yeast Res.* 10, 839–857. <https://doi.org/10.1111/j.1567-1364.2010.00677.x>
- Pike, S., Patel, A., Stacey, G., Gassmann, W., 2009. Arabidopsis OPT6 is an Oligopeptide Transporter with Exceptionally Broad Substrate Specificity. *Plant Cell Physiol.* 50, 1923–1932. <https://doi.org/10.1093/pcp/pcp136>
- Pincus, D., Chevalier, M.W., Aragón, T., van Anken, E., Vidal, S.E., El-Samad, H., Walter, P., 2010. BiP Binding to the ER-Stress Sensor Ire1 Tunes the Homeostatic Behavior of the Unfolded Protein Response. *PLoS Biol.* 8, e1000415. <https://doi.org/10.1371/journal.pbio.1000415>
- Pirie, N.W., Pinhey, K., 1929. THE TITRATION CURVE OF GLUTATHIONE. *J. Biol. Chem.* 84, 321–333. [https://doi.org/10.1016/S0021-9258\(18\)77063-4](https://doi.org/10.1016/S0021-9258(18)77063-4).
- Pirneskoski, A., Klappa, P., Lobell, M., Williamson, R.A., Byrne, L., Alanen, H.I., Salo, K.E.H., Kivirikko, K.I., Freedman, R.B., Ruddock, L.W., 2004. Molecular Characterization of the Principal Substrate Binding Site of the Ubiquitous Folding Catalyst Protein Disulfide Isomerase *. *J. Biol. Chem.* 279, 10374–10381. <https://doi.org/10.1074/jbc.M312193200>
- Pollard, M.G., Travers, K.J., Weissman, J.S., 1998. Ero1p: A Novel and Ubiquitous Protein with an Essential Role in Oxidative Protein Folding in the Endoplasmic Reticulum. *Mol. Cell* 1, 171–182. [https://doi.org/10.1016/S1097-2765\(00\)80018-0](https://doi.org/10.1016/S1097-2765(00)80018-0)
- Ponsero, A.J., Igarria, A., Darch, M.A., Miled, S., Outten, C.E., Winther, J.R., Palais, G., D'Autréaux, B., Delaunay-Moisan, A., Toledano, M.B., 2017. Endoplasmic Reticulum Transport of Glutathione by Sec61 Is Regulated by Ero1 and Bip. *Mol. Cell* 67, 962-973.e5. <https://doi.org/10.1016/j.molcel.2017.08.012>
- Potter, M.D., Nicchitta, C.V., 2002. Endoplasmic Reticulum-bound Ribosomes Reside in Stable Association with the Translocon following Termination of Protein Synthesis*. *J. Biol. Chem.* 277, 23314–23320. <https://doi.org/10.1074/jbc.M202559200>
- Potter, M.D., Seiser, R.M., Nicchitta, C.V., 2001. Ribosome exchange revisited: a mechanism for translation-coupled ribosome detachment from the ER membrane. *Trends Cell Biol.* 11, 112–115. [https://doi.org/10.1016/S0962-8924\(00\)01905-X](https://doi.org/10.1016/S0962-8924(00)01905-X)
- Presley, J.F., Smith, C., Hirschberg, K., Miller, C., Cole, N.B., Zaal, K.J.M., Lippincott-Schwartz, J., 1998. Golgi Membrane Dynamics. *Mol. Biol. Cell* 9, 1617–1626.
- Preuss, D., Mulholland, J., Kaiser, C.A., Orlean, P., Albright, C., Rose, M.D., Robbins, P.W., Botstein, D., 1991. Structure of the yeast endoplasmic reticulum: localization of ER proteins using immunofluorescence and immunoelectron microscopy. *Yeast* Chichester Engl. 7, 891–911. <https://doi.org/10.1002/yea.320070902>
- Qin, M., Wang, W., Thirumalai, D., 2015. Protein folding guides disulfide bond formation. *Proc. Natl. Acad. Sci.* 112, 11241–11246. <https://doi.org/10.1073/pnas.1503909112>
- Quijano, C., Trujillo, M., Castro, L., Trostchansky, A., 2016. Interplay between oxidant species and energy metabolism. *Redox Biol.* 8, 28–42. <https://doi.org/10.1016/j.redox.2015.11.010>
- Quintana-Cabrera, R., Fernandez-Fernandez, S., Bobo-Jimenez, V., Escobar, J., Sastre, J., Almeida, A., Bolaños, J.P., 2012. γ -Glutamylcysteine detoxifies reactive oxygen species by acting as glutathione peroxidase-1 cofactor. *Nat. Commun.* 3, 718. <https://doi.org/10.1038/ncomms1722>
- Rahman, I., Kode, A., Biswas, S.K., 2006. Assay for quantitative determination of glutathione and glutathione disulfide levels using enzymatic recycling method. *Nat. Protoc.* 1, 3159–3165. <https://doi.org/10.1038/nprot.2006.378>

- Ray, P.D., Huang, B.-W., Tsuji, Y., 2012. Reactive oxygen species (ROS) homeostasis and redox regulation in cellular signaling. *Cell. Signal.* 24, 981–990. <https://doi.org/10.1016/j.cellsig.2012.01.008>
- Rebbeor, J.F., Gregory, C.C., Dumont, M.E., Ballatori, N., 1998. ATP-dependent Transport of Reduced Glutathione on YCF1, the Yeast Orthologue of Mammalian Multidrug Resistance Associated Proteins *. *J. Biol. Chem.* 273, 33449–33454. <https://doi.org/10.1074/jbc.273.50.33449>
- Reddie, K.G., Carroll, K.S., 2008. Expanding the functional diversity of proteins through cysteine oxidation. *Curr. Opin. Chem. Biol., Biopolymers/Model Systems* 12, 746–754. <https://doi.org/10.1016/j.cbpa.2008.07.028>
- Rees, D.C., Johnson, E., Lewinson, O., 2009. ABC transporters: the power to change. *Nat. Rev. Mol. Cell Biol.* 10, 218–227. <https://doi.org/10.1038/nrm2646>
- Remington, S.J., 2011. Green fluorescent protein: A perspective. *Protein Sci. Publ. Protein Soc.* 20, 1509–1519. <https://doi.org/10.1002/pro.684>
- Rietsch, A., Belin, D., Martin, N., Beckwith, J., 1996. An in vivo pathway for disulfide bond isomerization in *Escherichia coli*. *Proc. Natl. Acad. Sci.* 93, 13048–13053. <https://doi.org/10.1073/pnas.93.23.13048>
- Rietsch, A., Bessette, P., Georgiou, G., Beckwith, J., 1997. Reduction of the periplasmic disulfide bond isomerase, DsbC, occurs by passage of electrons from cytoplasmic thioredoxin. *J. Bacteriol.* 179, 6602–6608. <https://doi.org/10.1128/jb.179.21.6602-6608.1997>
- Rodrigues-Pousada, C., Devaux, F., Caetano, S.M., Pimentel, C., da Silva, S., Cordeiro, A.C., Amaral, C., 2019. Yeast AP-1 like transcription factors (Yap) and stress response: a current overview. *Microb. Cell* 6, 267–285. <https://doi.org/10.15698/mic2019.06.679>
- Roscoe, J.M., Sevier, C.S., 2020. Pathways for Sensing and Responding to Hydrogen Peroxide at the Endoplasmic Reticulum. *Cells* 9, 2314. <https://doi.org/10.3390/cells9102314>
- Rothe, C., Lehle, L., 1998. Sorting of invertase signal peptide mutants in yeast dependent and independent on the signal-recognition particle. *Eur. J. Biochem.* 252, 16–24. <https://doi.org/10.1046/j.1432-1327.1998.2520016.x>
- Schafer, F.Q., Buettner, G.R., 2001. Redox environment of the cell as viewed through the redox state of the glutathione disulfide/glutathione couple. *Free Radic. Biol. Med.* 30, 1191–1212. [https://doi.org/10.1016/S0891-5849\(01\)00480-4](https://doi.org/10.1016/S0891-5849(01)00480-4)
- Schultz, L.W., Chivers, P.T., Raines, R.T., 1999. The CXXC motif: crystal structure of an active-site variant of *Escherichia coli* thioredoxin. *Acta Crystallogr. D Biol. Crystallogr.* 55, 1533–1538. <https://doi.org/10.1107/s0907444999008756>
- Schulz, G.E., Schirmer, R.H., Sachsenheimer, W., Pai, E.F., 1978. The structure of the flavoenzyme glutathione reductase. *Nature* 273, 120–124. <https://doi.org/10.1038/273120a0>
- Schwarzländer, M., Dick, T.P., Meyer, A.J., Morgan, B., 2016. Dissecting Redox Biology Using Fluorescent Protein Sensors. *Antioxid. Redox Signal.* 24, 680–712. <https://doi.org/10.1089/ars.2015.6266>
- Scirè, A., Cianfruglia, L., Minnelli, C., Bartolini, D., Torquato, P., Principato, G., Galli, F., Armeni, T., 2019. Glutathione compartmentalization and its role in glutathionylation and other regulatory processes of cellular pathways. *BioFactors Oxf. Engl.* 45, 152–168. <https://doi.org/10.1002/biof.1476>
- Seres, T., Ravichandran, V., Moriguchi, T., Rokutan, K., Thomas, J.A., Johnston, R.B., 1996. Protein S-thiolation and dethiolation during the respiratory burst in human monocytes. A reversible post-translational modification with potential for buffering the effects of oxidant stress. *J. Immunol.* 156, 1973–1980.
- Sevier, C.S., Qu, H., Heldman, N., Gross, E., Fass, D., Kaiser, C.A., 2007. Modulation of Cellular Disulfide-Bond Formation and the ER Redox Environment by Feedback Regulation of Ero1. *Cell* 129, 333–344. <https://doi.org/10.1016/j.cell.2007.02.039>

- Shamu, C.E., Walter, P., 1996. Oligomerization and phosphorylation of the Ire1p kinase during intracellular signaling from the endoplasmic reticulum to the nucleus. *EMBO J.* 15, 3028–3039.
- Sharma, D., Masison, D.C., 2009. Hsp70 Structure, Function, Regulation and Influence on Yeast Prions. *Protein Pept. Lett.* 16, 571–581.
- Sies, H., 1999. Glutathione and its role in cellular functions. *Free Radic. Biol. Med.* 27, 916–921. [https://doi.org/10.1016/S0891-5849\(99\)00177-X](https://doi.org/10.1016/S0891-5849(99)00177-X)
- Simoni, R.D., Hill, R.L., Vaughan, M., 2002. The Discovery of Glutathione by F. Gowland Hopkins and the Beginning of Biochemistry at Cambridge University. *J. Biol. Chem.* 277, 27–28. [https://doi.org/10.1016/S0021-9258\(20\)70350-9](https://doi.org/10.1016/S0021-9258(20)70350-9)
- Sipos, K., Lange, H., Fekete, Z., Ullmann, P., Lill, R., Kispal, G., 2002. Maturation of cytosolic iron-sulfur proteins requires glutathione. *J. Biol. Chem.* 277, 26944–26949. <https://doi.org/10.1074/jbc.M200677200>
- Sousa, C.A., Hanselaer, S., Soares, E.V., 2015. ABCC Subfamily Vacuolar Transporters are Involved in Pb (Lead) Detoxification in *Saccharomyces cerevisiae*. *Appl. Biochem. Biotechnol.* 175, 65–74. <https://doi.org/10.1007/s12010-014-1252-0>
- Srikanth, C.V., Vats, P., Bourbonloux, A., Delrot, S., Bachhawat, A.K., 2005. Multiple cis-regulatory elements and the yeast sulphur regulatory network are required for the regulation of the yeast glutathione transporter, Hgt1p. *Curr. Genet.* 47, 345–358. <https://doi.org/10.1007/s00294-005-0571-7>
- Staudacher, V., Trujillo, M., Diederichs, T., Dick, T.P., Radi, R., Morgan, B., Deponte, M., 2018. Redox-sensitive GFP fusions for monitoring the catalytic mechanism and inactivation of peroxiredoxins in living cells. *Redox Biol.* 14, 549–556. <https://doi.org/10.1016/j.redox.2017.10.017>
- Suda, Y., Nakano, A., 2012. The Yeast Golgi Apparatus. *Traffic* 13, 505–510. <https://doi.org/10.1111/j.1600-0854.2011.01316.x>
- Suzuki, T., Yokoyama, A., Tsuji, T., Ikeshima, E., Nakashima, K., Ikushima, S., Kobayashi, C., Yoshida, S., 2011. Identification and characterization of genes involved in glutathione production in yeast. *J. Biosci. Bioeng.* 112, 107–113. <https://doi.org/10.1016/j.jbiosc.2011.04.007>
- Tan, S.-X., Greetham, D., Raeth, S., Grant, C.M., Dawes, I.W., Perrone, G.G., 2010. The Thioredoxin-Thioredoxin Reductase System Can Function in Vivo as an Alternative System to Reduce Oxidized Glutathione in *Saccharomyces cerevisiae**. *J. Biol. Chem.* 285, 6118–6126. <https://doi.org/10.1074/jbc.M109.062844>
- Tanner, W., Lehle, L., 1987. Protein glycosylation in yeast. *Biochim. Biophys. Acta* 906, 81–99. [https://doi.org/10.1016/0304-4157\(87\)90006-2](https://doi.org/10.1016/0304-4157(87)90006-2)
- Thibault, G., Ng, D.T.W., 2012. The Endoplasmic Reticulum-Associated Degradation Pathways of Budding Yeast. *Cold Spring Harb. Perspect. Biol.* 4, a013193. <https://doi.org/10.1101/cshperspect.a013193>
- Toledano, M.B., Delaunay-Moisan, A., Outten, C.E., Igarria, A., 2013. Functions and Cellular Compartmentation of the Thioredoxin and Glutathione Pathways in Yeast. *Antioxid. Redox Signal.* 18, 1699–1711. <https://doi.org/10.1089/ars.2012.5033>
- Toledano, M.B., Kumar, C., Le Moan, N., Spector, D., Tacnet, F., 2007. The system biology of thiol redox system in *Escherichia coli* and yeast: differential functions in oxidative stress, iron metabolism and DNA synthesis. *FEBS Lett.* 581, 3598–3607. <https://doi.org/10.1016/j.febslet.2007.07.002>
- Torres-Quiroz, F., García-Marqués, S., Coria, R., Randez-Gil, F., Prieto, J.A., 2010. The activity of yeast Hog1 MAPK is required during endoplasmic reticulum stress induced by tunicamycin exposure. *J. Biol. Chem.* 285, 20088–20096. <https://doi.org/10.1074/jbc.M109.063578>
- Townsend, D.M., Manevich, Y., He, L., Xiong, Y., Bowers, R.R., Hutchens, S., Tew, K.D., 2009. Nitrosative stress-induced s-glutathionylation of protein disulfide isomerase leads to

- activation of the unfolded protein response. *Cancer Res.* 69, 7626–7634. <https://doi.org/10.1158/0008-5472.CAN-09-0493>
- Travers, K.J., Patil, C.K., Wodicka, L., Lockhart, D.J., Weissman, J.S., Walter, P., 2000. Functional and genomic analyses reveal an essential coordination between the unfolded protein response and ER-associated degradation. *Cell* 101, 249–258. [https://doi.org/10.1016/s0092-8674\(00\)80835-1](https://doi.org/10.1016/s0092-8674(00)80835-1)
- Trotter, E.W., Grant, C.M., 2002. Thioredoxins are required for protection against a reductive stress in the yeast *Saccharomyces cerevisiae*. *Mol. Microbiol.* 46, 869–878. <https://doi.org/10.1046/j.1365-2958.2002.03216.x>
- Tsunoda, S., Avezov, E., Zyryanova, A., Konno, T., Mendes-Silva, L., Pinho Melo, E., Harding, H.P., Ron, D., 2014. Intact protein folding in the glutathione-depleted endoplasmic reticulum implicates alternative protein thiol reductants. *eLife* 3, e03421. <https://doi.org/10.7554/eLife.03421>
- Tu, B.P., Ho-Schleyer, S.C., Travers, K.J., Weissman, J.S., 2000. Biochemical Basis of Oxidative Protein Folding in the Endoplasmic Reticulum. *Science* 290, 1571–1574. <https://doi.org/10.1126/science.290.5496.1571>
- Tu, B.P., Weissman, J.S., 2002. The FAD- and O(2)-dependent reaction cycle of Ero1-mediated oxidative protein folding in the endoplasmic reticulum. *Mol. Cell* 10, 983–994. [https://doi.org/10.1016/s1097-2765\(02\)00696-2](https://doi.org/10.1016/s1097-2765(02)00696-2)
- Ulrich, K., Jakob, U., 2019. The role of thiols in antioxidant systems. *Free Radic. Biol. Med.* 140, 14–27. <https://doi.org/10.1016/j.freeradbiomed.2019.05.035>
- Van Laer, K., Hamilton, C.J., Messens, J., 2013. Low-molecular-weight thiols in thiol-disulfide exchange. *Antioxid. Redox Signal.* 18, 1642–1653. <https://doi.org/10.1089/ars.2012.4964>
- van Leeuwen, J., Pons, C., Tan, G., Wang, J.Z., Hou, J., Weile, J., Gebbia, M., Liang, W., Shuteriqi, E., Li, Z., Lopes, M., Ušaj, M., Dos Santos Lopes, A., van Lieshout, N., Myers, C.L., Roth, F.P., Aloy, P., Andrews, B.J., Boone, C., 2020. Systematic analysis of bypass suppression of essential genes. *Mol. Syst. Biol.* 16, e9828. <https://doi.org/10.15252/msb.20209828>
- van Lith, M., Tiwari, S., Pediani, J., Milligan, G., Bulleid, N.J., 2011. Real-time monitoring of redox changes in the mammalian endoplasmic reticulum. *J. Cell Sci.* 124, 2349–2356. <https://doi.org/10.1242/jcs.085530>
- Vitu, E., Kim, S., Sevier, C.S., Lutzky, O., Heldman, N., Bentzur, M., Unger, T., Yona, M., Kaiser, C.A., Fass, D., 2010. Oxidative activity of yeast Ero1p on protein disulfide isomerase and related oxidoreductases of the endoplasmic reticulum. *J. Biol. Chem.* 285, 18155–18165. <https://doi.org/10.1074/jbc.M109.064931>
- Wall, S., Oh, J.-Y., Diers, A., Landar, A., 2012. Oxidative Modification of Proteins: An Emerging Mechanism of Cell Signaling. *Front. Physiol.* 3, 369. <https://doi.org/10.3389/fphys.2012.00369>
- Wang, J., Pareja, K.A., Kaiser, C.A., Sevier, C.S., 2014. Redox signaling via the molecular chaperone BiP protects cells against endoplasmic reticulum-derived oxidative stress. *eLife* 3, e03496. <https://doi.org/10.7554/eLife.03496>
- Wang, J., Sevier, C.S., 2016. Formation and Reversibility of BiP Protein Cysteine Oxidation Facilitate Cell Survival during and post Oxidative Stress. *J. Biol. Chem.* 291, 7541–7557. <https://doi.org/10.1074/jbc.M115.694810>
- Wang, L., Li, S.-J., Sidhu, A., Zhu, L., Liang, Y., Freedman, R.B., Wang, C.-C., 2009. Reconstitution of human Ero1-L α /protein-disulfide isomerase oxidative folding pathway in vitro. Position-dependent differences in role between the a and a' domains of protein-disulfide isomerase. *J. Biol. Chem.* 284, 199–206. <https://doi.org/10.1074/jbc.M806645200>
- Wawrzycka, D., Sobczak, I., Bartosz, G., Bocser, T., Ułaszewski, S., Goffeau, A., 2010. Vmr 1p is a novel vacuolar multidrug resistance ABC transporter in *Saccharomyces cerevisiae*. *FEMS Yeast Res.* 10, 828–838. <https://doi.org/10.1111/j.1567-1364.2010.00673.x>

- Wei, W., Smith, N., Wu, X., Kim, H., Seravalli, J., Khalimonchuk, O., Lee, J., 2014. YCF1-Mediated Cadmium Resistance in Yeast Is Dependent on Copper Metabolism and Antioxidant Enzymes. *Antioxid. Redox Signal.* 21, 1475–1489. <https://doi.org/10.1089/ars.2013.5436>
- Weill, U., Krieger, G., Avihou, Z., Milo, R., Schuldiner, M., Davidi, D., 2019. Assessment of GFP Tag Position on Protein Localization and Growth Fitness in Yeast. *J. Mol. Biol.* 431, 636–641. <https://doi.org/10.1016/j.jmb.2018.12.004>
- Weissman, J.S., Kimt, P.S., 1993. Efficient catalysis of disulphide bond rearrangements by protein disulphide isomerase. *Nature* 365, 185–188. <https://doi.org/10.1038/365185a0>
- Wemmie, J.A., Wu, A.L., Harshman, K.D., Parker, C.S., Moye-Rowley, W.S., 1994. Transcriptional activation mediated by the yeast AP-1 protein is required for normal cadmium tolerance. *J. Biol. Chem.* 269, 14690–14697. [https://doi.org/10.1016/S0021-9258\(17\)36680-2](https://doi.org/10.1016/S0021-9258(17)36680-2)
- Wheeler, G.L., Trotter, E.W., Dawes, I.W., Grant, C.M., 2003. Coupling of the transcriptional regulation of glutathione biosynthesis to the availability of glutathione and methionine via the Met4 and Yap1 transcription factors. *J. Biol. Chem.* 278, 49920–49928. <https://doi.org/10.1074/jbc.M310156200>
- Wiedemann, C., Kumar, A., Lang, A., Ohlenschläger, O., 2020. Cysteines and Disulfide Bonds as Structure-Forming Units: Insights From Different Domains of Life and the Potential for Characterization by NMR. *Front. Chem.* 8, 280. <https://doi.org/10.3389/fchem.2020.00280>
- Wiles, A.M., Naider, F., Becker, J.M., 2006. Transmembrane domain prediction and consensus sequence identification of the oligopeptide transport family. *Res. Microbiol.* 157, 395–406. <https://doi.org/10.1016/j.resmic.2005.10.004>
- Wilkinson, B., Xiao, R., Gilbert, H.F., 2005. A structural disulfide of yeast protein-disulfide isomerase destabilizes the active site disulfide of the N-terminal thioredoxin domain. *J. Biol. Chem.* 280, 11483–11487. <https://doi.org/10.1074/jbc.M414203200>
- Winterbourn, C.C., Metodiewa, D., 1999. Reactivity of biologically important thiol compounds with superoxide and hydrogen peroxide. *Free Radic. Biol. Med.* 27, 322–328. [https://doi.org/10.1016/s0891-5849\(99\)00051-9](https://doi.org/10.1016/s0891-5849(99)00051-9)
- Wu, A.L., Moye-Rowley, W.S., 1994. GSH1, which encodes gamma-glutamylcysteine synthetase, is a target gene for yAP-1 transcriptional regulation. *Mol. Cell. Biol.* 14, 5832–5839.
- Wu, B., Qiao, J., Wang, X., Liu, M., Xu, S., Sun, D., 2021. Factors affecting the rapid changes of protein under short-term heat stress. *BMC Genomics* 22, 263. <https://doi.org/10.1186/s12864-021-07560-y>
- Wu, G., Fang, Y.-Z., Yang, S., Lupton, J.R., Turner, N.D., 2004. Glutathione Metabolism and Its Implications for Health. *J. Nutr.* 134, 489–492. <https://doi.org/10.1093/jn/134.3.489>
- Wu, H., Ng, B.S.H., Thibault, G., 2014. Endoplasmic reticulum stress response in yeast and humans. *Biosci. Rep.* 34, e00118. <https://doi.org/10.1042/BSR20140058>
- Xiong, Y., Manevich, Y., Tew, K.D., Townsend, D.M., 2012. S-Glutathionylation of Protein Disulfide Isomerase Regulates Estrogen Receptor α Stability and Function. *Int. J. Cell Biol.* 2012, 273549. <https://doi.org/10.1155/2012/273549>
- Xu, M., Marsh, H.M., Sevier, C.S., 2016. A Conserved Cysteine within the ATPase Domain of the Endoplasmic Reticulum Chaperone BiP is Necessary for a Complete Complement of BiP Activities. *J. Mol. Biol.* 428, 4168–4184. <https://doi.org/10.1016/j.jmb.2016.08.011>
- Ye, Z.-W., Zhang, J., Ancrum, T., Manevich, Y., Townsend, D.M., Tew, K.D., 2017. Glutathione S-Transferase P-Mediated Protein S-Glutathionylation of Resident Endoplasmic Reticulum Proteins Influences Sensitivity to Drug-Induced Unfolded Protein Response. *Antioxid. Redox Signal.* 26, 247–261. <https://doi.org/10.1089/ars.2015.6486>
- Yu, J., Zhou, C.-Z., 2007a. Crystal structure of glutathione reductase Glr1 from the yeast *Saccharomyces cerevisiae*. *Proteins* 68, 972–979. <https://doi.org/10.1002/prot.21354>
- Yu, J., Zhou, C.-Z., 2007b. Crystal structure of glutathione reductase Glr1 from the yeast *Saccharomyces cerevisiae*. *Proteins Struct. Funct. Bioinforma.* 68, 972–979. <https://doi.org/10.1002/prot.21354>

- Yun, H., Tianwen, W., Xianyan, L., Guocheng, D., Jian, C., Jigai, X., 2010. Anti-Oxidative Stress and Beyond: Multiple Functions of the Protein Glutathionylation. *Protein Pept. Lett.* 17, 1234–1244.
- Zechmann, B., Liou, L.-C., Koffler, B.E., Horvat, L., Tomašić, A., Fulgosi, H., Zhang, Z., 2011. Subcellular distribution of glutathione and its dynamic changes under oxidative stress in the yeast *Saccharomyces cerevisiae*. *Fems Yeast Res.* 11, 631–642. <https://doi.org/10.1111/j.1567-1364.2011.00753.x>
- Zeida, A., Guardia, C.M., Lichtig, P., Perissinotti, L.L., Defelipe, L.A., Turjanski, A., Radi, R., Trujillo, M., Estrin, D.A., 2014. Thiol redox biochemistry: insights from computer simulations. *Biophys. Rev.* 6, 27–46. <https://doi.org/10.1007/s12551-013-0127-x>
- Zhang, J., Ye, Z.-W., Chen, W., Culpepper, J., Jiang, H., Ball, L.E., Mehrotra, S., Blumental-Perry, A., Tew, K.D., Townsend, D.M., 2020. Altered redox regulation and S-glutathionylation of BiP contribute to bortezomib resistance in multiple myeloma. *Free Radic. Biol. Med.* 160, 755–767. <https://doi.org/10.1016/j.freeradbiomed.2020.09.013>
- Zhang, L., Niu, Y., Zhu, L., Fang, J., Wang, X., Wang, L., Wang, C., 2014. Different interaction modes for protein-disulfide isomerase (PDI) as an efficient regulator and a specific substrate of endoplasmic reticulum oxidoreductin-1 α (Ero1 α). *J. Biol. Chem.* 289, 31188–31199. <https://doi.org/10.1074/jbc.M114.602961>
- Zimmermann, J., Oestreicher, J., Geissel, F., Deponte, M., Morgan, B., 2021. An intracellular assay for activity screening and characterization of glutathione-dependent oxidoreductases. *Free Radic. Biol. Med.* 172, 340–349. <https://doi.org/10.1016/j.freeradbiomed.2021.06.016>
- Zimmermann, J., Oestreicher, J., Hess, S., Herrmann, J.M., Deponte, M., Morgan, B., 2020. One cysteine is enough: A monothiol Grx can functionally replace all cytosolic Trx and dithiol Grx. *Redox Biol.* 36, 101598. <https://doi.org/10.1016/j.redox.2020.101598>
- Zimmermann, R., Eyrich, S., Ahmad, M., Helms, V., 2011. Protein translocation across the ER membrane. *Biochim. Biophys. Acta BBA - Biomembr., Including the Special Section: Protein translocation across or insertion into membranes 1808*, 912–924. <https://doi.org/10.1016/j.bbamem.2010.06.015>
- Zito, E., 2015. ERO1: A protein disulfide oxidase and H₂O₂ producer. *Free Radic. Biol. Med.* 83, 299–304. <https://doi.org/10.1016/j.freeradbiomed.2015.01.011>

List of Abbreviations

%	Percent
°C	Grade Celsius
Å	Ångström
<i>A. Thaliana</i>	<i>Arabidopsis Thaliana</i>
Bp	Base pairs
clonNAT	Nourseothricin
<i>D. Melanogaster</i>	<i>Drosophila Melanogaster</i>
Da	Dalton
dH ₂ O	Distilled water
DNA	Deoxyribonucleic acid
dNTP	Deoxyribonucleoside triphosphate
DTNB	5,5'-dithio-bis-[2-nitrobenzoic acid]
<i>E. coli</i>	<i>Escherichia coli</i>
EDTA	Ethylene diamine tetraacetate
<i>E</i> _{GSH}	Glutathione redox-potential
ER	Endoplasmic reticulum
FAD	Flavin adenine dinucleotide
g	Gram
GFP	Green fluorescent protein
GSH	Glutathione reduced
GSSG	Glutathione oxidized
GSx	Total glutathione concentration
h	Hour
H ₂ O	Water
H ₂ O ₂	Hydrogen peroxide
HC	Hartwell complete
HDEL	Histidine, Aspartic acid, Glutamic aci, Leucine – ER retention-signal
HPV	Human papillomavirus
Kb	Kilo base pairs
Km	Michaelis constant

I	Liter
LB	Lysogeny broth media
LB _{AMP}	Lysogeny broth + ampicillin
Leu	Leucine
Leu	Leucine
M	Molar
Met	Methionine
MiliQ-H ₂ O	Sterilized water using <i>MilliQ</i> -system of <i>Merck</i>
min	Minute
ml	Milliliters
mM	Milli molar
mRNA	Messenger Ribonucleic acid
mRNA Perturbation library	DAmP library
mV	Milli volts
NADP(H)	Nicotinamide adenine dinucleotide phosphate
<i>natNT2</i> -cassette	Nourseothricin resistant-gene
NBD1	Nucleotide- binding-domain1
NEB	<i>New England Biolabs GmbH</i>
ng	Nano gram
nm	Nano meters
OD ₆₀₀	Optical density at 600 nm
OH	Hydroxide
OPT	Oligopeptide-transporter
ORF	Open reading frame
OxD	Degree of probe oxidation
PCR	Polymerase chain reaction
pKa value	Acid dissociation constant
qPCR	Quantitative PCR
R-domain	Regulatory domain
redox	Reduction oxidation
roGFP2	Redox-sensitive GFP
ROS	Reactive oxygen species
rpm	Rounds per minute
RT	Room temperature

rxYFP	Redox sensitive YFP
<i>S. cerevisiae</i>	<i>Saccharomyces cerevisiae</i>
SDS	Sodium dodecyl sulfate
sec	Second
SGA	synthetic genetic array
SRP	Signal recognition particle
SRPR	Signal recognition particle receptors
SS	Signal sequence
SS-DNA	Salomon-sperm DNA
Su9	Subunit 9 of F0F1-ATPase from <i>Neurospora crassa</i>
TAE	Tris-acetate EDTA
TM	Tunicamycin
Tris	Tris-(hydroxymethyl)-aminomethane
TRX	thioredoxin superfamily
U	Unit
UPR	Unfolded protein response
Ura	Uracile
UV-light	Ultra-violette light
V	Volt
vDNA	Viral DNA
xg	Gravity of earth
YNB	Yeast Extract Nitrogen Base Media
YPD	Yeast Extract Peptone Dextrose
YPG	Yeast Extract Peptone Glycerol
γ -GC	γ -L-glutamyl-L-cysteine
μ g	Microgram
μ l	Microliter

Appendix

Supplementary Table 1: SGA Hits

Supplementary Table 1 Hits from the SGA high throughput screen. All genes are listed, which had a negative growth phenotype when deleted together with *OPT3*.

Gene	Gene description from Saccharomyces Database
CCR4	Component of the CCR4-NOT transcriptional complex
FUN12	Translation initiation factor eIF5B
YAL037W	Putative protein of unknown function
TSC3	Protein that stimulates the activity of serine palmitoyltransferase; involved in sphingolipid biosynthesis
AIM3	Protein that inhibits barbed-end actin filament elongation
CMD1	Calmodulin
LYS2	Alpha amino adipate reductase
ALG7	UDP-N-acetyl-glucosamine-1-P transferase
MRPS5	Mitochondrial ribosomal protein of the small subunit
PAF1	Component of the Paf1p complex involved in transcription elongation
SRO9	Cytoplasmic RNA-binding protein
MRC1	S-phase checkpoint protein required for DNA replication
VMS1	Component of a Cdc48p-complex involved in protein quality control
RRG1	Protein of unknown function; required for vacuolar acidification and mitochondrial genome maintenance
DOA4	Ubiquitin hydrolase
SVF1	Protein with a potential role in cell survival pathways
YDR526C	Dubious open reading frame; unlikely to encode a functional protein
HEM14	Protoporphyrinogen oxidase
EDC2	RNA-binding protein that directly activates mRNA decapping
CEM1	Mitochondrial beta-keto-acyl synthase
LYS5	Phosphopantetheinyl transferase involved in lysine biosynthesis
GND1	6-phosphogluconate dehydrogenase (decarboxylating)
NVJ1	Nuclear envelope protein
YIL055C	Putative protein of unknown function
ICE2	Integral ER membrane protein with type-III transmembrane domains; required for maintenance of ER zinc homeostasis
GSH1	Gamma glutamylcysteine synthetase; catalyzes the first step in glutathione (GSH) biosynthesis

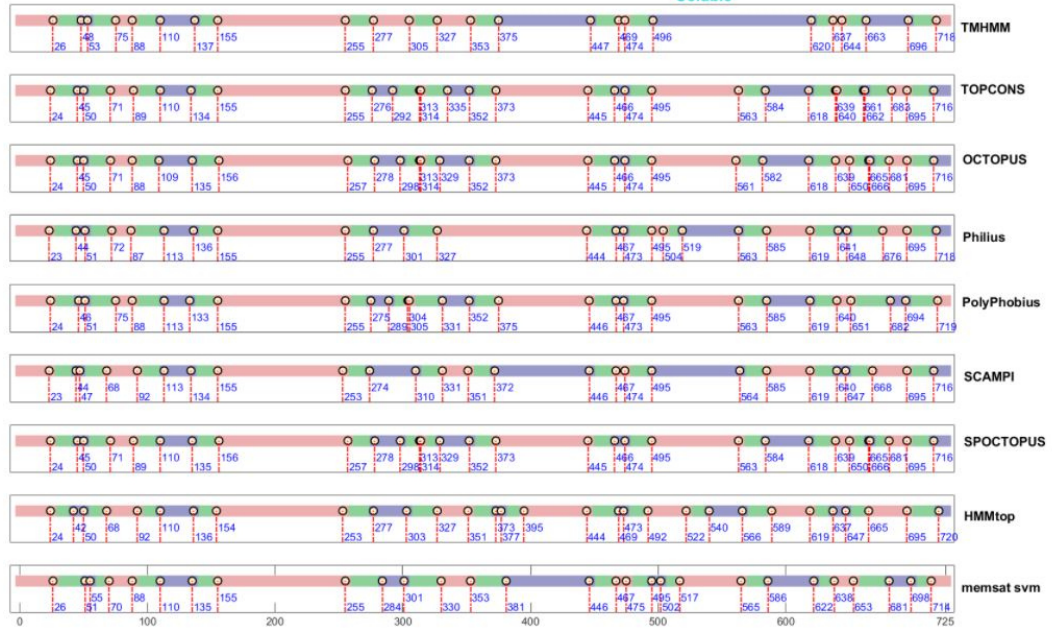
CDC6	Essential ATP-binding protein required for DNA replication
COF1	Cofilin, involved in pH-dependent actin filament depolarization
YPS1	Aspartic protease
YLR317W	Dubious open reading frame
RCH1	Putative transporter; member of the SLC10 carrier family
CCS1	Copper chaperone for superoxide dismutase Sod1p; involved in oxidative stress protection
RPS16A	Protein component of the small (40S) ribosomal subunit
NIP1	eIF3c subunit of the eukaryotic translation initiation factor 3 (eIF3)
YAF9	Subunit of NuA4 histone H4 acetyltransferase and SWR1 complexes
PFA4	Palmitoyltransferase with autoacylation activity
ARG1	Arginosuccinate synthetase
ELP4	Subunit of hexameric RecA-like ATPase Elp456 Elongator subcomplex
SAR1	ARF family GTPase; component of the COPII vesicle coat
YPR170C	Dubious open reading frame

YGL114W YGL114W

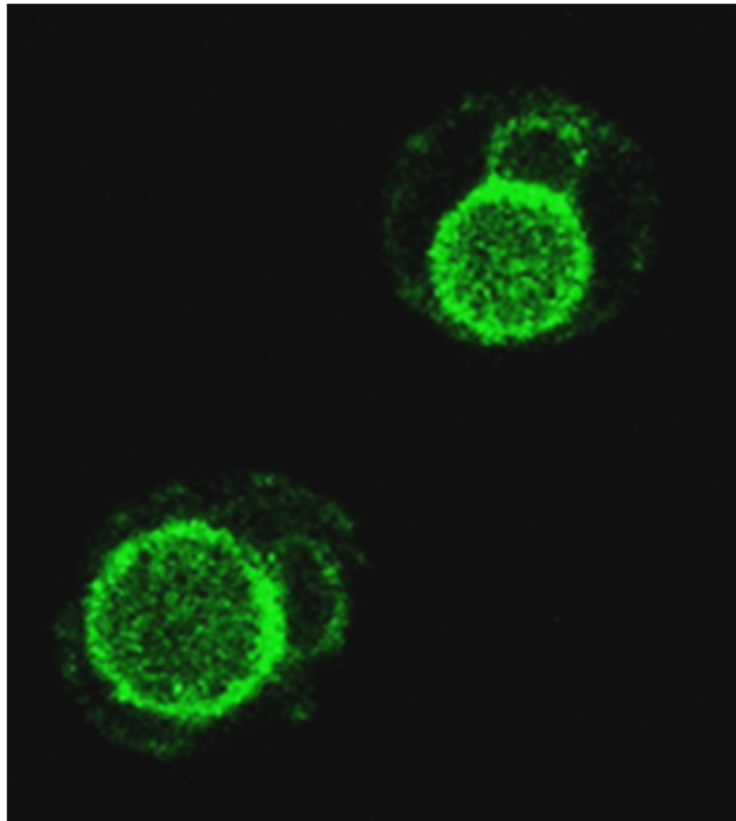
SGD description:
Putative protein of unknown function; predicted member of the oligopeptide transporter (OPT) family of membrane transporters

Legend

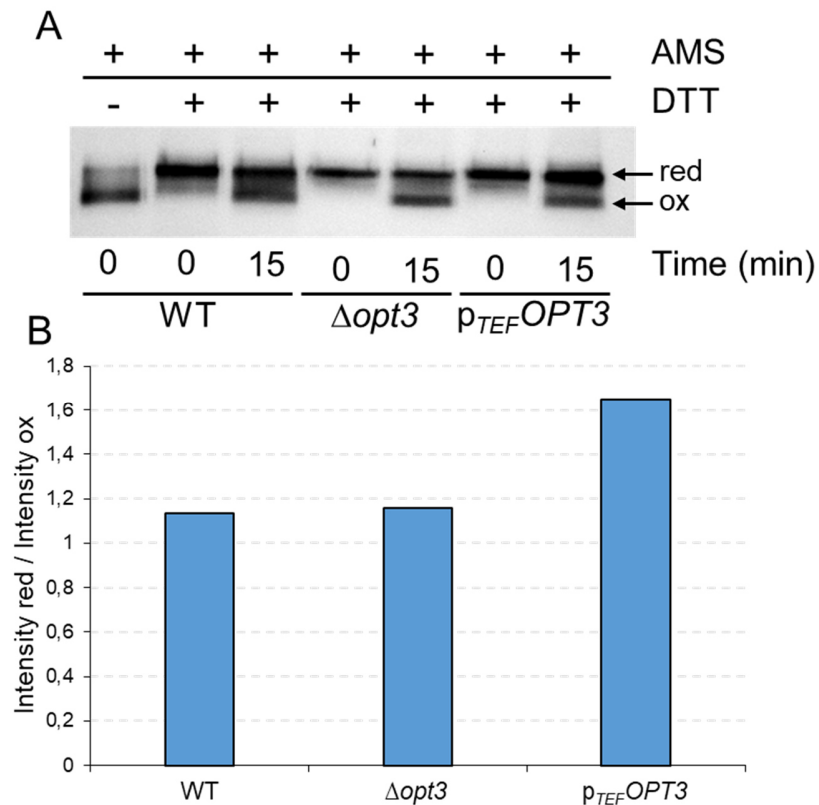
Out (Luminal or Extra-Cellular)
Trans Membrane Domain
Cleavable Signal peptide (SP)
In (Cytosol)
Mitochondrial Targeting Sequence (MTS)
Soluble



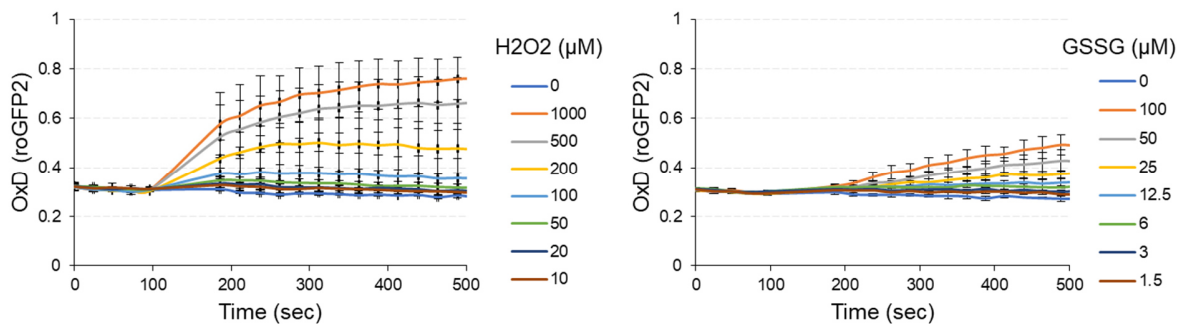
Supplementary Figure 1 Transmembrane prediction Opt3. The transmembrane prediction was carried out using the online available tool “TopologYeast” (<http://www.weizmann.ac.il/molgen/TopologYeast/home>). This online tool bundles and provides graphic output of nine different prediction algorithms (TMMHMM, TOPCONS, OCTOPUS, Philius, PolyPhobius, SCAMPI, SPCTOPUS, HMMtop, memsat svm). The here presented analysis was carried out on the 21 of September 2021.



Supplementary Figure 2 Microscopy GPD sfGFP OPT3. sfGFP-Opt3 has dual localization in the ER and the vacuole when it is strongly overexpressed. At the 5' prime termini of *OPT3* in a $\Delta opt3$ mutant strain, a super folder GFP (sfGFP) under the control of the strong constitutive promoter *GPD* was introduced. sfGFP-Opt3 was imaged using a Leica TCS SP5 and pictures were analyzed using the Leica Application Suite Advanced Fluorescence (LAS AF) software. Pictures were taken with the help of Lucas Schuck from the group of *Plant Physiology* at the TU Kaiserslautern.



Supplementary Figure 3 Ero1 re oxidation assay. Ero1 regulatory cysteines remain longer reduced in an *OPT3* overexpression strain. The strains WT, $\Delta opt3$ and $P_{TEF}OPT3$ containing Ero1 with a C-terminal 6X HA-tag were growing overnight in HC media. Next day 3 OD₆₀₀/ml per strain was harvested, samples were taken up in 1 ml fresh HC media and 5 mM DTT was added. As control, one wild-type sample was not treated with DTT. Samples of each strain were harvested and washed with 1 ml dH₂O directly after incubation in DTT-containing media and after 15 min incubation at 30°C in glutathione free media before taken up in non-reducing SDS sample-buffer (1M Tris/Cl, pH 6.8; 20% SDS; glycerin, 0.1% bromophenol blue) containing 20 mM AMS followed by incubation on ice for 15 min. Afterwards, all samples were cooked at 95°C for 5 min before diluted 1:4 in 50 mM sodium citrate (pH 5.5) with 100 U EndoHf (*NEB*) to remove glycosylation. After 2h incubation at 37°C all samples were loaded on a non-reducing SDS page before western blot analysis and detection of the HA-tag (A). To analyze how fast Ero1 returns to its oxidized low activity state, the ratio between the western blot band intensity of reduced Ero1 and oxidized Ero1 of each sample was analyzed (B).



Supplementary Figure 4 roGFP2 Pdi1 measurements. Pdi1 transfers oxidation from GSSG to roGFP2. The plasmids p416-*TEF-roGFP2-PDI1* and p415-*TEF-OPT1* were expressed in $\Delta glr1\Delta grx1\Delta grx2$ mutant strain. Cells were incubated overnight in corresponding growth media and resuspended the next day to an $OD_{600} = 7.5$ in fresh growth media. The cells were transferred to a 96-well plate and fluorescent roGFP2 signal was recorded in a fluorescent-plate-reader based assay. After 5 cycles measurement was paused and either H₂O₂ (A) or GSSG (B) was added to the samples before recording was continued. At least three independent experiments were performed. Error bars denote standard derivations. The experiment was performed with the help by Halie Ropp during her Bachelor Thesis.

Sequences of *OPT3* cysteine mutants from gene script

P416-*TEF-OPT3* seq. opt. with *Xba*I/*Xho*I cutting sites

All highlighted cysteine residues were mutated separately to alanine

TCTAGAATGCCTCAATCTACTCCAAGTCAAGAAGTACAGCGTGTACCATGGGATAATAAACCC
TGCTTTGAAGCAGATAAACTCCGAGCAACCATAGCAGGTATCGCTATAGGGTCTCTGGTG
CTAACATCAAATTTTCAATTTGGCCTGCAAACCGGTTGGGTTTCCATGATGTCCCTGCCATC
GGCATTGTTAGCTTGTGCTTTCTTTAAAAATATCTGGCCATTAATATTTCCGAACGACAGGC
CTTTCAGTGACGTTGAAAATGTATACGTACAAAGTATGGCAGTAGCTG

TCGGAACAGGCCCATAGCCTTTGGGTTTGTGCGCGTCATACCTGCCATCGAGAAGTTCCT
TACTAACGACGAAAGTGGTGGATTAAGGGAACAAGGACAGTCCTTCACTTTTAGAGAATTGT
TAATATGGTCCACAGCCCTAGCATTCTTCGGTATTTTTTTTTGCAGTTCCTCTAAGAAAGCAA
GTAATTGTTAGAGAGAACTTCCCTTCCCAGTGGTAGCGCCACGGCCACTTTAATTTTCAGT
GCTAAATGGAAGTGAAGATTTTACAAGAGGTTTCTAAGTCAGAGTTATTGAAATGAGGCAGA
GGAGATTGAATGAATGCTGCTGCTACAACCCAACAGAGATCCAGAGGAGGCGGATT
ATTTAATGAAGTCTTCTCATAGCGAACTTGGTGAATATACGGCAACTAGCCAAGATGGAAGT
TCTATCCTTTCTACTGGCTCTGAGAACTACAGAGCGAATATTATTATTTTATTGAAAACCTTT
GTTGTTTCTTCGCTTTACACCATGGTGTATATTTGTACCGGTAATACGGTCTATTCCAGTC
TTCGGAAAATACCTCTCGAACAATTATCTCTGGAATTTTTCAGCCGTCGCCTGCGTATATAGG
CCAAGGGATAATAATGGGTCTTCCAACAGTATCGTATATGCTTATCGGGTGTCTTAGGCT
GGGGTGTGTTAGCACCATTGGCGAGATACAAAAGATGGGTACCACCAGATGCTGATGTCCA
CGACTGGGAGGAGGGAGTGCAAGGATGGATTCTTTGGTCGTCGCTTTCAATAATGGTTGCT
GACAGTGTAGTCGCTTTTATTGTTGTGACAGTGAAGTCCATTGTGAAATTTATTCTTATAGAT
GACAAAGCTGCTTTACTGAACAACATAATCGATGATACATTTCAATCTATGTTACTGGAGGA
GGAACGCGCCATTAATAGCAGCAGAAGAAATACATATGTTGATGGAAGGCAGGACACCGTA
AGATTAGTGAGTAGAGATAACGAAATAGAAGTAGATTTCGAAGCATTTGGTTCGCTATACCAC
CGTTATCAGTGGATGTCTAGTCTCCTCGATAATAATTGTTTCCATAATATATTTGTTTGG
GATACAAGTAATTTCCCTATATGCTATTATCACTGCTTTGATACTTGC GTTGTCTATCTATT
CTCGGTATTTCGAGCACTTGGAGAGACCGATCTGAATCCTGTGAGCGGCATTGGTAAGATCT
CTCAATTGATTTTTGCCTTTATCATACCAAGGGATAGACCTGGATCAGTGTTAATGAACGTG
GTATCGGGAGGTATTGCAGAAGCCTCTGCCAACAGGGCGGGCGATTTAATGCAGGATTTG
AAAACGGGGCACCTCCTCGGCGCCTCCCCAAGAGCTCAGTTCGTGCCCAATTGATAGGG

GCC**TGT**TGGTCAATTATTTTGTCTAGCTTCATGTATTTG**TGC**TACAATAAAGTTTATTCAATTC
CGAGTGAGCAATTCAGGATACCGACAGCAGTAGTGTGGATAGATT**TGT**GCAAGACTAGTAAC
TGGTAAAGGGCTCCCTGATAAGGCCTTGGAG**TGC**TCCATGATTCTCGGAGTCATATTTGCC
GTTTTATCATTAAATCAGAAACACTTATAGAGATTACGGATACGGGTGGATATTATATATTCCG
TCTGGTGTAGCAGTCGGTGTGGTATATTTAATTCTCCAGTTTTACAATTGCAAGATTCATC
GGCGGGTGGGCTTCGCATTTTTGGTTGAAGAATCATAGGGGTGACTTAAATGCGAAAACAA
AAATGATTGTATTCAGTTCGGGGTTGGTCTTAGGTGAAGGTATCTTTAGCGTAATAAACATG
CTCTTCATC**TGC**TTAAATGTCCCTCACTATTAGCTCGAG